2017

Effect of charged species on the gradient properties

Kayesh Ashraf
Virginia Commonwealth University

Effect of charged species on the gradient properties

A dissertation submitted in partial fulfillment of the requirements for the degree of Doctor of Philosophy at Virginia Commonwealth University.

by

Kayesh M Ashraf

Doctor of Engineering, Yokohama National University, Japan, 2012

Masters of Science, University of Dhaka, Bangladesh, 2001

Bachelor of Science, University of Dhaka, Bangladesh, 2000

Director: Maryanne M. Collinson

Professor, Department of Chemistry

Virginia Commonwealth University

Richmond, Virginia

April 2017

Acknowledgement

I am extremely thankful to my advisor Professor Maryanne M. Collinson for the opportunity to work under her supervision and also for her immeasurable guidance and support throughout my graduate research at VCU. I would like to thank her especially for the in-depth analysis of my work and her receptiveness on various occasions. I would like to thank Professor Daniel Higgins Professor, Kansas State University, for his valuable suggestions for all the projects I was involved with. I would like to thank my committee members especially Prof. Sarah Rutan for her invaluable advice and in-depth analysis of my work. I would also like to thank Professor Kenneth J. Wynne for his help on streaming potential measurements and for allowing me to use his laboratory facilities. I sincerely appreciate the guidance and instructions of Dr. Dmitry Pestov with X-ray photoelectron spectroscopy, atomic force microscopy and water contact angle analyses.

I would like to thank my friend Rezaul Karim Khan for his invaluable support and help, especially during the time in need. Finally, I am thankful to my parents for their moral and emotional support throughout these years. Lastly, I would like to thank my loving wife Nadia Afruz for her sacrifice for my family that helped me finish this work without hassle.

Table of contents

List of abbreviations

A	Aligned
AFM	Atomic force microscopy
Ag/AgCl	Ag/AgCl reference electrode
APTEOS	3-aminopropyltriethoxysilane
BE	Binding energy
C8	Octyltrimethoxysilane
CAH	Contact angle hysteresis
CRI	Controlled-Rate infusion
ζ	Zeta potential
EDL	Electrical double layer
DCA	Dynamic water contact angle
DMDMOS	Dimethyldimethoxysilane
ESCA	Electron spectroscopy for chemical analysis
FWHM	Full width at half maxima
FTIR	Fourier transform infra-red
G	Gradient
GO	Graphene oxide

H_2O_2	Hydrogen peroxide
HBr	Hydrobromic acid
IEP	Isoelectric point
IWDC	Infusion-withdrawal dip coating
KBr	Potassium bromide solution
MPA	Mercaptopropanoic acid
MPTEOS	3-Mercaptopropyltriethoxysilane
MPTMOS	3-Mercaptopropyltrimethoxysilane
NC	Negative control
O	Opposed
OT	Octanethiol
OTMOS	Octyltrimethoxysilane
pKa	Log of acid dissociation constant
pKb	Log of base dissociation constant
PMMA	Polymethylmethacrylate
PC	Positive control
PDMS	Poly di-methyl siloxane
POI	Point of intersection

PP	Polypropylene
PTMOS	Phenyltrimethoxysilane
SEM	Scanning electron microscopy
SAM	Self –assembled monolayer
SCA	Static water contact angle
SIMS	Secondary ion mass spectrometry
SPM	Scanning probe microscopy
STM	Scanning tunneling microscopy
T	TMOS base layer
θ_{adv}	Advancing contact angle
θ_{rec}	Receding contact angle
TEOS	Tetraethoxysilane
TMOS	Tetramethoxysilane
WCA	Water contact angle
WP-DCA	Wilhelmy Plate dynamic contact angle
XPS	X-ray photoelectron spectroscopy

List of figures

Chapter 1 **Page**

Chapter 3

Chapter 5

Chapter 6

List of schemes

List of tables

Effect of charged species on the gradient characteristics

Abstract

Surface chemical gradients are materials that exhibit continuous, gradually varying chemical or physical properties along and across the length of a substrate. As a result, each point on the gradient surface can represent an individual sample. They are broadly classified as chemical and physical gradients depending upon the properties that the gradient exhibits. A physical gradient involves a continuous variation of physical properties such as surface roughness and film porosity on the micrometer scale. Chemical gradients involve a gradual variation of chemical properties such as polarity, acidity and basicity, etc. Such gradients have found various applications in cell adhesion, nanoparticle absorption, etc. Because of the multitude of potential applications of acid-base gradient materials in separation science and biological applications, the main work of this dissertation work is focused on the preparation and fundamental, molecular level investigation of acid-base gradients on siloxane surfaces.

In this work, we focused on the preparation and characterization of surface charge gradients. Charged gradients are gradients that contain charged functional groups that are spatially distributed along the length of the substrate. They can interact with each other or with other species in solution by electrostatic interactions. They can also play a key role in governing the interaction of macromolecules and bacteria on surfaces, the wetting of surfaces, the layer-by-layer (LBL) assembly of thin films, reactions in catalysis, and the separation of charged species in chromatography. Therefore, understanding localized interactions between surface functional groups and charged species in solution are particularly relevant to the development of surfaces resistant to biofouling, antimicrobial surfaces, catalytic surfaces, multi-layered composite thin

films, and imprinted surfaces for chemical sensing and separations. Thus, it is of great of interest to develop methodologies to create and study heterogeneous and homogeneous charged surfaces with well-defined properties.

There have been several different methods developed for the preparation of charged gradients. First a chemical gradient is prepared and then the chemical gradient is converted to charged gradient by a chemical approach. Silane-based methods for the preparation of chemical gradients are among those that are widely used because of the straightforwardness of the chemistry involved and also the availability of silanes with various chemical functionalities. A few of these silane based approaches such as the vapor-diffusion method and liquid diffusion method have been used for various applications so far. Most of these methods are only able to prepare surface chemical gradients for a specific application mainly because of their limitations in terms of gradient-length scale and chemistry involved.

In this work, we used a procedure already developed in our lab to prepare chemical gradients from different functionalized alkoxysilanes; we call this procedure the 'controlled-rate infusion method (***CRI***)'. This method can be adapted to different substrates and can form gradients at various length-scales, such as few hundred microns to tens of centimeters. The ***CRI*** method involves the infusion of an organoalkoxysilane solution into a container with a substrate mounted vertically so that time-dependent exposure along the substrate forms a gradient in chemical functionality from bottom to the top. The most important attribute of this method is that the local steepness of the gradient can be systematically controlled by simply changing the rate of infusion. The steepness of the gradient can also be changed at predefined positions along its length by programming the rate of infusion. ***CRI*** can also be used to prepare gradients containing multiple functionalities, termed multicomponent chemical gradients. The different chemical functionalities

can be oriented in different directions to produce gradients where functionalities can be oriented along the same or opposed directions producing aligned and opposed multicomponent chemical gradients, respectively.

In this work, the multicomponent gradients were converted to charge gradients via chemical reaction with 30% H_2O_2. Using controlled rate infusion and this technique, aligned or opposed multicomponent charge gradients containing NH_3^+, SO_3^- and SiO^- groups were prepared. By infusing 3-aminopropyltriethoxysilane (APTEOS) and 3-mercaptopropyltriethoxysilane (MPTMOS) in the same or opposed direction, gradients containing charged species in different locations relative to each other along the length of the substrate were made. The gradient properties in each case were different and correlated to the way they were prepared i.e., where the gradients were oriented in an aligned or opposed fashion. Surface wettability and local surface charge, etc were found to be entirely different depending on the type of charge gradients (aligned and opposed). In another example, SiO^- and NH_3^+ opposed gradients were prepared by infusing APTEOS on different base layers prepared from tetramethoxysilane (TMOS), phenyltrimethoxysilane (PTMOS), dimethyldimethoxysilane (DMDMOS) or octyltrimethoxysilane (OTMOS) followed by protonation of the surface amines. The gradient profiles and surface wettability were found to be independent of each other and dependent of the type of the base layer.

In summary, this dissertation work focuses mainly on the preparation of multicomponent charge gradients and their molecular level characterization by a multitude of different analytical methods including **XPS** spectroscopy, tapping mode atomic force microscopy (**TM-AFM**), zeta potential measurement, and **SCA** and **DCA** measurements. ***CRI*** has incredible flexibility and adaptability, which was confirmed by extending it to different siloxane base films and creating

gradients with different functionalities. Multicomponent charge gradients containing acid and base functionalities can be prepared and optimized for and acid base catalysis reactions such Michael addition as well as aldol, Henry, and Knoevenagel condensations.

Chapter 1: Introduction

1.1 Abstract

The primary objective of this research work is to study the variation of surface chemical properties when a surface gradient is prepared with acidic and basic charged groups on uniform surfaces. Charged groups can interact with each other or with other species in solution by electrostatic interactions. They also play a key role in governing the interaction of macromolecules and bacteria on surfaces, the wetting of surfaces, the layer-by-layer (LBL) assembly of thin films, the reactions in catalysis, and the separation of charged species in chromatography. In order to study various microscopic properties along the length of these gradient materials, there is a need to prepare surface charge gradients in a way so that we can essentially vary the chemistry at each point along these materials and analyze the variation of the surface properties e.g., zeta potential (ζ), surface wettability, nanoparticles absorption characteristics, etc. All these gradients were prepared by a simple, straightforward and rapid method called "controlled-rate infusion or ***CRI*** method. ***CRI*** is primarily based on the time dependent reactivity of organoalkoxysilanes with surface silanol groups on various substrates. This chapter mainly discusses the classification and significance of surface chemical gradients and discusses various methods of chemical gradient preparation, especially time controlled gradient methods using organosilanes. This discussion is followed by a description of different types of charge gradients. An introduction to sol-gel process and a brief discussion of organoalkoxysilanes is continued. A brief account on the reactivity of different silanes used for the gradient preparation is proceeded next. Finally, brief description of ***CRI*** and its uniqueness relative to other methods for gradient preparation and a brief description of the substrates used before summarizing the scope of this dissertation work.

1.2 Gradient materials

Gradient materials are materials that exhibit continuous, gradually varying chemical or physical properties along and across the length of a substrate. As a result, each point on the gradient surface can represent an individual sample. According to Genzer[1,2] there are mainly two types of gradients. These are physical and chemical gradients. A physical gradient involves a continuous variation of physical properties such as surface roughness and film porosity on the micrometer scale[5] Chemical gradients involve a gradual variation of chemical properties such as polarity, acidity and basicity, etc.[1-5] Such gradients have found various applications in cell adhesion, nanoparticle absorption, etc.[3-5] Because of the multitude of potential studies of acid-base gradient materials in separation science and biological applications, the main work of this dissertation work is focused on the preparation and fundamental investigation of acid-base gradients on siloxane surfaces.

1.3 Surface chemical gradients

A surface chemical gradient is formed when a surface exhibits a gradual variation of chemical properties along the length of a surface.[6] These chemical properties can be made to vary in multi-dimensions along the substrate such as one, two or three dimensions.[1,2] Materials researchers use these gradients for high throughput, cost effective and time saving approaches for analysis of many biological and biochemical and chemical processes.[7] A surface chemical gradient properly designed on a substrate can save preparation and analysis time.[8,9] For example, a chemical gradient can be used as a screening tool for biomedical research eliminating the need to prepare numerous samples with varying surface properties such as wettability and charge. Besides, gradient materials have been found applications in various areas such as controlled transport,[10-15]

polymer-templating,[16] chromatographic separations,[17-19] and also in biosensing.[20-23] Surface chemical gradients are formed by modifying the surface typically in one of two ways.[6]

Type 1: Modifying the surface of a substrate further with one or more chemical functional groups by varying the exposure time in the precursor solution or concentration of the functionality in solution.

Type 2: Partially desorbing or converting an already formed modified layer on the surface in such a way that it forms a gradient on the substrate.

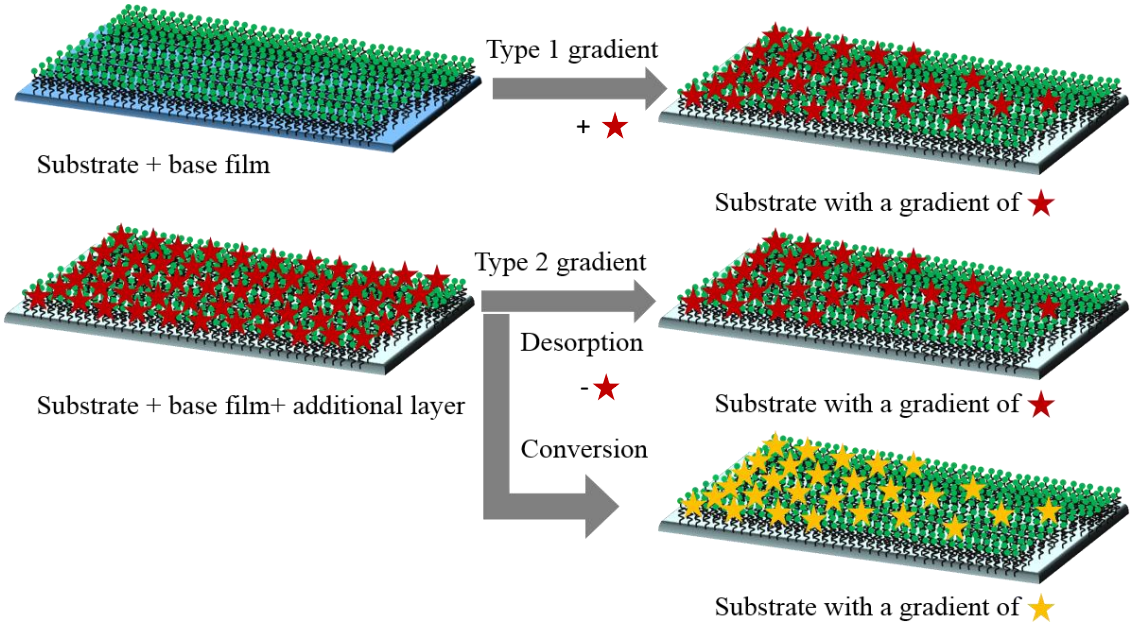

Figure 1.1: Gradient preparation methods based on modifying the surface (Type 1) or gradually converting the surface layers or partially removing the functional groups to generate a gradient (Type 2).

Numerous methods in both the categories have been reported in the past two decades. The former modifications are mainly performed by modifying the surface with silanes on glass or silica surfaces, with alkanethiols on gold or silver substrates, and with polymers.[1,2,6] In most of the cases, silane and alkanethiol approaches are based on forming self-assembled monolayers (SAM). The

latter approach involves the partial removal or conversion of a surface layer from the substrate in a gradient fashion. These types of surface chemical gradients are fabricated mostly by oxidation or photochemical or electrochemical desorption of a self-assembled monolayer.[24]

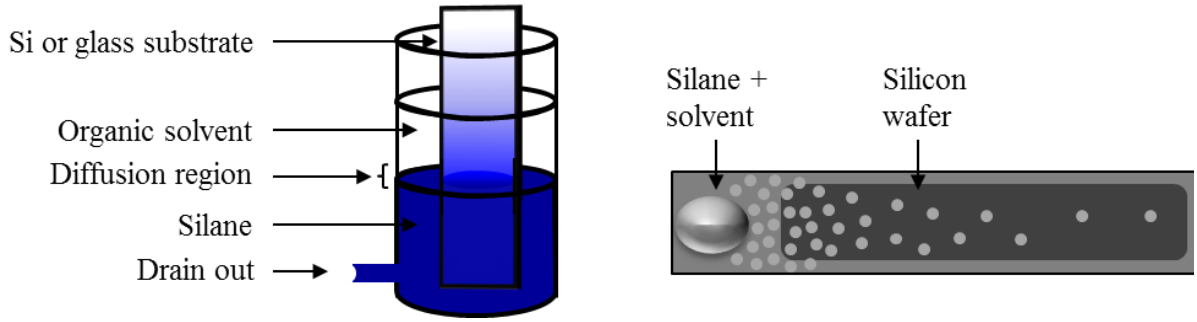

Figure 1.2: (a) Solvent-diffusion and (b) vapor-diffusion techniques.

1.3.1 Type 1 approach

The vapor diffusion method,[25-27] solvent diffusion method [7], and infusion of- and dipping into- the precursor solutions are widely used techniques for making silane-based gradients by this approach. A few mentionable works describing gradient preparation by the former technique reported in scientific journals are listed below. Elwing *et al.*[25-27] and Chaudhury *et al.*[7] developed solvent-diffusion and vapor-diffusion techniques, respectively (**Figure 1.2 (a)** and **(b)**). In the **solvent diffusion method**, a silane (e.g., functionalized chlorosilane) dissolved in a solvent was allowed to slowly diffuse through another solvent in which a substrate where a gradient will be formed is placed vertically. In the course of diffusion through the solvent, the functionalized silane reacts with the substrate where the bottom remains in contact with the silane for a longer time than the top, thereby forming a wettability gradient on the surface. In the **vapor diffusion method**, silane vapors slowly diffuse along the length of the substrate resulting in the formation of a wettability gradient.[28, 29] Other methods to generate wettability gradients from silanes include the use of microcontact printing,[30] the gradual oxidation of silanes by UV irradiation through a density filter[31, 32] or by varying irradiation time.[33-35] Han *et al.*[36] created a gradient from superhydrophobic

to superhydrophilic by combining the gradual oxidation of a silane SAM with a nanoporous substrate, prepared by the layer-by-layer assembly of negatively charged silica nanoparticles and positively charged poly(allylamine hydrochloride). Various applications have been reported for wettability gradients including mass (DNA) transport,[37] droplet movement,[7, 12] and protein and polymer adsorption.[28, 29]

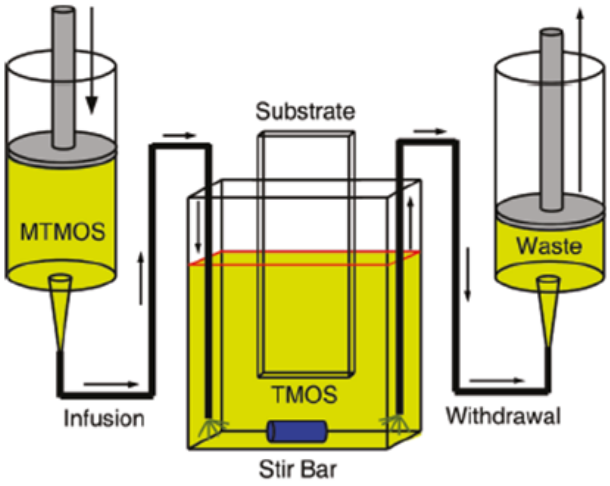

Figure 1.2 (c): Infusion-withdrawal dip coating for the preparation of polarity gradients. (Reprinted from ref. 38 with kind permission from American Chemical Society, Copyright 2010).[38]

Another method recently developed by our collaborators to prepare silane-based chemical gradients is termed 'infusion-withdrawal dip-coating" or **IWDC.**[38, 39] **IWDC** is a simple method for reproducibly preparing macroscopic (1-2 cm long) bulk (< 100 nm thick) silica film polarity gradients.[39] **IWDC** is easily generalized to prepare acid, charge, and dopant gradients. This method employs a reactive sol of time-varying composition that can be deposited on substrates of arbitrary size and geometry. The experimental setup is depicted in **Figure 1.2 (c)**. Gradient formation is accomplished by suspending the substrate in a reactive sol. Synchronized syringe pumps are used to infuse another reactive sol into the deposition reservoir, while the mixed sol (or alternatively the substrate) is withdrawn to produce a film.[38, 39] The change in sol composition during dipping

yields a film exhibiting gradually changing polarity along its length. Using this method, Cui *et al*.[38] prepared a gradient of methyltrimethoxysilane (MTMOS) on a slide modified with a tetramethoxysilane (TMOS) derived base layer. In their work, the substrate was first immersed totally into a cell containing a TMOS sol and withdrawn at a controlled rate using computer-operated device. At the same time, the MTMOS sol containing a methyl group was infused into the cell and the mixture was withdrawn from the cell at the same rate. The solution level in the cell was kept constant through the process while the substrate was slowly withdrawn, thereby, exposing the bottom of the substrate to the MTMOS solution for a longer time than the top. **Figure 1.2 (c)** shows the preparation of a polarity gradient on TMOS derived base film with the high MTMOS end being more hydrophobic. Gradients prepared by this method are few tens of nanometers thick as measured by the spectroscopic ellipsometry. By changing the organosilane and temporally varying its concentration in solution, this method enables the preparation of chemical gradients of various functionalities such as thiol, nitrile, isobutyl, etc.

Recently, our laboratory developed a time-based method for preparing surface chemical gradients with gradient thickness of 1 nm to 3 nm. We call it 'controlled-rate infusion', or ***CRI***.[40] A surface chemical gradient is formed on a siloxane coated substrate by slowly infusing a silica sol containing an organoalkoxysilane with the desired functional group into a container housing the substrate. The commonly used substrate for this method is a silicon wafer uniformly coated with a siloxane base layer prepared with different organic moieties or a TLC plate. This method provides flexibility in controlling the profiles of the gradient on a substrate just by changing the infusion rate and/or concentration in the solution. By varying the functionalities attached to the central atom (Si), 1-D or multidimensional gradients containing different organic groups can be prepared. For example, Kannan *et al.*[40] reported the preparation of surface amine gradients that

exhibit a wide variety of profiles from shallow to steep. In their work, a substrate that incorporates dimethyl and Si-OH groups was temporally modified with an aminoalkoxysilane ($NH_2(CH_2)_3Si(OC_2H_5)_3$) using ***CRI*** to build a gradient film for which the amine content changed over a 10-20 mm distance. Both **XPS** spectroscopy and contact angle measurements were used to confirm the presence of a chemical gradient across the surface of the film. The preparation of the multidimensional gradients with different functionalities in this dissertation work was performed by the ***CRI*** method, and a detailed procedure of this method will be discussed later.

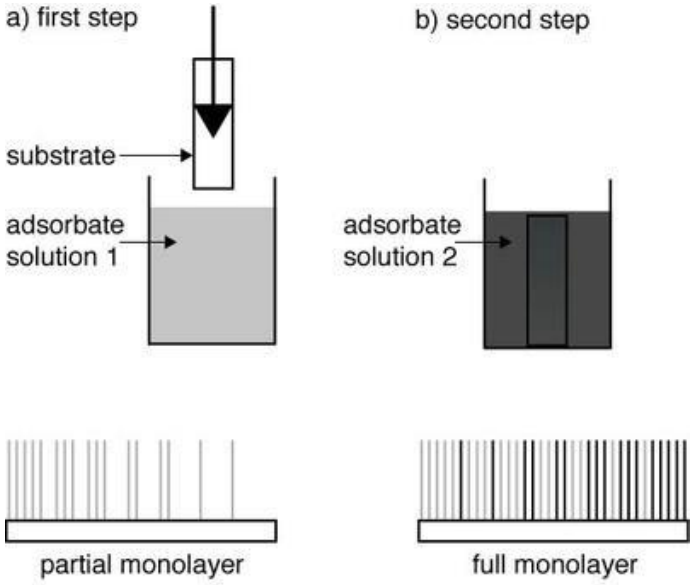

Figure 1.3: Gradient preparation procedure by sequential immersion method. During a first step a coverage gradient is generated that can optionally be saturated with a second component during a subsequent immersion (Reprinted from ref. 44 with the kind permission).[44]

Alkanethiols are also used widely to prepare type 1 gradients on noble metals such as gold, where alkanethiols have been shown to spontaneously assemble to form a self-assembled monolayer (SAM).[41] This area of research provides a simple way of creating surfaces of virtually any desired chemistry by placing a gold substrate into a solution of an alkanethiol in ethanol. It is now well established that thiol groups covalently bind to the gold resulting in the formation of

crystalline-like monolayers on the metal surface, called SAMs. Liedberg and Tengvall[42] used a diffusion method to generate an alkanethiol gradient by allowing two different alkanethiols to cross-diffuse from two ends of a polysaccharide-coated gold surface. The two alkanethiols having different alkyl chain lengths were placed at two glass filters separated by a distance of 40 mm for gradient formation.[43]

Recently Spencer and co-workers[44] developed a new method called "sequential immersion method" for making thiol gradient on gold substrates (**Figure 1.3**). In their technique, the substrate (glass slide) was slowly immersed in an 11-aminoundecanethiol solution by means of a linear-motion drive at a controlled speed resulting in the formation of a gradient from bottom to the top. The surface chemical composition and its distribution on the substrate were monitored by **XPS** spectroscopy. Beurer *et al*.[45] prepared an orthogonal surface-chemical gradient on gold by successive, controlled immersions in orthogonal directions into dilute solutions of dodecanethiol and perfluorododecanethiol. In their work, they evaluated the chemical composition, homogeneity and the ordering of the self-assembled monolayer by **XPS**, **DCA** measurements and polarization-modulation infrared reflection-absorption spectroscopy. Chemical gradients using alkanethiols with various substitutions such as hydroxyl and long-chain alkyl groups on gold substrates have also been reported by Morgenthaler *et al.*[46-47] The gradients were prepared by slowly immersing the gold substrate in the alkanethiol solution in a gradual fashion. The gradients were characterized by **XPS**, contact angle measurements and Infrared spectroscopy.

Other methods that are used for preparing alkanethiol functional gradients include regular contact printing to generate gradients with a wide variety of different shapes[48] by applying very thin, contoured, alkanethiol-saturated PDMS stamps to a substrate. Ink-jet printing was also used

to generate alkanethiol gradients in the centimeter range by printing one component and backfilling with a second.[49,50]

1.3.2 Type 2 approach

The type 2 approach is based on the removal of a surface layer from the substrate or gradually converting the surface layer. Ruardy *et al*.[24] discussed a few methods based on type 2 modification in their review.[24] Most of these methods utilize either photochemical or electrochemical desorption of self-assembled monolayer on a polymer surface to form a surface chemical gradient. Since these methods encounter disadvantages such as limited control on surface chemistry and roughness, these methods are relatively less common compared to constructive modification.

There are, however, many examples, such as those based on alkanethiols,[51] polymer coatings, etc. Electrochemical desorption[51- 55] of thiols on Au surface was reported by Terrill *et al*.[52] to form a gradient in surface composition by cycling electrode potential while the surface is withdrawn from the solution. This method relies on the electrochemical desorption of alkanethiols from a fully covered SAM by application of a potential in a flow-cell. These methods were used to prepare one-[51, 55] and two-[52, 53] component gradients and have found applications in cell adhesion studies[52] and in the evaluation of a new mass spectroscopic technique.[54] Two-component gradients by electrochemical process have also been prepared by fine-tuning of monolayer adsorption and then gradually desorbing it by applying the increasing electrode potential. For example, a two-component gradient of octanethiol (OT) and mercaptopropylamine or $HS(CH_2)_2$- CO_2H, (MPA) obtained by exploiting a linear potential variation with position along a gold surface, by poising the two ends of a thin Au strip at different potentials relative to a common solution Ag/AgCl reference couple.[53] A 2-component linear gradient in composition, i.e., OT/MPA, wetting

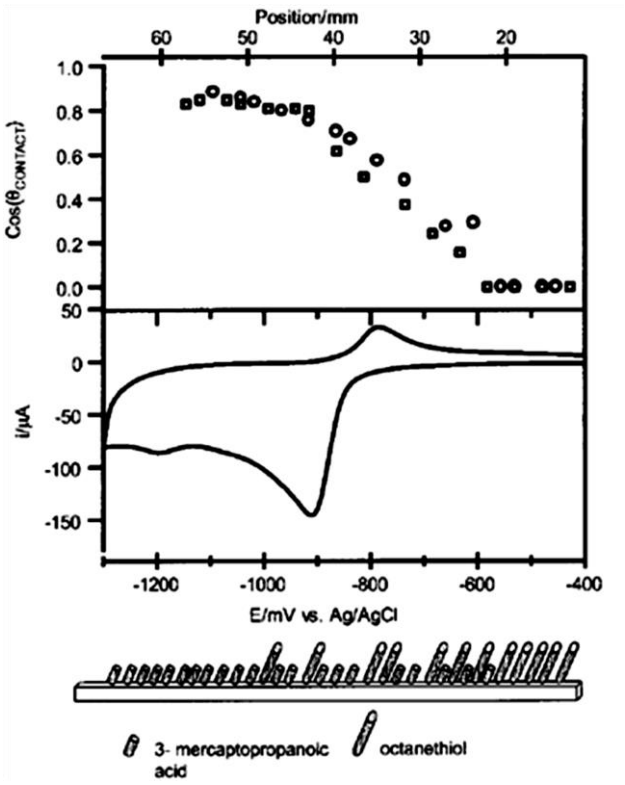

Figure 1.4: Plot correlating spatial position (top abscissa) and applied potential (bottom abscissa) along a single 60 mm long Au electrode containing a 2-component counter propagating gradient of OT and MPA. The bottom panel is a plot of the cyclic voltammogram showing how electrochemical phenomena are mapped onto position along the electrode surface. The top panel plots the sessile drop H_2O contact angle vs. spatial position (different symbols represent replicate trials). The bottom illustration schematically gives the composition of the 2-component gradient as a function of position, referenced to the distance (top) axis (Reprinted from ref. 53 with the kind permission).[53]

properties, and surface energy was thereby created (**Figure 1.4**). Several papers reported the electrochemical method for the preparation of gradients using several kinds of thiols by controlling the electrode potential performed by combining CV, cycling in the established voltage range with

mechanical withdrawal from the solution.[55,56] Alkanethiol desorption has also been accomplished using a X-ray beam by controlling the exposure time of irradiation.[57]

In another example[48,58], polyvinylenecarbonate (PVC) coated glass plate was gradually immersed into sodium hydroxide (NaOH) aqueous solution at a controlled rate. NaOH hydrolyzed the carbonate carbon (-OC(=O)O-) of PVC to of hydroxymethyl carbon (>CH-OH) (PHM). The end that was exposed for a longer time in the NaOH solution was more hydrophilic than the other end since it had more hydroxyl groups. The other end is rich in carbonate groups, which are relatively more hydrophobic as shown in **Figure 1.5**. Gradients prepared by these approaches have been used to study protein adsorption and cellular responses.[58]

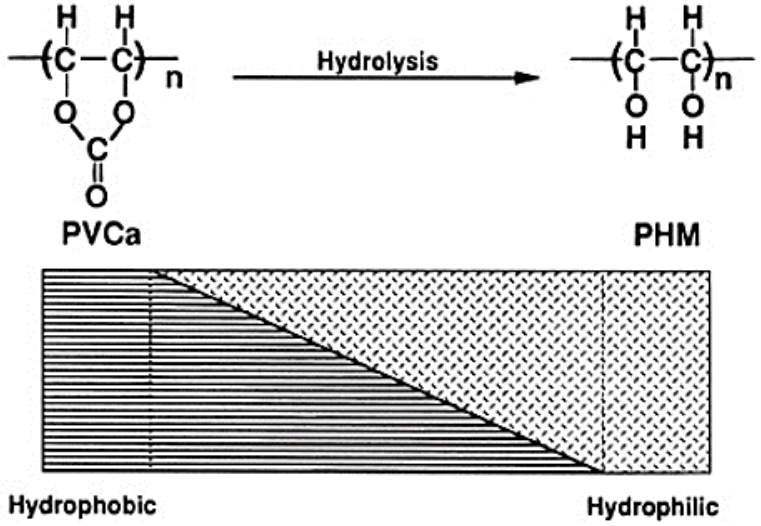

Figure 1.5: Conversion of hydrophobic poly(viny1ene carbonate) (PVCa) to very hydrophilic poly(hydroxymethy1ene) (PHM) as a function of hydrolysis time (Reprinted from ref. 58 with the kind permission).[58]

In polymer-based gradient preparation methods, the polymer substrate is generally exposed to radiation or an etching solution.[59-60] For example, a wettability gradient was prepared by treating

a polyethylene surface with corona discharge. The polymer surfaces were oxidized gradually from one end to the other end with increasing discharge power, and a wettability gradient (**Figure 1.6**) on the sample surface was created.[59]

Cavallini and coworkers[61] reported a new method to fabricate a surface chemical gradient of alkanethiols by the reductive electrochemical desorption/partial readsorption of thiols on Au substrate. The whole process was carried out by cycling the electrode potential while the surface is withdrawn from the solution. During the forward scan, reductive desorption of the thiol SAM occurs and during the reverse scan while the sample is being withdrawn, partial readsorption of thiol took place, thereby a spatial variation of the thiol functional groups was formed. The gradients thus prepared were characterized by contact angle, X-ray photoelectron analysis, Kelvin Probe (KP), and electrochemical techniques. Alkanethiol gradients have found a variety of applications in protein and cell adsorption,[62,63] nanoparticle attachment,[53] etc. Although the various preparation methods mentioned above enjoy some advantages, such as covalent interaction between gold and thiol molecules, the process is limited to a few metal substrates such as gold, silver, and copper.

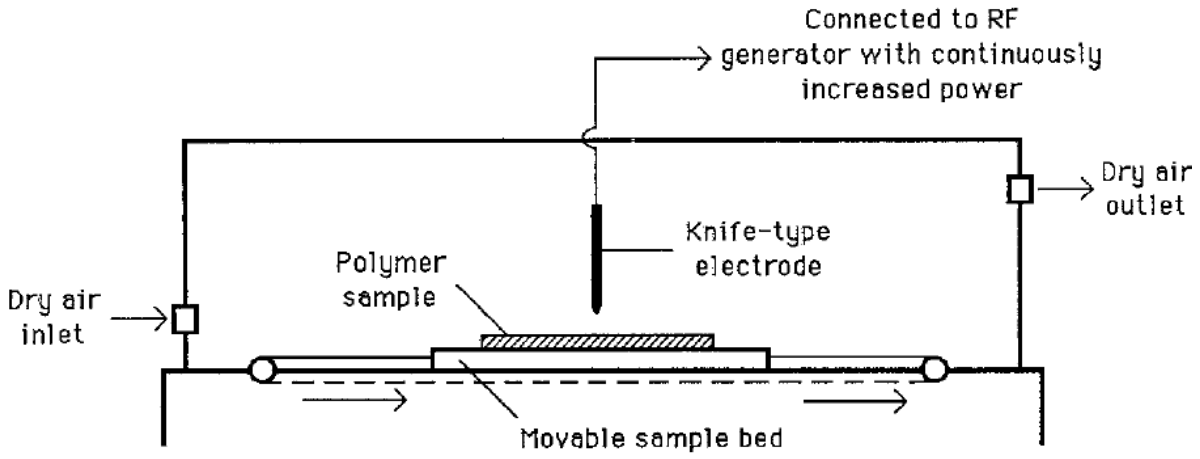

Figure 1.6: Schematic diagram showing the corona-discharge apparatus for the preparation of wettability gradient surfaces time (Reprinted from ref. 59 with the kind permission).[59]

All the gradients prepared in this work is based on the type 2 modification i.e., multicomponent gradients are formed first, later converted into charged species so that gradients where charge species are spatially distributed along the gradient is formed. The following section briefly accounts for the background and types of the charge gradient.

1.4 Charge gradient

Charged gradients are gradients that contain charged functional groups that are spatially distributed along the length of the substrate. They can interact with each other or with other species in solution by electrostatic interactions. They also play a key role in governing the interaction of macromolecules and bacteria on surfaces, the wetting of surfaces, the layer-by-layer (LBL) assembly of thin films, the reactions in catalysis, and the separation of charged species in chromatography.[64-68] Therefore, understanding localized interactions between surface functional groups and charged species in solution has become particularly relevant to the development of surfaces resistant to biofouling,[64] antimicrobial surfaces,[68] catalytic surfaces, multi-layered composite thin films,[66] and imprinted surfaces for chemical sensing and separations.[67] Thus it is of great of interest to develop methodologies to create and study heterogeneous and homogeneous charged surfaces with well-defined properties.

There have been a number of studies reported so far where charge gradients have been made and evaluated. Charge gradients can be of cationic[69], anionic[44,70] or dual (cationic and anionic) nature.[72,73]

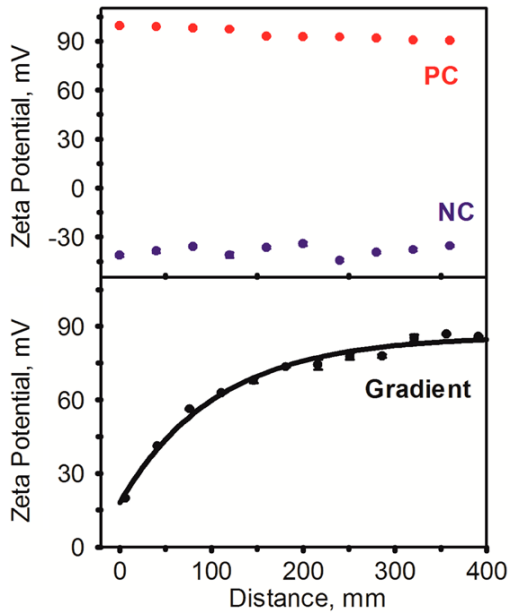

Figure 1.7: ζ profile on (top) the negative (NC) and positive (PC) control capillaries and (bottom) a gradient capillary. The solid line depicts a fit of the data to a first-order kinetic model using kC_{sol} = 12.9 h^{-1} time (Reprinted from ref. 73 with the kind permission). [73]

Cationic charge gradients are prepared when the positively charged functional groups are spatially distributed along the gradient surface. For example, Kannan *et al.*[73] reported the formation of surface amine charge gradients on the inside surface of silica capillaries via controlled rate infusion using 3-aminopropyltriethoxysilane as the reactive precursor. Using ζ measurements, they reported that the ζ values varied over 60 mV from one end of the capillary to the other (**Figure 1.7**). Other examples of cationic charge gradients include the preparation of $-N(CH_3)_3^+$ charged gradients by attaching amine-terminated reagents ($-NH_2$) and subsequent quaternarization, typically with methyl iodide,[69] to yield a $-N(CH_3)_3^+$ gradient or simply by protonation to give $-NH_3^+$ gradient.[73]

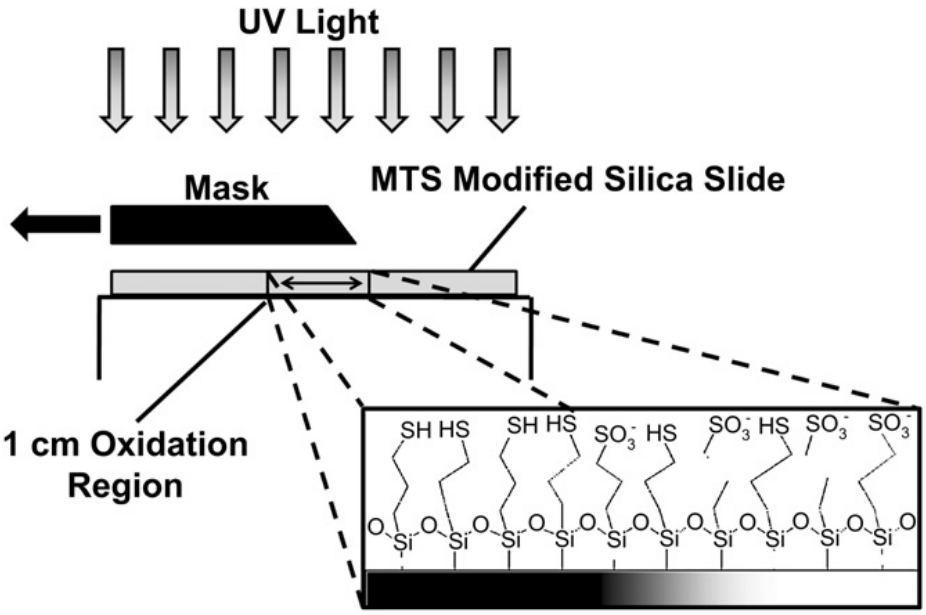

Figure 1.8: Creation of the surface charge gradient is accomplished by translating the edge mask at a constant rate over a 1 cm region of the uniformly modified MTS silica slide. On the UV exposed region the surface thiol group is oxidized into a negatively charged sulfonate group (Reprinted from ref. 73 with the kind permission).[74]

Anionic charge gradients are gradients where the negatively charged functional groups are spatially distributed along the surface. For example a sulfonate charge (anionic charge) gradient was formed on fused silica slides using selective oxidation of a 3-mercaptopropyltrimethoxysilane (MTS) monolayer to prepare a high throughput and cost effective approach for screening platelets adhesion[74] and protein adsorption.[69] UV radiation was used for the oxidation process which slowly translated from one end to the other end converting surface thiol groups (–SH) into negatively charged sulfonate ($-SO_3^-$) groups in a gradient fashion (**Figure 1.8**). The resultant gradient samples were characterized by **WCA** and electron spectroscopy for chemical analysis (ESCA). Other examples include negatively charged gradients prepared from

thiol-terminated functionalities (-SH) followed by oxidation to yield sulfonate groups ($-SO_3^-$)[75,76] or deprotonation of -COOH terminated groups spatially organized on a surface.[44, 70]

Dual charge gradients are gradients where both cationic and anionic charged species are spatially distributed along the gradients**.** A number of works has been reported about the preparation of dual charge gradients. These include opposed gradients prepared from polyelectrolyte brushes incorporating oppositely charged weak electrolytes such as poly(acrylic acid) and poly(2-vinyl pyridine)[71] or plasma polymerized amine and carboxylic acid polymers,[72] as well as binary and ternary mixed self-assembled alkanethiols on gold.[44] Such gradients offer an unique opportunity to explore localized intermolecular interactions in a time-efficient fashion, particularly when the placement of the individual functional groups can be carefully controlled. Such interactions are experimentally evaluated for a $-NH_3^+$ $-SO_3^-$ dual charge gradients on siloxane surface and are interpreted in **Chapter 3**.

Dual charge gradients containging SO_3^- and NH_3^+ groups oriented either in an aligned or opposed fashion were prepared by the hydrolysis and condensation reactions of the organoalkoxysilanes.[77,] Aminosilane and mercaptosilane precusors were used to make amine and thiol gradients via controlled rate infusion and then they were treated with hydrogen peroxide (H_2O_2) to create the dual charges on the surface. Because the hydrolysis and condensation of the silane precursors via the sol-gel chemistry is fundamental to the work described in this thesis, a brief account of the sol-gel process, organoalkoxysilane and the reactivity of the aminosilane and mercaptosilane is discussed in the following sections.

1.4 Sol-Gel process

The sol-gel process is utilized in the preparation of gradients via the **IWDC**[38,39] and ***CRI***[40] methods. The formation of reactive silane solutions is vital for the successful deposition of the silane monolayer/multilayer on various substrates. The sol-gel process is a wet chemical process where monomeric metal alkoxides or silicon alkoxides undergo simultaneous hydrolysis and condensation to produce a sol-gel derived product containing networks of metal oxide or silicon oxide bonds depending on the type of alkoxides used.[78] The sol-gel process involves two reaction steps; hydrolysis and condensation. A small amount of acid or base facilitates these types of reactions.[7]

A sol consists of colloidal particles (amorphous or crystalline) or polymers dispersed in a solvent. When the particles are dispersed in a gas phase, it is known as an aerosol. When these colloidal particles are agglomerated due to the Van der Waals forces or hydrogen bonding, they form a continuous network extending three dimensionally thereby creating a gel. A gel can also be formed by the covalent linkages of the polymeric units. Thus, a gel is a three dimensional continuous form due to the condensation or agglomeration of colloidal particles or from linking polymer chains.

The sol-gel process may be defined as the "formation of an oxide network through polycondensation reactions of a molecular precursor such as organoalkoxysilane in a liquid."[78, 80] **Scheme 1.1** shows a generalized reaction of a trialkoxysilane precursor with a species having silanol groups. The alkoxy groups of trialkoxysilanes are hydrolyzed to form Si-OH containing compounds. This hydrolysis may occur during the preparation of aqueous solutions of the silane or in the presence of trace moisture in the atmosphere or adsorbed on the substrates. The rate of hydrolysis of alkoxysilanes depends on steric and inductive effects, and thus the size of the alkoxy group ($OCH_3 > OCH_2CH_3 > OCH_2CH_2CH_3$), replacement of an alkoxy group with an alkyl group

and the presence and concentration of catalysts such as a mineral acid or base, and temperature.[78,81]

$$(RO)_3 - Si - OR \ + \ H_2O \ \xrightarrow{H^+/OH^-} \ (RO)_3 - Si - OH \ + \ ROH$$

$$(RO)_3 - Si - OH \ + \ H_2O \ \xrightarrow{H^+/OH^-} \ (RO)_2Si - (OH)_2 + ROH$$

$$(RO)_2 - Si - (OH)_2 + H_2O \ \xrightarrow{H^+/OH^-} \ RO - Si - (OH)_3 + ROH$$

$$RO - Si - (OH)_3 \ + H_2O \ \xrightarrow{H^+/OH^-} \ Si - (OH)_4 \ + ROH$$

Scheme 1.1: Generalized sol-gel reaction of a trialkoxysilane precursor, where $-R$ is the$-C_xH_{2x+1}$

In the hydrolysis step, the alkoxide groups (−OR) are replaced by the hydroxyl groups(−OH). Subsequent condensation reactions lead to the formation of siloxane networks where central Si atom is covalently bonded to the **O** atoms.

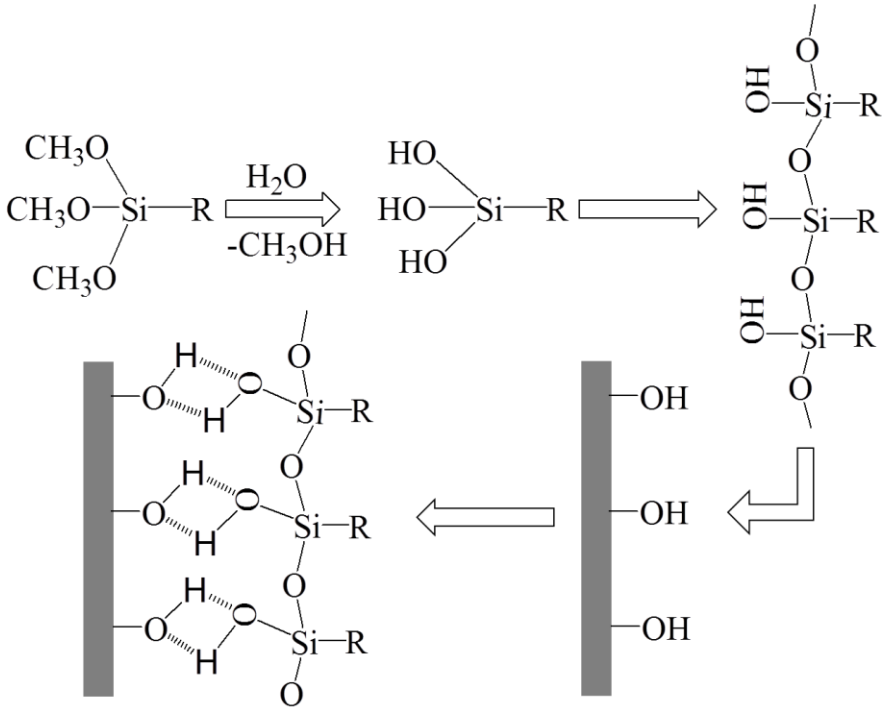

Scheme 1.2: Schematic represents hydrolysis and condensation with neighboring silane on the surface.

Condensation takes place concurrently with hydrolysis. In this step, a reaction takes place between the hydrolyzed precursor and the silanol groups resulting in covalent Si-O-Si bond formation. But before condensation, a molecular layer of hydrolyzed alkoxysilanes resulting from hydrogen bonding interaction occurs between a hydroxyl group of the silane and surface silanols.[81] The condensation reaction between these groups occurs on the surface as shown in **Scheme 1.2**, as well in most cases to form polymeric siloxane structures and this can occur anytime during the process, either before or after adsorption.

The above factors that affect the hydrolysis rate also affect the rate of condensation. Moreover, as the hydrolysis proceeds, the self-condensation of silanetriol to form polymeric compounds will also occur. The organic substituent (R) on the alkoxysilane can also influence the rate of hydrolysis and condensation.[78,82] For example, the amine group in 3-aminopropyltriethoxysilane (APTEOS) can self-catalyze the rate of hydrolysis and condensation and increase the rate of hydrolysis and condensation.[83] The condensation of an aminosilane with substrates containing silanol groups will be discussed in more detail in the following section as these reactions play a key role in this research study. Multi-component gels may be prepared with a controlled stoichiometry by mixing sols of different species or organoalkoxysilanes. The following section briefly describes the sol-gel chemistry of organoalkoxysilanes featuring some of the chemical properties.

1.5. Organoalkoxysilanes

Organoalkoxysilanes contain an organic functional groups covalently bonded to a central silicon atom as shown below.[84, 85]

$$R_n\text{-Si-}(OR')_{4-n}$$

R is a non-hydrolysable moiety covalently bonded to the silicon. *R* can be alkyl, aryl, organic-functional or a combination of any of these groups. *R*' is a hydrolysable alkoxy substituent, which is typically a methoxy or ethoxy group (-OCH_3 or -OCH_2CH_3). The organic moiety (*R*) of the organoalkoxysilanes can react with other organic compounds and the inorganic moiety such as silicon, metal, etc. Organoalkoxysilanes can act as mediators for the coupling of organic polymers, such as epoxy resin to inorganic materials and hence they are called as 'silane coupling agents'.[78] They can also react with themselves and with other silanes by a series of hydrolysis and

condensation reactions.[78, 85] The *R* groups in organoalkoxysilanes imparts various physico-chemical properties of a materials, such as optical and mechanical properties,[86,87] wettability[88] and pKa.[89] The R group is also a reactive group that can further undergo chemical reactions with other reactive groups including amino, thiol, cyano, phenyl and azide. A general structure of alkoxysilane with reactive and non-reactive R groups is listed in the following **Table 1.1**.

Table 1.1: Structures of some organoalkoxysilanes.

Name of the silane	Abbreviation	Chemical structure	R group
3-aminopropyltrimethoxysilane	APTMOS	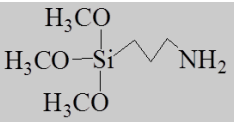	propylamine
3-mercaptopropyltrimethoxysilane	MPTMOS	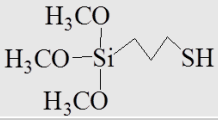	propylthiol
3-nitrilepropyltrimethoxysilane	CNTMOS	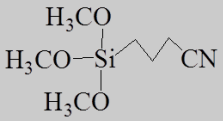	propylnitrile
dimethyldimethoxysilane	DMDMOS	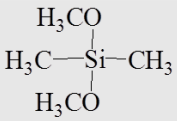	methyl
octyltrimethoxysilane	C8	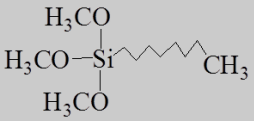	octyl
phenyltrimethoxysilane	PTMOS	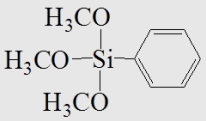	phenyl

1.6 Reactivity of aminosilane

In section 1.5, some of the important features of the organoalkoxysilanes were discussed. In this section, the chemical features originating from the attached alkyl and amine functional

group and the siloxane networks are discussed. Aminosilane is an organoalkoxysilane compound having a reactive amine functional group either directly covalently bonded to the silicon atom or linked to silicon atom by other organic groups. The reactivity of the aminoalkoxysilane compounds depends on the size of the organic linkages and alkoxy group, and also whether the amine is primary, secondary or tertiary. The hydrolysis and condensation reactions of aminoalkoxysilanes with various substrates such as glass, silicon and silica gels have been studied using different techniques including X-ray photoelectron spectroscopy,[90] Fourier transfer-infrared spectroscopy,[91,92] and Nuclear magnetic Resonance Spectroscopy.[93] Most researchers use APTEOS as the aminoalkoxysilane precursor.[94] A general formula for the aminosilanes used in this work is

NH_2-R-Si-$(OR')_3$ or

3-aminoalkyltrialkoxysilane

where *R* is a propyl and *R'* can be either a methoxy or ethoxy group. The amino group (-NH_2) is responsible for the high reactivity of aminosilanes. The N atom in NH_2 group is also involved in hydrogen bonding with neighboring OH groups either from surface silanol groups or from the hydrolyzed silane itself.[8] Fourier transform infrared spectroscopic (**FTIR**) studies suggest that once APTEOS starts hydrolyzing, it can form a cyclic structure by hydrogen bonding interactions.[91] The reaction for this is given below in **Scheme 1.3**.

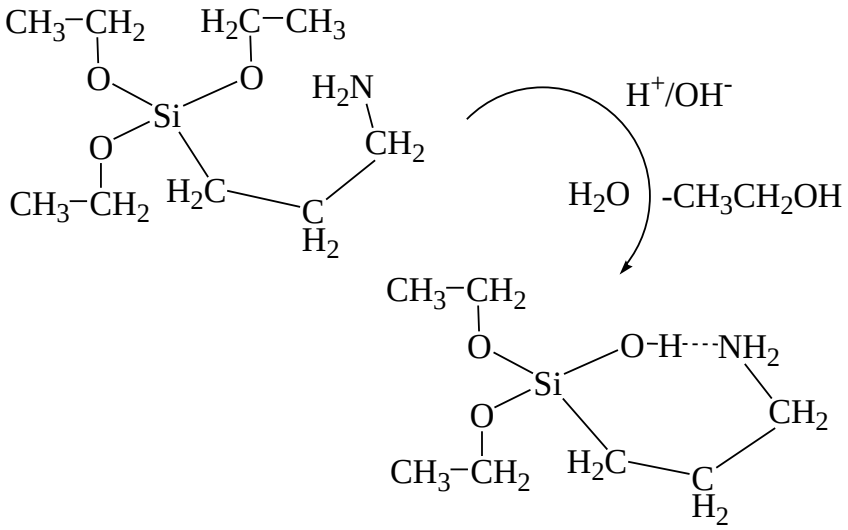

Scheme 1.3: 3-aminopropyltriethoxysilane hydrolyzes and forms a cyclic structure through hydrogen bonding.

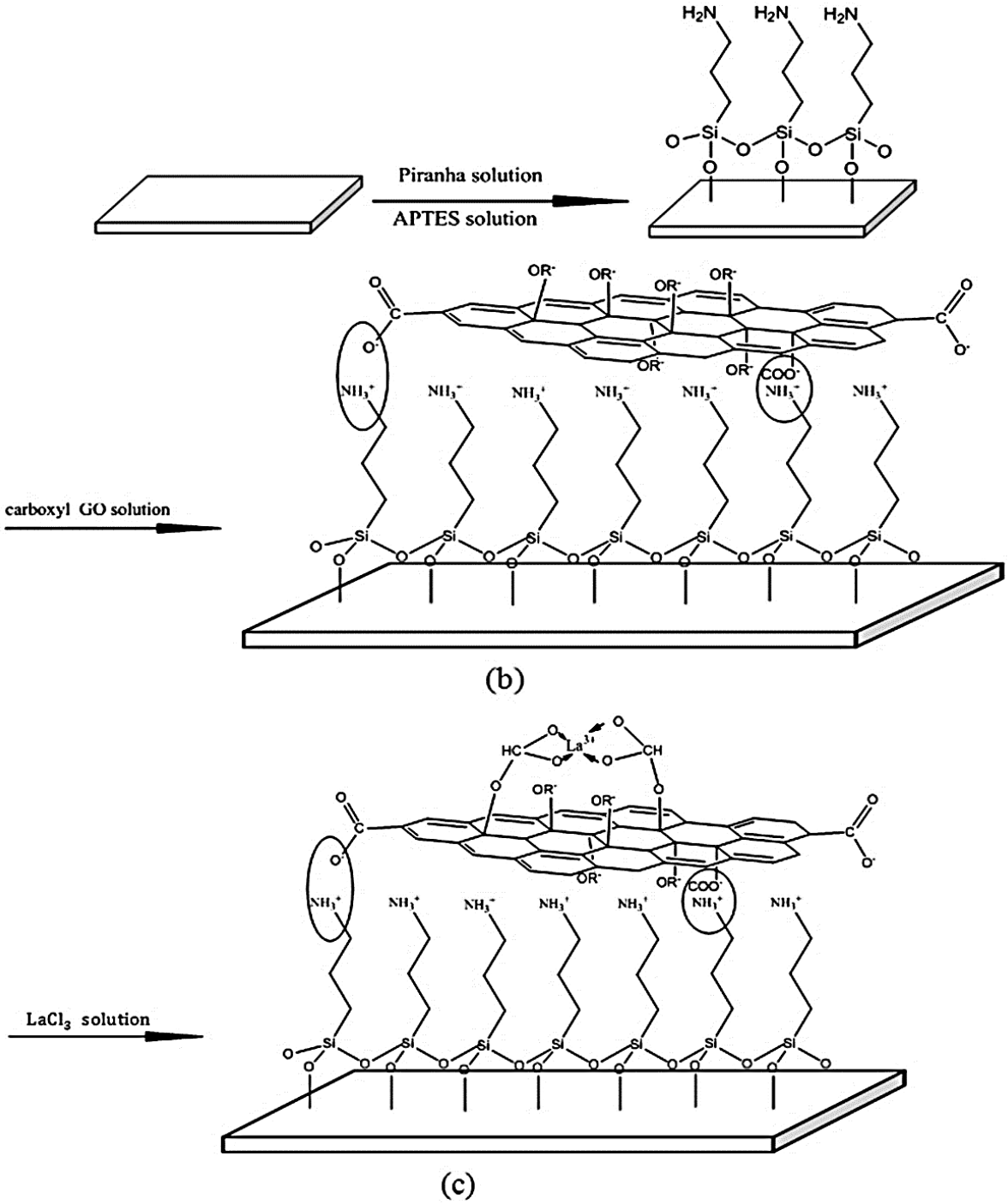

Figure 1.9: Schematic diagram illustrates the preparation of samples: (a) carboxy functionalized GO sheet (GO–COOH), (b) APTEOS-SAM film and APTEOS–GO film, (c) APTEOS–GO–La film (Reprinted from ref. 94 with the kind permission).[94]

The reactivity of the amine group is widely exploited in its use as a coupling agent. Liu *et al*.[95] reported APTEOS as a coupling agent for preparing low friction coefficient and good wear-

resistant carboxylated graphene oxide (GO) complexes with lanthanum on a silicon substrate (**Figure 1.9**). The chemical composition, microstructure, and surface morphology of the samples were analyzed by **XPS** spectroscopy, **WCA**, **AFM** microscopy, and scanning electron microscopy (**SEM**).[94]

The amine groups in the aminosilane precursors are involved in hydrogen bonding interactions with surface silanol groups initially and then catalyze condensation to form Si-O-Si bonds.[92, 96] In the case of aminosilanes containing multiple amine groups, the rate of the reaction is further increased and the condensation to surface silanol groups happens quickly.[40] However, alkyl substitution on the amine nitrogen such as secondary and tertiary amines increases the steric effect on the transition state, which reduces the condensation rate relative to the primary amines. [97] Since the aminosilane reaction with substrates containing silanol groups is very rapid and straightforward, surface modification using APTEOS has been commonly used to modify various substrates with amine groups for a wide range of applications. [92, 96,98]

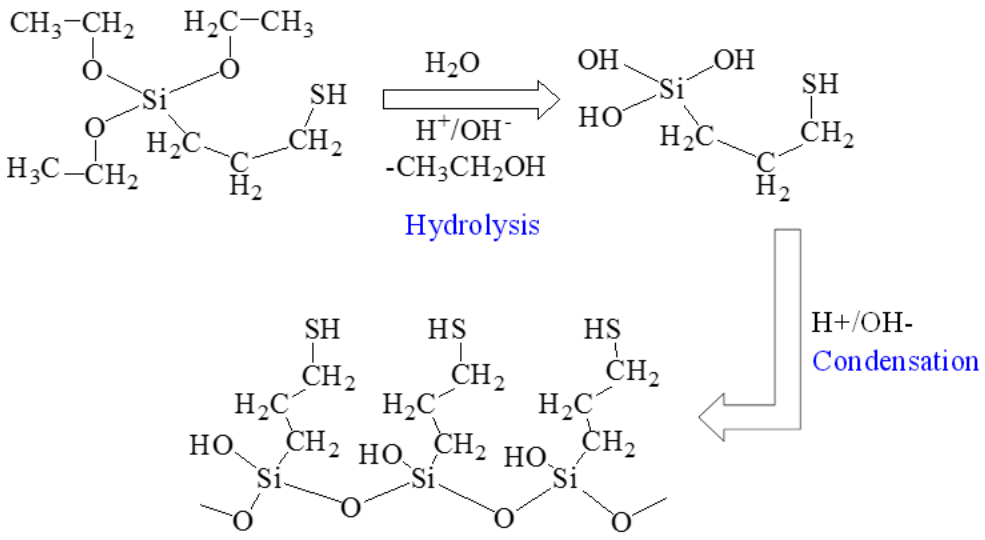

Scheme 1.4: A general scheme for the hydrolysis and condensation of the thiolsilane.

1.7 Reactivity of thiolsilane

Similar to aminosilanes, a thiolsilane can be used to modify a base-layer coated substrate or an amine-modified surface. Thiolsilane is an organoalkoxysilane having a slightly acidic thiol functional group either covalently bonded to the silicon atom or linked to silicon atom by another organic groups. Unlike aminosilanes that have a lone pair of electrons and can function as Lewis base catalyst for catalyzing the hydrolysis and condensation reaction, the thiol functional groups in the thiolsilanes do not. Thus, thiolsilanes are less reactive towards hydrolysis and condensation as compared to aminosilanes. To enhance hydrolysis and condensation, a small amount of acid or base is necessary. Similar to the aminosilanes, the hydrolysis and condensation of the thiolsilanes are highly influenced by the size and the reactivity of the attached groups (acid or basic). A general scheme for the hydrolysis and condensation of the thiolsilane is depicted in **Scheme 1.4**.

The mercapto/thiol group is known to bond with many metals, including gold, silver, copper, and lead due to underlying soft acid-base interaction between the thiol and metal. In addition, mercaptoalkoxysilane is wildly used as a molecular linker between metal and silica.[99] A general formula for the thiolsilanes used in this work is

SH-R-Si-(OR')$_3$ or 3-mercaptoalkyltrialkoxysilane

where *R* is a propyl in MPTEOS/ MPTMOS and *R'* can be either a ethoxy or methoxy group. It contains a slightly acidic thiol group (-SH) connected to the Si atom through an alkyl group (R). The widely explored mercaptoalkoxysilanes are 3-mercaptopropyltrimethoxysilane (MPTMOS) and 3-mercaptopropyltriethoxysilane (MPTEOS). In most studies, the interaction of the surface thiol and metal are exploited. The behavior of thiolsilanes on metal surface and their organization structure are influenced by following forces:

(i) Interactions between thiols head groups and Au lattice;

(ii) Interactions between alkyl chains having dispersion character; and

(iii) Interactions between end groups of thiols.

The final molecular organization and topography of thiol-bound metal are the result of the balance between these three forces.[52] When the two systems e.g., alkanethiol on Au (111) versus MPTMOS on Au(111) is compared, it is clear that interactions mentioned above are not the same in both cases.[100] Although it can be assumed that interactions between thiol head group and gold surface are the same in both cases, the remaining two interactions are different. The main difference is that MPTMOS has a bigger end-group and a shorter hydrocarbon chain. Therefore, a weak interaction between hydrocarbon chains in MPTMOS exists and is additionally screened by a large end group. Scanning tunneling microscopic (**STM**) images indicate that the main factor that governs the final structure of MPTMOS on gold is the presence of end groups. [100]

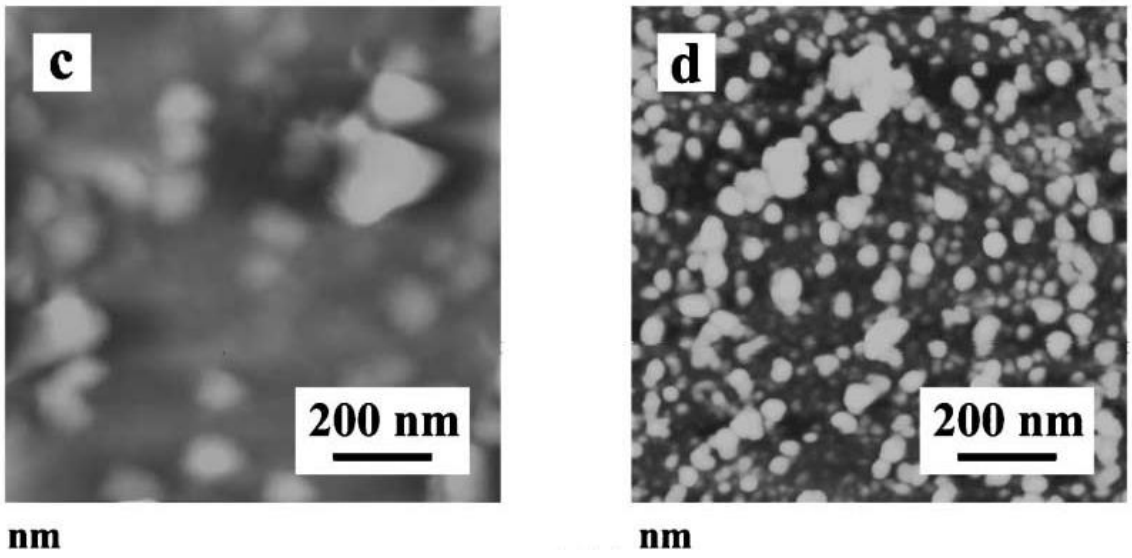

Figure 1.10: AFM micrograph of SiO_2 after treatment with MPTMOS. MPTMOS layers formed dispersed domain ranging in size from 20-200 nm (Reprinted from ref. 101 with the kind permission).[101]

The surface structure and morphology of the self-assembled 3-mercaptopropyltrimethoxysilane (MPTMOS, $(CH_3O)_3SiCH_2CH_2CH_2SH$) layers on hydroxyl-terminated silicon oxide (SiO_2) were characterized by **XPS** spectroscopy, contact angle measurements, **SEM**, and **AFM** microscopy[101]. The authors found that the MPTMOS layers on SiO_2 consisted of dispersed domains 20-200 nm in diameter flat monolayers via **AFM**, as shown in the **Figure 1.10**. They concluded that with increasing MPTMOS concentration, the domain shape changed from flat to steep. The effect of the hydrolysis of the MPTMOS SAM on the morphological change on a Au surface was investigated by **STM** and secondary ion mass spectrometry (**SIMS**) by Grobelny and coworkers. They found that the hydrolysis and condensation processes of MPTMOS end-groups on the Au surface leads to the creation of a 2D silica-like network, called a glass monolayer. MPTEOS, in particular, has been widely studied for biomolecule adhesion due to its affinity towards biological molecules.[102-103]

1.8 Methods of preparation

1.8.1. Controlled-rate infusion (*CRI*)

In the present study, a sol-gel based immersion method that we call ***CRI***[40] was used to create the surface chemical gradients. The gradients are prepared by a simple time-based method and largely dominated by the reactivity of the organoalkoxysilanes. This approach takes advantage of the versatility provided by silane chemistry and, most importantly, affords explicit control over the gradient profile (i.e., the local steepness of the gradient surface).[40]

The process begins with the deposition of a universal base layer incorporating reactive silanol groups on the substrate (e.g., glass slide, electrode, silicon wafer, etc.). Gradients are then prepared by time-dependent exposure of the base layer to a reactive organoalkoxysilane as

depicted in **Figure 1.11.** In ***CRI***, a reactive silane solution is slowly infused using a syringe pump into a vial containing the substrate[77,104] As a result, the bottom of the substrate gets more time to react with the silane solution whereas the top gets the minimum time to react with the solution thereby creating a gradient from the bottom to the top. For substrates other than planar surfaces (such as for capillary tubes), the infusion procedure is modified accordingly.[73] For example, Kannan *at el.*[73] prepared charged amine gradient inside a capillary column by connecting the syringe tip with the hydroxylated silica capillary column. The infusion of the aminosilane solution into the column created a gradient of amine functional group from one to the other end resulting from the chemical bonding between the aminoalkoxysilane on the hydroxylated silica surface.

CRI provides flexibility for controlling the steepness (shallow or deep) of the gradients by simply varying the infusion rates and/or the concentration of the silane. A shallow gradient forms when using faster infusion rates and a steeper gradient is formed at relatively slower rates (**Figure**

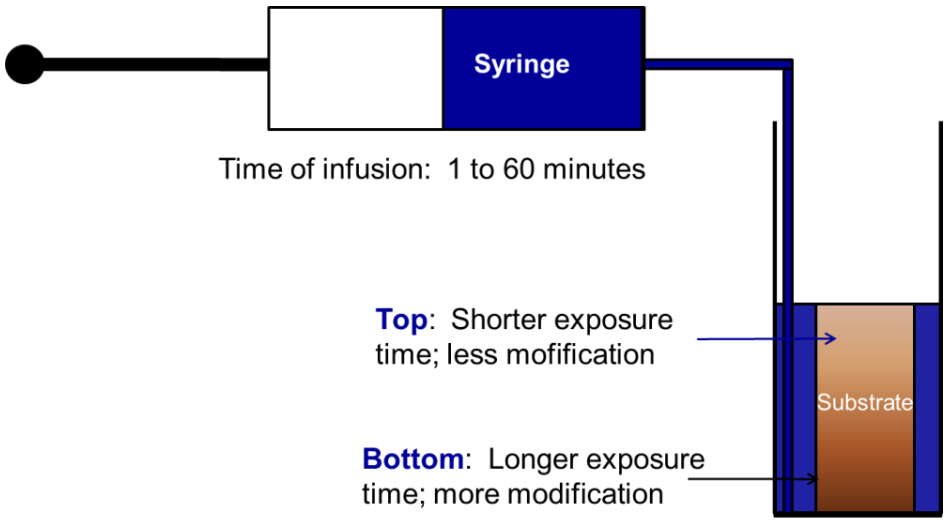

Figure 1.11: Schematic of Controlled-Rate Infusion (***CRI***). (Reprinted from Ref 40 with permission from American Chemical Society, Copyright 2011).[40]

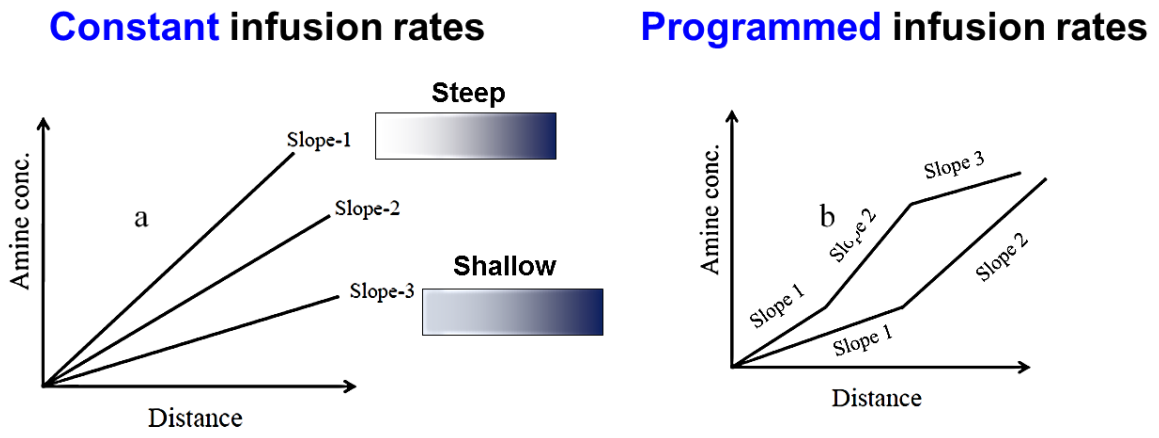

Figure 1.12: Plot represents the effect of infusion rate on steepness of the gradient in ***CRI***: a) Gradients prepared with different infusion rates; b) Programmed gradients where infusion rates are programmed within the gradient formation. (Reprinted from Ref 40 with permission from American Chemical Society, Copyright 2011).[40]

1.12(a)). By changing the infusion rate at different position along the length of the substrate, the steepness within a gradient can also be varied (**Figure 1.12(b)**). This is one of the two most important attributes of the ***CRI*** method. The other attribute of the ***CRI*** method is its ability to tailor the surface hydrophobicity. This method is used for preparing polarity gradients on any arbitrary flat substrate by using reactive silane sol(s) with appropriate polar group and controlling the infusion rate. Multi-component chemical gradients can be formed using ***CRI*** with a high degree of control by simply changing the gradient constituting sols in the syringe and repeating the infusion process. ***CRI*** also allows for making chemical gradients in multiple directions, for example 1D and 2D single and dual gradients. In a dual gradient, the individual gradients can align or oppose each other leading to surfaces with very different chemistry. The key criterion for the ***CRI*** to work successfully for the gradient formation is to match the reactivity of the silane with the timescale of the infusion.

1.8.2 Substrate for gradient preparation

In our work, gradients of aminosilane or thiolsilane SAMs were prepared on the base-layer modified substrates. Typically, silicon wafers and glass cover slips serve as the substrates. These substrates are prepared in a two-step process. First, the substrate is sonicated in ethanol, then piranha solution (H_2SO_4:H_2O_2::50:50 v/v; (CAUTION: Piranha solutions are extremely dangerous and react violently with organic materials) and then finally rinsed with copious amount of water. The cleaned surface is then spin coated with a previously hydrolyzed sol to form a thin film.[77,104] This film is termed 'base-layer' since it forms the base for further gradient formation. This base layer helps ensure there is a uniform surface containing reactive silanol groups for further chemical modification regardless of the nature of the underlying substrate. The presence of a base layer also ensures consistency when the gradient is formed on different substrates like glass coverslips, silicon wafers, gold slides, etc.

In this work, the base-layer films were made from sols prepared by hydrolyzing tetraethoxysilane (TEOS) or tetramethoxysilane (TMOS) and by hydrolyzing and co-condensing TEOS with dimethyldimethoxysilane (DMDMOS), phenyltriemthoxysilane (PTMOS) or

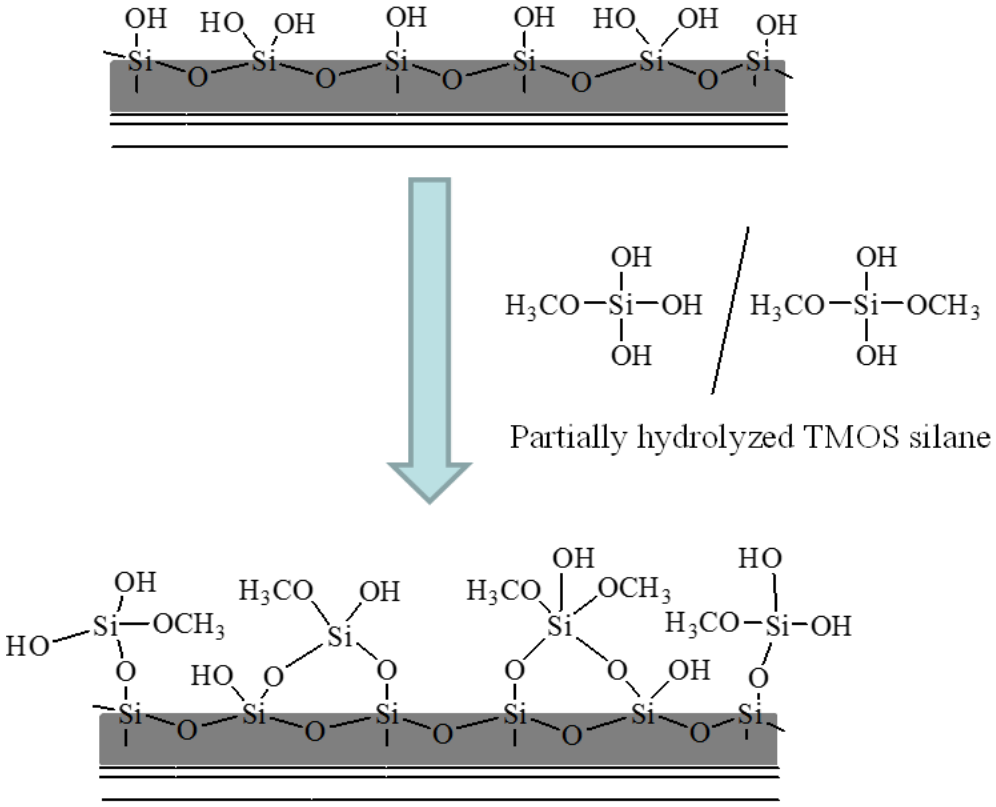

Figure 1.13: Base-layer formation by spin coating of TMOS sol on a substrate.

octyltriethoxysilane (C8) for gradient preparation and works on the principle of kinetically controlled Si-O-Si bond formation on surfaces. So, the main criterion for the substrate in the ***CRI*** method is the presence of reactive silanol groups which react with the silane precursors present in solution to make the siloxane networks. Base-layer formation is depicted in **Figure 1.13 and 1.14**.

The base-layer also serves as an additional tool to manipulate the surface properties of a substrate via the appropriate selection of an organalkoxysilanes that can be mixed with either TEOS or TMOS. For example, an amine gradient on a base-layer containing negatively charged sulfonate groups can provide a means to prepare charge density gradients from both the ends. A charge NH_3^+ gradient prepared on a bulky octyl base layer can have surface hydrophobicity entirely different from the $-NH_3^+$ gradient prepared on TMOS base layer as shown on **Chapter** 4. The effect of base layer prepared from different organalkoxysilanes on the various properties of the charged gradients are explained in that chapter.

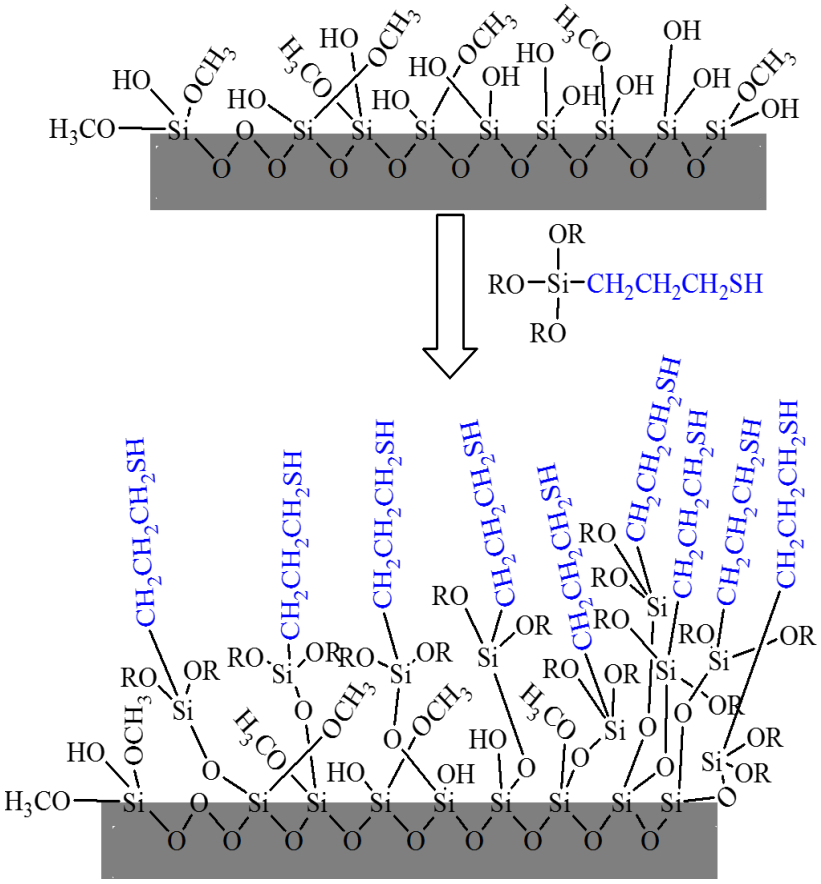

Figure 1.14: Thiol gradient formation by controlled-rate infusion from TMOS base-layer (For clarity, only terminal groups are shown).

1.13 Scope of research

Multicomponent charged gradients have found enormous application in biomaterials adsorption, chemical separation, chemical sensing, and directing transport of molecules, biomaterials, and even large objects such as water droplets, and as substrate for directing cellular differentiation.[102,103] Multicomponent charged materials are characteristically more complex than single-component charged materials due to the occurrence of simultaneous interactions between the various species at the molecular level. The cationic and anionic charge species in the multi-component charge gradients can function as a zwitterion thereby allowing these gradients to have a direct impact on the adsorption and surface confinement of biomolecules. For example, the positively charged lysozyme adsorbed preferentially on the negatively charged side and the negatively charged pepsin on the positively charged ammonium side on a $-COO^-$ and $-NH_3^+$ dual charge gradient.[76] Research work is being undertaken to develop new methods for preparing multicomponent charged gradients on the sub-micrometer scale, which are of interest for many of the above mentioned applications.[75] The successful applications of these multicomponent gradients depend on their chemical properties and the placement of the individual component species along the length of the gradients. Proper choice of the base substrate whether it's porous or solid, smooth or rough and its chemical characteristics plays a vital role in determining surface physical and chemical properties.

Cooperative interactions among different chemical (acid and base) species will also depend on the proximity of the individual charged species to each other and will thus depend on how the gradients are prepared, aligned versus opposed or cation first and then anion deposition and vice versa. For example, a multi-component charge gradient prepared by first modifying a base-layer coated slide with one functional group and subsequently with another may show entirely different

surface properties as compared to when the gradient is made by reversing the modification sequence. Thus, it is necessary to have sound fundamental insight into the macroscopic and microscopic properties of the charged materials, which can be evaluated by **XPS**, surface contact angle measurements, and by measuring net local surface charge at various points along the substrate. To obtain this insight, we need to investigate the molecular level properties of the different gradients prepared on different types of substrates e.g, silica, gold or slide glass and different types of base layers. In addition, we need to devise newer approaches to modify the base layers with desired functional groups in a gradient fashion and devise newer methods to convert the chemical gradient into a charge gradient without destroying the base layers.

The purpose of this dissertation work is to explore some of the fundamental properties originating from the interactions of different species (organic group, charge and polar groups) present in the gradients, their alignment (aligned or opposed to each other), and on different base-layer coated substrates with varying hydrophobicity. **Chapter 4** discusses the cooperative interactions between cationic (acidic), anionic (basic) and polar functionalities on the surface dual/multi-component charge gradients where the acidic (cationic) and basic (anionic) species are either aligned or opposed to each other along the length of the gradient. The effect of this alignment of the charged species on the cooperative interaction and other properties (surface wettability, surface roughness) were also studied by changing their relative concentration of the functionalities on the surface and by changing the base layer chemistry. The effect of various base layers having different hydrophobicity on the wettability of charge gradients was analyzed by the **WCA** measurements (**Chapter 5**). The catalytic effect of one functional group on the extent of the modification of the other functional groups at different positions along the gradients is also discussed in a separate chapter. Therefore obtaining quantitative information on the resulting

properties due to cooperative interactions taking place among different species on the gradient surface is a key attribute of this work. Sol-gel derived silica gradients represent an efficient means to understand these fundamental phenomena because a continuous library of samples can be produced and characterized along a single material. Such fundamental information is of importance to a broad range of biologically- and technologically-relevant systems. For example, the performance of bifunctional catalysts and molecularly imprinted materials strongly depend on cooperative interactions between neighboring functional groups and the target molecule (e.g., hydrogen bonding to a silanol site in close proximity to a basic amine group).[75,105] In adsorption chromatography, the strength of intermolecular interactions influences retention and ultimately the separation of complex, multi-component mixtures.[105] Micro/nanoscale interactions taking place between a material and a cell strongly affect its adhesion, motility, and proliferation.[106] This research will also help advance the development of sol-gel methods for the preparation of silica gradients and will yield a broader range of materials with possible applications in the transport of cells on a surface and the emerging method of stationary-phase-gradient chromatography.

1.14 References:

1. Genzer, J., Surface-Bound Gradients for Studies of Soft Materials Behavior. In *Annual Review of Materials Research, Vol 42*, Clarke, D. R., Ed. Annual Reviews: Palo Alto, **2012**; Vol. 42, 435-468.
2. Genzer, J.; Bhat, R. R., Surface-bound soft matter gradients. *Langmuir* **2008,** *24* (6), 2294-2317.
3. Kunzler, T. P.; Drobek, T.; Schuler, M.; Spencer, N. D., Systematic study of osteoblast and fibroblast response to roughness by means of surface-morphology gradients. *Biomaterials* **2007,** *28* (13), 2175-2182.
4. Kunzler, T. P.; Huwiler, C.; Drobek, T.; Voros, J.; Spencer, N. D., Systematic study of osteoblast response to nanotopography by means of nanoparticle-density gradients. *Biomaterials* **2007,** *28* (33), 5000-5006.
5. Pelham, R. J.; Wang, Y. L., Cell locomotion and focal adhesions are regulated by substrate flexibility (vol 94, 13661, 1997). *Proc. Natl. Acad. Sci. U.S.A.* **1998,** *95* (20), 12070-12070.
6. Morgenthaler, S.; Zink, C.; Spencer, N. D., Surface-chemical and -morphological gradients. *Soft Matter.,* **2008,** *4* (3), 419-434.
7. Bard, A. J.; Faulkner, L. R. Electrochemical Methods: Fundamentals and Applications; John Wiley & Sons, Inc.: New York, 2001.
8. Kannan, B.; Higgins, D. A.; Collinson, M. M., Chelation Gradients for the Investigation of Metal Ion Binding at Silica Surfaces", *Langmuir*, **2014**, *30*, 10019-10027.
9. Giri, D.; Hanks, C. N.; Collinson, M. M.; Higgins, D. A. Single Molecule Spectroscopic Imaging Studies of Polarity Gradients Prepared by Infusion-Withdrawal Dip-Coating, *J. Phys. Chem. C,* **2014**, *118*, 6423-6432.

10. Chaudhury, M. K.; Whitesides, G. M., How to make water run uphill. *Science* **1992,** *256* (5063), 1539-1541.

11. Petrie, R. J.; Bailey, T.; Gorman, C. B.; Genzer, J., Fast directed motion of "Fakir" droplets. *Langmuir,* **2004,** *20* (23), 9893-9896.

12. Moumen, N.; Subramanian, R. S.; McLaughlin, J. B., Experiments on the motion of drops on a horizontal solid surface due to a wettability gradient. *Langmuir,* **2006,** *22* (6), 2682-2690.

13. Shastry, A.; Case, M. J.; Bohringer, K. F., Directing droplets using microstructured surfaces. *Langmuir,* **2006,** *22* (14), 6161-6167.

14. Lai, Y. H.; Yang, J. T.; Shieh, D. B., A microchip fabricated with a vapor-diffusion self-assembled monolayer method to transport droplets across super hydrophobic to hydrophilic surfaces. *Lab on a Chip,* **2010,** *10* (4), 499-504.

15. Seidi, A.; Ramalingam, M.; Elloumi-Hannachi, I.; Ostrovidov, S.; Khademhosseini, A., Gradient biomaterials for soft-to-hard interface tissue engineering. *Acta Biomaterialia,* **2011,** *7* (4), 1441-1451.

16. Venkataraman, N. V.; Zurcher, S.; Spencer, N. D., Order and composition of methyl-carboxyl and methyl-hydroxyl surface-chemical gradients. *Langmuir,* **2006,** *22* (9), 4184-4189.

17. Stegall, S. L.; Ashraf, K. M.; Moye, J. R.; Daniel A. Higgins, D. A.; Collinson, M. M., "Separation of Transition and Heavy Metals Using Stationary Phase Gradients and Thin Layer Chromatography". *J. Chromatog. A,* **2016**, *1446*, 141-148.

18. Dewoolkar, V. C.; Kannan, B.; Ashraf, K. M.; Higgins, D. A.; Collinson, M. M., "Amine-Phenyl Multi-Component Gradient Stationary Phases". *J. Chromatog. A*, **2015**, *1410*, 190-199.

19. Kannan, B.; Marin, M. A.; Shrestha, K.; Higgins, D. A.; Collinson, M. M., Continuous stationary phase gradients for planar chromatographic media. *J. of Chromatog A,* **2011,** *1218* (52), 9406-9413.

20. Welin-Klintstrom, S.; Lestelius, M.; Liedberg, B.; Tengvall, P., Comparison between wettability gradients made on gold and on Si/SiO2 substrates. *Colloids and Surf. B-Biointerfaces*, **1999,** *15* (1), 81-87.

21. Gunawan, R. C.; Silvestre, J.; Gaskins, H. R.; Kenis, P. J. A.; Leckband, D. E., Cell migration and polarity on microfabricated gradients of extracellular matrix proteins. *Langmuir,* **2006,** *22* (9), 4250-4258.

22. Larsson, A.; Liedberg, B., Poly(ethylene glycol) gradient for biochip development. *Langmuir,* **2007,** *23* (22), 11319-11325.

23. Park, S. H.; Krull, U., A spatially resolved nucleic acid biochip based on a gradient of density of immobilized probe oligonucleotide. *Analytica Chimica Acta,* **2006,** *564* (2), 133-140.

24. Ruardy, T. G.; Schakenraad, J. M.; vanderMei, H. C.; Busscher, H. J., Preparation and characterization of chemical gradient surfaces and their application for the study of cellular interaction phenomena. *Surf. Sci. Reports,* **1997,** *29* (1), 3-30.

25. Elwing, H.; Askendal, A.; Lundstrom, I., Desorption of fibrinogen and gamma-globulin from solid surfaces induced by a nonionic detergent. *J. Colloid Interface Sci.,* **1989,** *128* (1), 296-300.

26. Elwing, H.; Welin, S.; Askendahl, A.; Lundstrom, I., Adsorption of fibrinogen as a measure of the distribution of methyl-groups on silicon surfaces. *J. Colloid Interface Sci.,* **1988,** *123* (1), 306-308.

27. Elwing, H.; Welin, S.; Askendal, A.; Nilsson, U.; Lundstrom, I., A wettability gradient-method for studies of macromolecular interactions at the liquid solid interface. *J. Colloid Interface Sci.,* **1987,** *119* (1), 203-210.

28. Hlady, V.; Ho, C. H., Human low density lipoprotein (LDL) and human serum albumin (HSA) co-adsorption onto the C18-silica gradient surface. *Materialwissenschaft Und Werkstofftechnik* **2001,** *32* (2), 185-192.

29. Genzer, J.; Fischer, D. A.; Efimenko, K., Fabricating two-dimensional molecular gradients via asymmetric deformation of uniformly-coated elastomer sheets. *Adv. Mater.,* **2003,** *15* (18), 1545.

30. Choi, S. H.; Newby, B. M. Z. Micrometer-Scaled Gradient Surfaces Generated Using Contact Printing of Octadecyltrichlorosilane. *Langmuir*, **2003**, *19*, 7427–7435.

31. Loos, K.; Kennedy, S. B.; Eidelman, N.; Tai,; Zharnikov, M.; Amis, E. J.; Ulman, A.; Gross, R. A. *Langmuir*, **2005**, *21*, 5237–5241.

32. S. V. Roberson, A. J. Fahey, A. Sehgal and A. Karim, Multifunctional ToF-SIMS: combinatorial mapping of gradient energy substrates. *J. Appl. Surf. Sci*., **2002**, *200*, 150–164.

33. Kennedy, S. B.; Washburn, N. R.; Simon, C. G.; Amis, J. Combinatorial screen of the effect of surface energy on fibronectin-mediated osteoblast adhesion, spreading and proliferation *Biomaterials*, **2006**, *27*, 3817–3824.

34. Gallant, N. D.; Lavery, K. A.; Amis, E. J.; Becker, M. L. Universal Gradient Substrates for "Click" Biofunctionalization. *Adv. Mater.,* **2007**, *19*, 965–969.

35. Ito, Y.; Heydari, M.; Hashimoto, A.; Konno, T.; Hirasawa, A.; Hori, S.; Kurita, K.; Nakajima, A. The Movement of a Water Droplet on a Gradient Surface Prepared by Photodegradation. *Langmuir*, **2007**, *23*, 1845–1850.

36. Han, J. T.; Kim, S.; Karim, A. UVO-Tunable Superhydrophobic to Superhydrophilic Wetting Transition on Biomimetic Nanostructured Surfaces. *Langmuir*, **2007**, *23*, 2608–2614.

37. Giri, D.; Li, Z.; Ashraf, K. M.; Collinson M. M.; Higgins, D. A. "Molecular Combing of lambda-DNA using Self-Propelled Water Droplets on Wettability Gradient Surfaces". *ACS Appl. Mater. Interfaces*, **2016**, *8*, 24265-24272.

38. Ye, F. M.; Cui, C. C.; Kirkeminde, A.; Dong, D.; Collinson, M. M.; Higgins, D. A., Fluorescence Spectroscopy Studies of Silica Film Polarity Gradients Prepared by Infusion-Withdrawal Dip-Coating. *Chem. Mater.* **2010,** *22* (9), 2970-2977.

39. Cui, C. C.; Kirkeminde, A.; Kannan, B.; Collinson, M. M.; Higgins, D. A., Spatiotemporal Evolution of Fixed and Mobile Dopant Populations in Silica Thin-Film Gradients as Revealed by Single Molecule Tracking. *J. Phys. Chem. C* **2011,** *115* (3), 728-735.

40. Kannan, B.; Dong, D.; Higgins, D. A.; Collinson, M. M., Profile Control in Surface Amine Gradients Prepared by Controlled-Rate Infusion. *Langmuir* **2011**, *27* (5), 1867-1873.

41. DiBenedetto, S. A.; Facchetti, A.; Ratner, M. A.; Marks, T. J., Molecular Self-Assembled Monolayers and Multilayers for Organic and Unconventional Inorganic Thin-Film Transistor Applications. *Adv. Mater,* **2009,** *21* (14-15), 1407-1433.

42. Liedberg, B.; Tengvall, P. Molecular Gradients of omega-Substituted Alkanethiols on Gold: Preparation and Characterization. *Langmuir*, **1995**, *11*, 3821–3827.

43. Liedberg, B.; Wirde, M.; Tao, Y. T.; Tengvall, P.; Gelius, U., Molecular gradients of omega substituted alkanethiols on gold studied by X-ray photoelectron spectroscopy. *Langmuir* **1997,** *13* (20), 5329-5334.

44. Beurer, E.; Venkataraman, N. V.; Sommer, M.; Spencer, N. D., Protein and Nanoparticle Adsorption on Orthogonal, Charge-Density-Versus-Net-Charge Surface-Chemical Gradients. *Langmuir* **2012**, *28*, 3159−3166.

45. Beurer, E.; Venkataraman, N. V.; Rossi, A.; Bachmann, F.; Engeli, R.; Spencer, N. D., Orthogonal, Three-Component, Alkanethiol-Based Surface-Chemical Gradients on Gold. *Langmuir* **2010**, *26* (11), 8392−8399.

46. Morgenthaler, S.; Lee, S. W.; Zurcher, S.; Spencer, N. D., A simple, reproducible approach to the preparation of surface-chemical gradients. *Langmuir* **2003**, *19* (25), 10459-10462.

47. Morgenthaler, S. M.; Lee, S.; Spencer, N. D., Submicrometer structure of surface-chemical gradients prepared by a two-step immersion method. *Langmuir*, **2006**, *22* (6), 2706-2711.

48. Kraus, T.; Stutz, R.; Balmer, T. E.; Schmid, H.; Malaquin, L.; Spencer, N. D.; Wolf, H. Printing chemical gradients. *Langmuir*, **2005**, *21* (17), 7796–7804.

49. Pardo, L.; Wilson W. C.; Boland, T. J. Characterization of Patterned Self-Assembled Monolayers and Protein Arrays Generated by the Ink-Jet Method. *Langmuir*, **2003**, *19*, 1462–1466.

50. Sankhe, A. Y.; Booth, B. D.; Wiker, N. J.; Kilbey, S. M. Inkjet-printed monolayers as platforms for tethered polymers. *Langmuir*, **2005**, *21* (12), 5332–5336.

51. Terrill, R. H.; Balss, K. M.; Zhang, Y. M.; Bohn, P. W., Dynamic monolayer gradients: Active spatiotemporal control of alkanethiol coatings on thin gold films. *J. Am. Chem. Soc.*, **2000**, *122* (5), 988-989.

52. Plummer, S. T.; Bohn, P. W., Spatial dispersion in electrochemically generated surface composition gradients visualized with covalently bound fluorescent nanospheres. *Langmuir*, **2002**, *18* (10), 4142-4149.

53. Balss, K. M.; Kuo, T. C.; Bohn, P. W. Direct Chemical Mapping of Electrochemically Generated Spatial Composition Gradients on Thin Gold Films with Surface-Enhanced Raman Spectroscopy. *J. Phys. Chem.* B **2003**, *107* (4), 994−1000.

54. Wang, Q.; Jakubowski, J. A.; Sweedler, J. V.; Bohn, P. W., Quantitative submonolayer spatial mapping of Arg-Gly-Asp-containing peptide organomercaptan gradients on gold with matrix-assisted laser desorption/ionization mass spectrometry. *Anal. Chem.*, **2004**, 76 (1), 1-8.

55. Balss, K. M.; Fried, G. A.; Bohn, P. W. Chemically Selective Force Mapping of Electrochemically Generated Two-Component ω-Substituted Alkanethiol Monolayer Gradients by Pulsed-Force-Mode Atomic Force Microscopy, *J. Electrochem. Soc.*, **2002**, *149*, C450–455.

56. Fuierer, R. R.; Carroll, R. L.; Feldheim, D. L.; Gorman, C. B. Patterning Mesoscale Gradient Structures with Self-Assembled Monolayers and Scanning Tunneling Microscopy Based Replacement Lithography, *Adv. Mater*., **2002**, 14, 154–157.

57. Klauser, R.; Chen, C. H.; Huang, M. L.; Wang, S. C.; Chuang, T. J.; Zharnikov, M., Patterning and imaging of self-assembled monolayers with a focused soft X-ray beam. *J. Electron. Spectrosc. Relat. Phenom.*, **2005**, *144*, 393-396.

58. Uedayukoshi, T.; Matsuda, T., Cellular-responses on a wettability gradient surface with continuous variations in surface compositions of carbonate and hydroxyl-groups. *Langmuir*, **1995**, *11*(10), 4135-4140.

59. Lee, J. H.; Kim, H. G.; Khang, G. S.; Lee, H. B.; Jhon, M. S., Characterization of wettability gradient surfaces prepared by corona discharge treatment. *J. Colloid Interface Sci.*, **1992**, *151* (2), 563-570.

60. Pitt, W. G., Fabrication of a continuous wettability gradient by radio-frequency plasma discharge. *J. Colloid Interface Sci.*, **1989**, *133* (1), 223-227.

61. Fioravanti, G.; Lugli, F.; Gentili, D.; Mucciante, V.; Leonardi, F.; Pasquali, L.; Liscio, A.; Murgia, M.; Zerbetto, F.; Cavallini. M. Electrochemical Fabrication of Surface Chemical Gradients in Thiol Self-Assembled Monolayers with Tailored Work-Functions. *Langmuir*, **2014**, *30*, 11591−11598.

62. Plummer, S. T.; Wang, Q.; Bohn, P. W.; Stockton, R.; Schwartz, M. A., Electrochemically derived gradients of the extracellular matrix protein fibronectin on gold. *Langmuir*, **2003,** *19* (18), 7528-7536.

63. Smith, J. T.; Tomfohr, J. K.; Wells, M. C.; Beebe, T. P.; Kepler, T. B.; Reichert, W. M., Measurement of cell migration on surface-bound fibronectin gradients. *Langmuir*, **2004,** *20* (19), 8279-8286.

64. Adamczyk, Z. Particle adsorption and deposition: Role of electrostatic interactions. *Adv. Colloid Interface Sci*., **2003**, *100−102*, 267−347.

65. Becker, A. L.; Henzler, K.; Welsch, N.; Ballauff, M.; Borisov, O. Proteins and polyelectrolytes: A charged relationship. *Curr. Opin. Colloid Interface Sci*. **2012**, *17*, 90−96.

66. Borges, J.; Mano, J. F. Molecular Interactions Driving the Layer-by-Layer Assembly of Multilayers. *Chem. Rev.*, **2014**, *114*, 8883−8942.

67. Boroudjerdi, H.; Kim, Y. W.; Naji, a.; Netz, R. R.; Schlagberger, X.; Serr, a. Statics and dynamics of strongly charged soft matter. *Phys. Rep*., **2005**, *416*, 129−199.

68. Chen, Z.; Kang, L.; Wang, Z.; Xu, F.; Gu, G.; Cui, F.; Guo, Z. Recent progress in the research of biomaterials regulating cell behavior. *RSC Adv.*, **2014**, *4*, 63807.

69. Lin, Y. S.; Hlady, V. The desorption of ribonuclease A from charge density gradient surfaces studied by spatially-resolved total internal reflection fluorescence. *Colloids Surf., B* **1995**, *4*, 65−75.

70. Riepl, M.; Östblom, M.; Lundström, I.; Svensson, S. C. T.; Van Der Gon, a. W. D.; Schäferling, M.; Liedberg, B. Molecular gradients: An efficient approach for optimizing the surface properties of biomaterials and biochips. *Langmuir*, **2005**, *21*, 1042−1050.

71. Mierczynska, A.; Michelmore, A.; Tripathi, A.; Goreham, R. V.; Sedev, R.; Vasilev, K. pH-tunable gradients of wettability and surface potential. *Soft Matter.*, **2012**, *8*, 8399.

72. Ionov, L.; Houbenov, N.; Sidorenko, A.; Stamm, M.; Luzinov, I.; Minko, S. Inverse and reversible switching gradient surfaces from mixed polyelectrolyte brushes. *Langmuir*, **2004**, *20*, 9916−9919.

73. Kannan, B.; Nokura, K.; Alvarez, J. C.; Higgins, D. A.; Collinson, M. M., Fabrication of Surface Charge Gradients in Open-Tubular Capillaries and Their Characterization by Spatially Resolved Pulsed Streaming Potential Measurements *Langmuir*, **2013**, *29* (49), 15260-15265.

74. Corum, L. E.; Hlady, V. Screening platelet-surface interactions using negative surface charge gradients. *Biomaterials*, **2010**, *31*, 3148−3155.

75. Koo, H. J.; Waynant, K. V.; Zhang, C.; Haasch, R. T.; Braun, P. V. General method for forming micrometer-scale lateral chemical gradients in polymer brushes. *Chem. Mater.*, **2014**, *26*, 2678−2683.

76. Shen, C. H.; Lin, J. C. Surface characterization and platelet compatibility evaluation of binary mixed self-assembled monolayers containing novel sulfonic acid terminated alkanethiol. *Colloids Surf. B,* **2010**, *79*, 156−163.

77. Ashraf, K. M.; Giri, D.; Wynne, K. J.; Higgins, D. A.; Collinson M. M. Cooperative effects in aligned and opposed multicomponent charge gradients containing strongly acidic, weakly acidic, and basic functional groups. *Langmuir*, **2016**, *32*, 3836−3847.

78. Brinker, C. J.; Scherer. G.W., *Sol-Gel Science: The Physics and Chemistry of Sol-Gel Processing*. **1990**; Vol. 1.

79. Sanchez, C.; Lebeau, B., Chaput, F.; Boilot, J. P. Optical properties of functional hybrid organic-inorganic nanocomposites, *Adv. Mater*., **2003,** *15*, 1969-1994.

80. Kurumada, K-i.; Ashraf K. M.; Matsumoto, S. Effects of heat treatment on various properties of organic–inorganic hybrid silica derived from phenyltriethoxysilane. *Mater. Chem. Phys.*, **2014**, *44*, 132-138.

81. Ashraf, K, M. The effect of temperature and catalyst on polycondensation of organic-inorganic hybrid silica derived from mono-substituted trialkoxysilanes using sol-gel method. *Doctoral thesis*, **2012**.

82. Arkles, B.; Steinmetz, J. R.; Zazyczny, J.; Mehta, P., Factors contributing to the stability of alkoxysilanes in aqueous-solution. *J. Adhesion Sci. Technol.* **1992**, *6* (1), 193-206.

83. Shimizu, I.; Yoshino, A.; Okabayashi, H.; Nishio, E.; Oconnor, C. J., Kinetics of interaction of 3-amimopropyltriethoxysilane on a silica gel surface using elemental

analysis and diffuse reflectance infrared Fourier transform spectra. *J. Chem. Soc.-Faraday Transactions* **1997**, *93* (10), 1971-1979.

84. Walcarius, A.; Collinson, M. M., Analytical Chemistry with Silica Sol-Gels: Traditional Routes to New Materials for Chemical Analysis. *Annual Review of Anal. Chem.*, **2009**; *2*, 121-143.

85. Thames, S. F.; Panjnani, K. G., Organosilane polymer chemistry: A review. *J. Inorg. Organomet. Polym.*, **1996,** *6* (2), 59-94.

86. Ronald, H.B. Itoh, M.; Sakakibara, A.; Suzuki, T. Silsesquioxanes, *Chem. Rev*., **1995**, 95, 1409-1430.

87. Loy, D.A.; Baugher, B.M.; Baugher, C.R.; Schneider, D.A.; Rahimian, K. Substituent effects on the sol-gel chemistry of organotrialkoxysilanes, *Chem. Mater.,* **2000**, *12*, 3624-3632.

88. Arkles, B.; Pan, Y. L.; Kim, Y. M., The Role of Polarity in the Structure of Silanes Employed in Surface Modification. *Silanes and Other Coupling Agents*, **2009**; 51-64.

89. Carre, A. B., W.; Lacarriere, V., Glass substrates modified with organosilanes for DNA immobilization *Silanes and Other Coupling Agents*, **2007,** *4*, 1-14.

90. Moses, P. R.; Wier, L. M.; Lennox, J. C.; Finklea, H. O.; Lenhard, J. R.; Murray, R. W. X-ray photoelectron-spectroscopy of alkylamine-silanes bound to metal-oxide electrodes. *Anal. Chem.*, **1978**, *50* (4), 576-585.

91. Pena-Alonso, R.; Rubio, F.; Rubio, J.; Oteo, J. L., Study of the hydrolysis and condensation of gamma-aminopropyltriethoxysilane by FT-IR spectroscopy. *J. Mater. Sci.*, **2007**, *42* (2), 595-603.

92. Shimizu, I.; Yoshino, A.; Okabayashi, H.; Nishio, E.; Oconnor, C. J., Kinetics of interaction of 3-amimopropyltriethoxysilane on a silica gel surface using elemental analysis and diffuse reflectance infrared Fourier transform spectra. *J. Chem Soc-Faraday Transactions* **1997**, *93* (10), 1971-1979.

93. Chiang, C. H.; Ishida, H.; Koenig, J. L., The structure of gamma-aminopropyltriethoxysilane on glass surfaces. *J. Colloid Interface Sci.*, **1980**, *74* (2), 396-404.

94. Chaudhury, M.; Pocius , A.V.; *Adhesion Sci. Eng.*. **2002**, 2.

95. Liu, Z.; Shu, D.; Lia, P.; Cheng, X. Tribology study of lanthanum-treated graphene oxide thin film on silicon substrate. *RSC Adv*., **2014**, *4*, 15937.

96. Vrancken, K. C.; Possemiers, K.; Vandervoort, P.; Vansant, E. F., Surface modification of silica-gels with amino-organosilanes. *Colloids and Surfaces a-Physicochemical and Engineering Aspects*, **1995**, *98* (3), 235-241.

97. Adachi, K.; Hirano, T., Controllable silane water-cross-linking kinetics and curability of ethylenepropylene copolymer by amine compounds. *Ind. Eng. Chem. Res.*, **2008**, *47* (6), 1812-1819.

98. Vandenberg, E. T.; Bertilsson, L.; Liedberg, B.; Uvdal, K.; Erlandsson, R.; Elwing, H.; Lundstrom, I., Structure of 3-aminopropyl triethoxysilane on silicon-oxide. *J. Colloid Interface Sci.* **1991**, *147* (1), 103-118.

99. Sainsbury, T.; Ikuno, T.; Okawa, D.; Pacile, D.; Frechet, J. M. J.; Zettl, A. Self-assembly of gold nanoparticles at the surface of amine and thiol-functionalized boron nitride nanotubes. *J. Phys. Chem. C*, **2007**, *111*, 12992−12999.

100. Piwonski, I.; Grobelnya, J.; M. Cichomskia, M. Celichowski, G.; Rogowski, J. Investigation of 3-mercaptopropyltrimethoxysilane self-assembled monolayers on Au(111) surface. *Applied Surface Science*, **2005**, *242*,147–153.

101. Lin, J.C.; Chung, W.H. Synthesis, surface characterization, and platelet reactivity evaluation for the self-assembled monolayer of alkanethiol with sulfonic acid functionality, *J. Biomed. Mater. Res.*, **2000**, *51*, 413–423.

102. M.Y. Tsai, Lin, J.C. Surface characterization and platelet adhesion studies of self-assembled monolayer with phosphonate ester and phosphonic acid functionalities, *J. Biomed. Mater. Res.*, **2001**, *55*, 554–565.

103. Ostuni, E. Yan, L. Whitesides, G.M. The interaction of proteins and cells with self-assembled monolayers of alkanethiols on gold and silver, *Colloid Surf. B*, **1999**, *15*, 3–30.

104. Kannan, B.; Higgins, D. A.; Collinson, M. M., Aminoalkoxysilane Reactivity in Surface Amine Gradients Prepared by Controlled-Rate Infusion". *Langmuir*, **2012**, *28*, 16091-16098.

105. Shen, C. H.; Lin, J. C. Surface characterization and platelet compatibility evaluation of binary mixed self-assembled monolayers containing novel sulfonic acid terminated alkanethiol. *Colloids Surf. B* **2010**, *79*, 156−163.

106. Brochier Salon, M.-C.; Bardet, M.; Belgacem, M., Solvolysis–hydrolysis of N-bearing alkoxysilanes: Reactions studied with 29Si NMR. *Silicon Chemistry*, **2008**, *3* (6), 335-350.

Chapter 2: Characterization Techniques

2.1 Introduction

Surface chemical gradients have chemical constituents that increase or decrease from one end to the other end along a substrate. A plethora of techniques are available to characterize surface chemical gradients. Some techniques involve the quantification of the chemical species on the surface and others provide physical insights about their spatial arrangements. The basic principles and experimental conditions for all the characterization techniques utilized to study charge gradients prepared in this work will be discussed in this chapter. To measure the surface coverage of nitrogen (both in the form of protonated and unprotonated amines) and sulfur in the form of thiol and sulfonate groups along on the length of the Si wafer, **XPS** spectroscopy was employed. Quantification of the net charge on the surface at various locations was performed by measuring the streaming potential followed by charge calculation using Helmholtz-Smoluchowski equation. The wettability across the surface of the gradient was evaluated by both dynamic and **SCA** measurements. **DCA** experiments are especially important since they provide information regarding the interaction of the surface with Millipore water at almost every point along the surfaces of both the gradients and control samples. The binding of gold nanoparticles to the as-synthesized gradients and the surface roughness of the gradients and control samples were performed by **TM-AFM** microscopy.

2.2 XPS spectroscopy

Surface elemental composition and the chemical and electronic state of elements on the top 5-10 nm of the surface have been characterized by the **XPS** spectroscopic technique. X-rays are emitted usually from an Mg or Al anode. When a surface is irradiated by X-rays of sufficient

energy, electrons are removed from the surface atoms by the high energy X-rays. This is a process known as the photoelectric effect. In **Figure 2.1**, a schematic of an electron being removed from the carbon 1s orbital by an X-ray photon is depicted. In **XPS**, an X-ray ejects an electron and the kinetic energy of the ejected electron is measured. The kinetic energy of the removed electron depends on the binding energy (BE) of the electron, the energy of the X-ray irradiation beam ($h\nu$) and the work function (ϕ) of the instrument.[106] Thus, the binding energy of the electron can be calculated using the equation below (equation 2.1).[1]

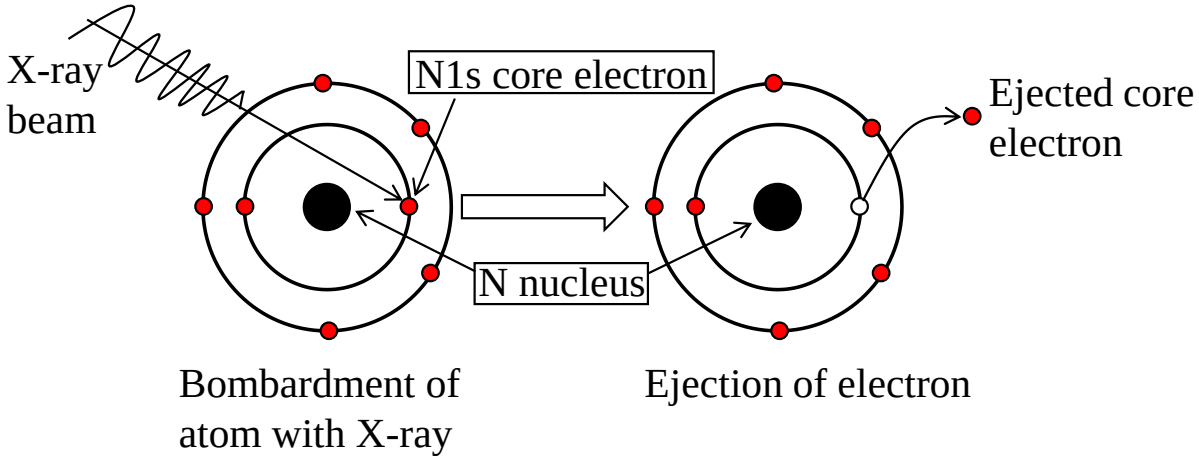

Figure 2.1: Removal of a nitrogen 1s electron by photoelectric effect.

The binding energies of the electrons are characteristic of the elements and their orbitals. Thus, by comparing the measured binding energy with reference values, the various chemical components present on a surface can be identified from the spectra. The peak intensity (I_A) of each signal is proportional to the amount of that particular species present on the surface (N_A). This proportionality depends on various factors such as ionization cross-section (sensitivity factor σ_A), transmission function (T_A) of the instrument, the inelastic mean free path (λ_A) and the sine of the take-off angle (θ).[1, 2]

$$N_A = \frac{I_A}{(\sigma_A T_A \lambda_A \sin\theta)} \qquad (2.1)$$

The sensitivity factor and mean free path are characteristic of each element. These are necessary for quantifying atomic ratios for different elements provided the spectrum is acquired with high-resolution. The binding energy of the electrons varies slightly depending on the chemical environment of an atom. This results in a characteristic shift of the **XPS** signal which provides valuable information about the surface composition, chemical bonds, substitutions, chemical state, etc.[3] The **XPS** analysis is performed under ultra-high vacuum to avoid collision of the emitted electrons with the gaseous atoms and to reduce contamination of the surface from the atmosphere. A general representation of an **XPS** instrument consisting of an X-ray source, an analyzer where the electrons are separated based on their kinetic energy, and a detector is shown in **Figure 2.2**. The source of X-ray beam is an Al Kα or a Mg Kα emission having narrow bandwidths leading to well resolved **XPS** signals[1] Sometimes a monochromator such as quartz crystal is used to narrow the line-width before it is focused on the sample. The emitted electrons are focused by the lens set-up before they reach the analyzer, where the electrons are separated based on their kinetic energy. The detector detects an electron at a particular binding energy and results in a plot of intensity versus binding energy. The **XPS** instrument measurements can go as far as 10 nm deep by varying the angle between the sample and analyzer (the take-off angle).[2, 3] Although **XPS** requires the ultra-high vacuum and the long acquisition times, it has a great advantage of providing a wide range of information regarding the surface composition of materials. Almost all the elements can be detected quantitatively.[4, 5]

Samples were usually placed on top of a piece of conducting tape on a 5 x 2 cm sample holder. **XPS** spectra were acquired in regular fashion (typically every 1-2 mm) across the wafer

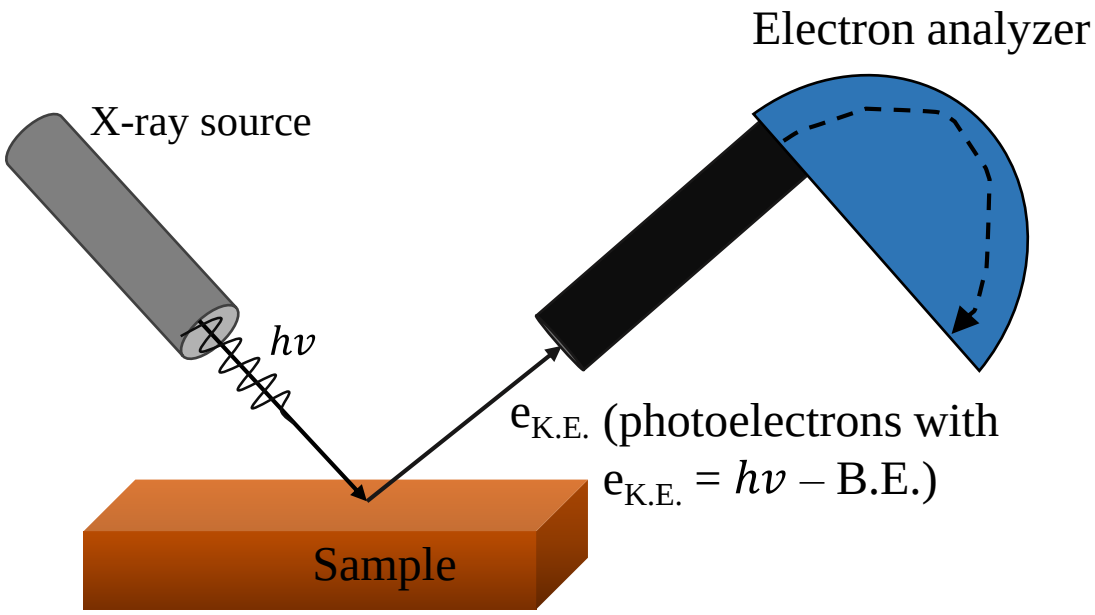

Figure 2.2: Schematic sketch of an X-ray Photoelectron Spectrometer.

starting about ~ 2 mm from the edge. Spectra were calibrated by taking the C1s peak as occurring at 284.6 eV. The X-ray photoelectron spectra in this work were acquired with a ThermoFisher ESCAlab 250 equipped with a radian lens, a concentric hemi-spherical analyzer and a two-dimensional channel-plate detector. A monochromatic Al Kα source with a spot size of 500 μm was used. The instrument was operated with 50 eV pass energy and 0.1 eV step size. Data analyses were carried out by the Thermo Avantage program (Version 4.33) and CASA software. 'Smart' background correction was used for the integration of all peaks. This is the type of background correction is preferred by the Avantage software itself. It gives an 'S-shaped' background similar to Shirley background but it will adjust the background positions so that they will not go above the data-curve. This research focused the quantitative determination of the area under the peaks of

N or S or both in the protonated and unprotonated amine and oxidized and non-oxidized thiol respectively across the surface of the samples.

2.2.1 Area normalization and peak fit

A. N 1s peak fit

The area under N 1s peak of the protonated and free amine groups was determined by deducing their ratio by curve fitting. The fitting was performed by using Avantage and CASA software where N1s spectrum was loaded and the area under the peak from ~ 396-404 eV was amended with 'smart background' correction. It was then curve-fit using Gaussian-Lorentzian (70:30) function in such a way to give a normalized chi-square value that was close to 1 (0.7-1.20) and the Abbe criterion was close to 0 (0.1-0.4) in order to qualify as a good fit. The peak fitting function used for the Gaussian- Lorentzian product function is shown below (equation 2.2)

$$f(x) = \frac{peak\ height}{[1+ M(x-x_0)^2/\beta^2 exp\{ (1-M) [ln2\ (x-x0)^2]/ \beta^2\}} \qquad (2.2)$$

where x_o is the peak center, β is a parameter which is 0.5 (FWHM) and M is the mixing ratio. The value of M is 1 for a pure Lorentzian peak and 0 for Gaussian peak.

Once the N1s curve was successfully fitted into two N1s peaks, the ratio of N1s peaks of protonated and free amine was determined and plotted as function of distance along the gradient. This way we obtain information about how the surface basicity changes along the length of the gradient.

B. S2p peak fit

S2p has two peaks: one at lower energy ca. 163 eV and the other at higher binding energy ca. 168 eV.[6] The lower energy peak corresponds to the S2p in SH group and the higher energy peak corresponds to S2p in sulfonate group (HSO_3^-). Similar to the N 1s peak fitting, a Gaussian-Lorentzian (70:30) function was used. The peaks from 160-165 eV and 166 – 170 eV were adjusted with the smart background correction. The plots of the S2p peak area under thiol (SH) and sulfonate peaks were then plotted to obtain their information about their differential spatial distribution along the length of the substrates. A more detailed discussion about determining the area under S2p peak using smart background correction is presented in **Chapter 3**.

2.3 AFM microscopy

The surface roughness, topography and morphology along the length of the gradients and control samples were analyzed by **AFM** microscopy. **AFM** is a Scanning Probe Microscopy (**SPM**) technique first reported in 1981 by Binnig.[7] **SPM** techniques operated by detecting the deflection in the cantilever and modern **SPM** use a split photodiode to detect the deflection.[7-10] **STM**, the first of these techniques to be developed, produces images by measuring the current decay in electron tunneling between a conductive surface and a sharp tip (probe). STM operates in many different modes such as constant current mode, constant height mode, conductance mapping, and tunneling spectroscopy. The key process in STM is the quantum tunneling of electrons through a thin potential barrier separating two electrodes. By applying a voltage (V) between the tip and a metallic or semiconducting sample, a current can flow (I) between these electrodes when their distance is reduced to a few atomic diameters. Change in current is a result

of a change in the tip-sample separation. The resolution and quality produced by STM is very high (0.1 nm wide, 0.01 nm deep).

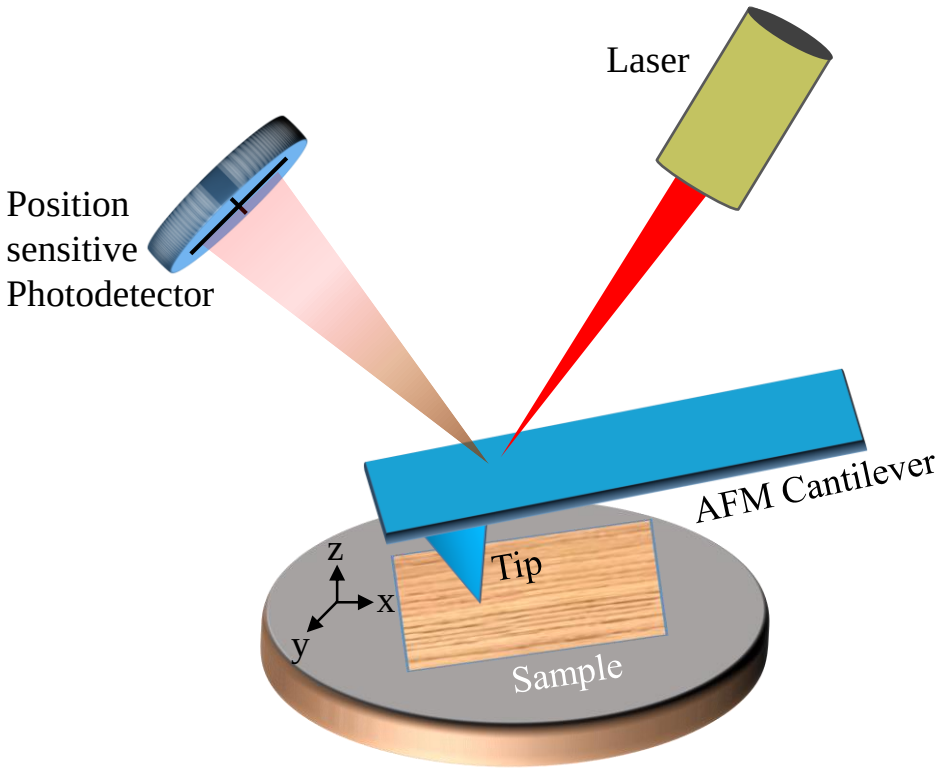

Figure 2.3: Schematic representation of the **AFM** apparatus

STM microscopy is influenced by the sample's electronic states (conductance of the samples) and roughness[10] The introduction of **AFM**, however, greatly expanded SPM's applicability to image in both air and liquid and allowed for imaging of larger, particularly, nonconductive samples.[7] Although **AFM** has lower resolution relative to STM, it has been widely employed for micro-imaging of biological samples[11, 12] in electrochemistry[7] and material science by providing an alternative technique that avoids some of the weaknesses of STM while still giving the potential for sub-micron resolution.

Figure 2.3 illustrates the basic apparatus of the **AFM**. The working principle of the **AFM** involves the instrument's interaction with the sample through the use of an extremely sharp tip (probe) (commonly called 'tip'), which is located on the bottom side of a cantilever and is typically made out of silicon or silicon nitride.[7] Due to the controlled bending that the cantilever experiences during scanning, cantilevers generally have very low spring constants. Normally, the sample specimen is placed on an **AFM** sample stage which can be moved in the xyz position as shown in the **Figure 2.3** thus allowing the proper focusing of the laser.

AFM can be used for both topographical imaging and force measurements[13]. Topographical imaging involves scanning the cantilever/tip across the sample surface. A laser beam is reflected off the back of the cantilever, and small changes in cantilever deflection are detected with a position-sensitive photodiode detector. This deflection is processed by the system

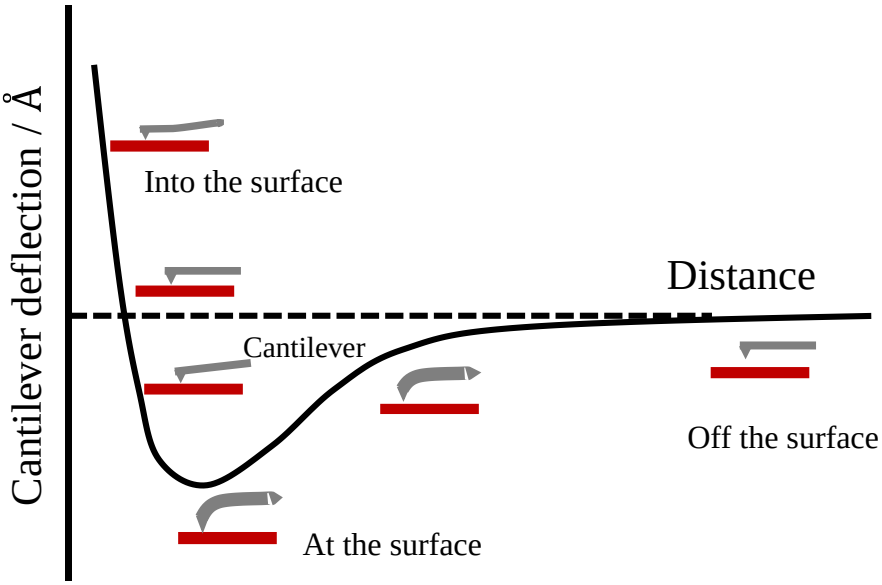

Figure 2.4: Cantilever deflection vs. distance curve.

detector to determine topological height changes on the sample surface. The lateral resolution that can be achieved by the **AFM** instrument depends on the geometry of the tip but can approach sub-nanometer levels, whereas the height resolution is sub-angstrom[11, 12]. Imaging can be

accomplished with either contact mode or tapping mode or non-contact mode, and these modes can be used in either air or fluid. In contact mode, the tip is in constant contact with the sample surface, whereas in tapping mode the cantilever is oscillated as it is rastered across the sample surface. Here in this work the surface topographic image and roughness of the samples were determined by **TM-AFM** microscopy. In **TM-AFM**, the lateral forces on the sample are reduced thereby reducing the sample damage. The tapping mode is, therefore, more commonly used when imaging very soft materials. The **AFM** has been increasingly used for the imaging of soft biological materials, since 1994 with the introduction of the tapping mode fluid cell in fluid,[14, 15] allowing the tapping mode to be used with samples in fluid.

The **TM-AFM** technique involves the measurement of different forces [16, 17] (include attractive, repulsive, polymer transition and relaxation temperatures, electrostatic, and van der Waals) between a sharp tip and the sample surface. Imaging is accomplished by measuring the interaction forces via deflection of a cantilever as the tip approaches the surface. Signal generation in **AFM** is essentially based on interatomic repulsive forces. Interactions between the tip and sample can be described by force-distance curves.[18] **Figure 2.4** shows how the force changes as the tip approaches the surface. At large separations there is no interaction between the tip and the substrate surface and thus the net force is zero. As the tip approaches the surface, however attractive van der Waals interactions begin to draw the tip to the surface, resulting in a slight bend in the cantilever. As the tip moves further towards the sample the total force acting on the cantilever becomes repulsive due to shell electron repulsion. Eventually the tip and the surface will touch and the cantilever will experience significant bending. When the distance between the sample and the tip is decreased further, the cantilever will straighten out and then eventually curve outward as

the sample is pushed into the surface. Below the zero force line the net force acting on the cantilever become attractive due to adhesion thus leading to the tip being held to the surface.

Here in this work the **TM AFM** employed was a Dimension-3100 (Digital Instruments) and dimension icon atomic force microscope with a NanoScope V controller. Imaging was performed in the tapping mode using a microfabricated silicon cantilever (40 N/m, Bruker, Santa Barbara, CA) in air. In tapping mode as shown in **Figure 2.4**, the tip is oscillated near its resonating frequency is brought close enough to the sample so that the oscillating tip repeatedly engages and disengages with the surface. Depending on the topography of the surface, the amplitude of the oscillating tip will either increase or decrease, information which is then used to construct the image.[19] With softer tapping, even if the sample surface has good phase separation produces a featureless phase image. With harder tapping, the tip interacts more with the near surface's hard segment. This produces an image that contains features whose intensity increases with harder

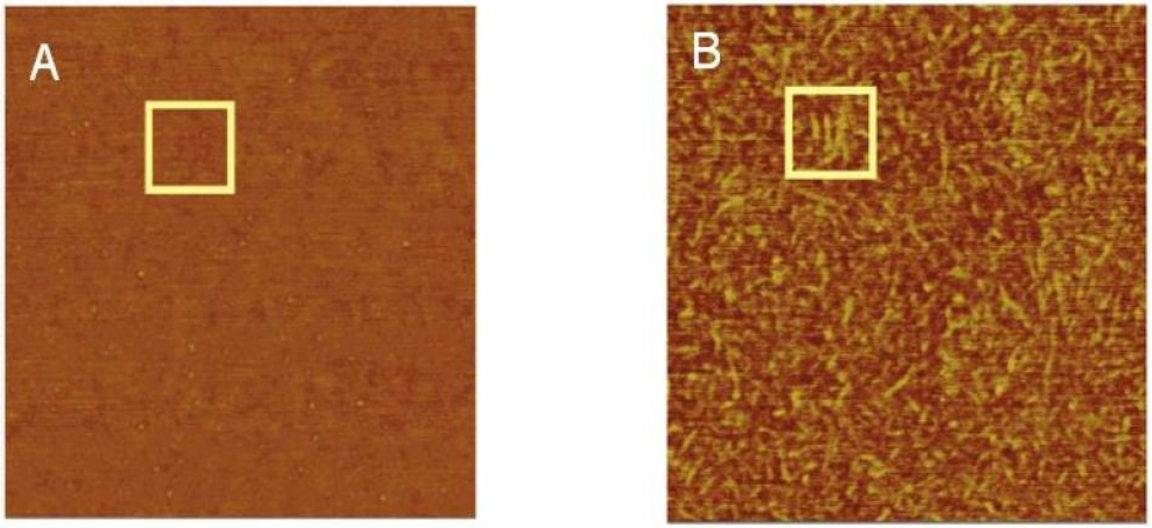

Figure 2.5: TM-**AFM** phase images of polyurethane-urea. Scan size = 500 x 500 nm phase angle 25°. A) Amplitude set point ratio (A_{sep}/A_o) = 0.9, B) Amplitude set point ratio (A_{set}/A_o) =0.8. (Reprinted from Ref 19 with permission from American Chemical Society, Copyright 2011).[19]

tapping. Changing of the cantilever amplitude or "tapping" is done by decreasing the amplitude setpoint voltage (A_{set}). The ratio of the A_{set} to the initial amplitude setpoint voltage (A_o) is the setpoint ratio (r_{sp}) or A_{set}/A_o, Thus with a smaller r_{sp} the cantilever taps harder.

An example of this phenomenon[19] is given in a study of polyurethane-urea block morphology via **TM-AFM**. As seen from **Figure 2.5**, the featureless images taken at the higher setpoint ratio (soft tapping) is indicative of the amorphous soft segment being dominant at the surface. At the lower setpoint ratio (harder tapping) the near surface hard segment can be seen in the form of ordered domains previously described. This surface segregation of the soft segment is typical for polyurethanes due to the soft segment having a lower surface energy that the hard segment.

Tapping mode tips require particularly stiff cantilevers because, as when they disengage, they must overcome capillary forces produced by the condensation of water as the tip first approaches the surface. The nanoscopic features of the micro-images obtained by **TM-AFM** were analyzed by NanoScope V software (1.5 v) and the number of gold nano particles adhered to the surface bound amine groups was analyzed with the help of ImageJ (1.48v) and NanoScope V software. **Chapter 3** describes in detail the preparation and adsorption of nanoparticles on sample surface and obtaining micrographs by **TM-AFM**, whereas **Chapter 4** discusses the analysis of some microfeatures of the samples having different base layers. Overall, **AFM** is a very successful technique for imaging small areas on a substrate under atmospheric conditions and can provide information about surface roughness and depths of small pores.

2.4 Electrokinetic measurements

Electrokinetic measurements can provide detailed information correlating surface composition and charge density, and ultimately interactions between functional groups. This is because the net charge depends on the functional groups present on the surface, their location relative to each other, and the solution pH. By studying the sign and magnitude of the ζ and how it changes with composition, detailed information about the surface composition and the interactions between surface bound functionalities can be elucidated, particularly when combined with **XPS** and the nanoparticle binding experiments. An electrokinetic potential or ζ develops during flow of electrolyte over a solid[20] This charge is attributed to an electrical double layer formed at the interface. The initial step in evaluating charge density is the measurement of

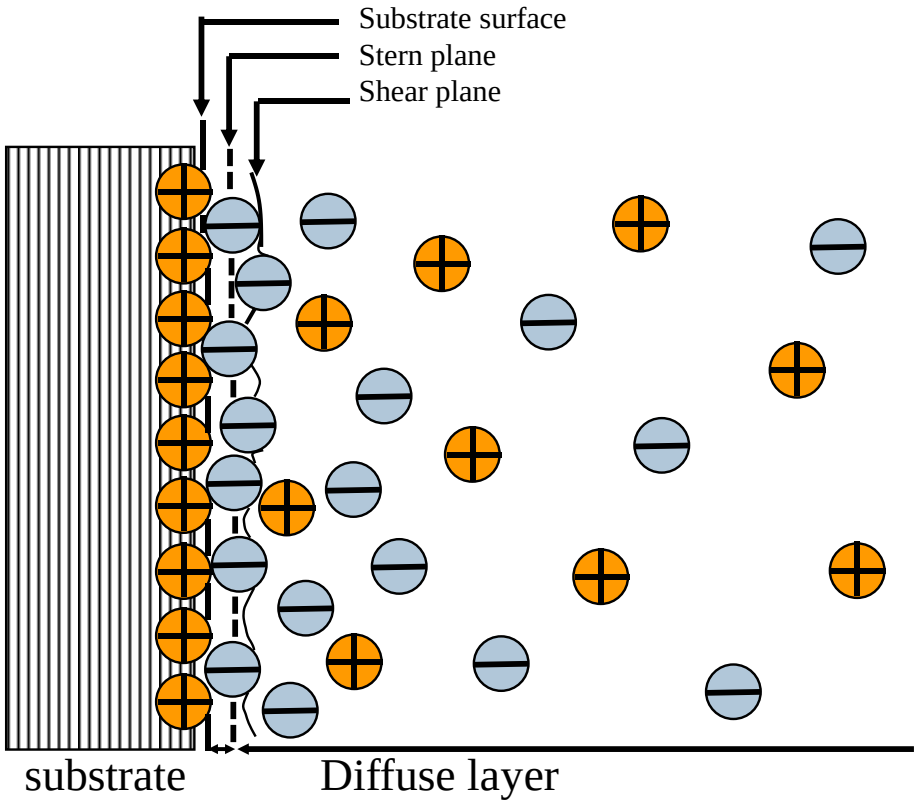

Figure 2.6. Schematic sketch of the double-layer.

streaming potentials resulting from the pressure-driven flow of an electrolyte solution across a substrate.[20, 21] The ζ values are calculated using the Helmholtz−Smoluchowski equation 2.3,

$$\zeta = \frac{\kappa\eta}{\varepsilon\varepsilon_0 \, (\Delta E / \Delta P)} \qquad (2.3)$$

where ΔE is the streaming potential in volts, ζ is the zeta potential in volts, η is the viscosity of the solution in Pascal seconds (Pa·s), κ is the solution conductivity in Siemens per meter (S/m), ε is the dielectric constant of the solution, ε_0 is the dielectric permittivity of vacuum, and ΔP is the pressure in Pa.[22]

Streaming potential measurements have long been used for the characterization of modified surfaces especially surface charge densities on capillaries.[20, 23] It is one of the several electrokinetic effects that is influenced by the surface charge. On a charged surface such as a flat substrate or a microchannel or colloidal particles, an electrical double layer (EDL) is formed at the interface by the surface charge and the surrounding counter ions in solution. This layer has two distinct parts, a Stern layer where the counter ions are strongly attached to the surface and 'diffuse layer' where the ions are less strongly bound.[24, 25] The ions that exist at the Stern layer and the diffuse layer close to it can move when the charged solution moves. The rest of the counter ions remain static in bulk solution. The plane that separates the moving and stationary layer of ions is called 'Shear plane'. The potential corresponding to the shear plane is called 'Zeta potential'[26] (**Figure 2.6**).

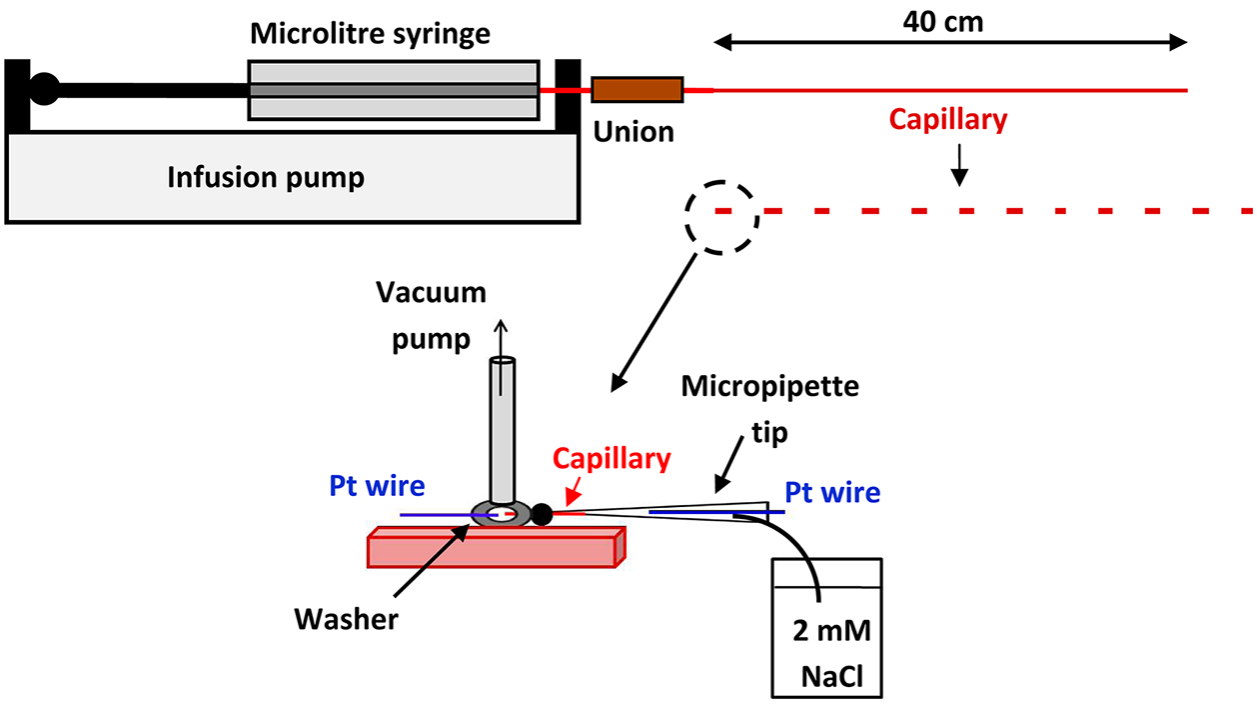

Figure 2.7: Top: Infusion setup for the fabrication of an amine gradient on the inside of a silica capillary by CRI. After gradient preparation, the capillary was cut into 12 mm segments. Bottom: The surface charge was evaluated for each segment of the capillary using a pulsed streaming potential apparatus based on pressure driven flow. (Reprinted from Ref 29 with permission from American Chemical Society, Copyright 2011).[29]

ζ measurements have been used to characterize charged surfaces such as glass modified with aminosilanes,[27] silica nanoparticles,[28] and most recently a glass capillary (75 μm id) 400 mm in length containing a gradient in amine and SiOH groups.[29] In the latter case, as shown in **Figure 2.7**, spatially resolved streaming potential measurements were made by cutting the gradient capillary into small pieces and measuring the average ζ of each of the segments using a custom built system.[29] because the capillary was long and the segments small, this method of characterization proved valuable and the charge at discrete locations along the length of the gradient could be directly evaluated. Using a similar capillary cell design, near surface quaternary

charge was investigated for polycation-based modified polyurethanes.[20] Decreasing charge density upon immersion in water was correlated with the instability of contact antimicrobial effectiveness.[20]

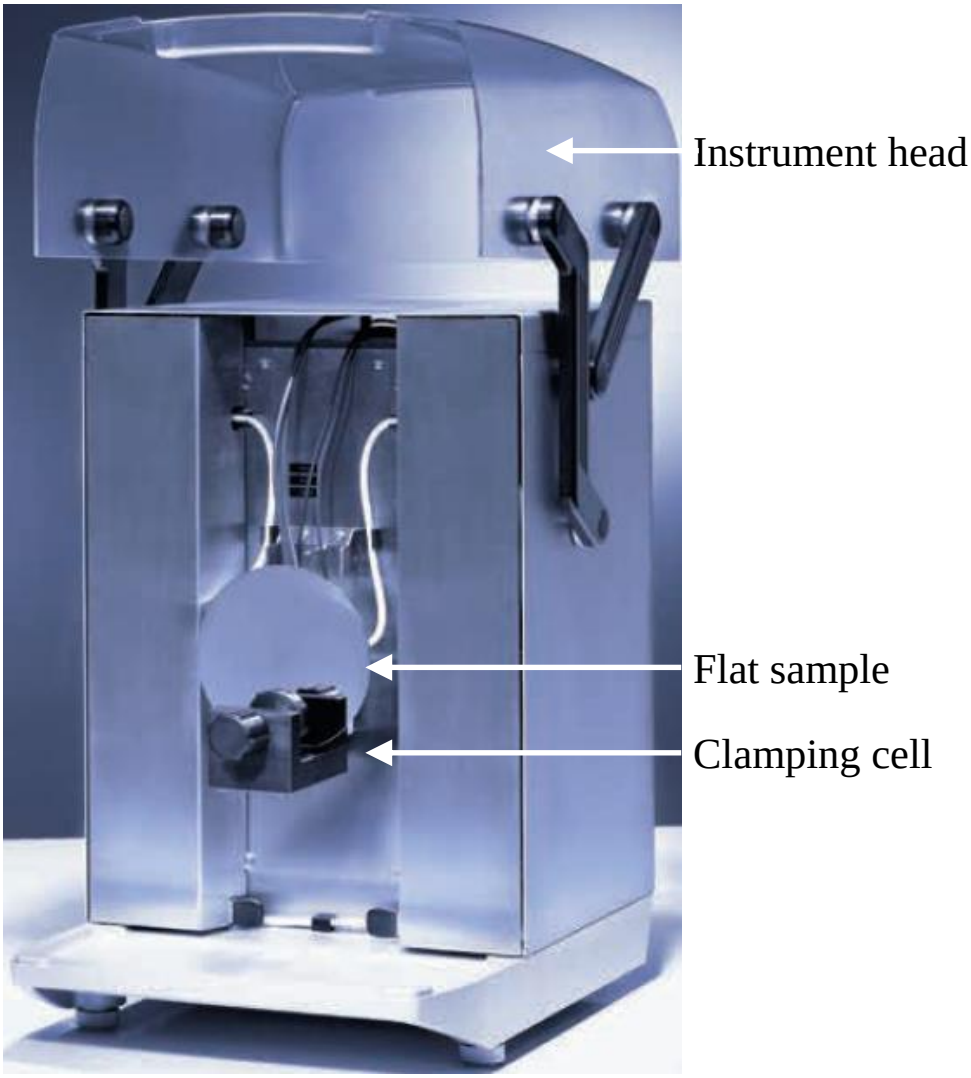

Figure 2.8: Anton paar electrokinetic containing clamping cell analyzer.[30]

For flat substrates, which are the subject of analysis herein, a commercial clamping cell was used with streaming potentials resulting from electrolyte flow through a channel between a polypropylene (***PP***) reference film and the substrate. The instrument works on the principle of acid base titration, where the pH of the electrolyte in contact with the sample surface is continuously

changing by continuously adding acid or base from the container connected via plastic tube. The final data or ζ values are presented as a function of the solution pH. The commercial name of the instrument containing the clamping cell is Anton paar electrokinetic analyzer, which is shown in **Figure 2.8.** Using the Helmholtz−Smoluchowski equation, ζ values can be obtained, which reflect the charge on the sample relative to the ***PP*** reference. The ζ values of ***PP*** reference must be done before any sample measurement since ζ value of reference indicates whether the analyzer is working correctly or not. A correct measurement of the samples' ζ values can be obtained only if the iso-electric point or ***IEP*** of the ***PP*** reference is 4±0.2. The ζ of ***PP*** was measured as a function of pH and then appropriately subtracted from the measured ζ for the full channel at each pH as described by the manufacturer. The formula that the instrument uses to calculate ζ is shown in the following expression. The sample setup on a clamping cell is shown in **Figure 2.9**. All the

$$The\ instrument\ reading = \frac{\zeta of\ sample + \zeta of\ PP}{2}$$

$$\zeta of\ sample = 2 \times intrument\ reading - \zeta of\ PP$$

solutions including acid and base and the electrolyte solutions are prepared fresh and the instrument is calibrated for the pH and conductivity once at every 7 and 14 days respectively.

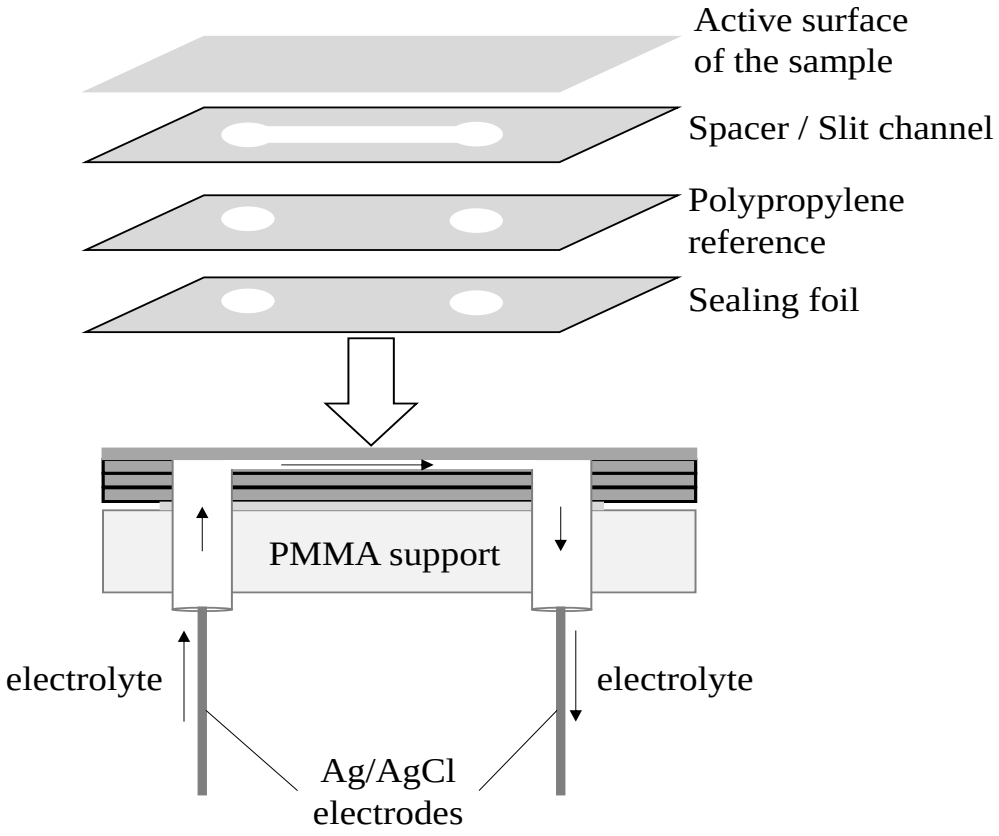

Figure 2.9: Assembly of the sample stack in the clamping cell.

To estimate the surface charge density, the Gouy equation (equation 2.4)[31] and measured ζ values were used,

$$\sigma = \sqrt{(8\varepsilon\varepsilon_0\ \mathrm{kNc})}\sinh\frac{ze\xi}{2kT} \qquad (2.4)$$

where σ = charge density ($C/m2$), k = Boltzmann constant ($1.38 \times 10^{-23}\ J/K$), T = 293 K, N = Avogadro's number ($6.02 \times 10^{23}\ \mathrm{mol}^{-1}$), z = counterion charge (+1), e is the charge on the electron,

and c = bulk electrolyte concentration (mol/m^3). The following values were used to calculate the charge density: ε = 80 and $\varepsilon_0 = 8.85 \times 10^{-12}\ F/m$.

2.5 Contact angle measurements

The wettability of SAMs has received great interest from both fundamental and applied points of view. It plays an important role in many industrial processes, such as oil recovery, lubrication, liquid coating, printing, and spray quenching.[32-37] Wettability studies usually involve the measurement of contact angles as the primary data, which indicates the degree of wetting when a solid and liquid interact. Contact angle measurement is a fast, simple and reproducible method to evaluate surface wettability and it can give valuable information on hydrophobicity differences across the length of a gradient film. A drop of a liquid on a surface in the contact angle measurement involves three interfaces. The angle between the solid-liquid interface and the liquid-

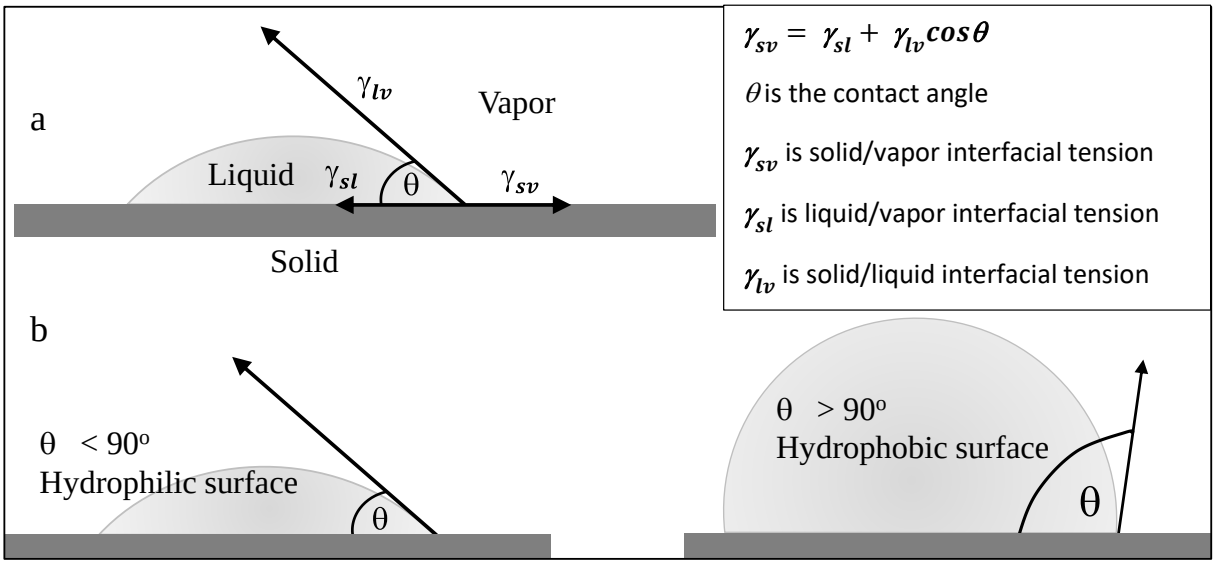

Figure 2.10: a. Schematic sketch of a droplet on a surface.

b. Schematic sketch of a water droplet on a hydrophilic and hydrophobic surface.

vapor interface is referred to as the contact angle. Small contact angles (≪90°) correspond to high wettability, while large contact angles (≫90°) correspond to low wettability. It is represented in **Figure 2.10**.

A drop on surfaces with a contact angle above 90° is considered to be hydrophobic and below 90° is considered to be hydrophilic (**Figure 2.10 (b)**). Normally, water is used as standard liquid for the contact angle measurement. Other liquids such as hexadecane have also been used for characterizing the surface oleophobicity. The extent that a contacting liquid wets depends on the wetting characteristics of the surface, its interfacial surface tension (γ) between surface (s), liquid (*l*) and gas (*g*). The contact angle of a liquid drop on an ideal solid surface is defined by the mechanical equilibrium of the drop under the action of three interfacial tensions (inset of **Figure 2.10 (a)**).

There are two ways to measure the surface contact angle using water as the wetting liquid: (1) **SCA** and (2) **DCA**. In **DCA**, the sample containing identical surface on either side of the siloxane substrate is slowly immersed into and withdrawn from Millipore water thereby measuring the contact angle continuously from bottom to near the top. The contact angle in the **DCA** instrument is measured by converting the net force between the surface and the liquid water by using Wilhelmy plate method.[38] In the following subsections these two approaches are discussed.

2.5.1 SCA analysis

The **SCA** measures the contact angle by the sessile drop method where a small drop (~1 μL) of water is carefully placed on the substrate surface and an optical image is captured immediately by a camera. In this work, **SCA** method was used to study the spatial variation of contact angle along the length of the gradients prepared on base layer coated Si wafers as well as

study the uniformity of various control samples. Contact angles were measured by a contact-angle goniometer as shown in **Figure 2.11**, which contains the optical unit for capturing the liquid-drop profile on a flat solid surface. A RameHart goniometer equipped with a high-resolution camera was used measure the contact angles at various positions along the length of the gradients. The camera captures the water droplet and the software called 'ImageJ v 1.48 (free version) was used to analyze the contact angle. In the ImageJ software, at first, the image is converted into 8-bit pixel image and analyzed by drop analysis plugin. This plugin uses Low-Bond Axisymmetric Drop Shape Analysis (*LBADSA*) method to measure the contact angle. The LBADSA[39] method is based on perturbation solution of the axisymmetric Laplace equation. It is thus suited to drops that are under the only force of gravity on a horizontal substrate. Contact angle values in the sessile drop

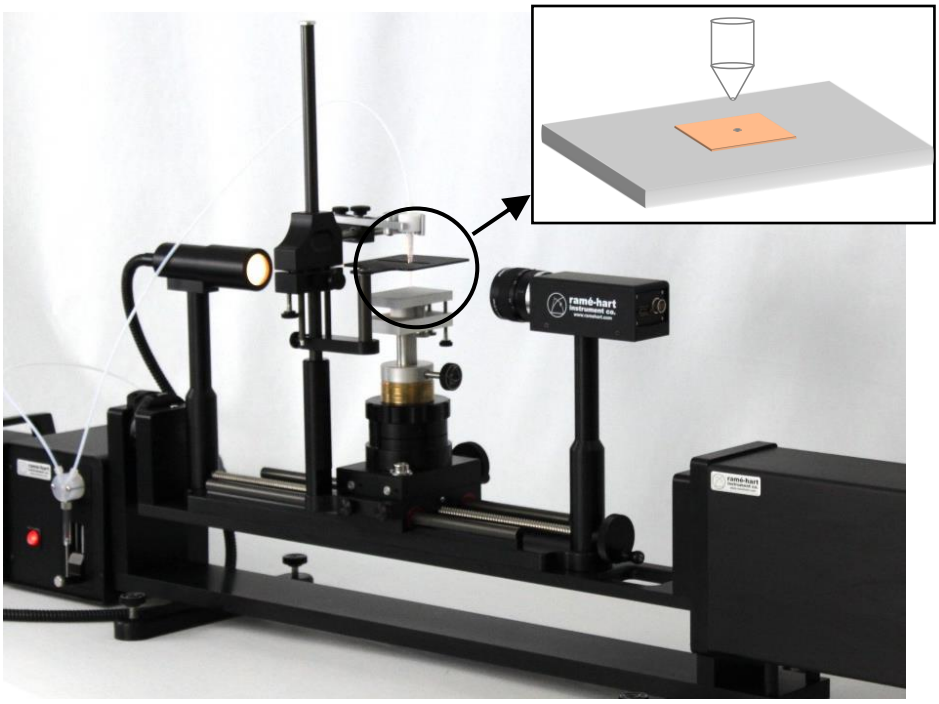

Figure 2.11: RameHart goniometer equipped with a high-resolution camera. Inset: zoomed view of the circled portion where a water drop from the pipette tip is falling on the sample surface.[40]

method largely depend on the smoothness of surface or surface inhomogeneity and the drop size. The size of the drop can vary from 1 to 10 μL; we typically use 1 μL. The water used must be fresh and distilled and deionized. The shape of the water drop is largely affected by local surface composition or surface heterogeneities. Since the surface heterogeneities of the various gradients and the control samples prepared from different base films could not be controlled therefore the drop size and the volume of water was kept constant (~1 μL) throughout the measurements.

2.5.2 Dynamic contact angle (DCA)

Wetting behavior and surface inhomogeneity and contact angle hysteresis were characterized by **DCA** measurements. The significance of contact angle hysteresis has been extensively investigated,[41-45] and the general conclusion is that it arises from surface roughness and/or heterogeneity.[38] For surfaces that are not homogeneous, there exist domains that present barriers to the motion of the contact line. In a heterogeneous surface, hydrophobic domains will

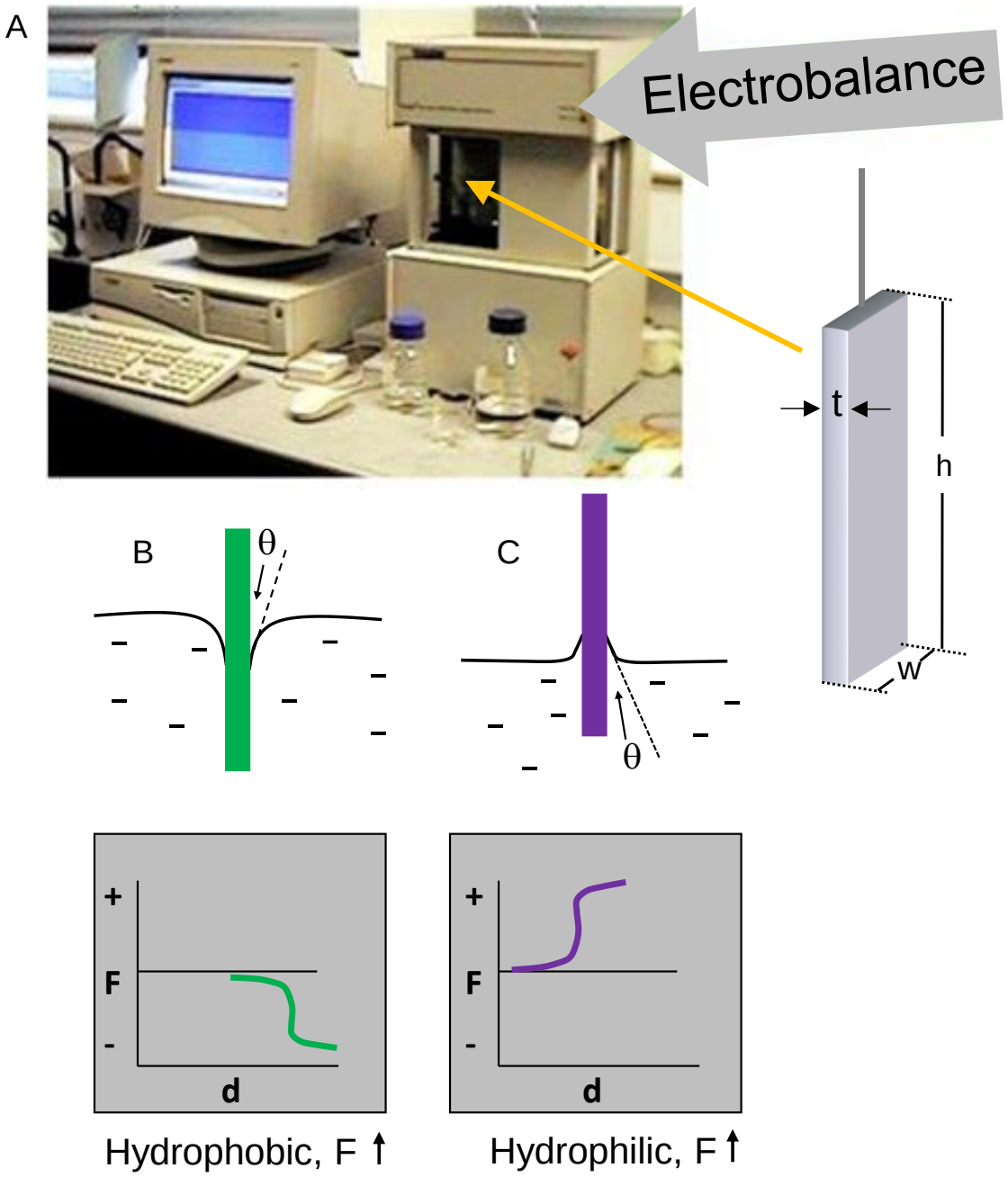

Figure 2.12: Model of Dynamic Contact Angle Analysis. A) Cahn dynamic Contact Angle (DCA) Model 312 Analyzer, B) Depiction of advancing force-distance curve for hydrophobic surface, C) Depiction of advancing force-distance curve for hydrophilic surface.

pin the motion of the water front as it advances, causing an increase in the observed contact angle; the same domains however will hold back the contracting motion of the water front when the water recedes, thus leading to a decrease in the observed contact angle.[42, 43] The data were analyzed by analyzed using the Wilhelmy Plate Method via a Cahn dynamic Contact Angle (DCA) Model 312 Analyzer (Cerritos, CA) instrument (**Figure 2.12**). Such method is useful in studying the continuous variation of the contact angle for a certain length of the sample. The figures show a photograph of the Cahn dynamic Contact Angle (DCA) Model 312 Analyzer, and depict how the meniscuses look when the surface is hydrophobic (B) and hydrophilic (C). The surface tension quantification limit of the instrument is 0.1 dyne/cm. The probe liquid was ~18 M/cm deionized Millipore water. The surface tension of the probe liquid was checked daily (72.6 ± 0.5 dynes/cm). Beakers used for DCA analysis were cleaned by soaking in an isopropanol/potassium hydroxide base bath for at least 24 hour, rinsed for 30 sec with hot tap water and then rinsed another 30 sec with Millipore water. In a typical determination, a freshly prepared sample was attached to the electro-balance via a clip and the clip with the sample was automatically raised and lowered into a beaker of water to allow the water to impinge upon the slide. By analyzing the resulting force versus distance curves advancing and receding contact angles were obtained. Using the following relation among the force, samples perimeter, surface tension of the liquid the contact angle was determined.

$$F = mg + P\gamma_l cos\theta + F_b$$

Where, F is the force applied to the load cell

m, mass of the plate

P, perimeter of the sample

γ_l, surface tension of the liquid

g, acceleration due to gravity

θ, contact angle

F_b, buoyancy force.

For the correct measurement, the buoyancy force exerted by water on the sample surface must be corrected. Buoyancy force is determined by the mass of water that must be displaced by the sample times the acceleration due to gravity. The buoyancy force must be added to correctly measure the contact angle.

The stage speed was kept 100 μm/sec and the wetted depth is from 20-25 mm. This was repeated 3 times during the course of analysis for each sample. To ensure the Millipore DI water is clean enough with surface tension at 72.43 mN/m (22º C) and to examine whether there was contamination from the siloxane samples, the wetting medium was tested with a flamed glass slide (water check) before and after the sample testing under the same conditions. In the water check test, the glass was heated carefully in a flame so that any volatile organic compound and salt were evaporated at the high temperature. The surface is then cooled down and connected to the hook for the DCA measurement. If the water is fresh i.e., not contaminated with sample, the flamed glass should show a contact angle around 0-10 º. Any bigger deviation from this values indicates that the water is contaminated from the leakage of the component from sample surface. The samples employed in the current work did not show any leakage in the water since the water check test before and after the DCA measurement remained unchanged. A DCA plot for a uniform sample looks like unchanged along the length of the substrate because the substrate has a uniform surface chemical composition. However, if the surface appears to be rougher surface[46] or nanoscale heterogeneity[47-48] can make the DCA curve take different form. For a gradient surface, as is the case of the current research takes entirely different form of DCA curves depending on how and

what is being used to modify the gradient surface. In this work, we investigated DCA analysis of gradient surface prepared by the programmed and non-programmed ***CRI*** method.

2.6 References

1. Vickerman , J. C.; Gilmore, I. *Surface Analysis- The Principle Techniques*. **2009**.
2. Bogart, K. H. A.; Donnelly, V. M. On the constant composition and thickness of the chlorinated silicon surface layer subjected to increasing etching product concentrations during chlorine plasma etching. *Journal of Applied Physics* **1999**, *86* (4), 1822-1833.
3. Biino, G. G.; Groning, P. X-Ray Photoelectron Spectroscopy (XPS) used as a structural and chemical surface probe on aluminosilicate minerals. *European Journal of Mineralogy* **1998**, *10* (3), 423-437.
4. Tougaard, S.; Ignatiev, A. Concentration depth profiles by xps - *a new approach. Surface Science* **1983**, *129* (2-3), 355-365.
5. Cumpson, P. J. Angle-resolved XPS depth-profiling strategies. *Applied Surface Science* **1999**, *144-45*, 16-20.
6. Koo, H. J.; Waynant, K. V.; Zhang, C.; Haasch, R. T.; Braun, P. V. General method for forming micrometer-scale lateral chemical gradients in polymer brushes. *Chem. Mater.*, **2014**, *26*, 2678−2683.
7. Gunning, A. P.; Morris, V. J. Atomic Force Microspcopy for Biologists. Second Edition ed.; Imperial College Press: London, **2010**.
8. Van-Putten, E. G.; Akbulut, D.; Bertolotti, J.; Vos, W. L.; Lagendijk, A.; Mosk, A. P. Scattering Lens Resolves Sub-100 nm Structures with Visible Light. *Physical Rev. Lett.*, 106, (19).
9. Bowen, W, R.; Hilal, N. Atomic Force Microscopy in Processing Engineering; Introduction to AFM for Improved Processes and Products.**2009**.
10. Bai, C. Scanning Tunneling Microscopy and Its Applications. Springer: Shanghai, **2000**.

11. Zhang, B. J.; Davis, S. A.; Mendelson, N. H.; Mann, S., Bacterial templating of zeolite fibres with hierarchical structure. *Chem. Com.*, **2000**, (*9*), 781-782.

12. Zhou, H.; Fan, T. X.; Zhang, D. Hydrothermal synthesis of ZnO hollow spheres using spherobacterium as biotemplates. *Microporous and Mesoporous Mater.*, **2007**, *100*, (1-3), 322-327.

13. Cranston, E. D.; Gray, D. G. Morphological and optical characterization of polyelectrolyte multilayers incorporating nanocrystalline cellulose. Biomacromolecules **2006**, *7*, (9), 2522-2530.

14. Tomcsik, J.; Guex-Holzer, S., A Specific Cell-Wall Reaction in Bacillus sp. *J. Gen. Microbiol.*, **1954**, *10*, 317-324.

15. Hansma PK, Cleveland JP, Radmacher M, *et al*. Tapping mode atomic-force microscopy in liquids. *Appl. Phys. Lett.* 1994; 64: 1738–1740.

16. Cooper, S. L.; Tobolsky, A. V., Viscoelastic behavior of segmented elastomers. *Text. Res. J.* **1966**, *36*, (9), 800-3.

17. Krause, S. Phase separation in block copolymers. *J. Polym. Sci., Part A: Polym. Chem.*, **1969**, *7*, 249.

18. Bubert, H.; Jenett, H. Surface and Thin Film Analysis. **2002**, Wiley-VCH.

19. Garrett, J.T.S., C.A.; Runt, J., Microdomain Morphology of Poly(urethane ureas) Mutiblock Copolymers. *Macromolecules*, **2001**. 34: 7066-7070.

20. Gupta, M. L.; Brunson, K.; Chakravorty, A.; Kurt, P.; Alvarez, J. C.; Luna-Vera, F.; Wynne, K. J. Quantifying surface-accessible quaternary charge for surface modified coatings via streaming potential measurements. *Langmuir* **2010**, 26, 9032−9039.

21. Pu, Q.; Elazazy, M. S.; Alvarez, J. C. Label-free detection of heparin, streptavidin, and other probes by pulsed streaming potentials in plastic microfluidic channels. *Anal. Chem.* **2008**, 80, 6532−6536.

22. Berezkin, V. V.; Volkov, V. I.; Kiseleva, O. A.; Mitrofanova, N. V.; Sobolev, V. D. The Charge of the Pores of Poly (ethylene terephthalate) Nucleopore Membranes. *Colloid J.* **2003**, 65 (1), 119−121.

23. Stanley, J. S. *J. Phys. Chem.* **1954**, 58, 533.

24. Kirby, B. J., Hasselbrink Jr., E. F., *Electrophoresis*, **2004**, 25, 187–202.

25. Lyklema, J. H., Fundamentals of Interface and Colloid Science, Academic Press, London **1991**.

26. Kralchevsky, P. A., Danov, K. D., Denkov, N. D., in: Birdi, K. S. (Ed.), *Handbook of Surface and Colloid Chemistry*, CRC Press, Boca Raton, FL, **2003**, 137–344.

27. Metwalli, E.; Haines, D.; Becker, O.; Conzone, S.; Pantano, C. G. Surface characterizations of mono-, di-, and tri-aminosilane treated glass substrates. *J. Colloid Interface Sci. 2006*, 298, 825−831.

28. Hayes, R. A.; Böhmer, M. R.; Fokkink, L. G. J. Study of silica nanoparticle adsorption using optical reflectometry and streaming potential techniques. *Langmuir* **1999**, 15, 2865−2870.

29. Kannan, B.; Nokura, K.; Alvarez, J. C.; Higgins, D. A.; Collinson, M. M. Fabrication of Surface Charge Gradients in Open-Tubular Capillaries and Their Characterization by Spatially Resolved Pulsed Streaming Potential Measurements. *Langmuir* **2013**, 29, 15260−15265.

30. Surpass electrokinetic Analyzer. http://www.anton-paar.com/sg-en/products/group/surface-analysis.

31. Bard, A. J.; Faulkner, L. R. Electrochemical Methods: Fundamentals and Applications; John Wiley & Sons, Inc.: New York, **2001**.

32. Prabhu, K.N.; Fernandes, P.; Kumar, G. Effect of substrate surface roughness on wetting behaviour of vegetable oils. *Mater. Des.*, **2009**, 2, 297.

33. Zhao, X.; Blunta, M.J.; Yao, J.J. Pore-scale modeling: Effects of wettability on waterflood oil recovery. *Pet. Sci. Technol. Eng.*, **2010**, 71, 169.

34. Wang, Y.Q.; Yang, H.F.; Hang, Q.G.; Fang, L.; Ge, S.R. Tribological and Lubrication Properties of Sandblast-Textured Surfaces with Varied Roughness. *Adv.Mater. Res.*, **2010**, 154–155, 1019.

35. Sakai, M.; Yanagisawa, T.; Nakajima, A.; Kameshima, Y.; Okada, K. Contact angle hysteresis: a different view and a trivial recipe for low hysteresis hydrophobic surfaces. *Langmuir*, **2009**, 25, 13.

36. Son, Y.; Kim, C.; Yang, D.H.; Ahn, D.J. Spreading of an Inkjet Droplet on a Solid Surface with a Controlled Contact Angle at Low Weber and Reynolds Numbers. *Langmuir*, **2008**, *24*, 2900.

37. Perelaer,J.; Hendriks, C. E.; de Laat, A. W. M.; Schubert, U. S. One-step inkjet printing of conductive silver tracks on polymer substrates. *Nanotechnology*, **2009**, *20*, 165303.

38. Shang, J.; Flury, M.; Harsh, J. B.; Zollars, R. L., Comparison of different methods to measure contact angles of soil colloids, *J. Colloid Interface Sci.*, **2008**, *328*, 299–307.

39. Aurélien F.; Staldera, A. F.; Melchiorb, T.; Müllerb, M.; Saged, D.; Bluc, T.; Unser M. Low-bond axisymmetric drop shape analysis for surface tension and contact angle

measurements of sessile drops, *Colloids and Surfaces A: Physicochem. Eng. Aspects*, **2010**, *364* (1-3), 72–81.

40. Nanomaterials Core Characterization Facility. http://www.nano.vcu.edu/

41. Johnson, R.E.; Dettre, R.H.J. Contact Angle Hysteresis. III. Study of an Idealized Heterogeneous Surface *J. Phys. Chem*., **1964**, 68, 1744.

42. Schwartz, L.W.; Garoff, S. Contact angle hysteresis on heterogeneous surfaces. *Langmuir*, **1985**, 1, 219.

43. Joanny, J.F.; de Gennes, P.G.J. A model for contact angle hysteresis. *J. Chem. Phys.*, **1984**, 81, 552

44. Krumpfer, J.W.; McCarthy, T.J. Contact angle hysteresis: a different view and a trivial recipe for low hysteresis hydrophobic surfaces. *Faraday Discuss*., **2010**, *146*, 103.

45. Gao, L.; McCarthy, T.J. Contact Angle Hysteresis Explained. *Langmuir*, **2006**, *22*, 6234.

46. Wang,Y.; Pitet, L. M.; Finlay, J. A.; Brewer, L. H.; Cone, G.; Betts, D. E.; Callow, M. E.; Callow, J.A.; Wendt, d. E.; Hillmyer, M.A.; DeSimone, J. M.Investigation of the role of hydrophilic chain length in amphiphilic perfluoropolyether/poly(ethylene glycol) networks: towards highperformance antifouling coatings. *Biofouling*: *J. Bioadhesion Biofilm Research*, **2011**, *27* (10), 1139–1150.

47. Lin, Y.; Hlady, V.; Gölander, C.-G. The surface density gradient of grafted poly (ethylene glycol): Preparation, characterization and protein adsorption. *Colloids Surf. B: Biointerfaces*, **1994**, *3* (1-2), 49-62.

48. Lin, Y.; Hlady, V. The desorption of ribonuclease A from charge density gradient surfaces studied by spatially-resolved total internal reflection fluorescence. *Colloids Surf. B: Biointerfaces*, **1995**, *4* (2), 65-75.

Chapter 3: Cooperative Effects in Aligned and Opposed Multi-Component Charge Gradients Containing Strongly Acidic, Weakly Acidic and Basic Functional Groups

Adapted from Kayesh M. Ashraf, Dipak Giri, Kenneth J. Wynne, Daniel A. Higgins, and Maryanne M. Collinson, *Langmuir* **2016**, *32*, 3836−3847.

3.1 Abstract

Bi-functionalized surface charge gradients in which the individual component gradients either align with or oppose each other have been prepared. The multi-component gradients contain strongly acidic, weakly acidic, and basic functionalities that cooperatively interact to define surface wettability, nanoparticle binding, and surface charge. The two-step process for gradient formation begins by modifying a siloxane coated silicon wafer in a spatially dependent fashion first with an aminoalkoxysilane and then with a mercapto-functionalized alkoxysilane. Immersion in hydrogen peroxide leads to oxidation of the surface immobilized sulfhydryl groups and subsequent protonation of the surface immobilized amines. Very different surface chemistries were obtained from gradients that either align with or oppose each other. **XPS** spectroscopy data show that the degree of amine group protonation depends on the local concentration of sulfonate groups, which form ion pairs with the resulting ammonium ions. Contact angle measurements show that these ion pairs greatly enhance the wettability of the gradient surface. Finally, studies of colloidal gold binding show that the presence of both amine and thiol moieties enhance colloid binding, which is also influenced by surface charge. Cooperativity is also revealed in the distribution of charges on uniform samples used as models of the gradient surfaces, as evaluated

via ζ measurements. Most significantly, the net surface charge and how it changes with distance and solution pH strongly depend on whether the gradients in amine and thiol align or oppose each other. The aligned multicomponent gradients show the most interesting behavior in that there appears to be a point at pH ~6.5 where surface charge remains constant with distance. Setting the pH above or below this transition point leads to changes in the direction of charge variation along the length of the substrate.

3.2 Introduction

Electrostatic interactions at charged surfaces play a key role in governing the interaction of proteins and bacteria on surfaces, the stabilization of colloids, the wetting of surfaces, the layer-by-layer (LBL) assembly of thin films, reactions in catalysis, and in the separation of charged species in chromatography.[1-5] Understanding localized interactions between surface functional groups and charged species in solution thus becomes particularly relevant to the development of surfaces resistant to biofouling, antimicrobial surfaces, catalytic surfaces, multi-layered composite thin films, and imprinted surfaces for chemical sensing and separations. It is therefore of interest to develop methodologies to create and study heterogeneous and homogeneous charged surfaces with well-defined properties.

An efficient approach to systematically study localized interactions is to generate a surface that exhibits a gradual change in charge density in a unidirectional or bidirectional fashion.[6-10] Such gradients provide different charge states along a single sample and bypass the need to prepare multiple uniform surfaces each with differing surface chemistry. Previous work on charge gradients have involved those prepared using self-assembled monolayers with functionalized alkane thiols,[11, 12] those employing silane chemistry,[13-16] and those made using polymer chemistry.[17-20] Specific examples include negatively charged gradients prepared from thiol-terminated functionalities (-SH) followed by oxidation to yield sulfonate groups ($-SO_3^-$)[18, 21] or deprotonation of COOH terminated groups spatially organized on a surface.[11, 12] Positively charged gradients have often been prepared by attachment of amine-terminated reagents ($-NH_2$) followed by quaternatization, typically with methyl iodide,[16] to yield $-N(CH_3)_3^+$ or simply by protonation to give $-NH_3^+$.[15] Multi-component charge gradients that contain negatively and positively charged components have also been prepared. These include ***opposed*** gradients prepared

from polyelectrolyte brushes incorporating oppositely charged weak electrolytes such as poly(acrylic acid) and poly(2-vinyl pyridine)[22] or plasma polymerized amine and carboxylic acid polymers,[19] as well as binary and ternary mixed self-assembled alkanethiols on gold.[11] Such gradients offer an unique opportunity to explore localized intermolecular interactions in a time-efficient fashion, particularly when the placement of the individual functional groups can be carefully controlled.

In this work, as a route to exploring cooperative interactions between acidic and basic functionalities on a surface,[23] dual/multi-component chemical gradients in which the individual component gradients ***either align with or oppose each other*** were prepared and characterized. These surfaces are interesting because they contain weakly acidic, strongly acidic and basic functional groups in close proximity. This work is relevant to acid-base functionalized silica,[24-28] which is a valuable support for cooperative catalysis, especially when the two functional groups are in juxtaposition. The spatial distribution of the individual components on the surface ultimately influences the local microscopic charge and hence, localized interactions between surface-bound functional groups and reagents in solution. In this work, we show how the distribution of charge on the surface is very different for *opposed* vs. *aligned* multi-component gradients and how by simply aligning the individual gradients differently, materials with very different surface chemistry can be obtained. Interestingly, in the aligned gradients, there appears to be a pH ~6.5 where the surface charge remains constant with distance.

3.3 Experimental

3.3.1 Sample preparation

Tetramethoxysilane (TMOS, 98%), 3-aminopropyltriethoxysilane (APTEOS, 99%), and 3-mercaptopropyltrimethoxysilane (MPTMOS, 98%) were purchased from Acros Organics. All

the silanes were used as received. Silicon wafers (University Wafer, B-doped, ⟨111⟩) were cut to the appropriate size ((1-2) × (2-3.5) cm) and then cleaned with fresh concentrated H_2SO_4:H_2O_2 (70:30) for 10 min at 70 °C in a water bath. *Caution:* piranha solutions are extremely dangerous and react violently with organic materials. The silica sol used for base layer preparation contained ethanol, TMOS, 0.1 M HCl, and water in a 0.4:0.2:0.06:0.06 volumetric ratio and was aged for 24−36 h prior to use. This sol was spin-coated on the wafers at 5000 rpm for 30 s and the modified substrates then dried in a desiccator overnight. This base layer helps ensure there is a uniform surface containing reactive silanol groups for further chemical modification regardless of the nature of the underlying substrate.[29]

The aminosilane solution used for infusion was prepared by mixing ethanol:silane:water in a 5:0.25:0.06 volumetric ratio. Surface amine gradients were prepared by slowly infusing a freshly prepared aminosilane solution into a vial containing the vertically aligned substrate by controlled-rate infusion (***CRI***).[29, 30] In this method, the rate of infusion was controlled by a programmable syringe pump (Harvard apparatus, PHD 2000 infusion; 0.3 mL/min). During infusion, the base-layer-coated substrate was exposed to the aminosilane solution for 30 min along its length, thus producing a gradual spatial variation in the extent of amine modification from top to bottom.

The mercaptosilane solution for subsequent use in ***CRI*** was prepared by mixing ethanol:silane:0.1 M HCl in a 11.8:0.12:0.12 volumetric ratio. The solution was vigorously stirred for 5 min, after which 0.12 ml of 0.3 M NH_4OH solution was added to neutralize the acid and ultimately increase the rate condensation of the silanols.[31] The pH of the resultant solution was ~ 6.4. The solution was stirred for an additional 25 min and sat quiescent for 90 min before use in ***CRI*** with an infusion rate of 0.3 mL/min. This two-step process[32, 33] affords efficient hydrolysis

(via the addition of acid) and condensation (via the addition of ammonia) of the mercaptosilane precursors.

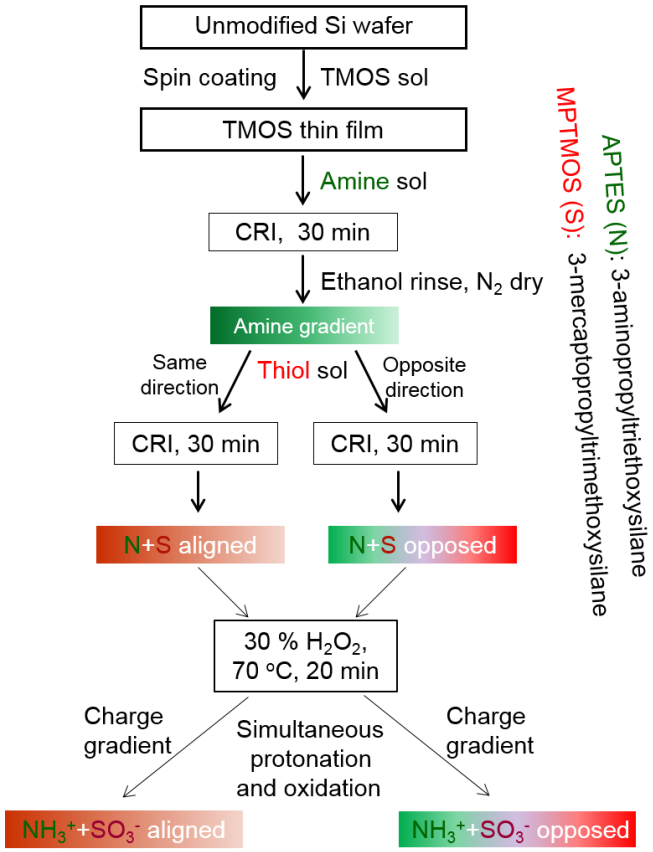

Scheme 3.1: Fabrication of multi-component aligned and opposed gradients by controlled-rate infusion (***CRI***).

Multi-component gradients were prepared by infusing a freshly prepared mercaptosilane sol along the same amine gradient. If the mercaptosilane is deposited in the same direction as the amine gradient, an aligned multicomponent gradient is obtained and is designated as N+S aligned; if in the opposite direction, an opposed gradient is obtained that is designated as N+S opposed. H_2O_2 was used to oxidize the thiol groups to sulfonic acid groups (SH→ SO_3H).[34, 35] Surface charge gradients were prepared by exposing the multi-component gradients to 30% H_2O_2 at 70 °C for 20 min. The oxidation of thiol subsequently leads to the protonation of the amine (NH_2 →NH_3^+)

to give rise to a dual charge surface. The duration of the reaction time with H_2O_2 was optimized as described below. After ***CRI***, the samples were rinsed with ultrapure water, dried with a stream of N_2 and stored in a desiccator. We denote the aligned charge gradients as (NH_3^+ + SO_3^- aligned) and the opposed charge gradients as (NH_3^+ + SO_3^- opposed). A flow chart outlining the steps associated with gradient formation is shown in **Scheme 3.1**.

Uniform samples were also prepared as controls. The base-layer coated silicon wafers were immersed in aminosilane solution for 30 min followed by rinsing with ethanol, drying with N_2 and storing in a desiccator for 2 h. After subsequent immersion in mercaptosilane solution for 30 min, the samples were again rinsed, dried, and desiccated; these are referred to as (N + S uniform). Oxidation via reaction with 30% H_2O_2 yielded uniformly charged surfaces designated as (NH_3^+ + SO_3^- uniform). Other controls include an unmodified silicon wafer and the base-layer coated silicon wafer.

3.3.2 Characterization

XPS spectroscopy was performed with a Thermo Fisher ESCAlab 250 imaging X-ray photoelectron spectrometer (Al Kα (1486.68 eV)), 500 μm spot size, 50 eV pass energy, 0.1 eV step size). Samples were placed on top of conducting tape on a 5 cm × 2 cm sample holder. **XPS** spectra were acquired at constant intervals (typically every 3 mm) across the wafer and starting ~ 3 mm from the edge. The spectra were calibrated by taking the C1s peak as 284.6 eV. Deconvolution of the N1s peak area was done using CASA software and a Gaussian−Lorentzian (70:30) function after smart background subtraction, similar to that reported by Unger *et al*.[36] To evaluate if any damage to the film by the X-ray beam takes place, a number of scans were acquired at a few locations while carrying out the experiments and no noticeable increase or decrease in the

peak size was observed. Other studies have also indicated minimal beam damage under their similar experimental conditions as well.[36, 37]

AFM microscopy was conducted on a Dimension-3100 (Digital Instruments, CA) atomic force microscope with a NanoScope V controller. Imaging was performed in the tapping mode using a microfabricated silicon cantilever (40 N/m, Bruker, Santa Barbara, CA) in air. The set point ratio r_{sp} or A_{exp} / A_o, where A_o is the free oscillation amplitude and A_{exp} is the experimental oscillation amplitude, which was held constant at 0.95 ("soft tapping").

Gold nanoparticles. A colloidal solution of citrate stabilized gold nanoparticles was prepared according to published procedures by heating $HAuCl_4$ in the presence of sodium citrate in dilute perchloric acid (pH ~ 4.3).[38] The substrates were soaked in the colloidal gold solution for two hours followed by rinsing with water. The number of gold particles/clusters on the surface was calculated with ImageJ software. From **AFM** sectional images, the number of individual nanoparticles were determined in each cluster. Using these numbers, the number of particles in each 2 x 2 μm^2 was determined.

Contact angle measurements were made with a Rame-Hart contact angle goniometer by the sessile drop method. The volume of the drop of water was 1 μL.

Ellipsometric measurements of film thickness were obtained by spectroscopic ellipsometry (α- SE, J.A. Woollam) under dry conditions with a continuous flow of nitrogen gas (relative humidity~ 18%). In these experiments, the ellipsometry data were acquired at ~ 2 mm intervals along the length of each base-layer coated substrate. Thin base layer coatings were employed in these studies to facilitate the measurements. Data were acquired from approximately the same locations (i.e., within ±0.5 mm) after modification by the aminosilane and then again after modification by the mercaptosilane. All spectroscopic ellipsometry data were globally fit to

a single layer model using the "Si with Transparent Film" model available in the CompleteEASE software provided with the instrument. Only those data that produced good fitting results (mean square error ≤ 0.9) were used to determine film thickness. Fitting of the data to a single layer model was assumed sufficient to properly determine film thickness, because the refractive indexes, n, of all films were determined to be very similar. The *n* values (at 632.8 nm) obtained from the base layer, and the films after aminosilane and mercaptosilane modification were all 1.456 ± 0.001. The film thickness is 0.456 ± 0.001 after modification with the aminosilane only. The thickness data are shown in **Figure 3.1**. All the samples were immersed in mercaptopropionic acid (**MPA**) for stabilization.

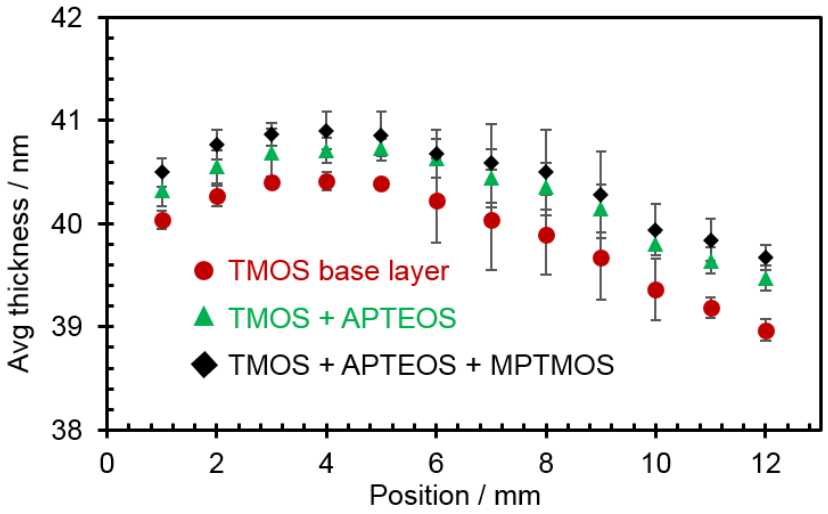

Figure 3.1: Thickness of the APTEOS and APTEOS+MPTMOS modified base layer. All the samples were immersed in MPA solution for stabilization.

Zeta potentials (ζ) were determined using an Anton-Paar SurPASS instrument and clamping cell including a standard electrokinetic analyzer. The sequence of the placement of the sample, spacer, reference and sealing foil on the clamping cell is illustrated in **Figure 3.2**. Samples used for ζ measurements were 5 cm × 2.5 cm. Flat polypropylene (***PP***) sheets (0.0125 in., 5 × 2

cm^2, McMaster-Carr) were used as a reference. The electrolyte was 0.001 M KBr (99%) (Sigma Aldrich). As shown in **Figure 3.2**, a polypropylene reference sheet with two holes 2.5 cm apart was placed on the PMMA support with a sealing foil on it. The spacer used to create a channel was covered by the sample substrate with its active surface facing down. The cell height was ~ 90-100 μm. The impact of the interfacial conductance from the sample surface was not considered. Measurements were made at 20 ± 2 °C and at a maximum pressure difference of 500 mbar. ζ values were measured in the pH range 3.0-8.5 monitored by two Ag/AgCl electrodes. The average value of four measurements was recorded.

3.4 Results and Discussion

3.4.1 Gradient fabrication

Gradient fabrication began by spin coating an acid-catalyzed silica sol prepared from TMOS onto a silicon or glass substrate to form a homogeneous base layer for covalently anchoring the organoalkoxysilanes.[29] Such films are relatively nonporous with effective pore sizes of less

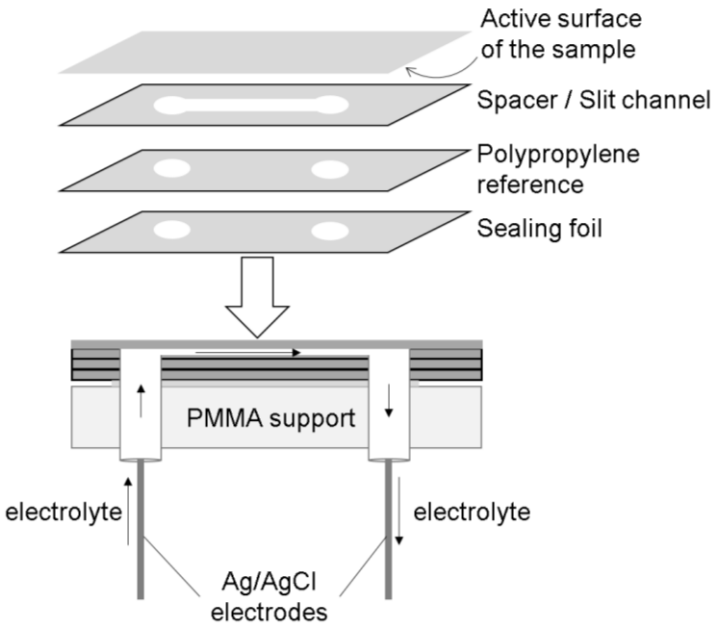

Figure 3.2: Assembly of the sample stack in the clamping cell

than a nanometer.[39, 40] Compared to previous work which used a base layer prepared in part from dimethyldiethoxysilane,[29] a TMOS sol was used to increase the hydrophilicity of the substrate and the area density of silanol groups. Using controlled rate infusion (***CRI***), the base-layer coated substrate was exposed to a solution containing APTEOS in a time-dependent fashion by slowly infusing it into a glass vial holding the vertically aligned substrate.[29] The bottom of the substrate has more time to react than the top, leading to the formation of a gradient in amine groups. Gradient formation is governed by the rate of infusion, the rate of reaction,[30] and the silane concentration.[29, 30] The condensation reaction between surface silanol groups and hydrolyzed APTEOS precursors results in covalent bonding of the aminopropyl groups to the substrate in a gradient fashion. The thickness of the aminopropyl layer as evaluated by ellipsometry[29] on a uniformly modified surface that was soaked in the APTEOS sol for 30 min was 0.5 ± 0.2 nm, which corresponds to approximately a monolayer.[41] The kinetics of the amine deposition on the substrate by ***CRI*** has been thoroughly studied, and shown to be first order following an initial fast reaction of the APTEOS precursors with surface silanol groups.[29, 30]

Following time-dependent modification by amine groups, the gradient surfaces were further modified with the mercaptopropyl silane precursors in a similar fashion for 30 minutes to form multi-component gradients. The thickness of the mercapto layer on the amine -modified surface as evaluated by ellipsometry was 0.3 ± 0.1 nm, which is slightly less than a monolayer. This result suggests that the SH-terminated silane partially inserts in the aminosilane layer to condense with surface or near surface silanol groups. Because surface immobilized amines can catalyze the condensation of organoalkoxysilanes as shown in previous work using a phenylalkoxysilane,[42] it is likely that the mercapto groups are attached in close proximity to the amines.

The ability to prepare multi-component gradients where the changes in surface density of the individual components either **align** (N+S aligned) or **oppose** each other (N+S opposed) is a unique advantage of the ***CRI*** method. Such aligned and opposed multi-component gradients exhibit very different surface chemistries, as demonstrated below. Whether (N+S aligned) or (N+S opposed) gradients are prepared, sol-derived surface silanol groups will also be present with surface concentrations that will vary from bottom to top depending on the level of modification. Oxidation of sulfhydryl to sulfonic acid, which was achieved via immersion in 30% H_2O_2 for 20 min also leads to concomitant protonation of the amine groups. Chemical characterization of these chemically complex surface functionalized surfaces is described below.

3.4.2 Gradient characterization

3.4.2.1 XPS spectroscopy

The presence and extent of modification of the surfaces with amine and thiol as well as the degree of protonation/oxidation were evaluated using **XPS** spectroscopy. **Figure 3.3** shows an overlay of five N1s and S2p **XPS** spectra for the aligned (**a**, **b**) and opposed (**c**, **d**) (N+S) gradients acquired at ~3 mm intervals from the high amine end (position 5) to the low amine end (position 1). The N1s peak in the **XPS** spectra shown in **Figure 3.3 (a, c)** appears as a doublet with binding energies (BE) ~399 and ~401 eV, corresponding to free amine and protonated/H-bonded amines, respectively, in accordance with the literature.[29, 36, 37, 43-46] Deconvolution of the N1s spectra into two components (protonated; nonprotonated) for the aligned gradient yields a N^+/N peak area ratio in the dry state of 0.50 at the top or low amine end of the gradient and 0.28 at the bottom of the gradient. Similar results were obtained for the opposed gradient. The extent of protonation is smaller at the bottom or high amine end of the gradient and could result from changes in the pK_b of the immobilized base due to changes in hydrogen bonding and the local chemical environment[47]

or because a greater number of surface silanol groups are present at the top of the gradient, which can protonate nearby amines. Alternatively, it could be due to the fact that the percent ionization of a weak base (or acid) depends on its concentration. As the surface concentration decreases, percent ionization (protonation) increases.

For S2p, the spectrum consists of one peak at a binding energy of 163.5 eV (see **Figure 3.3 (b, d)**) in agreement with reported values.[13, 14, 21] For the aligned gradient, both the N1s and S2p signals increase from top (low amine end, position 1) to bottom (high amine end, position 5) while for the opposed gradient the N1s signal increases while the S2p decreases. These trends indicate the presence of multi-component gradients in the same or opposing directions.

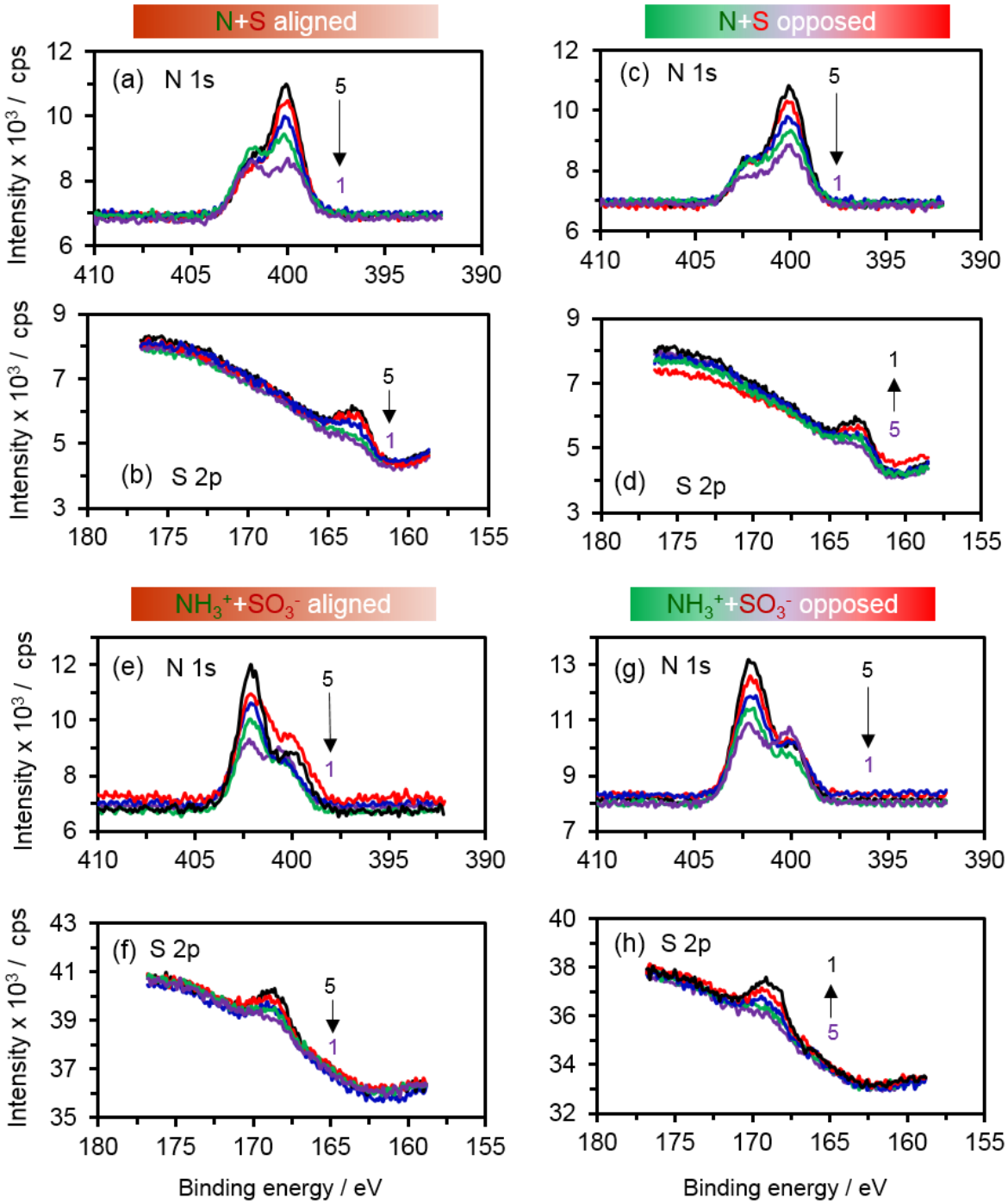

Figure 3.3: XPS spectroscopy N1s and S2p spectra acquired along the length of the charged and uncharged multicomponent gradients at ~3 mm intervals. Arrow indicates the direction from bottom (high amine end, 5) to top along the gradient (low amine end, 1). The charged gradients were prepared by exposure to hydrogen peroxide for 20 min.

To oxidize the sulfhydryl groups on the surface, the substrates were immersed in 30% H_2O_2 for 15, 20 or 30 min and **XPS** data were then acquired along the length of each substrate at ~ 3 mm intervals as shown in **Figure 3.4**. Following a 20-minute exposure to H_2O_2, the peak at 401.5 eV increases significantly and a new peak at a binding energy of 168.5 eV appears, consistent with the formation of $SO_3^{-\cdot}$ It's unlikely that the hydrogen peroxide simultaneously oxidizes NH_2 to a NO_2 compound because a new peak would then appear at 406 eV.[48] Oxidation to a nitroso compound cannot be completely ruled out because it has a similar binding energy to amine groups (~400 eV).[49] However, it's deemed to be unlikely because the peak at 400 eV drops in intensity while the peak at 401.5 eV (protonated amine) significantly increases upon oxidation (not the other way around).

The extent of protonation of the NH_2 peak and the appearance of the SO_3^- peak depend on time of exposure to H_2O_2. A 15 min exposure to H_2O_2 (**Figure 3.4**) caused partial oxidation of SH (BE: 163.5 eV) to SO_3^- (BE: 168.5 eV) and partial protonation of surface NH_2 (BE: 399.6 eV) to NH_3^+ (BE: 401.3 eV). Exposure for 20 and 30 min converted all SH to SO_3^- and a correspondingly larger fraction of NH_2 groups to NH_3^+. After the longer immersion times, **Figure 3.4 (a** and **b**), the peak intensity for NH_3^+ and SO_3^- decreases from the high amine end (bottom, position 5) to the low amine end (top, position 1), confirming the formation of an aligned multi-component charge gradient. Similarly, the gradual decrease in the intensity of NH_3^+ and increase in intensity of SO_3^- from bottom to top in **Figure 3.4 (c,** and **d)** confirms the presence of an opposed multi-component charge gradient. Deconvolution of the N1s spectra into two components now yields an N^+/N peak area ratio of 0.60 at the top or low amine end of the gradient and 0.75 at the bottom of the gradient indicative of a significantly greater protonation of the amine groups on the surface.

Given the well-known oxidation of thiols by hydrogen peroxide, the appearance of SO_3^- groups upon immersion of the thiolated substrates in hydrogen peroxide is expected.[50] However, the basis for protonation of amine groups is less obvious. Because the pK_a of H_2O_2 is 11.6,[51] it is unlikely that hydrogen peroxide is responsible for amine group protonation. If the degree of amine protonation were due to pH alone, it would be independent of exposure time to H_2O_2. Interestingly, based on **Figure 3.4,** it is clear that amine protonation parallels thiol oxidation, indicating that thiol

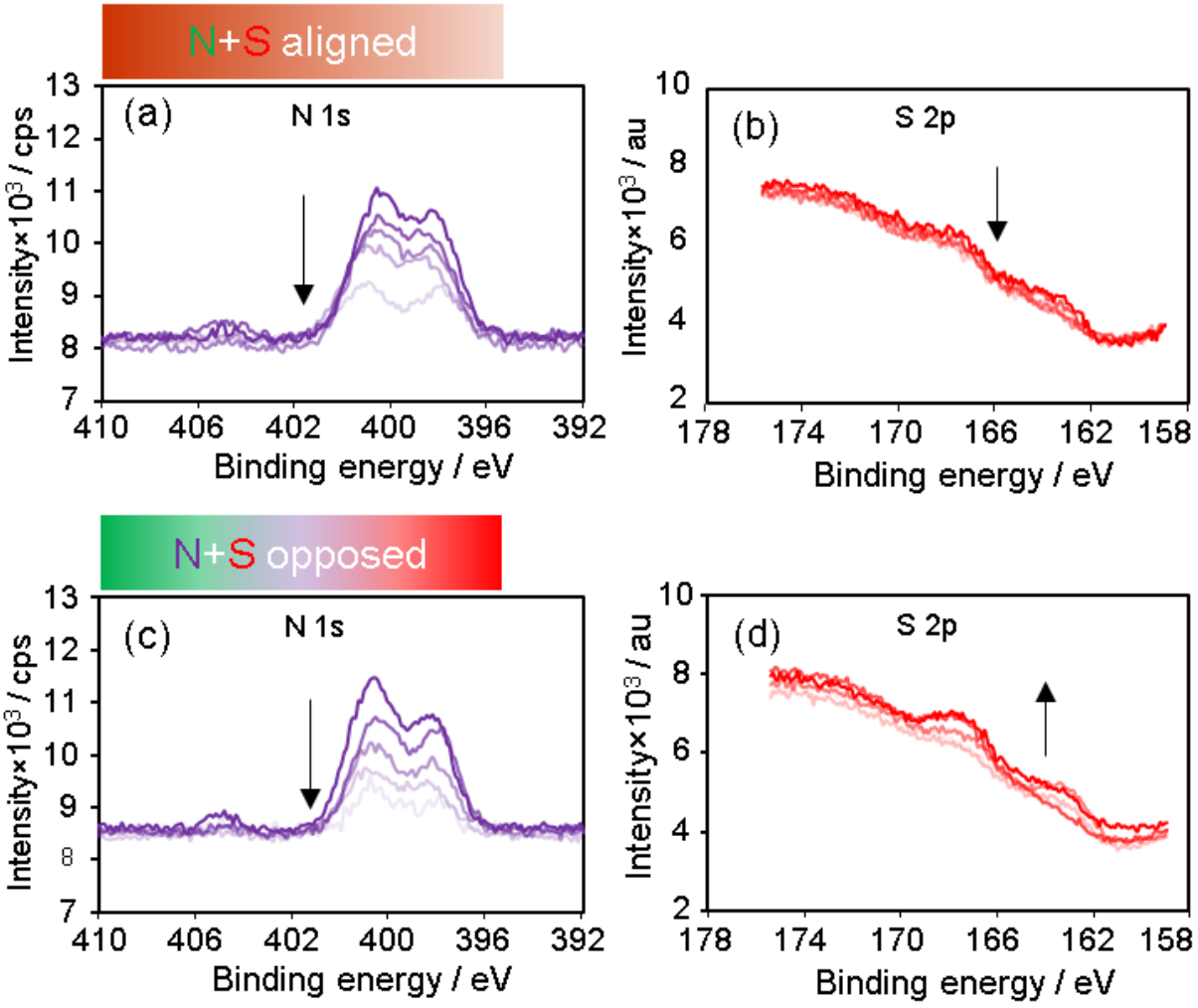

Figure 3.4: (**a, c**) N1s and (**b, d**) S2p **XPS** spectra acquired along the length of partially oxidized multi-component gradients at ~3 mm intervals after immersion in hydrogen peroxide for 15 minutes. The arrow indicates the direction from bottom to top along the gradient.

oxidation leads to contemporaneous amine protonation. Neighboring SO_3^- groups can then act as counter ions for nearby NH_3^+ groups. That is, when hydrogen peroxide oxidizes the sulfhydryl groups, the amine becomes protonated due to the close proximity of the two groups (acid and base) on the surface.[26-28] The two charged groups are cooperatively interacting in the sense that to obtain strong protonation of the amine groups, SO_3^- must be nearby and able to influence the amine pKa. The complete disappearance of the SH peak indicates that sulfhydryl groups have been oxidized, but some free amine remains **(Figure 3.3 a, c).** This result suggests that the surface concentration of thiol is lower than that of the amine, otherwise more of the free amines would have been

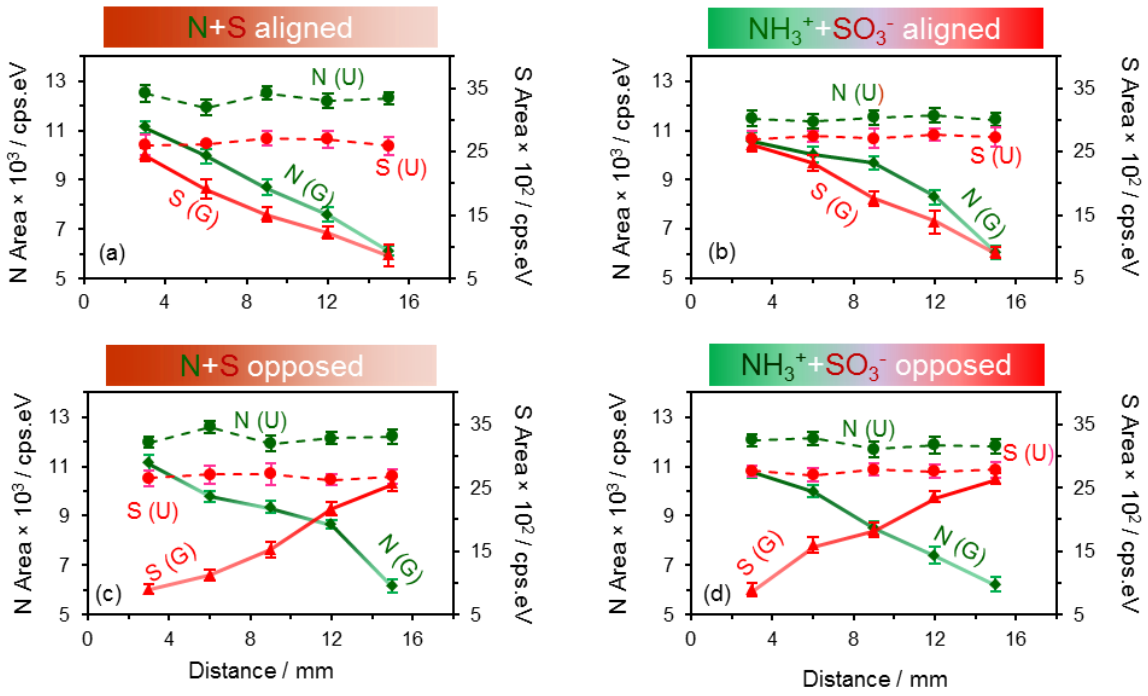

Figure 3.5: N1s and S2p **XPS** peak areas as a function of distance from bottom (3 mm) to top (15 mm) along the length of the multi-component gradients and uniformly modified ((N+S) or (NH_3^+ + SO_3^-)) substrates. Aligned and opposed gradients (G), solid lines; uniformly modified surfaces (U), dashed lines. Error bars represent the standard deviation of three replicate measurements acquired at each position.

protonated. This observation is consistent with the 5x lower concentration of thiol relative to amine in the respective alkoxysilane solutions. The weakly acidic silanol groups can also protonate the amine[36] as evident in the **XPS** spectra acquired from samples that have not been oxidized.

To better understand the gradient profile relative to uniformly modified substrates, the areas under the N1s and S2p peaks for the (N+S aligned), (N+S opposed) and (N+S uniform) and the oxidized/protonated analogs ($NH_3^+ + SO_3^-$ aligned), ($NH_3^+ + SO_3^-$ opposed), and ($NH_3^+ + SO_3^-$ uniform) were integrated. **Figure 3.5** shows the resultant profiles. The error bars represent standard deviations for three replicate measurements from a single sample; sample-to-sample variations are typically higher (~10%).[29, 30] As expected, the area under the N or S peaks changes along the length of the substrate for the gradient materials whereas for the uniformly modified controls, the areas are constant. The area under both N and S peaks increases from top to bottom (high amine end) for the aligned gradient; however, for the opposed gradients, the N peak area increases while the S peak decreases.

3.4.2.2 WCA analysis (Wettability)

WCAs facilitate rapid acquisition of information about hydrophobicity and hydrophilicity originating from the polarity differences along the length of the samples. The surface polarity and hence the WCA is determined by cooperative effects of the various component functional groups present on the film surface. **Figure 3.6A** shows images of water drops spaced ~ 3 mm apart along the length of the gradient surfaces while **Figure 3.6B** shows results for the uniformly modified substrates. The degree to which the water wets the surface depends on its position along the length of the gradient film as well as the type of surface. Water wets the (NH_3^++ SO_3^-) surfaces more than the (N + S) surfaces, reflecting stronger interactions with the former. WCAs are constant along the

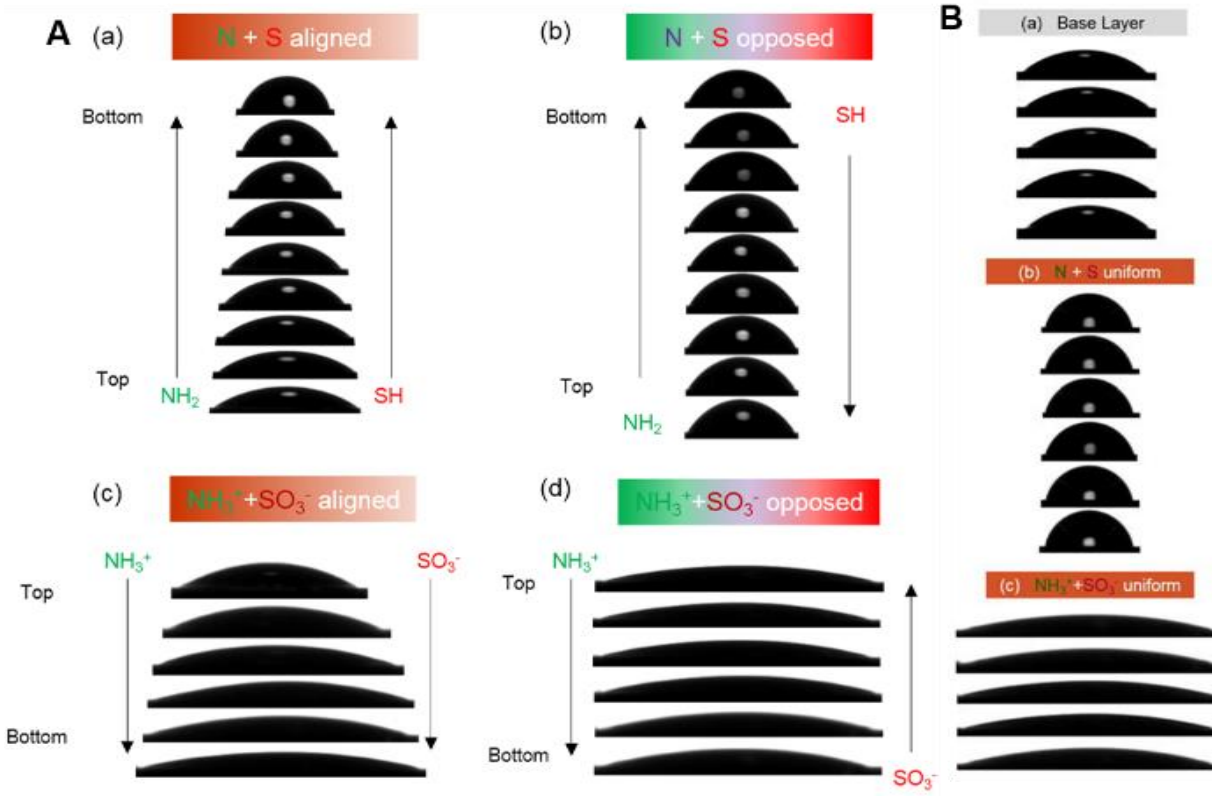

Figure 3.6: Photograph of water droplets along the multi-component gradient surfaces from bottom to top (A) and along a base-layer coated substrate and uniformly modified multi-component surfaces (B). The substrate dimensions were (30-35) mm x (15-20) mm.

length of the substrate for (N + S uniform), (NH_3^++ SO_3^- uniform) and base-layer coated substrates, indicative of a near uniform distribution of the functional groups.

To better understand how the WCAs change with distance, profile plots were constructed. **Figure 3.7a** shows WCAs obtained for (N + S) gradients while **Figure 3.7b** depicts values obtained for the (NH_3^++SO_3^-) gradients. For comparison, results are also shown for the uniformly

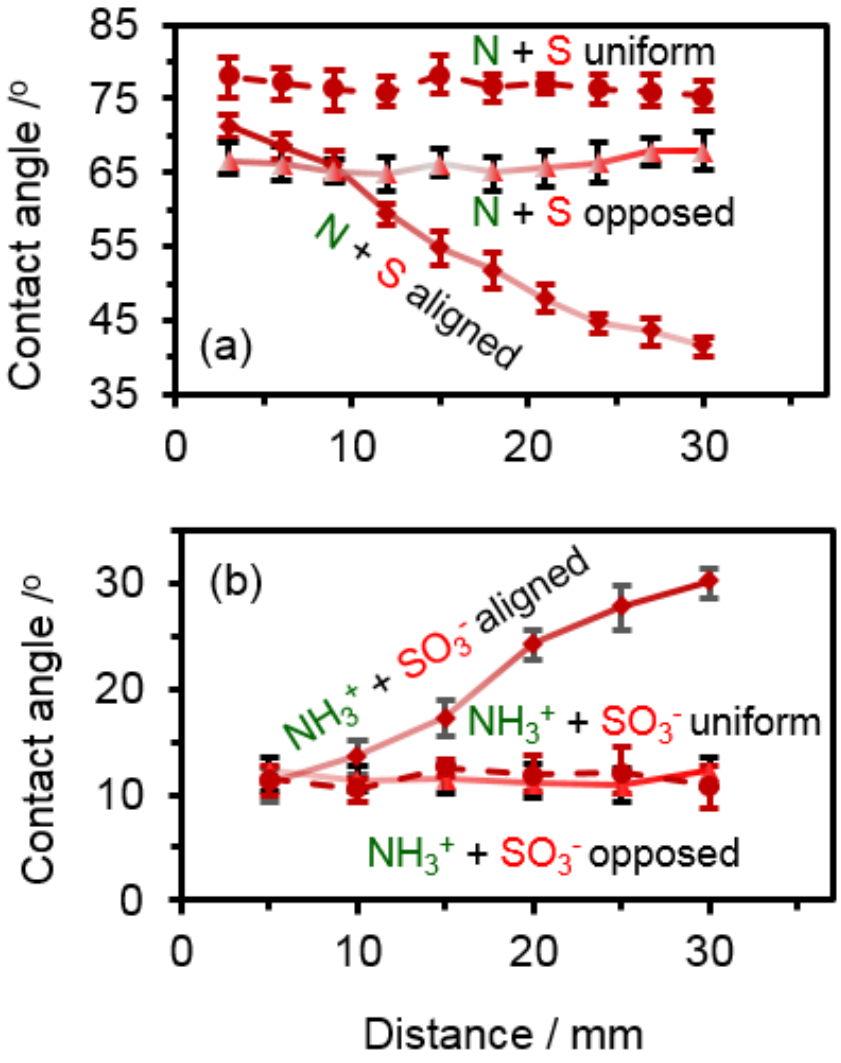

Figure 3.7: WCA as a function of distance from bottom (5 mm) to top (30 mm) along the multicomponent gradients (solid lines) and uniformly modified surfaces (dashed lines). Error bars represent the standard deviation of three replicate measurements acquired at each position.

modified substrates (dashed lines). WCAs for the uniformly modified surfaces are constant with distance. High WCAs (~71°) are found for (N+S) while low WCAs (~11^{o}) are found for the charged (NH_3^++ SO_3^-) surfaces. Uniformly high contact angles for the unoxidized substrate are attributed to the presence of the organic modifier on the surface.

For comparison, the base-layer coated substrate has a contact angle of 33-35^{o}, irrespective of exposure to hydrogen peroxide. For the (N+S aligned) gradient (**Figure 3.7a**), the contact angle gradually decreases from ~ 71^{o} to 42^{o} from bottom to top. This finding agrees with **XPS** analysis (**Figure 3.6**) that shows a greater concentration of organic moieties (aminopropyl and mercaptopropyl groups) at the bottom relative to the top, which contains mostly silanol functionality. The CA at the top of the multicomponent aligned gradient (~ 42^{o}) is only slightly higher than that observed on the base-layer coated substrate (~34^{o}), which is also consistent with a low degree of modification.

For the (N+S opposed) gradient, the WCA is ~ 63-65^{o} and essentially invariant with distance. In this case, both the bottom and the top each contain organic moieties in addition to residual unreacted silanol groups. The WCA is only slightly lower than that observed at the bottom on the (N+S aligned) gradient (~68^{o}) but ~7-10^{o} lower than the value observed on the (N+S uniform) film. This observation indicates the concentration of organic moieties is higher for uniform modification compared to an opposed gradient with predominately one component (mercapto or amine) on each end.

Overall, the oxidized/protonated gradients have 10 – 50° lower contact angles due to stronger interactions of NH_3^+ and SO_3^- with water. Emphasizing this point, for the (N + S uniform) substrate, WCAs are ~71-74^{o}, whereas (NH_3^++ SO_3^- uniform) WCAs are 11-13^{o}. For the oxidized/protonated gradients, similar trends are observed as that noted for the uncharged

gradients. That is, the opposed charge gradient shows little change in WCA with distance while the aligned charge gradient shows a significant change. In particular, for the (NH_3^++ SO_3^- aligned) gradient, the WCA increases from bottom (high degree of modification) to top (low degree of modification) while the reverse is true for the uncharged aligned gradient (N + S aligned) and a decrease is observed. The charged groups dominate the wettability in the former, while organic moieties are dominant in the latter. For the aligned charge gradient, the WCAs gradually increase from the bottom (~11°) to the top (30°) while for the (NH_3^+ + SO_3^- opposed) system, the contact angle stays constant (~11°) due to presence of charged species on either end of the gradient.

3.4.2.3 Nanoparticle binding

Another means to characterize the gradient profile and how the amine and thiol groups are spatially distributed involves examining the binding of gold nanoparticles along the length of gradient surfaces.[16, 52-57] It is well known that gold colloids bind to amine and thiol groups through weak and strong covalent bonding, respectively.[58] To explore this path for differentiation of functionality, the surface was first exposed to a slightly acidic citrate-stabilized gold colloid solution for two hours, washed and dried, and then imaged using **AFM** microscopy. Immobilized gold nanoparticles on a defined region along the length of the substrate were then counted and the results plotted with respect to distance along the length of the substrate. This approach has been previously used to characterize amine gradients.[16, 52-57]

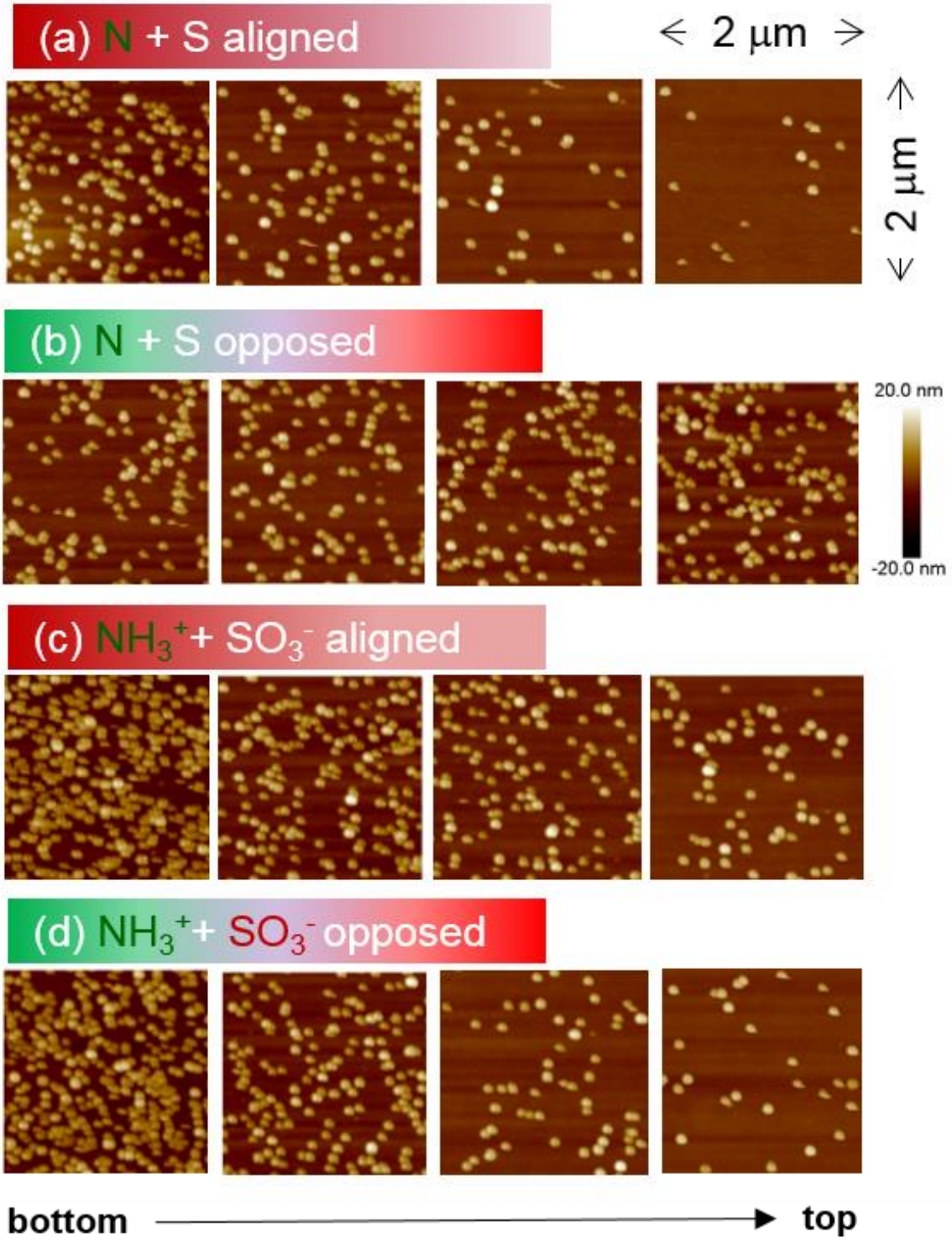

Figure 3.8: Atomic force microscope images (2×2 µm^2) at four different locations ~ 4 mm apart along the multi-component gradients following immersion in a solution containing gold nanoparticles for two hours followed by rinsing.

(NH_3^+ + SO_3^- aligned), and (NH_3^+ + SO_3^- opposed) surfaces after exposure to the gold colloid solution. **AFM** images were acquired from bottom (high amine end) to top at ~4 mm intervals. Images for all the modified samples show small clusters of nanoparticles (~20-35 nm in diameter) randomly scattered across the surface with surface density depending on the extent of modification. For the (NH_3^+ + SO_3^- uniform) film in **Figure 3.9**, the density of 'clusters' was approximately double that observed on the (N + S uniform) film. In contrast, negligible nanoparticle adsorption was observed on the unmodified base-layer coated substrate, which has only SiOH or $Si(OR)_n$ (**Figure 3.9**). The root-mean-square roughness for the base-layer coated substrate was ~1.8 nm for a 2 x 2 μm^2 region.

To better understand the gradient profile, the number of nanoparticles in three 2 × 2 μm^2 images was counted using the ImageJ and NanoScope V software as described in the experimental section and plotted as a function of distance (mm). **Figure 3.10** shows the total number of Au nanoparticles immobilized on the (a) (N+S aligned), (N+S opposed); (b) (NH_3^+ + SO_3^- aligned), (NH_3^+ + SO_3^- opposed) gradients and (c) uniformly modified substrates. The (N+S uniform) and (NH_3^+ + SO_3^- uniform) surfaces provide an interesting reference. First, the gold nanoparticle density is constant along the surface, reflecting a homogeneous substrate. The surface density for the (N+S uniform) is ~75 per μm^2 but the gold nanoparticle density is ~ 125 per μm^2 for the (NH_3^+ + SO_3^- uniform) surfaces. Given that the gold nanoparticles are stabilized by citrate ions and are therefore negatively charged, electrostatic interactions are clearly stronger than polar interactions under the experimental conditions employed. Overall, gold nanoparticle density provides a sensitive metric for electrostatic interactions at charged surfaces.

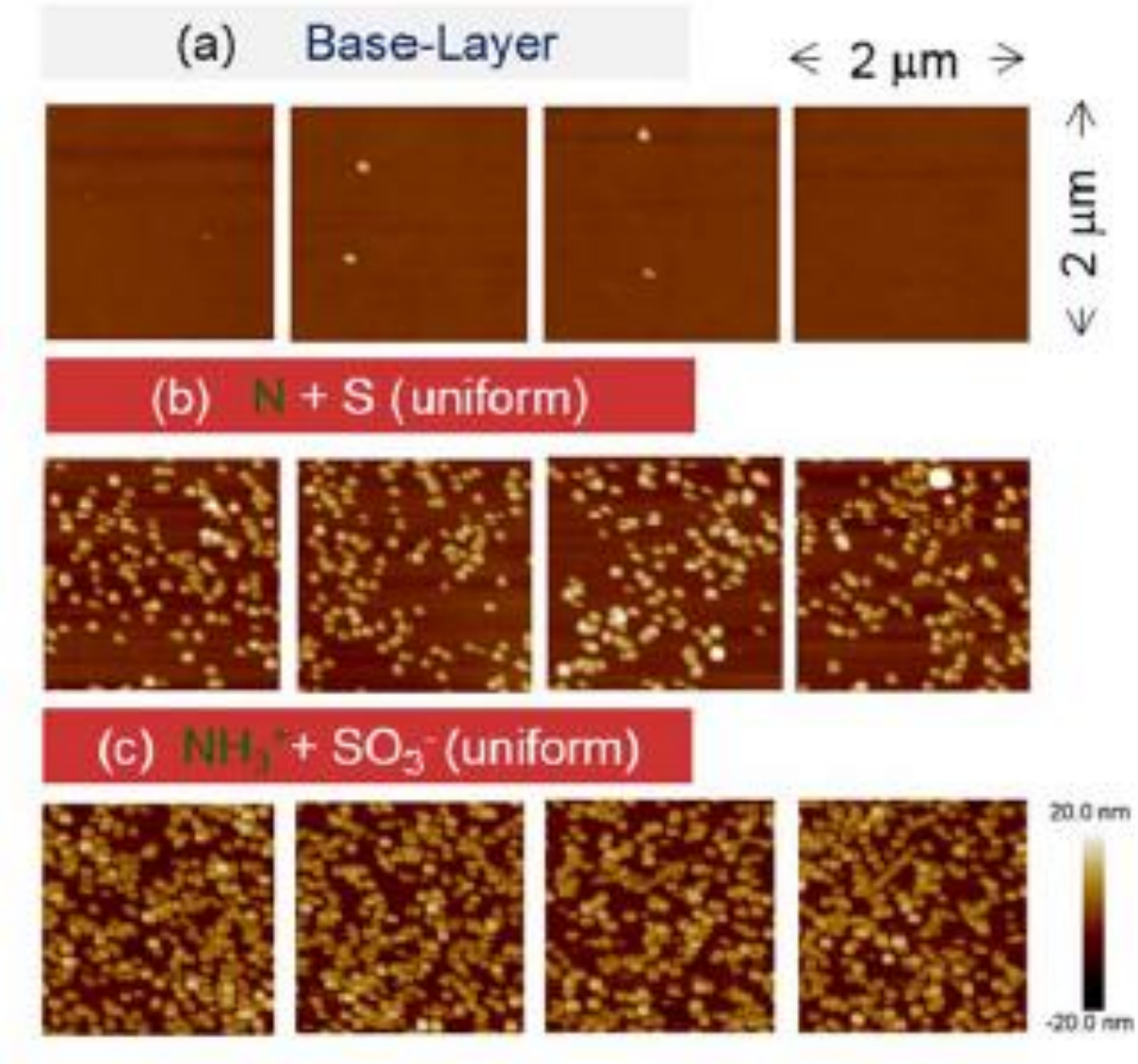

Figure 3.9: Atomic Microscopic images (2 × 2 µm2) of (a) a base-layer coated substrate and (b, c) uniformly modified multi-component films at four different locations ~ 4 mm apart along the length of the substrate following immersion in a solution containing gold nanoparticles for two hours.

For the aligned N+S gradient, there is a clear difference in the number of gold particles from the bottom (high amine/thiol, ~85 per μm^2) to the top (low amine/thiol, ~9 per μm^2), **Figure 3.10 (a)**. Furthermore, the (N+S aligned) gradient has a greater nanoparticle density compared to

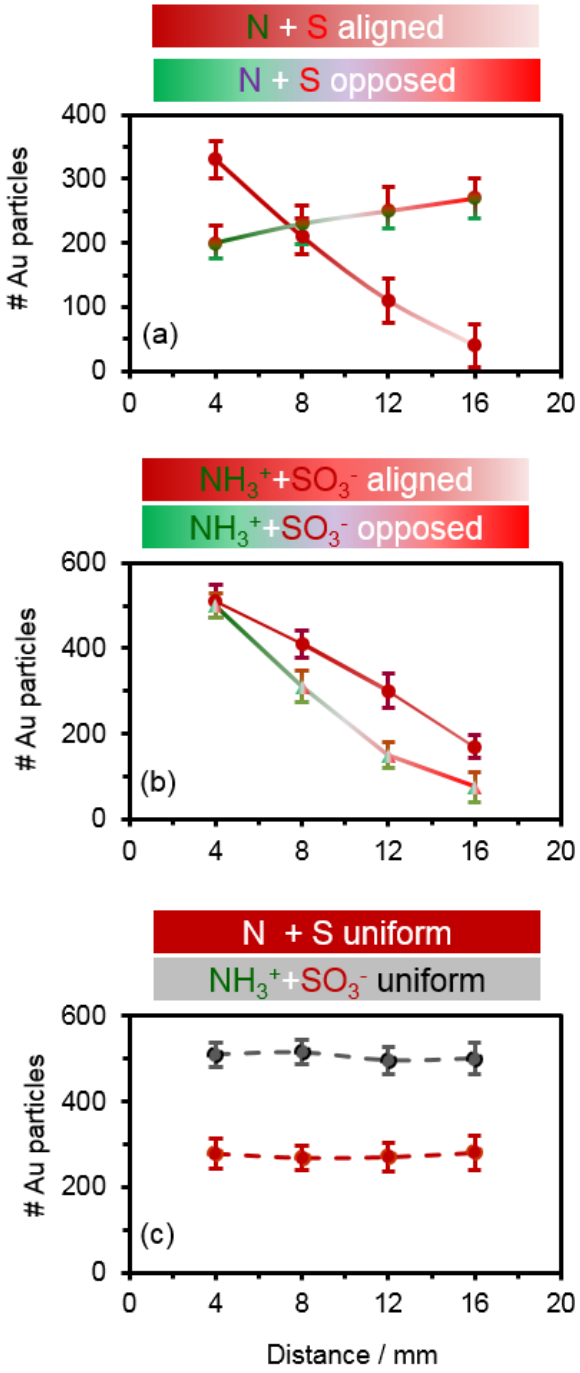

Figure 3.10: Number of gold nanoparticles immobilized on a 2 × 2 μm^2 section of (a, b) the multi-component gradients and (c) uniformly modified substrates as a function of distance from bottom (3 mm) to top (15 mm). The error bars represent the standard deviation of three images acquired at each position.

end leads to a larger number of bound gold nanoparticles. The nanoparticle density at the top or lightly modified end of this gradient is < 12 per μm^2, which approaches that for the substrate and is consistent with a low degree of modification.

For the opposed gradient, the variation in the number of Au nanoparticles with distance is much smaller because of the predominance of one surface group (either NH_2 or SH) at each end. The number of attached Au nanoparticles is somewhat higher on the SH end than the NH_2 end, consistent with the greater affinity of SH towards Au nanoparticles. In agreement with a somewhat higher coverage of organic moieties on the uniformly modified substrate noted in WCA measurements, there is a greater number of immobilized nanoparticles compared to either end of the opposed gradient, as shown in **Figure 3.10c**.

Different results are observed for the charge gradients (NH_3^+ + SO_3^- aligned and opposed) compared with uniformly modified substrates (**Figure 3.10 b, c**). As noted above, for uniformly modified substrates, a greater number of nanoparticles is immobilized on the charged surface compared to the original uncharged surface. For the charge gradients (NH_3^+ + SO_3^- aligned and opposed), a greater number of bound gold nanoparticles is observed on the high amine end, compared to the uncharged analogs (N+S) (~ 125/μm^2 vs. ~50-75/μm^2). There is also a substantially lower gold nanoparticle density for the SO_3^- end of the charged opposed gradient (~12/μm^2) compared to the original surface that contained predominately SH groups (~60/μm^2). Electrostatic repulsion between SO_3^- and the negatively charged gold nanoparticles accounts for this observation. Furthermore, for the opposed charge gradient, the number of nanoparticles drops significantly with distance from bottom to top, whereas on the uncharged opposed gradient, only a slight increase is observed instead. Given that the gold nanoparticles are stabilized by citrate ions and are therefore negatively charged, electrostatic interactions are likely important between the

charged functional groups on the surface and the gold nanoparticles. Understanding these results, requires an understanding of the effective charge along the gradient surfaces, which prompted the ζ investigation described next.

3.4.2.4 Electrokinetic measurements

Electrokinetic measurements can provide detailed information correlating surface composition and charge density, and ultimately interactions between functional groups. This is because the net charge depends on the functional groups present on the surface, their location relative to each other, and the solution pH. By studying the sign and magnitude of the ζ and how it changes with composition, detailed information about the surface composition and the interactions between surface bound functionalities can be elucidated, particularly when combined with **XPS** and the nanoparticle binding experiments.

An electrokinetic potential or ζ develops during flow of electrolyte over a solid (e.g., a polymer coating).[59] This charge is attributed to an electrical double layer formed at the interface. The initial step in evaluating charge density is the measurement of streaming potentials resulting from the pressure-driven flow of an electrolyte solution across a substrate.[59, 60] The ζ values are calculated using the Helmholtz-Smoluchowski equation 3.1,

$$\zeta = \frac{\Delta \mathrm{E}}{\Delta P} \frac{\kappa \eta}{\varepsilon \varepsilon_0} \qquad (3.1)$$

where ΔE is the streaming potential in Volts, ζ is the zeta potential in volts, η is the viscosity of the solution in Pascal-seconds (Pa-s), κ is the solution conductivity in Siemens per meter (S/m), ε is the dielectric constant of the solution, ε_0 is the dielectric permittivity of vacuum, and ΔP is the pressure in Pa.[61]

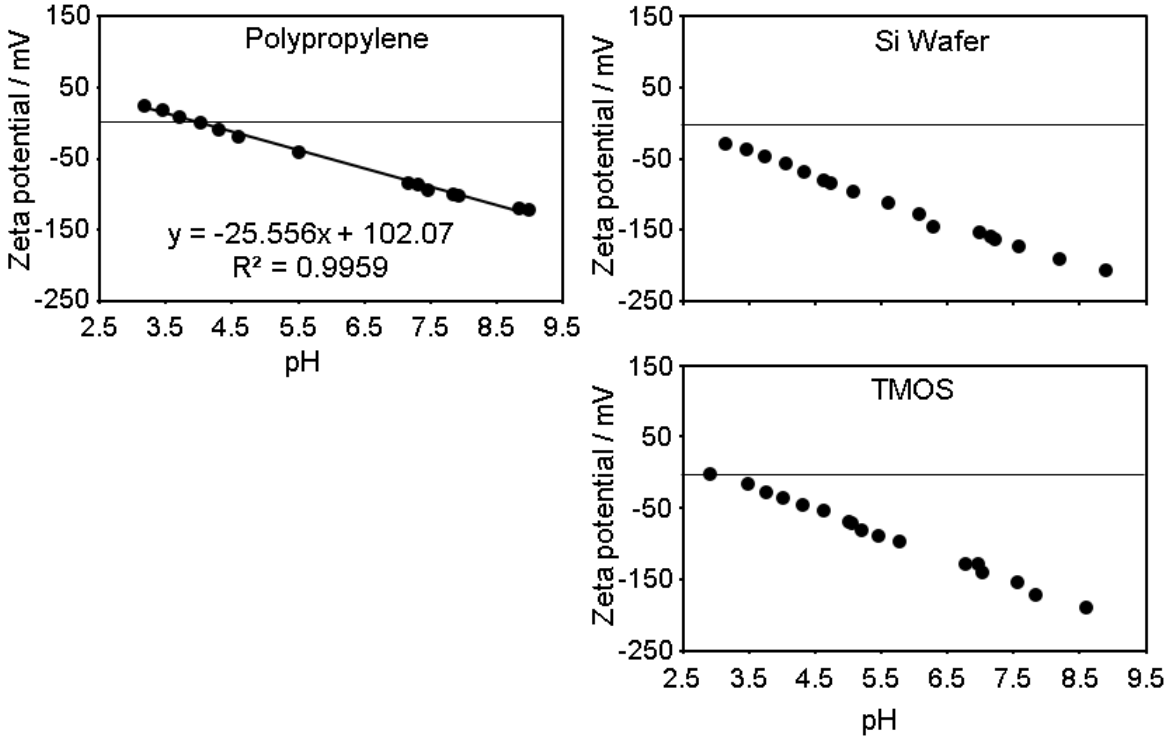

Name	pH	ζ (mV)
Si wafer	5.5	-115
TMOS	5.5	-90
Polypropylene	5.5	-37

Figure 3.11: ζ measured at pH varying from 3 to 9. The ***IEP*** for polypropylene is 3.9, whereas the ***IEP*** for the piranha cleaned Si wafer is 2.6 and 3.4, respectively.

ζ measurements have been used to characterize charged surfaces such as glass modified with aminosilanes,[45] silica nanoparticles[62] and most recently a glass capillary (75 μm id) 400 mm in length containing a gradient in amine and SiOH groups.[15] In the latter case, spatially resolved streaming potential measurements were made by cutting the gradient capillary into small pieces and measuring the average ζ value of each of the segments using a custom built system.[15] Because

the capillary was long and the segments small, this method of characterization proved valuable and the charge at discrete locations along the length of the gradient could be directly evaluated. Using a similar capillary cell design, near surface quaternary charge was investigated for polycation-based modified polyurethanes.[59] Decreasing charge density upon immersion in water was correlated with the instability of contact antimicrobial effectiveness.[59]

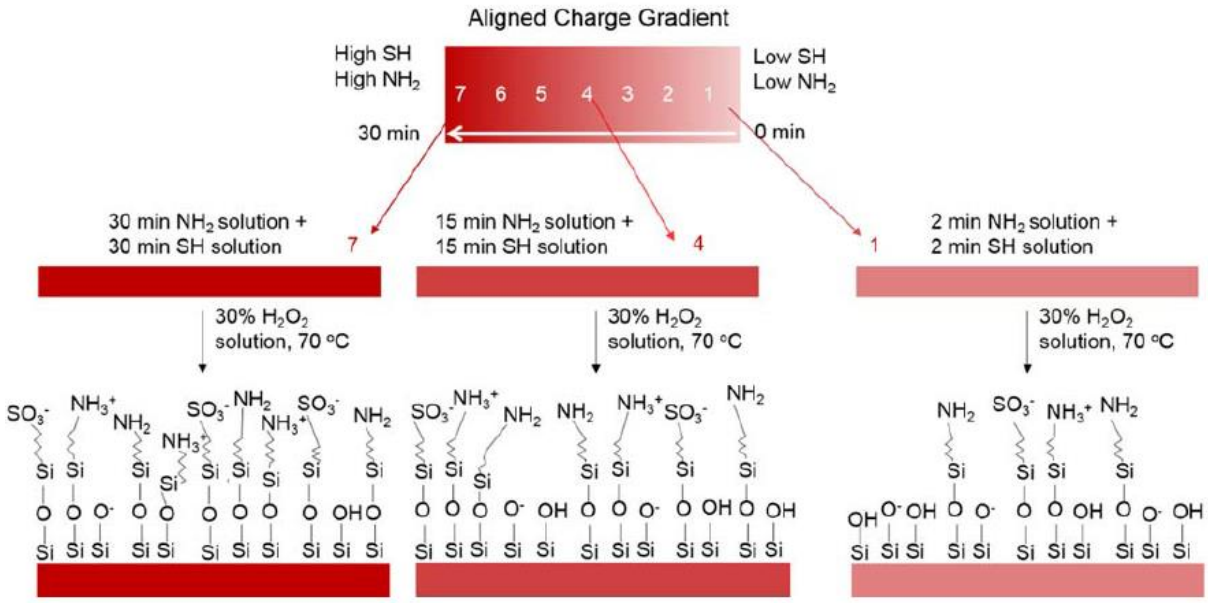

Figure 3.12: Representative samples and surface chemical structure for the ζ measurement. Samples for the ζ measurements were prepared to mimic the surface chemical composition of seven representative regions on an **aligned** charge gradient as shown above.

For flat substrates, which are the subject of analysis herein, a commercial clamping cell was used with streaming potentials resulting from electrolyte flow through a channel between a polypropylene (***PP***) reference film and the substrate **(Figure 3.2)**. From the Helmholtz-Smoluchowski equation, ζ values were obtained, which reflect the charge on the sample relative to the ***PP*** reference. The ζ of ***PP*** was measured as a function of pH (**Figure 3.11)** and then appropriately subtracted from the measured ζ for the full channel at each pH as described by the

manufacturer. The ζ values and isoelectric point (***IEP***) of ***PP*** were in agreement with Anton Paar electrokinetic analyzer specifications. As references, the ζ value of a piranha cleaned silicon wafer and the base-layer coated substrate at pH 5.5 were found to be -90 and -115 mV, respectively.

With a gradient substrate, only the average ζ can be measured. To obtain information about surface charge at discrete positions along the gradient, seven samples (size: 2 × 5 cm) were prepared as shown in **Figure 3.12**. Each sample mimics a certain surface chemical composition along the length of the multi-component gradient. The first set of substrates was designed to mimic various positions from bottom to top on an **aligned** multi-component gradient. Thus, sample 7 was immersed in the aminosilane for 30 min followed by mercaptosilane for 30 min to represent a position at the high amine/high sulfur end (bottom) of an aligned gradient, while sample 1 was immersed in the respective solutions for 2 min each to represent a position at the low amine/low

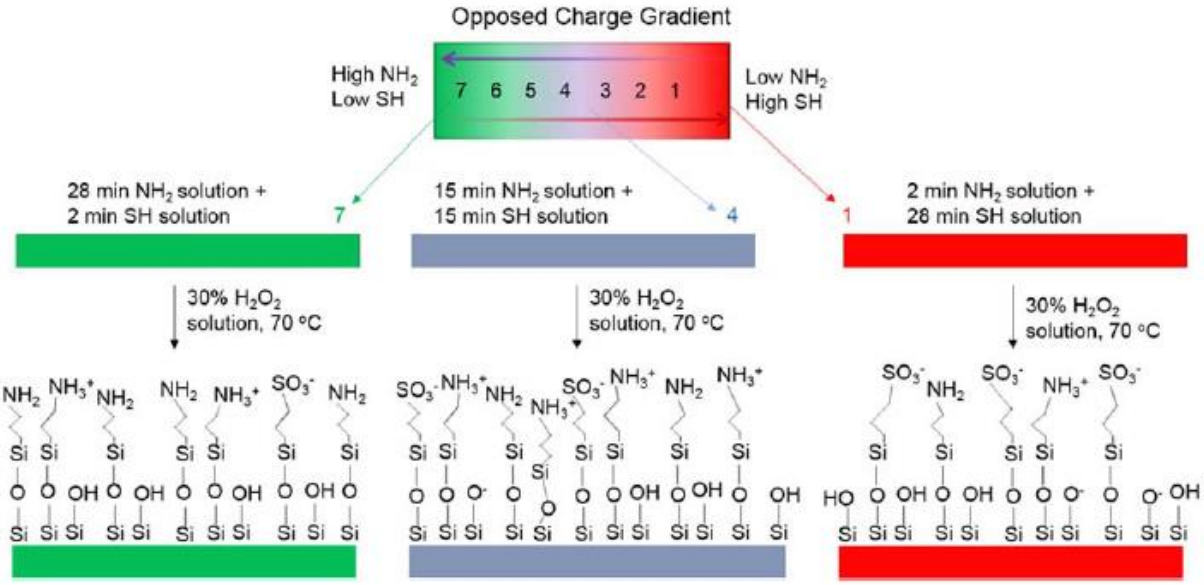

Figure 3.13: Representative samples and surface chemical structure for the ζ measurement. Samples for the ζ measurements were prepared to mimic the surface chemical composition of seven representative regions ion the **opposed** gradient as shown above.

sulfur end (top) of the gradient. To oxidize/protonate the surface, the samples were immersed in H_2O_2 for 20 min. Another set of samples with a constant total reaction time in the two different alkoxysilane solutions was prepared to mimic the surface chemical composition of the **opposed** multi-component charge gradient as shown in **Figure 3.13**. In this case, sample 7 was immersed for 28 min in aminosilane and 2 min in mercaptosilane while sample 1 was immersed in aminosilane for 2 min and mercaptosilane for 28 min. Sample 1 represents a particular position at the low amine/high sulfur end of the opposed gradient while sample 7 represents a position on the high amine/low sulfur end of the gradient. To oxidize/protonate the surface functional groups, the samples were immersed in H_2O_2 for 20 min. In all these samples, surfaces contain the desired functional groups and residual surface silanols.

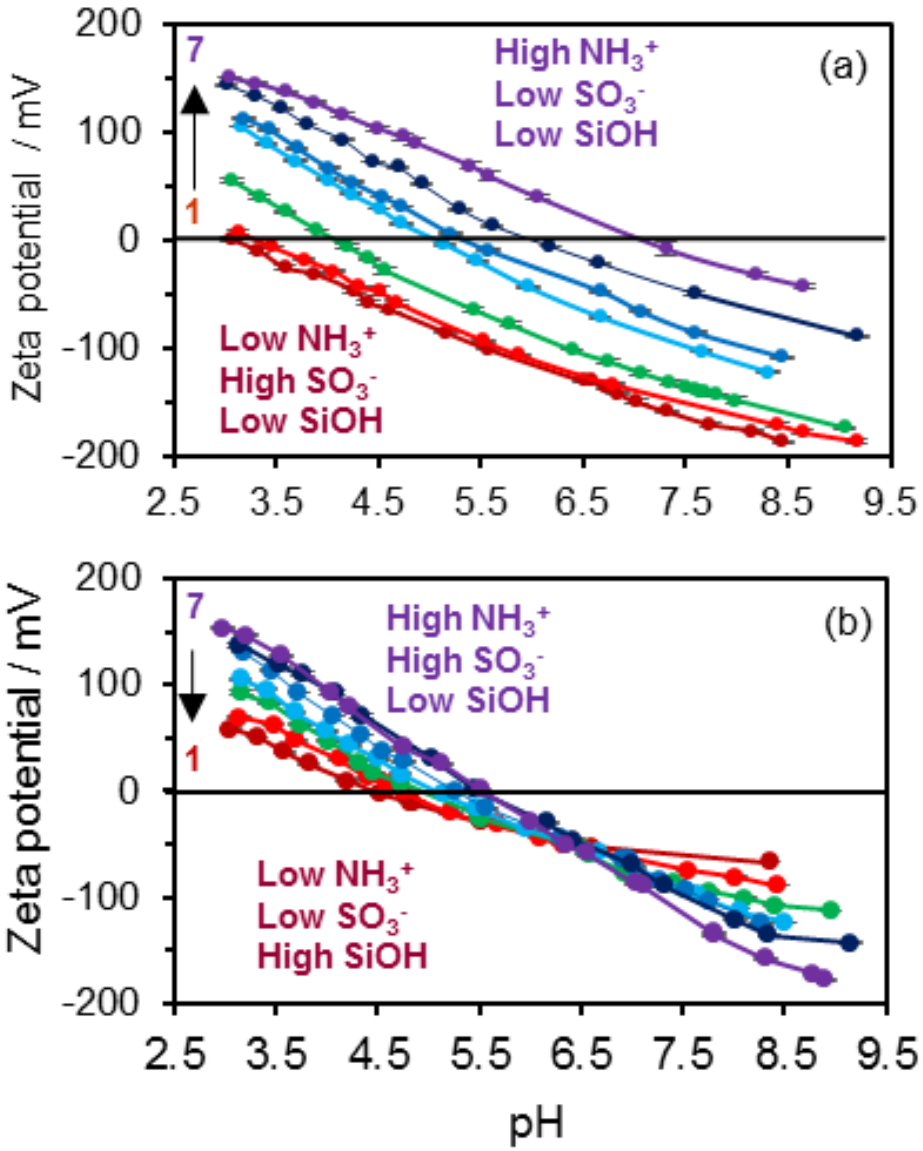

Figure 3.14: ζ values as a function of pH for the samples that mimic (a) an opposed multi-component gradient and (b) an aligned multi-component gradient. For (a) the reaction time in the aminosilane solution decreased from 28, 25, 20, 15, 10, 5 to 2 min while the reaction time in the mercaptosilane solution increased from 2, 5, 10, 15, 20, 25 to 28 min. Total reaction time with both silanes was 30 min. For (b), the reaction time in each silane solution increased from 2, 5, 10, 15, 20, 25 to 30 min. The total reaction time in the silane solutions was thus 4 10, 20, 30, 40, 50, and 60 min.

Figure 3.14 shows the variation in ζ values from pH ~3 to ~8.5 for the multi-component films designed to mimic the surface of an opposed gradient (**Figure 3.14a**) and an aligned gradient (**Figure 3.14b**). For comparison, the ζ values were determined for samples that mimic "single"-component amine and sulfonic acid gradients, **Figure 3.15,** and a base-layer coated slide **(Figure 3.12).** In both these cases, an opposing gradient in silanol groups also exists. For all samples, the ζ decreases in a near linear fashion as the electrolyte pH increases. Interestingly, the variation in ζ with pH is very different on the surfaces designed to mimic an opposed vs. aligned gradient. For the surfaces that mimic an aligned gradient, in particular, there is a distinct change in slope near pH 6.5 for the substrates that were not modified as heavily and thus have a higher density of silanol groups on the surface (e.g., samples 1→5). On the "single"-component sulfonic acid surfaces, a change in slope is also observed but is not quite as pronounced as that observed on the multicomponent surfaces, **Figure 3.15.** As a consequence of this change in slope, for the aligned gradient, there is a point at pH ~6.5 where all seven surfaces have the same surface charge (**Figure 3.14b**). This "point of intersection" does not appear in the samples that represent an opposed gradient, which look very similar to the "single"-component amine samples but have a smaller positive surface charge due to neutralization by nearby sulfonic acid. What this result signifies is that at pH 6.5, the aligned multi-component surface is not a gradient at all since the surface has a near constant ζ of ~ –55 mV at all positions along its length. At a pH > 6.5, however, the surface charge becomes more positive as the extent of modification decreases (7→1) whereas at a pH < 6.5, the surface charge becomes more negative as the modification decreases (7→1). In contrast, for the seven samples representing the opposed gradient, the ζ vs. pH curves are parallel and there is no single pH at which the surface charge is uniform. The gradient in charge always becomes more negative as the extent of amine modification decreases (sample 7 → 1) just as it does on the

"single"- component amine gradients. Further work is needed to confirm the origin of the abrupt change in slope near pH 6.5 for the samples representing an aligned gradient.

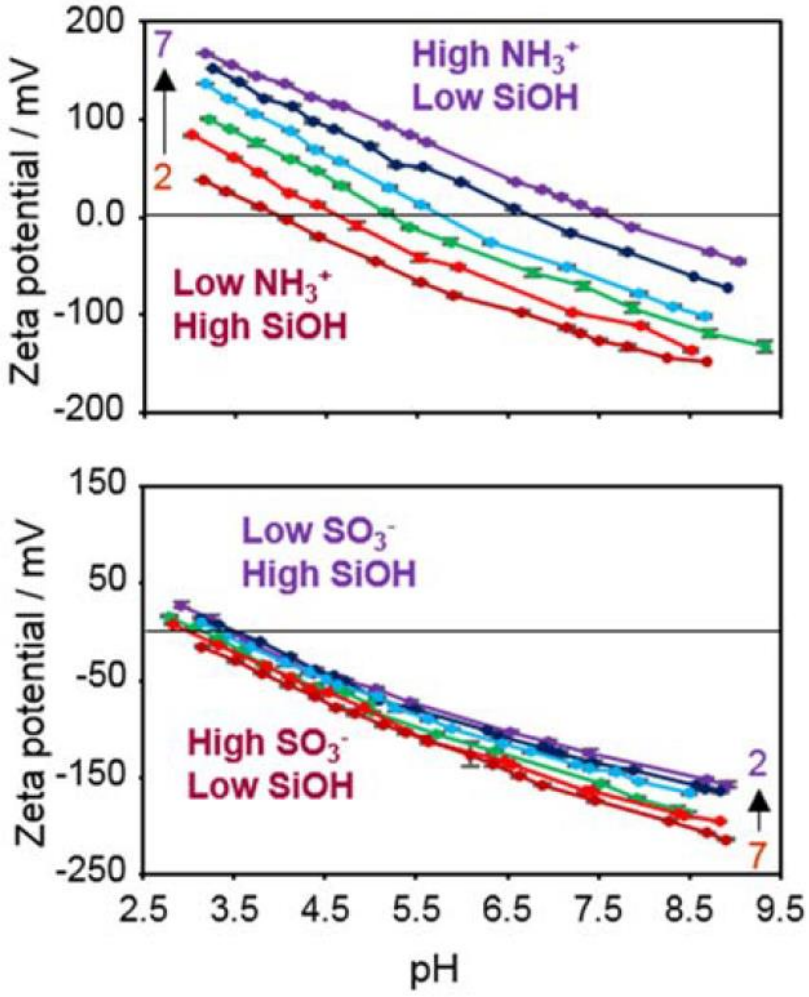

Figure 3.15: ζ values as a function of pH for the samples that mimic (a) a "single"-component amine gradient and (b) a 'single'-component sulfonate gradient. The reaction time in the modifying solution decreased from 30, 25, 20, 15, 10, to 5 min from samples 7→2.

The net charge on the surface at each pH will depend on the extent of modification by amine and thiol, the presence of unreacted silanol groups, and the pKa's of the surface immobilized acidic and basic functionalities. In solution, the pKa's of SO_3H and NH_3^+ are ~ -2.0 and ~10.0,

respectively,[28, 63] while the majority of SiOH groups exhibit a pKa ~ 8.[64] On a surface, however, the pKa's of acidic and basic functionalities can be significantly different from their solution values and can also depend of the local chemical environment.[65-68] As an example, for surface immobilized propylsulfonic acid in mesoporous silica, the pKa obtained from potentiometric titrations was ~2.8-3.0, whereas the pKa for propane sulfonic acid in solution was found to be 1.57 using the same method.[69]

To more easily show how ζ values change with surface modification, the values obtained at one of three different pHs (3.0, 5.5, and 8.0) for each of the seven samples are shown in **Figure 3.16**. At pH 3, more than ~ 100 mV difference in ζ is observed between the surfaces representing the top (sample 1) and bottom (sample 7) of the gradients. Under this condition, the isolated amine groups and residual silanol groups will be fully protonated (e.g., -SiOH, $-NH_3^+$) while the sulfur moieties will exist as either sulfonate or sulfonic acid, depending on the exact value of the surface pKa. The positive ζ values implies there are more free NH_3^+ groups on the surface than SO_3^-. As expected, the surface becomes even more protonated as the immersion time in the aminosilane solution increased (from 1→7). The lowest ζ (near 0) was found on the surface that had a low concentration of amine and a high concentration of sulfonate/sulfonic acid groups (e.g., the top of an opposed gradient) while the largest value was obtained on the surface that had a high surface concentration of amine (e.g., bottom of an aligned or opposed gradient).

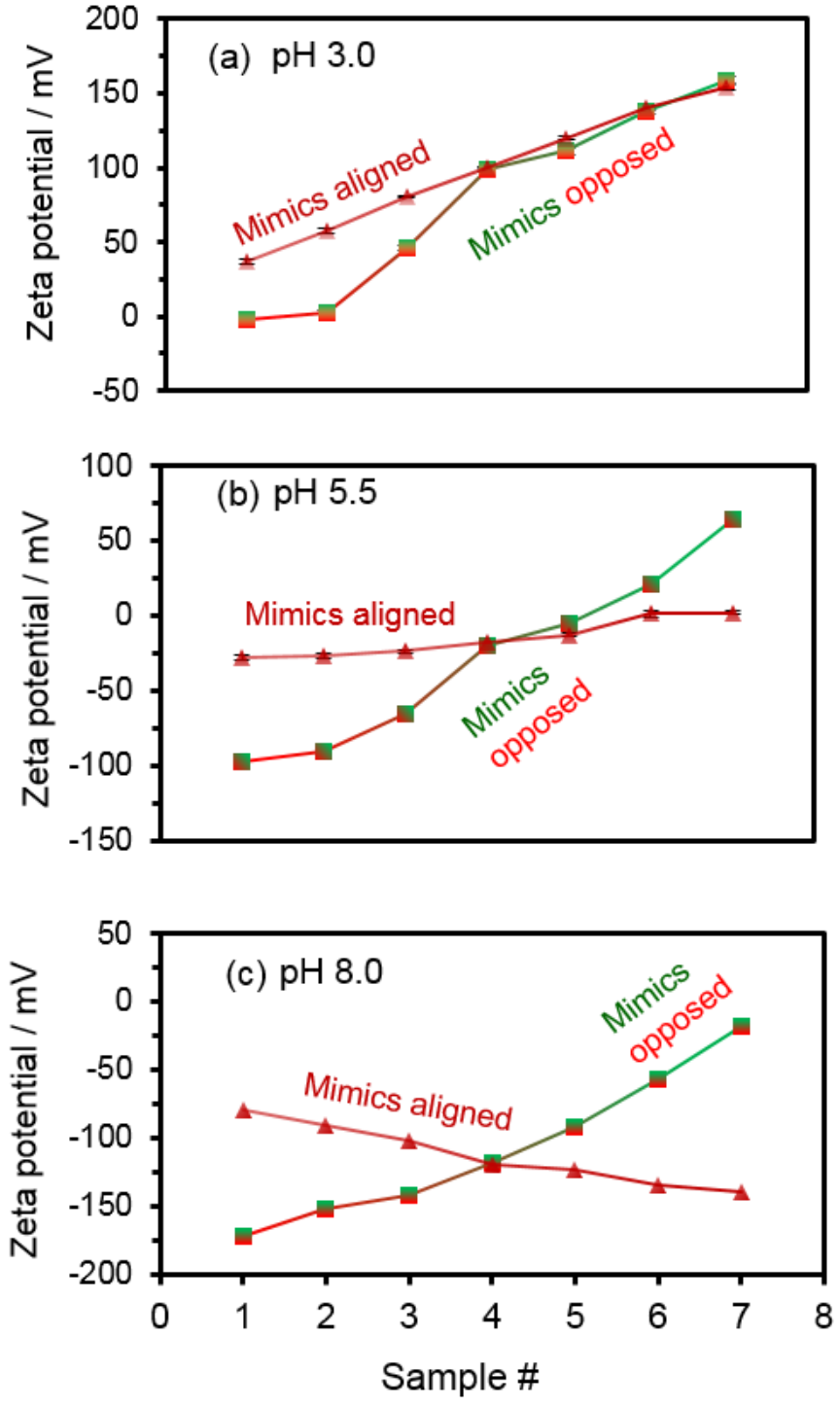

Figure 3.16: ζ measured for the different samples designed to mimic an opposed and aligned multi-component gradient at (a) pH 3, (b) 5.5, and (c) 8.0. Sample 7 represents the bottom (or high amine end) of the gradients.

mimic an aligned and opposed surface. At intermediate pH (5.5), the net charge on the surface was ~ zero for the samples that mimic an aligned gradient; while for the samples that mimic an opposed gradient, the surface charge becomes more positive from top (low amine/high sulfonic acid, sample 1) to bottom (high amine/low sulfonic acid, sample 7). At the opposite end of the pH scale, pH 8, it can be seen that all the ζ values are negative, indicating the functional groups on the

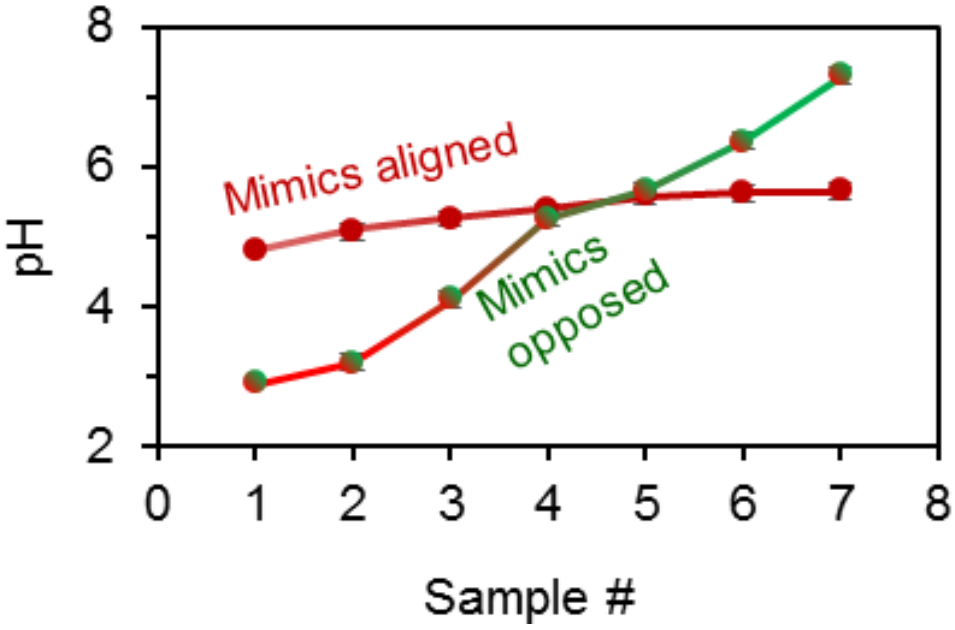

Figure 3.17: pH at the isoelectric point.

surface are largely deprotonated (e.g., $-SO_3^-$, $-SiO^-$, $-NH_2$). Deprotonation is expected based on pKa values of the immobilized acids/bases. For the surfaces that mimic the opposed gradient, ζ values become more positive as the extent of modification by amine increases. This gradient in positive charge is similar to that observed at pH 3 and 5.5. However, for surfaces that represent the aligned gradient, the surface charge becomes ***negative*** by more than 50 mV from samples 1 (low degree of modification) → 7 (high degree of modification). The ability to manipulate the direction of increasing positive charge with pH is clearly evident in the surfaces that mimic the

aligned but not the opposed gradient. For the latter, the change in surface charge with degree of modification always occurs in the same direction regardless of the pH.

Figure 3.17 shows a plot of the pH at the isoelectric point (***IEP***) or zero ζ of the multicomponent samples as a function of the immersion time in the modifying solutions. As the immersion time in the aminosilane solution increases (sample 1 → sample 7), the pH at the ***IEP*** shifts to more basic values (from pH ~3-4 to pH ~ 7-8) for the surfaces designed to mimic the opposed gradient. In contrast, for the samples designed to mimic the aligned gradient, the ***IEP*** changes only slightly (pH ~ 5.1 to 5.6). The neutralization effect or the cooperative effect between the components present in equal amounts keeps the net charge relatively constant.

To estimate the surface charge density, the Gouy equation (equation 3.2 2)[70] and measured ζ values were used,

$$\sigma = \sqrt{8\varepsilon\varepsilon_0}kTNc\ sinh\left\langle\frac{ze\zeta}{2kT}\right\rangle \qquad (3.2)$$

where σ = charge density (C/m^2), k = Boltzmann constant (1.38 × 10^{-23} J/K)), T = 293 K, N = Avogadro's number (6.02 × 10^{23} mol^{-1}), z = counter ion charge (+1), e is the charge on the electron, and c = bulk electrolyte concentration (mol/m^3). The following values were used to calculate the charge density: ε = 80 and ε_o = 8.85 × 10^{-12} F/m. **Table 3.1** shows charge densities and number of charged groups at pH 5.5. There is a much larger difference in surface charge for the surfaces that correspond to an opposed gradient compared to those that represent an aligned gradient. The overall surface charge density of these materials, however, is highly dependent on the pH of the external solution and the surface functional groups (NH_3^+, SO_3^-, SiO^-) present in the films. For a fully deprotonated film such as that shown in **Figure 3.18**, sample 7, the charge density is 0.15 C/cm^2.

Table 3.1: Charge density (C/m^2) (non-absolute) for the different samples designed to mimic an opposed and aligned multi-component gradient at pH 5.5 calculated by Gouy-Chapman equation.

Charge density × 10^{-3} (C/m^2) pH 5.5			Net # charge groups ($1/m^2$)	
Sample #	Mimics opposed	Mimics aligned	Mimics opposed	Mimics aligned
1	-13	-2.2	7.9×10^{16}	1.4×10^{16}
2	-11	-2.1	6.8×10^{16}	1.3×10^{16}
3	-6.4	-1.8	4.0×10^{16}	1.1×10^{16}
4	-1.5	-1.4	0.95×10^{16}	0.8×10^{16}
5	-0.4	-1	0.23×10^{16}	0.6×10^{16}
6	1.5	0.08	9.7×10^{16}	0.05×10^{16}
7	6.1	0.15	3.8×10^{16}	0.1×10^{16}

3.5 Surface chemistry

Based on **XPS** analysis, both aligned and opposed oxidized gradients contain an excess of amine groups relative to thiol groups over the entire substrate from top to bottom. Since the amine is deposited first and can act as a condensation catalyst,[42] thiol likely deposits in close proximity to the amine sites and then elsewhere. Upon oxidation of sulfhydryl to sulfonic acid, the adjacent amine becomes protonated, forming an ionic pair. The remaining amine groups not adjacent to sulfonic acid remain free or weakly H-bonded to adjacent weakly acidic surface silanol groups.

At pH ~3, positive ζ values support the results of **XPS** studies in that protonated amine groups dominate charge on the surface for all samples. Isolated amine and residual silanol groups will be fully protonated but a large fraction of the free sulfonate groups will be negatively charged. As the degree of modification by amine increases, the surface charge increases. For samples 5-7

that represent the high amine end on the aligned (high amine, high sulfonic acid) and opposed (high amine, low sulfonic acid) gradient (**Figure 3.16**), ζ values are nearly identical. The surface charge is therefore not dominated by the sulfonate groups and there are relatively few free groups. This follows from the much lower quantity of mercaptosilane in the reacting sol. The majority of sulfonate groups have been neutralized by neighboring protonated amines to form an ionic complex that does not contribute strongly to the surface charge. This neutralization has been noted before for the fabrication of mesoporous materials containing acidic and basic functional groups.[28]

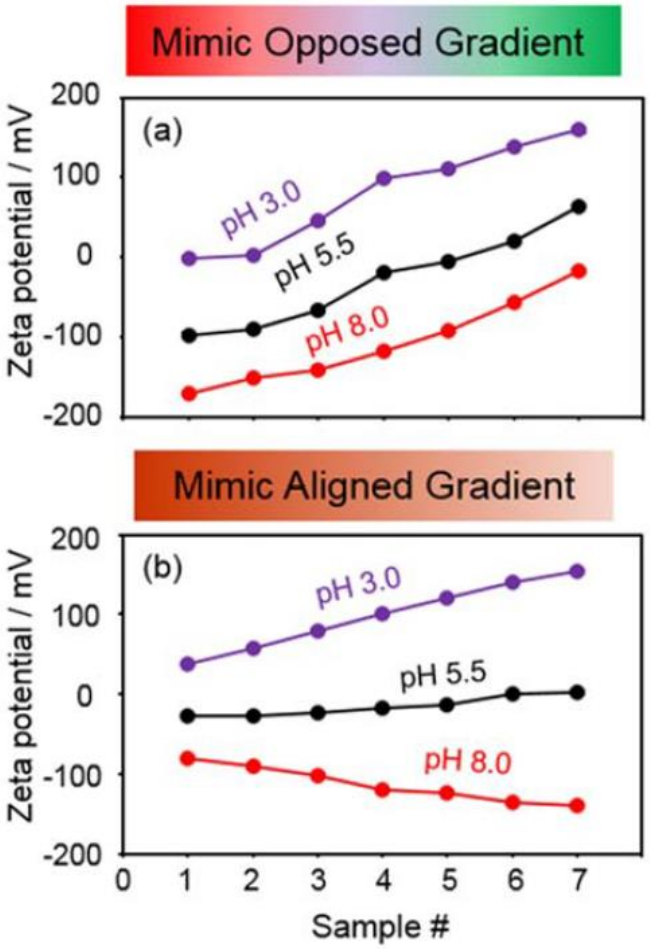

Figure 3.18: ζ measured for the samples designed to mimic an (a) opposed and (b) aligned multi-component gradient at three different pHs (3, 5.5, 8). Sample 7 represents the bottom (or high amine end) of the gradients.

Free sulfonate/sulfonic acid groups are evident when the degree of amine functionalization is low. For example, at pH 3 (**Figure 3.16**) the ζ is ~ zero for sample 1, which represents the low amine/high sulfonic acid end of the opposed gradient. At pH 3, the majority of the silanol groups exist as SiOH and because there are free amines on the surface (as evidenced from **XPS**), the near neutral ζ indicates the surface contains a balance of isolated negatively charged sulfonate groups and isolated protonated amines. For the low amine/low sulfonic acid surface (sample 1; mimics top of aligned gradient), there are clearly more amine groups than free sulfonate groups present as the ζ is about 50 mV more positive than the low amine/high sulfonic acid surface (mimics top of opposed gradient).

The surface concentration of unreacted silanol groups will vary from top to bottom depending on the extent of modification by amine and thiol. The aligned gradient, in particular, is expected to have a silanol gradient whereas the opposed gradient may only have a weak gradient. These silanol groups play an important role in governing the net charge on the surface, particularly at neutral to high pH where they will be largely deprotonated. The pKa's of sulfonic acid and amines is ~2.8 and ~ 7.6, respectively, while they range from ~4-8 for surface silanols.[64] To more clearly see the importance of surface silanol groups in governing the net charge, the data shown in **Figure 3.16** has been replotted in **Figure 3.18.** At pH 5.5 and pH 8, the ζ is negative for almost all of the samples. At a pH above the pKa of immobilized amine, a neutral species will reside on the surface. Thus, for the surfaces to have a negative ζ, there must be an excess of negatively charged surface silanol groups (SiO^-). At pH 8, the ζ value is significantly more negative for all seven substrates compared to pH 5.5. These changes can be attributed to loss of positive charge from the free amine groups and an increase in negative charges due to the deprotonation of the majority of surface silanol groups.

Interestingly, the change in ζ value (~50 mV) with the degree of surface modification under pH 5.5 and pH 8.0 track each other for surfaces that mimic an opposed gradient while they do not for the surfaces that mimic an aligned gradient. For the samples that represent an aligned gradient, however, the change observed in the ζ for the seven samples measured at pH 5.5 and 8 is not the same. Rather, the difference varies from about 50 mV for the sample 1 (slightly modified; relatively high amount of SiOH) to 150 mV for sample 7 (heavily modified with amine and thiol; relatively lower amount of SiOH). This change in ζ suggests the presence of a gradient in silanol groups on the surface, which is expected to be more pronounced in an aligned gradient but not in an opposed gradient.

The **AFM**-nanoparticle results can also be explained by a consideration of surface charge. As shown in **Figure 3.8**, there are a greater number of nanoparticles immobilized on the high amine end of both multi-component charge gradients compared to the uncharged surfaces. At pH ~ 4.3 , which is the pH of the gold colloid solution, the surface of both multicomponent gradients is positively charged at the high amine end due to the excess of protonated amines as all (or most) of the sulfonate groups will form an ionic pair with the amines. The ζ value takes on a large positive value at the high amine ends of both gradients. Thus, electrostatic interactions explain the increase in the number of gold nanoparticles bound to the surface. At the opposite end of the gradient, where the surface bound amine is low, and negatively charged sulfonate groups are comparably high, electrostatic repulsion leads to a significantly lower amount of immobilized gold nanoparticles.

3.6 Summary

Aligned and opposed multi-component gradients containing strongly acidic, weakly acidic, and basic functionalities were prepared and studied using **XPS**, **AFM**, contact angle, and ζ

measurements. Very different surface chemistry was observed when the mercaptoalkoxysilane precursors and the aminoalkoxysilane precursors were deposited in the same direction (aligned) vs. opposite directions (opposed). Surface charge and charge distribution from the bottom to the top of the substrate strongly influenced **WCA**s, binding of metal nanoparticles, and ζ values. In acidic solutions (pH ~ 3), the surface charge was positive and there was more than a 100 mV difference in ζ values from the bottom of the gradient surface to top. In basic solutions (pH > 7.5), the surfaces were negatively charged and depending on whether the individual gradients (SO_3^-, NH_3^+) were aligned or opposed, the ζ values varied from ~50 to > 100 mV. For aligned multi-component gradients, the choice of pH allows the net charge to be tailored and also provides control over the direction of increasing or decreasing charge. Such behavior was not observed for the opposed charge gradient. These results depict the ease at which the surface chemistry along the length of a substrate can be tuned by simply changing the direction at which the individual gradients run with respect to each other, something that has received little attention in the literature. They also reveal the value that multi-component charge gradients provide in understanding the intermolecular interactions between neighboring surface functionalities. Such information is relevant to the development of surfaces that resist biofouling, are antimicrobial, have catalytic properties, are pH responsive, or are imprinted for chemical sensing and separations.

3.7 References

1. Z. Adamczyk. Particle adsorption and deposition: Role of electrostatic interactions, *Advances in Colloid and Interface Science* **2003,** *100-102*, 267-347.
2. A. L. Becker, K. Henzler, N. Welsch, M. Ballauff and O. Borisov. Proteins and polyelectrolytes: A charged relationship, *Current Opinion in Colloid and Interface Science* **2012,** *17*, 90-96.
3. J. Borges and J. F. Mano. Molecular Interactions Driving the Layer-by-Layer Assembly of Multilayers., *Chemical reviews* **2014,** *114*, 8883-8942.
4. H. Boroudjerdi, Y. W. Kim, a. Naji, R. R. Netz, X. Schlagberger and a. Serr. Statics and dynamics of strongly charged soft matter, *Physics Reports* **2005,** *416*, 129-199.
5. Z. Chen, L. Kang, Z. Wang, F. Xu, G. Gu, F. Cui and Z. Guo. Recent progress in the research of biomaterials regulating cell behavior, *RSC Advances* **2014,** *4*, 63807.
6. R. R. Bhat, M. R. Tomlinson, T. Wu and J. Genzer. Surface-grafted polymer gradients: Formation, characterization, and applications, *Advances in Polymer Science* **2006,** *198*, 51-124.
7. J. Genzer. Surface-Bound Gradients for Studies of Soft Materials Behavior, *Annual Review of Materials Research, Vol 42* **2012,** *42*, 435-468.
8. J. Genzer and R. R. Bhat. Surface-bound soft matter gradients, *Langmuir* **2008,** *24*, 2294-2317.
9. X. Lin, Q. He and J. Li. Complex polymer brush gradients based on nanolithography and surface-initiated polymerization, *Chemical Society Reviews* **2012,** *41*, 3584.

10. T. G. Ruardy, J. M. Schakenraad, H. C. van der Mei and H. J. Busscher. Preparation and characterization of chemical gradient surfaces and their application for the study of cellular interaction phenomena, *Surface Science Reports* **1997,** *29,* 3-30.

11. E. Beurer, N. V. Venkataraman, M. Sommer and N. D. Spencer. Protein and nanoparticle adsorption on orthogonal, charge-density-versus- net-charge surface-chemical gradients, *Langmuir* **2012,** *28,* 3159-3166.

12. M. Riepl, M. Östblom, I. Lundström, S. C. T. Svensson, a. W. D. Van Der Gon, M. Schäferling and B. Liedberg. Molecular gradients: An efficient approach for optimizing the surface properties of biomaterials and biochips, *Langmuir* **2005,** *21,* 1042-1050.

13. L. E. Corum and V. Hlady. Screening platelet-surface interactions using negative surface charge gradients, *Biomaterials* **2010,** *31,* 3148-3155.

14. Y. X. Ding, S. Streitmatter, B. E. Wright and V. Hlady. Spatial variation of the charge and sulfur oxidation state in a surface gradient affects plasma protein adsorption, *Langmuir* **2010,** *26,* 12140-12146.

15. B. Kannan, K. Nokura and J. C. Alvarez. Fabrication of Surface Charge Gradients in Open-Tubular Capillaries and Their Characterization by Spatially Resolved Pulsed Streaming Potential Measurements, *Langmuir* **2013,** *29,* 15260-15265.

16. Y. S. Lin and V. Hlady. The desorption of ribonuclease A from charge density gradient surfaces studied by spatially-resolved total internal reflection fluorescence, *Colloids and Surfaces B: Biointerfaces* **1995,** *4,* 65-75.

17. J. T. Han, S. Kim and A. Karim. UVO-tunable superhydrophobic to superhydrophilic wetting transition on biomimetic nanostructured surfaces, *Langmuir* **2007,** *23,* 2608-2614.

18. H. J. Koo, K. V. Waynant, C. Zhang, R. T. Haasch and P. V. Braun. General method for forming micrometer-scale lateral chemical gradients in polymer brushes, *Chemistry of Materials* **2014,** *26*, 2678-2683.

19. A. Mierczynska, A. Michelmore, A. Tripathi, R. V. Goreham, R. Sedev and K. Vasilev. pH-tunable gradients of wettability and surface potential, *Soft Matter* **2012,** *8*, 8399.

20. T. Wu, P. Gong, I. Szleifer, P. Vlček, V. Šubr and J. Genzer. Behavior of surface-anchored poly(acrylic acid) brushes with grafting density gradients on solid substrates: 1. Experiment, *Macromolecules* **2007,** *40*, 8756-8764.

21. C. H. Shen and J. C. Lin. Surface characterization and platelet compatibility evaluation of binary mixed self-assembled monolayers containing novel sulfonic acid terminated alkanethiol, *Colloids and Surfaces B: Biointerfaces* **2010,** *79*, 156-163.

22. L. Ionov, N. Houbenov, A. Sidorenko, M. Stamm, I. Luzinov and S. Minko. Inverse and reversible switching gradient surfaces from mixed polyelectrolyte brushes, *Langmuir* **2004,** *20*, 9916-9919.

23. J. Lee, I. Choi and W. S. Yeo. Preparation of gradient surfaces by using a simple chemical reaction and investigation of cell adhesion on a two-component gradient, *Chemistry - A European Journal* **2013,** *19*, 5609-5616.

24. Y. Huang, S. Xu and V. S. Y. Lin. Bifunctionalized mesoporous materials with site-separated Bronsted acids and bases: Catalyst for a two-step reaction sequence, *Angewandte Chemie - International Edition* **2011,** *50*, 661-664.

25. S. Huh, H. T. Chen, J. W. Wiench, M. Pruski and V. S. Y. Lin. Cooperative catalysis by general acid and base bifunctionalized mesoporous silica nanospheres, *Angewandte Chemie - International Edition* **2005,** *44*, 1826-1830.

26. F. Shang, J. Sun, H. Liu, C. Wang, J. Guan and Q. Kan. One-pot cascade reactions catalyzed by acid-base mesoporous MCM-41 materials, *Materials Research Bulletin* **2012,** *47*, 801-806.

27. F. Shang, J. Sun, S. Wu, H. Liu, J. Guan and Q. Kan. Direct synthesis of acid-base bifunctionalized hexagonal mesoporous silica and its catalytic activity in cascade reactions, *Journal of Colloid and Interface Science* **2011,** *355*, 190-197.

28. R. K. Zeidan and M. E. Davis. The effect of acid-base pairing on catalysis: An efficient acid-base functionalized catalyst for aldol condensation, *Journal of Catalysis* **2007,** *247*, 379-382.

29. B. Kannan, D. Dong, D. A. Higgins and M. M. Collinson. Profile Control in Surface Amine Gradients Prepared by Controlled-Rate Infusion, *Langmuir* **2011,** *27*, 1867-1873.

30. B. Kannan, D. A. Higgins and M. M. Collinson. Aminoalkoxysilane reactivity in surface amine gradients prepared by controlled-rate infusion, *Langmuir* **2012,** *28*, 16091-16098.

31. C. J. Brinker. Hydrolysis And Condensation Of Silicates - Effects On Structure, *Journal of Non-Crystalline Solids* **1988,** *100* (1-3), 31-50.

32. C. J. Brinker, K. D. Keefer, D. W. Schaefer and C. S. Ashley. Sol-gel transition in simple silicates, *Journal of Non-Crystalline Solids* **1982,** *48* (1), 47-64.

33. A. Fidalgo and L. M. Ilharco. Chemical tailoring of porous silica xerogels: Local structure by vibrational spectroscopy, *Chemistry-a European Journal* **2004,** *10* (2), 392-398.

34. E. Cano-Serrano, G. Blanco-Brieva, J. M. Campos-Martin and J. L. G. Fierro. Acid-functionalized amorphous silica by chemical grafting-quantitative oxidation of thiol groups, *Langmuir* **2003,** *19*, 7621-7627.

35. E. Cano-Serrano, J. M. Campos-Martin and J. L. G. Fierro. Sulfonic acid-functionalized silica through quantitative oxidation of thiol groups., *Chemical communications (Cambridge, England)* **2003**, DOI: 10.1039/b210766j, 246-247.

36. N. Graf, E. Yegen, T. Gross, A. Lippitz, W. Weigel, S. Krakert, A. Terfort and W. E. S. Unger. XPS and NEXAFS studies of aliphatic and aromatic amine species on functionalized surfaces, *Surface Science* **2009,** *603* (18), 2849-2860.

37. E. M. E. Kristensen, F. Nederberg, H. Rensmo, T. Bowden, J. Hilborn and H. Siegbahn. Photoelectron spectroscopy studies of the functionalization of a silicon surface with a phosphorylcholine-terminated polymer grafted onto (3-aminopropyl)trimethoxysilane, *Langmuir* **2006,** *22* (23), 9651-9657.

38. K. C. Grabar, R. G. Freeman, M. B. Hommer and M. J. Natan. Preparation and Characterization of Au Colloid Monolayers, *Anal Chem* **1995,** *67* (4), 735-743.

39. C. J. Brinker, A. J. Hurd, P. R. Schunk, G. C. Frye and C. S. Ashley. Review Of Sol-Gel Thin-Film Formation, *Journal of Non-Crystalline Solids* **1992,** *147*, 424-436.

40. G. C. Frye, S. J. Martin, A. J. Ricco and C. J. Brinker. Monitoring Thin-Film Properties With Surface Acoustic-Wave Devices - Diffusion, Surface-Area, And Pore-Size Distribution, *Acs Symposium Series* **1989,** *403*, 208-221.

41. M. Zhu, M. Z. Lerum and W. Chen. How To Prepare Reproducible, Homogeneous, and Hydrolytically Stable Aminosilane-Derived Layers on Silica, *Langmuir* **2012,** *28* (1), 416-423.

42. V. C. Dewoolkar, B. Kannan, K. M. Ashraf, D. A. Higgins and M. M. Collinson. Amine-phenyl multi-component gradient stationary phases, *Journal of Chromatography A* **2015,** *1410*, 190-199.

43. F. X. Zhang and M. P. Srinivasan. Self-assembled molecular films of aminosilanes and their immobilization capacities, *Langmuir* **2004,** *20* (6), 2309-2314.

44. E. T. Vandenberg, L. Bertilsson, B. Liedberg, K. Uvdal, R. Erlandsson, H. Elwing and I. Lundstrom. Structure Of 3-Aminopropyl Triethoxy Silane On Silicon-Oxide, *Journal of Colloid and Interface Science* **1991,** *147* (1), 103-118.

45. E. Metwalli, D. Haines, O. Becker, S. Conzone and C. G. Pantano. Surface characterizations of mono-, di-, and tri-aminosilane treated glass substrates., *Journal of colloid and interface science* **2006,** *298*, 825-831.

46. D. G. Castner, K. Hinds and D. W. Grainger. X-ray photoelectron spectroscopy sulfur 2p study of organic thiol and bisulfide binding interactions with gold surfaces, *Langmuir* **1996,** *12*, 5083-5086.

47. K. Kim and J. Kwak. Faradaic impedance titration of pure 3-mercaptopropionic acid and ethanethiol mixed monolayers on gold, *Journal of Electroanalytical Chemistry* **2001,** *512* (1-2), 83-91.

48. O. Ivashenko, J. T. van Herpt, B. L. Feringa, W. R. Browne and P. Rudolf. Rapid reduction of self-assembled monolayers of a disulfide terminated para-nitrophenyl alkyl ester on roughened Au surfaces during XPS measurements, *Chemical Physics Letters* **2013,** *559*, 76-81.

49. C. D. Batich and D. S. Donald. X-Ray Photoelectron-Spectroscopy Of Nitroso-Compounds - Relative Ionicity Of The Closed And Open Forms, *Journal of the American Chemical Society* **1984,** *106* (10), 2758-2761.

50. D. Margolese, J. A. Melero, S. C. Christiansen, B. F. Chmelka and G. D. Stucky. Direct Syntheses of Ordered SBA-15 Mesoporous Silica Containing Sulfonic Acid Groups, *Chemistry of Materials* **2000,** *12*, 2448-2459.

51. R. Sundara. Hot peroxide bleaching, *Canadian Chemical News* **1998,** *17*, 15-17.

52. R. R. Bhat, D. a. Fischer and J. Genzer. Fabricating planar nanoparticle assemblies with number density gradients, *Langmuir* **2002,** *18*, 5640-5643.

53. R. R. Bhat, J. Genzer, B. N. Chaney, H. W. Sugg and A. Liebmann-Vinson. Controlling the assembly of nanoparticles using surface grafted molecular and macromolecular gradients, *Nanotechnology* **2003,** *14*, 1145-1152.

54. R. R. Bhat, M. R. Tomlinson and J. Genzer. Assembly of Nanoparticles using Surface-Grafted Orthogonal Polymer Gradients, *Macromolecular Rapid Communications* **2004,** *25*, 270-274.

55. R. V. Goreham, A. Mierczynska, M. Pierce, R. D. Short, S. Taheri, A. Bachhuka, A. Cavallaro, L. E. Smith and K. Vasilev. A substrate independent approach for generation of surface gradients, *Thin Solid Films* **2013,** *528*, 106-110.

56. R. V. Goreham, R. D. Short and K. Vasilev. Method for the generation of surface-bound nanoparticle density gradients, *Journal of Physical Chemistry C* **2011,** *115*, 3429-3433.

57. X. Wang, R. T. Haasch and P. W. Bohn. Anisotropic hydrogel thickness gradient films derivatized to yield three-dimensional composite materials, *Langmuir* **2005,** *21*, 8452-8459.

58. T. Sainsbury, T. Ikuno, D. Okawa, D. Pacile, J. M. J. Frechet and A. Zettl. Self-assembly of gold nanoparticles at the surface of amine-and thiol-functionalized boron nitride nanotubes, *The Journal of Physical Chemistry C* **2007,** *111*, 12992-12999.

59. M. L. Gupta, K. Brunson, A. Chakravorty, P. Kurt, J. C. Alvarez, F. Luna-Vera and K. J. Wynne. Quantifying surface-accessible quaternary charge for surface modified coatings via streaming potential measurements, *Langmuir* **2010,** *26*, 9032-9039.

60. Q. Pu, M. S. Elazazy and J. C. Alvarez. Label-free detection of heparin, streptavidin, and other probes by pulsed streaming potentials in plastic microfluidic channels, *Anal Chem* **2008,** *80*, 6532-6536.

61. V. V. Berezkin, V. I. Volkov, O. A. Kiseleva, N. V. Mitrofanova and V. D. Sobolev. The Charge of the Pores of Poly (ethylene terephthalate) Nucleopore Membranes, *Colloid Journal* **2003,** *65* (1), 119-121.

62. R. A. Hayes, M. R. Böhmer and L. G. J. Fokkink. Study of silica nanoparticle adsorption using optical reflectometry and streaming potential techniques, *Langmuir* **1999,** *15*, 2865-2870.

63. H. K. Hall. Steric Effects on the Base Strengths of Cyclic Amines, *Journal American Chemical Society* **1957,** *79*, 5444-5447.

64. S. Ong, X. Zhao and K. B. Eisenthal. Polarization of water molecules at a charged interface: second harmonic studies of the silica/water interface, *Chemical Physics Letters* **1992,** *191*, 327-336.

65. S. E. Creager and J. Clarke. Contact-Angle Titrations of Mixed Omega-Mercaptoalkanoic Acid Alkanethiol Monolayers on Gold - Reactive vs. Nonreactive Spreading, and Chain-Length Effects on Surface Pk(a) Values, *Langmuir* **1994,** *10*, 3675-3683.

66. E. W. Van der Vegte and G. Hadziioannou. Acid-base properties and the chemical imaging of surface-bound functional groups studied with scanning force microscopy, *Journal of Physical Chemistry B* **1997,** *101*, 9563-9569.

67. D. V. Vezenov, A. Noy, L. F. Rozsnyai and C. M. Lieber. Force titrations and ionization state sensitive imaging of functional groups in aqueous solutions by chemical force microscopy, *Journal of the American Chemical Society* **1997,** *119*, 2006-2015.

68. H. Zhang, H.-X. He, T. Mu and Z.-F. Liu. Force titration of amino group-terminated self-assembled monolayers of 4-aminothiophenol on gold using chemical force microscopy, *Thin Solid Films* **1998,** *327-329*, 778-780.

69. B. Cinlar and B. H. Shanks. Applied Catalysis A : General Characterization of the acidic sites in organic acid functionalized mesoporous silica in an aqueous media, *Applied Catalysis A, General* **2011,** *396*, 76-84.

70. A. J. Bard, Faulkner, L.R., *Electrochemical Methods: Fundamentals and Applications*, John Wiley & Sons, Inc, New York, 2001.

Chapter 4: Base Layer Influence on Protonated Aminosilane Gradient Wettability

Adapted from Kayesh M. Ashraf, Chenyu Wang, Sithara S. Nair, Kenneth J. Wynne, Daniel A. Higgins, Maryanne M. Collinson, *Langmuir*, **2017**, DOI: 10.1021/acs.langmuir.7b00614.

4.1 Abstract

Protonated amine gradients have been prepared on silicon wafers via programmed controlled rate infusion (CRI) with varying degrees of hydrophobicity and characterized by XPS spectroscopy and static and Wilhelmy plate dynamic contact angle measurements. Initially, base layers were spin coated from sols containing tetramethoxysilane (TMOS) and either phenyltrimethoxysilane (PTMOS), dimethyldimethoxysilane (DMDMOS) or octyltrimethoxysilane (OTMOS, C8). Amine gradients were then prepared from 3-aminopropyltrimethoxysilane (APTEOS) via CRI. Gradients were exposed to concentrated HCl vapor for amine protonation. XPS showed that NH_2 functional groups were distributed in a gradient fashion as a result of CRI controlling the time of exposure to APTEOS. Interestingly, the overall extent of N modification depended on the type of base layer used for gradient formation. The C8 derived base layer had about half the amount of nitrogen on the surface as compared to those prepared from TMOS, which was attributed to a reduction in the number and accessibility of surface silanol groups. The wettability and contact angle (CA) hysteresis were also dependent on the base layer and varied along the length of the gradient. The greatest CA change across the length of the gradient was observed on the gradient formed on the C8-derived base layer. Likewise, the CA hysteresis was ~ 2X larger on the C8-modified surfaces, indicative of greater chemical inhomogeneity. In contrast to uniformly modified substrates, Wilhelmy plate CA analysis that involves immersion of samples gave a unique S-shaped CA-distance curve for the gradients. The three curve segments correspond to hydrophilic,

hydrophobic, and a middle connecting region. Importantly, these curves give precise CAs along the gradient that reflect surface chemistry and coverage defined by programmed CRI processing.

4.2 Introduction

Surfaces functionalized with amine groups have wide versatility. They have been used as coupling agents to promote the bonding and adhesion between organic resins and inorganic substrates, for the extraction of metal ions, and as linkers to immobilize proteins, enzymes, antibodies, DNA or nanoparticles to a substrate via covalent or electrostatic binding.[1-9] Amine functionalized surfaces have been used to build complex, multi-layered three-dimensional systems for biosensors, immunosensors and/or sensor arrays.[10] Bi-functional surfaces containing both amine groups and acidic functionalities have also been used to catalyze organic reactions.[11-12] For example, acid–base cooperative catalysis has been involved in reactions such as Michael addition as well as aldol, Henry, and Knoevenagel condensations.[12-13] Cooperative catalysis, however, requires careful positioning of reactive groups and can be affected by the hydrophobic/hydrophilic properties of the substrate.[12]

One approach for efficient and systematic study of localized chemical interactions is to create a surface that incorporates a gradual change in density of one or more functionalities unidirectionally or bidirectionally.[14-15] Methods to prepare one-, two-, or three-component gradients containing amine groups have included vapor- or liquid-diffusion,[16-20] sequential immersion,[21] e-beam exposure,[22] controlled exposure UV oxidation,[23] plasma copolymerization,[24] controlled rate infusion,[25] contact printing,[26] and electrochemical methods.[27]

Aminoalkoxysilanes such as 3-aminopropyltrimethoxysilane (3-APTEOS) are ideal for generating gradients because the amine can catalyze condensation of silanols to glass, a silicon wafer, or mesoporous silica.[28-29] Our group has prepared gradient amine surfaces with

alkoxysilanes using controlled-rate infusion (CRI) for studying metal ion binding,[30] silane reaction kinetics[31] and to influence a separation process.[32-34] In CRI, a silica surface is exposed to a solution containing organoalkoxysilanes such as APTEOS in a time-dependent fashion to form a gradient in chemical functionality (viz., amine) and a corresponding counter gradient in silanol groups.[35] An important feature of CRI is control over the distribution of functional groups on a surface. That is, the local chemistry can be changed at predefined positions along the substrate by changing the rate of infusion.[25] Furthermore, the local hydrophilicity or hydrophobicity of the surface can be uniquely tailored as shown herein. The ability to manipulate the gradient profile and the local surface chemistry is particularly important for applications that rely on mass transport and/or those that require spatial control of gradient properties such as in cooperative catalysis.

Gradient preparation on planar surfaces by CRI typically begins with the formation of a "base layer".[25] Base-layer formation on the substrate (e.g., silicon wafer) is achieved by spin coating a silica sol comprised of tetramethoxysilane (TMOS) and an organoalkoxysilane. The base-layer has several functions including a source of reactive silanols for covalently anchoring the aminosilane and ensuring uniformity when gradients are prepared on surfaces that lack sufficient silanol concentration.[34] The chemical composition of the base layer is important as it can control (1) the hydrophobicity/hydrophilicity of the surface, (2) the pK_b of the amine group,[31] (3) the amount of amine deposited along the length of the substrate, (4) whether deposition is homogeneous or heterogeneous (e.g., islands) and (5) whether liquid droplet motion can occur ("sticky or slippery").[36]

In this work, ammonium ($-NH_3^+$) gradients were prepared on base-layer coated silicon substrates to manipulate and control the hydrophobicity/hydrophilicity and thus wettability. These base layers were prepared from silica sols containing TMOS, TMOS/ phenyltrimethoxysilane

(PTMOS), TMOS/dimethyldimethoxysilane (DMDMOS) or TMOS/octyltrimethoxysilane (OTMOS). **XPS** spectroscopy and sessile drop contact angle (CA) measurements were used to characterize the gradient. In addition, the Wilhelmy Plate dynamic contact angle (WP-DCA) method[37] was used following pioneering work of Elwing,[38] Andrade[39] and later Hlady[40-41] to evaluate continuous, position dependent changes in gradient wetting behavior. In prior studies[36, 42-45] and in homogeneously functionalized surfaces described herein, contact angles (CAs) are constant with depth of immersion. In contrast, for these gradient surfaces, the three phase contact line on sample immersion and emersion provides continuously changing CAs that track gradient chemistry. In particular, hysteresis loops comprised of advancing (θ_{adv}) and receding (θ_{rec}) CAs provide a sensitive metric for degree of surface modification. Inspection of DCA curves on sample immersion indicates sensitivity to CA changes along the gradient is ~0.5 mm. This sensitivity arises from the WP instrument electrobalance that detects a mass increase for water wetting at the three phase contact line (hydrophilicity) or apparent mass loss for dewetting (hydrophobicity). Our results show a strong influence of the base layer on gradient characteristics including amine surface coverage, amine basicity, surface wettability, and degree of heterogeneity. Importantly, we also find that the choice of base layer can provide a facile approach for tailoring surface chemistry of gradient films.

4.3 Experimental

4.3.1 Sample Preparation. Silicon wafers (University Wafer, B-doped, ⟨111⟩) were cut to the appropriate size and then cleaned with fresh concentrated H_2SO_4:H_2O_2 (70:30) for 10 min. *Caution*: "piranha solutions" are extremely dangerous and react violently with organic materials. The silica sols used for base-layer preparation contained a mixture of ethanol, silanes (TMOS, PTMOS, DMDMOS, or OTMOS), 0.1 M HCl, and water. The TMOS sol was prepared by mixing

ethanol : TMOS : 0.1 M HCl : H_2O with volume ratios of 0.4 : 0.1 : 0.06 : 0.06 ml (v/v) and aged for 36 h prior to use. The hybrid sols were prepared by mixing ethanol : TMOS : silane (PTMOS or DMDMOS or OTMOS) : 0.1 M HCl : H_2O in a volume ratio of 0.4 : 0.1 : 0.06 : 0.06 :0.06 ml (v/v) and aged for 36 h prior to spin coating. These sols were spin-coated on the silicon wafers at 5000 rpm for 30 s and dried in a desiccator overnight.

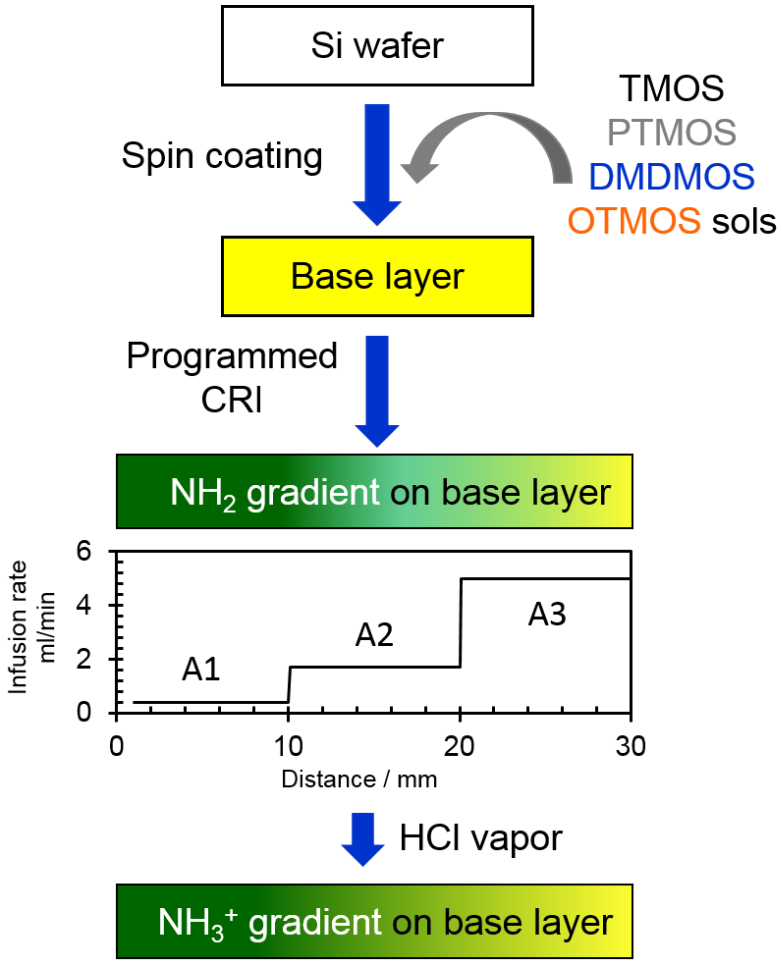

Figure 4.1: Preparation of NH_3^+ gradients on different base-layer coated substrates by programmed CRI. Designations for NH_3^+ concentrations: A1, high; A2, medium, A3, low; Details in **Table 4.1**.

The aminosilane solution used for infusion was prepared by mixing ethanol : silane : water in a 5 : 0.25 : 0.06 volumetric ratio. Amine gradients were prepared using controlled rate infusion (CRI) at pre-programmed rates by infusing the freshly prepared aminosilane solution into a vial containing the vertically aligned substrate.[25] The rate of infusion is controlled by a programmable syringe pump (Harvard apparatus, PHD 2000 infusion). The infusion rate was changed during modification of the base-layer coated slide such that the first 1/3 of the substrate was exposed to solution for ~15 min, the middle third for ~ 3 min, and the top for ~ 1 min. To protonate the amine groups, substrates were exposed to concentrated HCl vapor for 30 minutes. The gradients are designated to indicate base layer: NH_3^+-SiO_x, NH_3^+-Ph, NH_3^+-DM, and NH_3^+-C8. The gradient preparation process is depicted in **Figure 4.1.** Uniformly modified substrates were used as controls and consisted of the base-layer formed from the respective sol and spin coated piranha-cleaned silicon wafers. These control samples were exposed to the HCl vapor under the same conditions as the gradient surfaces.

For Dynamic Contact Angle (DCA) analysis using the Wilhelmy Plate method (DCA-WP), both sides of the substrate needed similar modification. Importantly, the CRI method modifies both sides of the substrate by default. Each side of the double-side polished silicon wafer was first spin coated with the hybrid sol prepared from one of the organoalkoxysilanes and/or TMOS. Next, the base-layer coated substrate was vertically positioned in the reaction chamber (vial) so that modification took place on both sides of the substrate during infusion. Each side of the substrate was then exposed to concentrated HCl vapor to protonate the amine groups.

4.3.2 Characterization. XPS spectroscopy, Static CA and TM-AFM are described in **Chapter 4**. Dynamic water contact angle measurements were performed using a Cahn Dynamic Contact Angle (DCA) Model 312 Analyzer (no longer manufactured) instrument by the Wilhelmy plate method.

To verify that the water was not contaminated by components leaching out of the films during DCA analysis,[46] water checks with a flamed glass slide were performed before and after sample runs. If water contamination is negligible, superposed advancing and receding force distance curves are obtained for the flamed glass slide that correspond to near zero contact angles. This test is sensitive for species that migrate to the water surface and thus change the water surface tension.[46] In all cases, negligible contamination was found for all samples.

4.4 Results and Discussion

4.4.1 Gradient Fabrication. As outlined in **Figure 4.1**, the process for gradient fabrication began by spin coating silica sols containing either TMOS or TMOS:R-Si(OR')$_x$ (1:0.6 v/v; x = 2 or 3) where R = phenyl (Ph), dimethyl (DM) or octyl (C8) onto a silicon or glass substrate to form base layers. The objective was to achieve gradient surfaces with differing hydrophobicity. During infusion, the base-layer coated substrate was exposed to the aminosilane solution for selected time sequences. As a result of the condensation reaction between surface silanol groups on the base layer and the hydrolyzed APTEOS precursors in solution, the aminopropyl groups were covalently bonded to the planar substrate.[25] In this study, the rate of infusion was changed in steps so as to heavily modify the first 1/3 of the substrate (**Figure 4.1, A1**), lightly modify the middle 1/3 (**Figure 4.1, A2**), and sparsely modify the top 1/3 (**Figure 4.1, A3**). This was achieved by exposing the bottom third to the aminosilane solution for 15 min, the middle third for 3 min and the top of the substrate for 1 min as summarized in **Table 4.1**. Protonation of the amine groups takes place via exposure to concentrated HCl vapor for 30 min. As described in later sections, this process results in varying surface functional density so as to amplify differences in wettability along the length of

the substrate. Previous ellipsometric results indicate that the aminopropyl film is thin (~ 0.5 nm) and near a monolayer thick.[35]

Table 4.1. Designations for infusion areas exposed to APTEOS

Designation	Time (min)	Flow rate (ml/min)	Time (min)	Flow Rate (ml/min)	Time (min)	Flow rate (ml/min)	Total Exposure Time (min)
A1	15	0.4	3	1.7	1	5.0	19
A2	-	-	3	1.7	1	5.0	4
A3	-	-	-	-	1	5.0	1

4.4.2 Gradient Characterization

4.4.2.1 XPS Spectroscopy. The presence and extent of modification with amine groups and the degree of protonation/oxidation was evaluated using XPS. **Figure 4.2** shows an overlay of six N1s XPS spectra for the NH_3^+ gradient on TMOS, PTMOS, DMDMOS and OTMOS derived base layers. Spectra were acquired at ~3 mm intervals along the length of the substrate. For all samples, the N1s peak intensity increases from top (low amine end; A3) to bottom (high amine end; A1), which is consistent with the formation of amine gradients. The N1s peak appears as a doublet with binding energies near 399.5 and 401.5 eV, corresponding to free amine and protonated/H-bonded amines, respectively.[35, 47] The peak intensity at 401.5 eV for the protonated amine is higher than the peak at 399.5 eV, indicating that in the dry state the concentration of $–NH_3^+$ is higher than $–NH_2$ following exposure to HCl. However, the continued presence of the peak at 399.5 eV indicates that not all amines are protonated. This result is consistent with prior XPS studies on alkylamine-silanized metal oxides, which indicated that three forms of nitrogen are on the outermost surface (to ~5 nm): free amine that resists protonation in acid, $–NH_3^+$ that resists deprotonation, and "active amine", that can be reversibly protonated.[48]

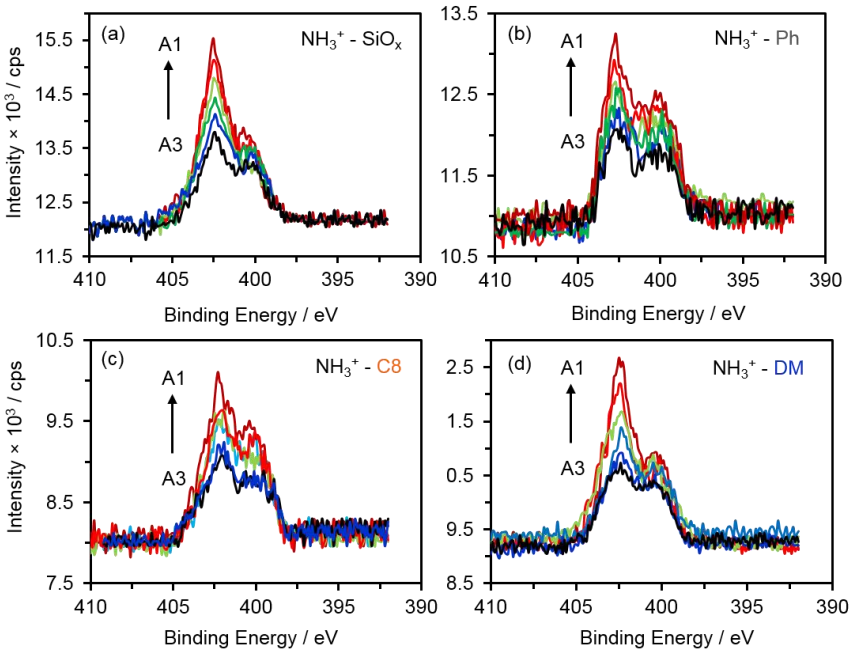

Figure 4.2: N1s high resolution XPS spectra at ~3 mm intervals along the length of the multicomponent NH_3^+ gradient surfaces: (a) NH_3^+ - SiO_x, (b) NH_3^+ - Ph, (c) NH_3^+ - C8, and (d) NH_3^+ - DM. Arrow indicates the direction from top (**black curves, A3**) to bottom (**red curves, A1**). Designation details are in **Table 4.1**.

The area under the N1s peaks as a function of distance along the length of substrates was used to generate the gradient profiles shown in **Figure 4.3.** As can be seen, the area under the N1s peak increases from top (A3) to bottom (A1) consistent with gradient formation. In contrast, a variation was not observed for the uniformly modified films, which is consistent with our previous gradient studies.[25, 31] Some adventious nitrogen is observed on the SiO_x and DM base layer coated slides **Figure 4.4** , and is believed to result in part from impurities present in the base layer sols.[25] In both cases, the nitrogen observed on the unmodified base layer is well below that observed on the top (least modified) end of the respective NH_3^+ gradients.

From **Figure 4.3** it is seen that the extent of amine modification depended on the composition of the base layer and follows the trend: SiO_x > DM ~ Ph >> C8. The highest amine concentration on the TMOS-derived base layer is taken as evidence for the highest Si-OH concentration/availability on the SiOx base layer. For the C8 base layer, the amount of amine immobilized on the surface was significantly smaller, viz., about half that observed on the SiO_x surface. The C8 base layer is the most hydrophobic of the four examined and also contains the largest functional group. Hydrophobicity and/or restricted access to surface silanol groups apparently hinder deposition.

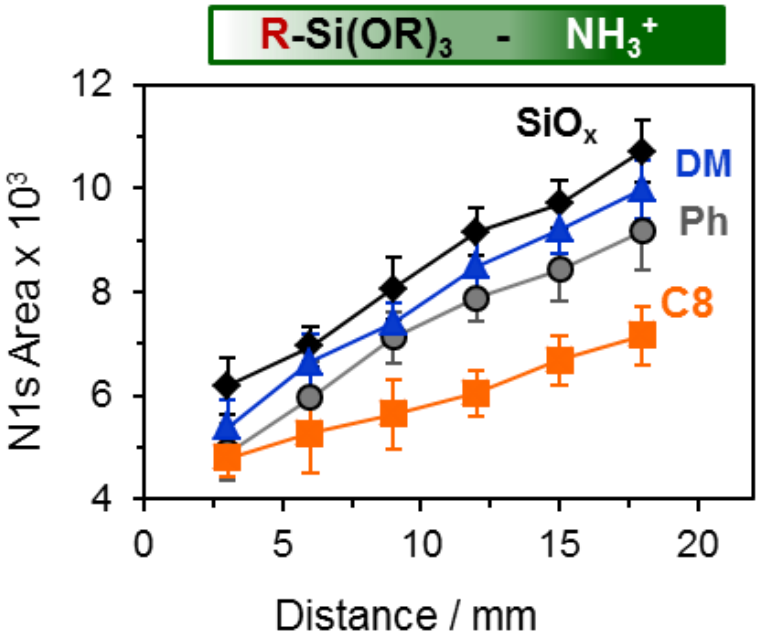

Figure 4.3: N1s area (CPS eV) as a function of distance along the length of the substrate for the gradient amine coated base-layers. The error bars represent the standard deviation of three replicate measurements on a single sample.

To obtain more information about the extent of N-protonation as a function of distance along the length of the substrate, the N1s peak was fit to two components, one corresponding to

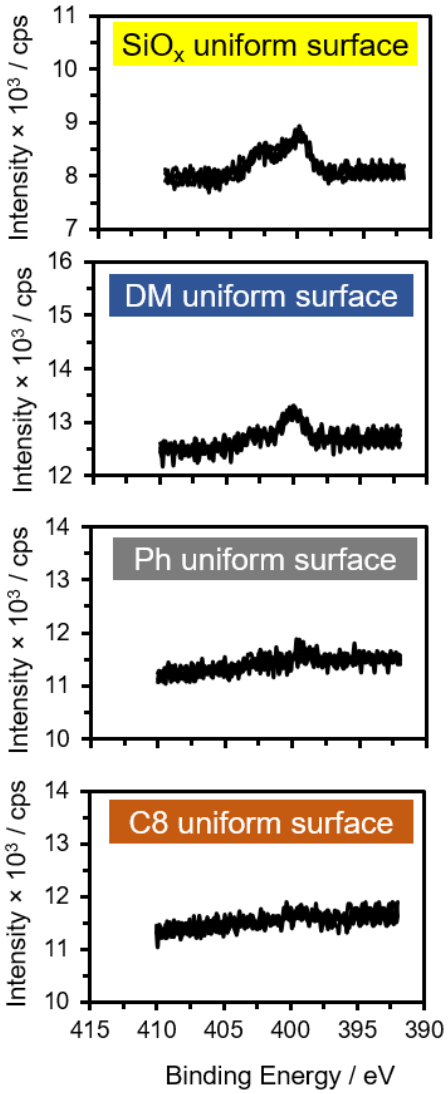

Figure 4.4: N1s high resolution XPS spectra acquired on the base-layer coated substrates.

NH_3^+ (~401 eV) and the other to NH_2 (~399 eV).[31] The ratio of NH_3^+ to total nitrogen (NH_3^+ + NH_2) as a function of distance along the length of the gradient is listed in the **Table 4.2**. The protonated form is predominant and the extent of protonation is higher at the more heavily modified end for all base-layer modified substrates, a finding similar to our previous work.[35] It is also observed that the extent of protonation is smaller on the more hydrophobic base layer (C8) compared to the SiO_x base-layer coated substrate even when the adventitious nitrogen present in

Table 4.2: Ratio of NH_3^+ to total N, (NH_3^+/(NH_3^+ + NH_2)) for each gradient on modified base-layer coated substrates

Position	C8	SiOx		DMDMOS		PTMOS
A1	0.69	0.77		0.78		0.74
↓	0.69	0.76		0.80		0.72
	0.69	0.75		0.76		0.72
	0.64	0.75		0.76		0.71
	0.62	0.75		0.72		0.63
A3	0.64	0.72		0.64		0.63

the TMOS base layer is taken into account, suggesting an increase in the pK_b of the surface bound amine groups on the hydrophobic base layer.

4.4.2.2 WCA analysis (Wettability)

4.4.2.2.1 Static water contact angles. Sessile drop WCAs provide information about film hydrophobicity and hydrophilicity originating from polarity differences across the length of the substrate. WCAs are expected to be primarily affected by the charged and uncharged amine groups but also by the organic groups in the base layer and residual silanol groups. **Figure 4.5 and 4.6**

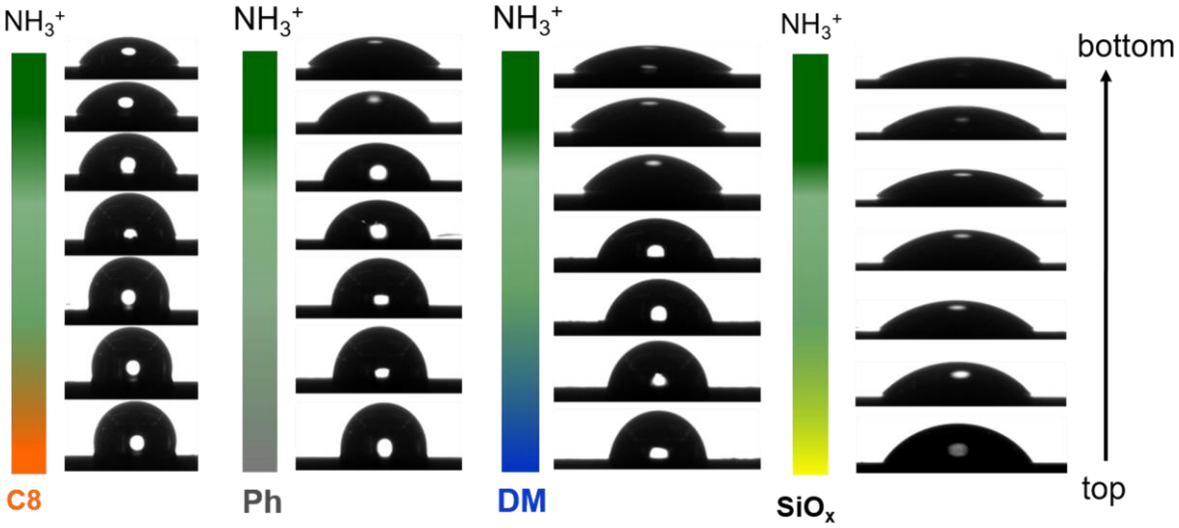

Figure 4.5: Photographs of water droplets along NH_3^+ gradients prepared on different base-layers coated substrates

show images of water drops spaced ~ 3 mm along the length of the base-layer coated substrates and the uniformly modified and gradient surfaces. Water wets the NH_3^+ uniformly modified substrate better than the corresponding base-layer coated substrates, reflecting stronger molecular interactions with charged groups on the surface. The degree to which water wets the surface depends on the position along the length of the gradient film as well as the functional groups on the base layer. Water wets the bottom (NH_3^+ end) of the gradient better than the least modified end (viz., top). Water beads up more on the hydrophobic base layers especially C8 compared to the more hydrophilic base layer (SiO_x) derived from TMOS.

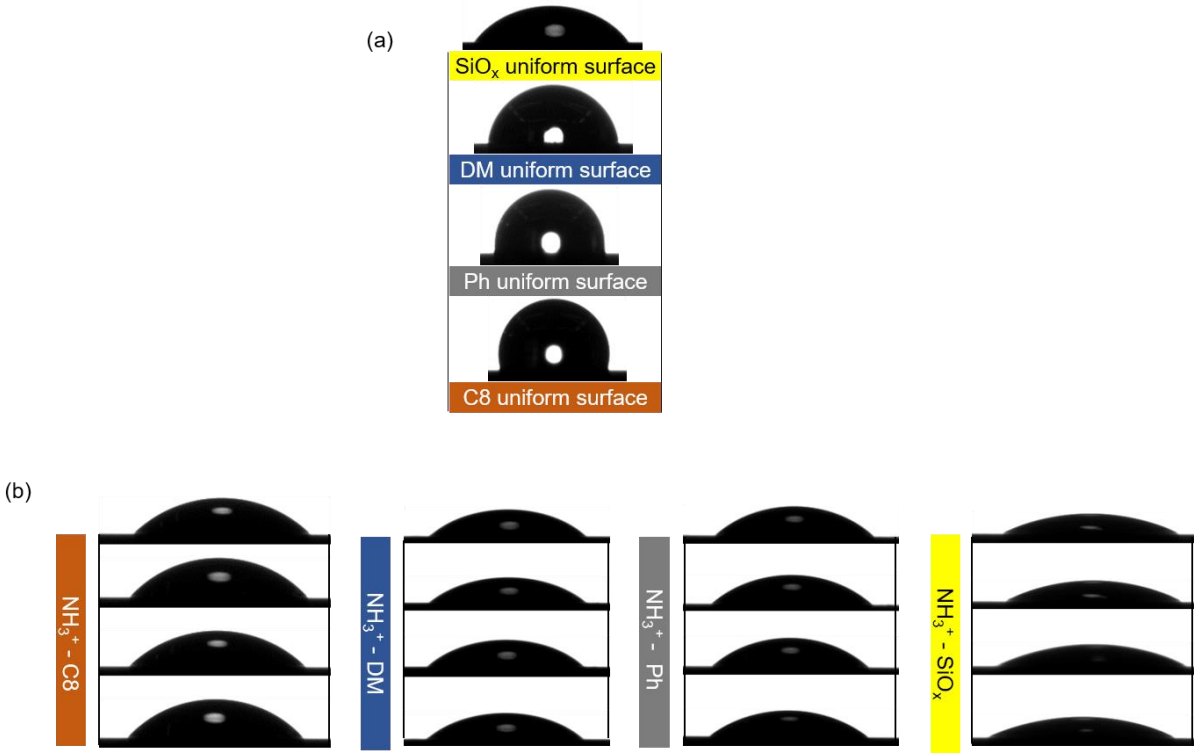

Figure 4.6: Photographs of water droplets as a function of distance along the (a) different base-layer coated substrates and the (b) base-layer coated substrates uniformly modified with NH_3^+.

To better understand the change in contact angle with distance, WCA profiles were prepared for the NH_3^+ gradients, the uniformly modified NH_3^+ films, and the base layers (**Figure**

4.7). For the base-layer substrates and the uniformly modified NH_3^+ surfaces, WCAs do not change significantly along the length of the substrate, indicating a uniform distribution of the functional groups. The average WCA across the length of the base-layer coated substrate is highest on the C8 surface (108 ± 3.3°) and lowest on the SiO_x surface (46.8 ± 4.4°). The base-layer formed

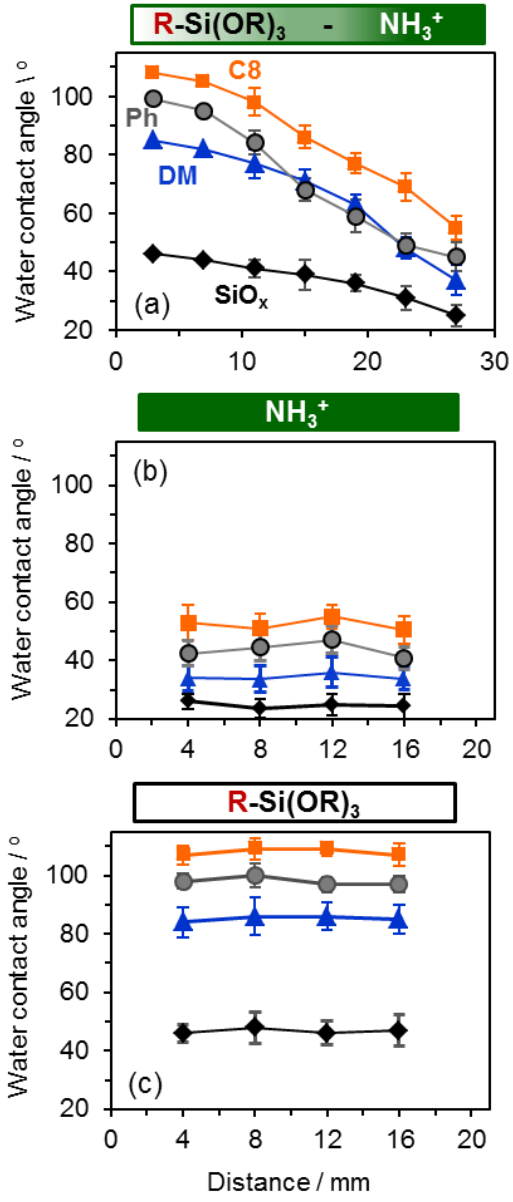

Figure 4.7: Water contact angles as a function of distance on the (a) gradient, (b) uniformly modified, and (c) base-layer coated substrates. Error bars are the standard deviation of the three replicate measurements.

from PTMOS has a contact angle of 98.0 ± 3.0º, which is higher than that obtained with the DMDMOS derived sol (85.3 ± 5.3º). Not surprisingly, these WCAs are similar to those obtained at the least modified end of the gradient surfaces.

The addition of charge to the base-layer coated substrates results in a ×2 drop in WCAs (**Figure 4.7b vs 4.7c**). WCAs for the uniformly modified NH_3^+ substrates depend on the hydrophilicity of the base layer and follow the trend C8 (52.4º) >Ph (43.8º) >DM (34º) >SiO_x (24º). The Ph-NH_3^+ uniform surface has a higher WCA than that observed for DM-NH_3^+. This observation is likely the result of a greater hydrophobicity of the Ph layer (**Figure 4.7c**) since both surfaces have a similar amount of amine as evaluated by XPS (**Figure 4.3**). On the gradient materials, the contact angle changes with distance with the gradient profiles being similar to those generated from XPS data. WCAs decrease as the extent of modification with -NH_3^+ increases; that is, water wets the highly modified end better than the least modified end. The steepness of the wettability gradient is also dependent on the base layer. On the TMOS-derived base layer, the difference in contact angle is only ~ 21º, but on the C8 and Ph base layers, the difference in WCAs from the top to bottom is more than 50º.

4.4.2.2. Dynamic contact angles (DCA). DCA measurements using the Wilhelmy plate method[37, 44] were performed to analyze the advancing (θ_{adv}) and receding (θ_{rec}) and thus contact angle hysteresis (CAH = $\theta_\Delta = \theta_{adv} - \theta_{rec}$) and to evaluate chemical heterogeneity. This conventional Wilhelmy Plate method for the determination of CAs has been reported in studies of silicones,[36, 44] fluorinated coatings[45, 49] and gradients prepared using a two-phase diffusion method.[38-43] Reproducibility of CAH for uniformly modified films during several immersion/emersion cycles was taken as a measure of stability in water and uniformity in the context of the present investigation.[36, 44]

Unlike the sessile drop method that probes only the area where the drop is placed, the Wilhelmy plate method provides a continuous average for θ_{adv} and θ_{rec} at the solid-liquid-vapor interface along the gradient. For gradients, WP-DCA is an efficient alternative to the sessile drop method, which requires the placement of water drops at selected points along the sample surface.[50] The Wilhelmy plate method is also advantageous in providing a continuous, real-time assessment of wettability along 2-4 cm of the substrate.[50] CAH can also be readily ascertained at various locations along the length of the substrate to obtain information regarding surface heterogeneity that is comprised of hydrophobic and hydrophilic functionality.[51]

For gradient films, the Wilhelmy plate method requires near-identical coatings on both sides of the substrate. The CRI method is easily adapted to this provision by spin coating each side of a double-side polished silicon wafer with the organic-inorganic sol prepared from the different organoalkoxysilanes followed by drying. For DCA, the sample was attached to a Cahn instrument electrobalance and a beaker of Milli-Q water was placed on the stage. The stage speed was 100 μms^{-1} enabling characterization of the entire surface in a few minutes. The resulting advancing and receding force-distance curves (fdc's) were converted to contact angles versus depth of immersion or emersion via the relationship $F = mg = P\gamma(\cos\theta)$, where F is the force derived from respective mass (m) changes on immersion and emersion, g is the gravitational constant (980.7 $cm.s^{-2}$), P is the perimeter (5.2 cm), γ is the water surface tension (72.6 $dyne.cm^{-1}$), and θ is the contact angle. A buoyancy correction was done prior to determining WCAs. For the gradient samples, the hydrophilic end ("bottom or A1) was immersed first.

Figure 4.8 shows the change in θ_{adv} and θ_{rec} with depth for gradient films (**Figure 4.8**, left hand column) and uniformly modified films (**Figure 4.8**, right hand column). **Figure 4.9** shows the results obtained on the base-layer coated slides. On all the base-layer coated slides and

uniformly modified charged surfaces, the WCA is constant for immersion and emersion, respectively. As noted above, this observation is similar to conventional, homogeneous coatings.[36,

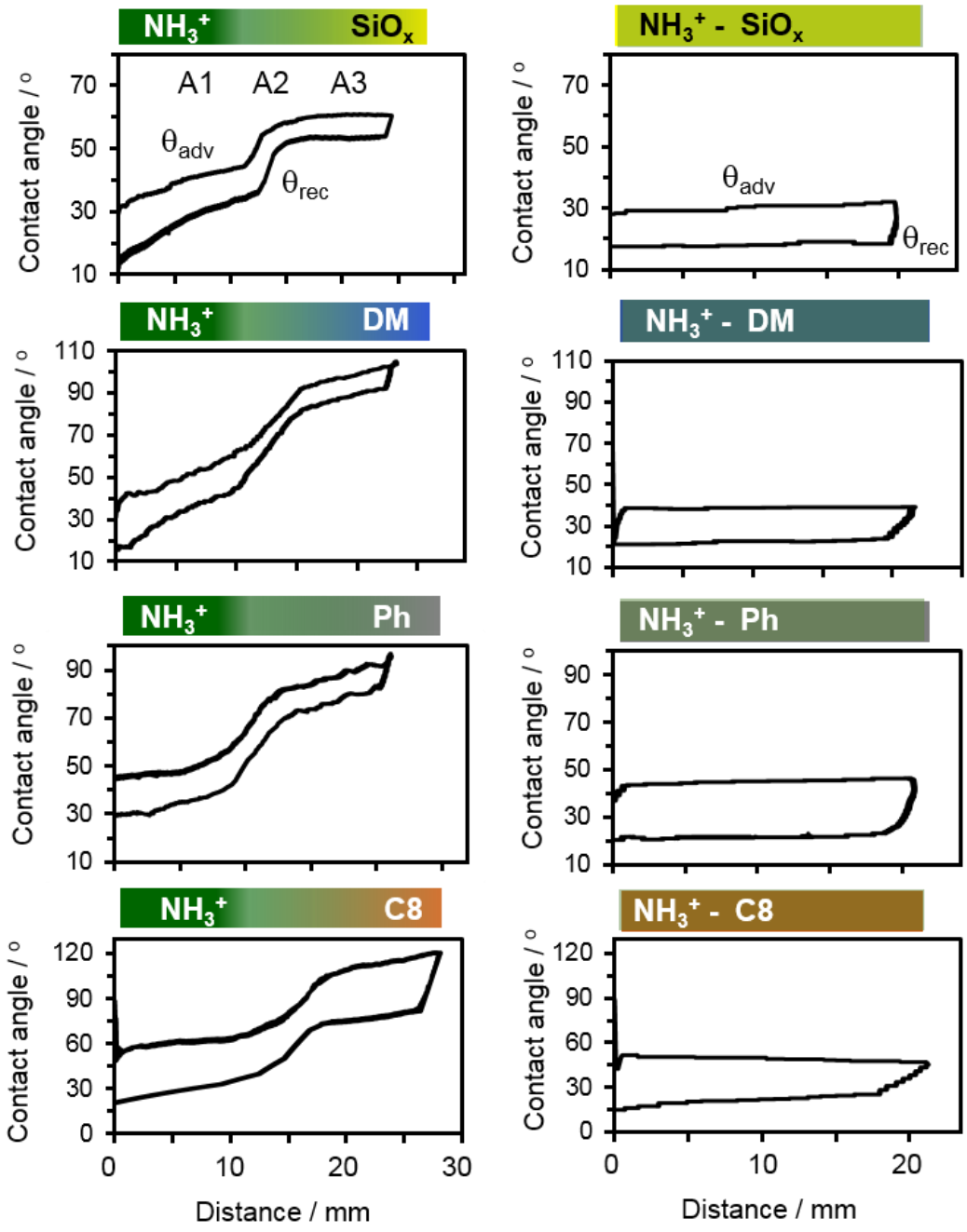

Figure 4.8. DCA contact angle / distance curves for NH_3^+ gradients (left) and NH_3^+ uniformly modified surfaces (right). The hydrophilic end A1 was immersed first. Immersion distances are normalized to begin at 0 mm.

[42-45] In contrast to the uniformly coated substrates, WCAs for the gradient films are not uniform along the length of the substrate but rather have a striking sigmoidal appearance (**Figure 4.8**, left column). A distinct change in slope of the WCA curve midway between the hydrophilic bottom (A1) and hydrophobic top (A3) is seen regardless of the composition of the base layer. In the ~3 mm A2 region, the WCAs change by ~ 30^0 for the hydrophobic base layers and ~ 15^0 for the TMOS derived base layer. Before and after this segment, WCAs change gradually with distance. These S-shaped CA curves are reminiscent of WP WCAs for gradients prepared using a two-phase diffusion method.[38-41] However, a more gradual gradient before and after the distinct change in slope is observed in the present work.

The midway point A2 is near the point where the infusion rate was increased from 0.4 to 1.7 mL/min and then to 5 mL/min during gradient preparation. In this short time span, distinct changes in amine group surface density of take place. Because XPS was collected every ~ 3 mm using a fairly large beam size, it did not identify these changes. However, it is evident that the Wilhelmy plate method has the sensitivity to detect abrupt changes in amine surface area fraction on the gradients.

When the hydrophobic end of the gradient was immersed first, the fdc's were noisier and less stable. In this case, a relatively low entrance force appears to be disrupted by asperities and inhomogeneities whereas when the hydrophilic end is immersed first, the high apparent gain in mass due to the hydrophilic surface may mask inhomogeneities. Further work is needed to understand these results as in principle force distance curves for gradient surfaces should be independent of which end is chosen for first immersion.

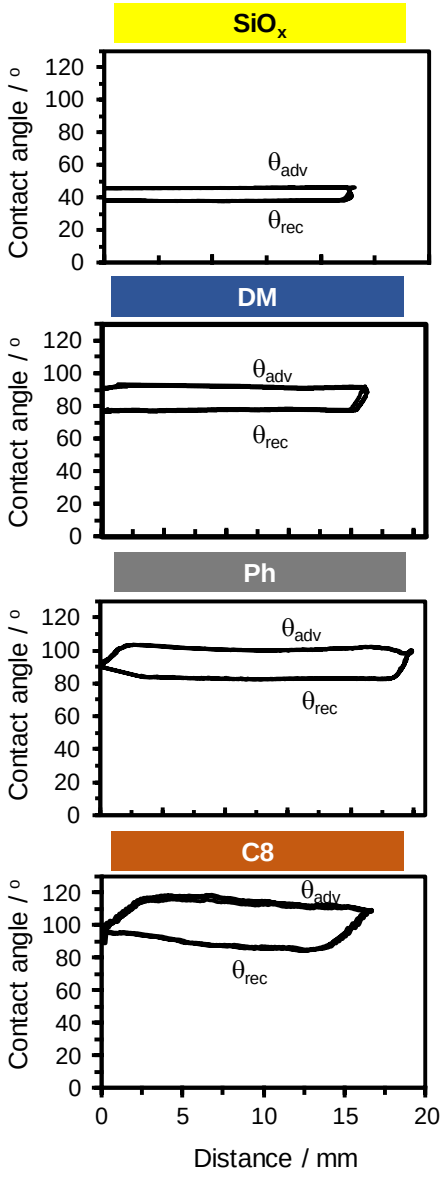

Figure 4.9: Dynamic water contact angle on the various base-layer coated substrates.

The advancing dynamic contact angle for each substrate is similar to the respective static contact angle measured with the sessile drop method. Furthermore, θ_{adv} and θ_{rec} follow the same trend for the base-layer coated substrates (**Figure 4.9**): C8 > Ph > DM > SiO_x. This result is expected since the C8 group has the highest hydrophobicity, followed by the phenyl group and the dimethyl group, and ending with the siloxane (TMOS) coating. Further examination of **Figure 4.8** also reveals that CAH depends on the chemical composition of the base layer and the gradient film. To better understand differences, θ_Δ along the gradient surface as well as the uniformly modified and base-layer substrates are shown in **Figure 4.10.** The average value acquired at the hydrophilic (A1 bottom) and hydrophobic (A3 top) ends began at 2 mm from the point of contact

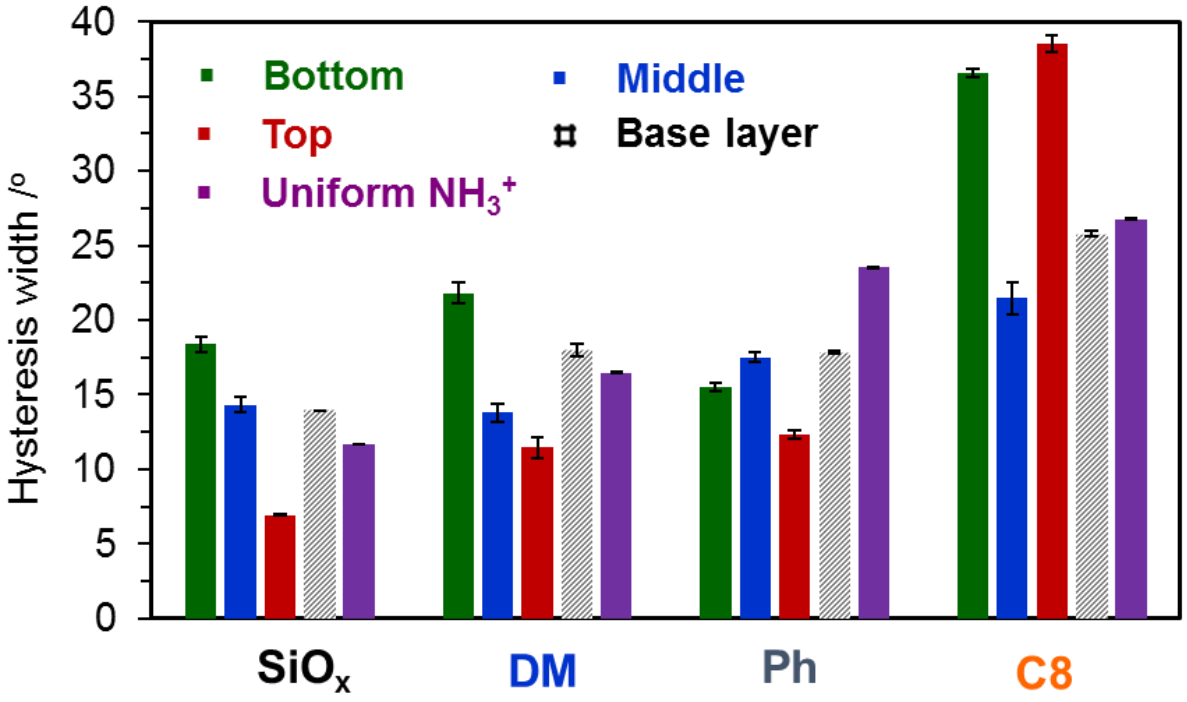

Figure 4.10. Average θ_Δ from DCA obtained at the beginning (green), middle (blue) and end (red) of the force-distance curves obtained from the gradient films. Uniformly modified base layers (hatched) and surfaces uniformly modified with NH_3^+ are shown for comparison. Error bars are standard deviations based on three measurements.

with water and ended at 3 mm. For the middle of the gradient A2, a first derivative was obtained to determine the inflection point. The average hysteresis was 0.5 mm before and after this point.

Several interesting results are evident from the CAH analysis in **Figure 4.10**. First, CAH varies across the length of the gradient substrate. As noted by Johnson and Dettre, θ_Δ is sensitive to small area fractions of hydrophilicity on a hydrophobic surface, and vice versa.[52] Gradient materials are particularly useful for interrogations of relative area fractions as coverage can be easily changed over a narrow range spanning short distances and underlying base films are changed systematically. In this regard θ_Δ increases as the base layer becomes more hydrophobic. For the hydrophilic base SiOx, θ_Δ is 14° and increases to 26° for the C8 (hatched bars in **Figure 4.10**). This trend may be understood in terms of hydrophilic area fractions influencing θ_{rec} while θ_{adv} is affected more by hydrophobic areas. After uniform modification with NH_3^+ a similar, regular trend is observed for θ_Δ.

The relatively high θ_Δ at both ends of the C8-NH_3^+ gradient is noteworthy. The high CAH stems from a relatively high advancing WCA along the gradient, which is attributed to the Si-C8 moiety. Johnson and Dettre recognized that for a surface with a high θ_{adv}, only a small area fraction of polar groups can cause water to "cling" to the surface resulting in a low θ_{rec}.[52-53] Lower advancing WCAs reduce this nonlinear effect. Thus, the most hydrophilic SiO_x gradient has the lowest θ_Δ. In the middle of the gradients A2, the magnitude of CAH depends on base-layer functionality with the C8-NH_3^+ gradient again having a larger CAH than the other three base layers.

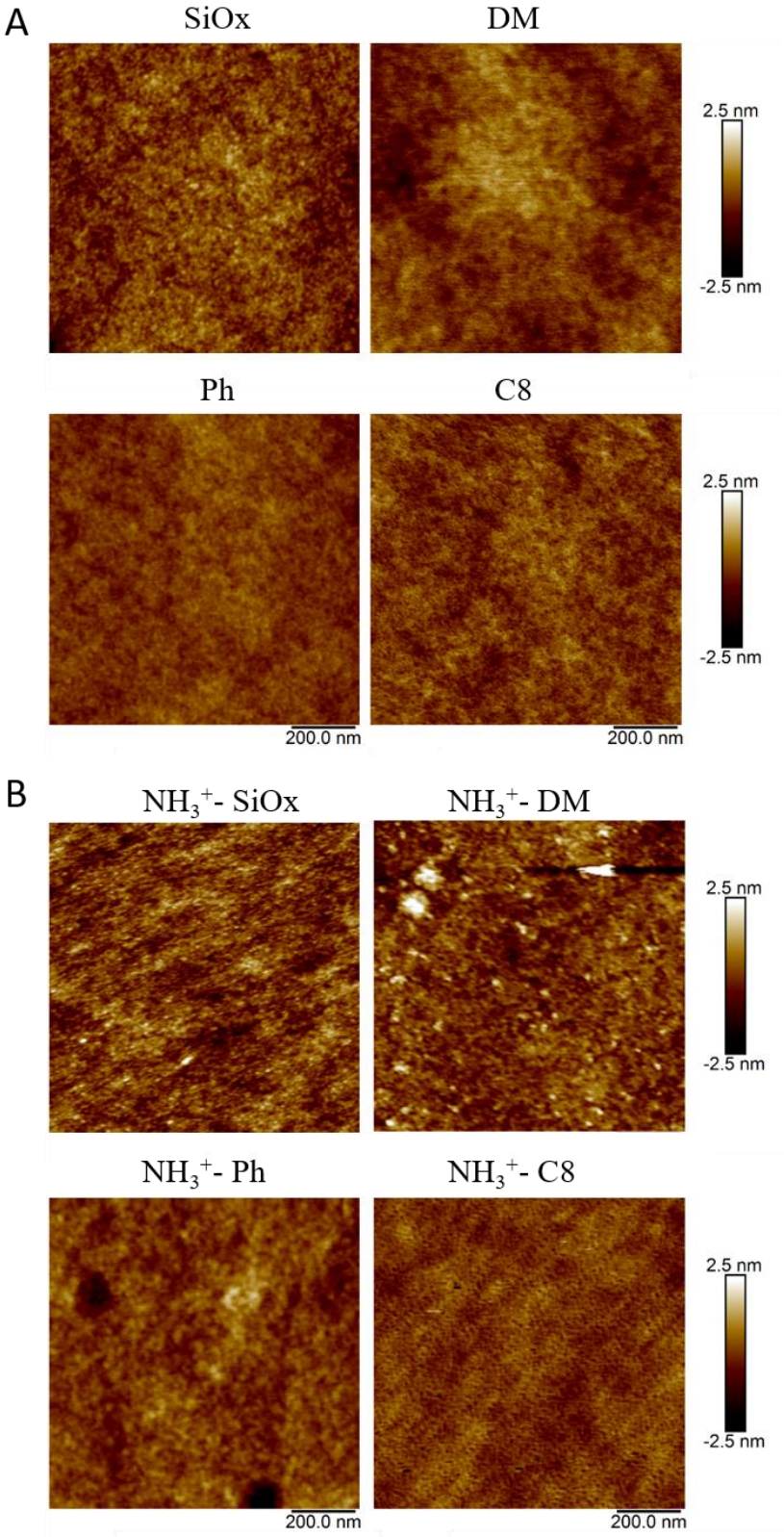

Figure 4.11: AFM images of the (A) base layer coated substrates and (B) NH_3^+ treated films

The RMS surface roughness (***R***q) of the base layers was investigated by TM-AFM (1 μm x 1 μm^2 area scans) and is shown in **Figure 4.11**. ***R***q of samples are listed in the **Table 4.3**. ***R***q was typically on the order of ~0.3-1.5 nm. Surface roughness alone does not usually contribute to contact angle hysteresis unless > 100 nm.[45, 54-55] Rather than roughness, the main contributor to CAH is chemical heterogeneity, which has been observed on amine functionalized gradient films.[40-41] With this result in mind, it is clear that gradient or uniform materials formed on a SiO_x base layer have a lower degree of nanoscale heterogeneity than those formed on substrates with bulky organic groups.

Table 4.3: Roughness data of the base films and the NH_3^+ modified base films

Sample	Base films	Stdev	NH_3^+ on base films	Stdev
TMOS	0.47	0.04	1.02	0.71
PTMOS	0.29	0.05	0.37	0.04
DMDEOS	0.73	0.17	0.51	0.22
C8	0.38	0.01	1.07	0.05

4.5 Conclusions

The most important function of a base layer is to provide a consistent and uniform source of surface silanol groups regardless of the type of substrate. An extra bonus of a base layer is that it also provides an easy route to add additional surface functionality before gradient formation begins. However, as shown herein via the fabrication of surface amine gradients on supports of differing hydrophobicity, the chemical composition of the base layer also influences the macroscopic and microscopic properties of the gradient itself. The number of amine groups that can be attached to the surface as well as whether they deposit homogeneously or heterogeneously.

Different surface chemistry was observed when the base layer was hydrophobic compared to more hydrophilic. The amount of amine deposited on the C8 surface, for example, was about half that observed on the SiO_x base layer. Likewise, the steepness of the gradient in wettability as observed by the change in static contact angle between the top and bottom of the substrate was much greater on the more hydrophobic base layers. A 50^0 change in WCA was observed for the gradient prepared on the most hydrophobic base layer while half that was observed on the SiO_x. However, greater microscopic heterogeneity was observed on the hydrophobic C8 base layer vs the SiO_x base layer as noted from contact angle hysteresis data.

The Wilhelmy plate method was particularly sensitive to changes in the extent of modification and the detection of heterogeneity along the length of the gradient films. In contrast to uniformly coated substrates, WCAs for gradient films are not uniform along the length of the substrate as evidenced by a striking sigmoidal curve. (**Fig 4.8**, left column). The three curve segments correspond to the hydrophilic bottom (A1), the hydrophobic top (A3) and a connecting region A2. The correlation of these curves give precise gradient CAs that reflect the controlled-rate infusion processing, which is an important finding of this study.

Collectively, these results show that the base layer is more than just a source of surface SiOH groups but can also be used as a means to appropriately tailor the microscopic and macroscopic properties of gradient surfaces. Furthermore, our findings demonstrate how gradient films can be a useful tool to experimentally evaluate the dependence of contact angle hysteresis on surface coverage and surface hydrophobicity as correlated with theory.

4.6 References

1. Sullivan, T. P.; Huck, W. T. S. Reactions on monolayers: Organic synthesis in two dimensions. *European Journal of Organic Chemistry* **2003,** (1), 17-29.

2. Shen, G.; Horgan, A.; Levicky, R. Reaction of N-phenyl maleimide with aminosilane monolayers. *Colloids and Surfaces B-Biointerfaces* **2004,** *35* (1), 59-65.

3. Rother, D.; Sen, T.; East, D.; Bruce, I. J. Silicon, silica and its surface patterning/activation with alkoxy- and amino-silanes for nanomedical applications. *Nanomedicine* **2011,** *6* (2), 281-300.

4. Jin, L.; Horgan, A.; Levicky, R. Preparation of end-tethered DNA monolayers on siliceous surfaces using heterobifunctional cross-linkers. *Langmuir* **2003,** *19* (17), 6968-6975.

5. Oh, S. J.; Cho, S. J.; Kim, C. O.; Park, J. W. Characteristics of DNA microarrays fabricated on various aminosilane layers. *Langmuir* **2002,** *18* (5), 1764-1769.

6. Chrisey, L. A.; Lee, G. U.; Oferrall, C. E. Covalent attachment of synthetic DNA to self-assembled monolayer films. *Nucleic Acids Research* **1996,** *24* (15), 3031-3039.

7. Xiao, S. J.; Textor, M.; Spencer, N. D.; Sigrist, H. Covalent attachment of cell-adhesive, (Arg-Gly-Asp)-containing peptides to titanium surfaces. *Langmuir* **1998,** *14* (19), 5507-5516.

8. Jiang, H.; Xu, F. J. Biomolecule-functionalized polymer brushes. *Chemical Society Reviews* **2013,** *42* (8), 3394-3426.

9. Aguado, J.; Arsuaga, J. M.; Arencibia, A.; Lindo, M.; Gascon, V. Aqueous heavy metals removal by adsorption on amine-functionalized mesoporous silica. *Journal of Hazardous Materials* **2009,** *163* (1), 213-221.

10. Willner, I.; Katz, E. Integration of layered redox proteins and conductive supports for bioelectronic applications. *Angewandte Chemie International Edition* **2000,** *39* (7), 1180-1218.

11. Shylesh, S.; Wagner, A.; Seifert, A.; Ernst, S.; Thiel, W. R. Cooperative Acid-Base Effects with Functionalized Mesoporous Silica Nanoparticles: Applications in Carbon-Carbon Bond-Formation Reactions. *Chemistry-a European Journal* **2009,** *15* (29), 7052-7062.

12. Margelefsky, E. L.; Zeidan, R. K.; Davis, M. E. Cooperative catalysis by silica-supported organic functional groups. *Chemical Society Reviews* **2008,** *37* (6), 1118-1126.

13. Bass, J. D.; Solovyov, A.; Pascall, A. J.; Katz, A. Acid-base bifunctional and dielectric outer-sphere effects in heterogeneous catalysis: A comparative investigation of model primary amine catalysts. *Journal of the American Chemical Society* **2006,** *128* (11), 3737-3747.

14. Genzer, J. Surface-Bound Gradients for Studies of Soft Materials Behavior. *Annual Review of Materials Research, Vol 42* **2012,** *42*, 435-468.

15. Genzer, J.; Bhat, R. R. Surface-bound soft matter gradients. *Langmuir* **2008,** *24*, 2294-2317.

16. Bhat, R. R.; Fischer, D. A.; Genzer, J. Fabricating planar nanoparticle assemblies with number density gradients. *Langmuir* **2002,** *18* (15), 5640-5643.

17. Bhat, R. R.; Genzer, J.; Chaney, B. N.; Sugg, H. W.; Liebmann-Vinson, A. Controlling the assembly of nanoparticles using surface grafted molecular and macromolecular gradients. *Nanotechnology* **2003,** *14* (10), 1145-1152.

18. Riepl, M.; Ostblom, M.; Lundstrom, I.; Svensson, S. C. T.; van der Gon, A. W. D.; Schaferling, M.; Liedberg, B. Molecular gradients: An efficient approach for optimizing the surface properties of biomaterials and biochips. *Langmuir* **2005,** *21* (3), 1042-1050.

19. Bhat, R. R.; Genzer, J. Tuning the number density of nanoparticles by multivariant tailoring of attachment points on flat substrates. *Nanotechnology* **2007,** *18* (2).

20. Usrey, M. L.; Strano, M. S. Adsorption of Single Walled Carbon Nanotubes onto Silicon Oxide Surface Gradients of 3-Aminopropyltri(ethoxysilane) Described by Polymer Adsorption Theory. *Langmuir* **2009,** *25* (17), 9922-9930.

21. Beurer, E.; Venkataraman, N. V.; Sommer, M.; Spencer, N. D. Protein and Nanoparticle Adsorption on Orthogonal, Charge-Density-Versus-Net-Charge Surface-Chemical Gradients. *Langmuir* **2012,** *28* (6), 3159-3166.

22. Toikkanen, O.; Doan, N.; Erdmanis, M.; Lipsanen, H.; Kontturi, K.; Parviz, B. Building molecular surface gradients with electron beam lithography. *Journal of Micromechanics and Microengineering* **2011,** *21* (5).

23. Ekblad, T.; Andersson, O.; Tai, F. I.; Ederth, T.; Liedberg, B. Lateral Control of Protein Adsorption on Charged Polymer Gradients. *Langmuir* **2009,** *25* (6), 3755-3762.

24. Goreham, R. V.; Short, R. D.; Vasilev, K. Method for the Generation of Surface-Bound Nanoparticle Density Gradients. *Journal of Physical Chemistry C* **2011,** *115* (8), 3429-3433.

25. Kannan, B.; Dong, D.; Higgins, D. A.; Collinson, M. M. Profile Control in Surface Amine Gradients Prepared by Controlled-Rate Infusion. *Langmuir* **2011,** *27,* 1867-1873.

26. Song, F.; Cai, Y. J.; Newby, B. M. Z. Fabricating tunable nanoparticle density gradients with the contact printing based approach. *Applied Surface Science* **2006,** *253* (5), 2393-2398.

27. Plummer, S. T.; Bohn, P. W. Spatial dispersion in electrochemically generated surface composition gradients visualized with covalently bound fluorescent nanospheres. *Langmuir* **2002,** *18* (10), 4142-4149.

28. Luechinger, M.; Prins, R.; Pirngruber, G. D. Functionalization of silica surfaces with mixtures of 3-aminopropyl and methyl groups. *Microporous and Mesoporous Materials* **2005,** *85* (1-2), 111-118.

29. Beari, F.; Brand, M.; Jenkner, P.; Lehnert, R.; Metternich, H. J.; Monkiewicz, J.; Siesler, H. W. Organofunctional alkoxysilanes in dilute aqueous solution: new accounts on the dynamic structural mutability. *Journal of Organometallic Chemistry* **2001,** *625* (2), 208-216.

30. Stegall, S. L.; Ashraf, K. M.; Moye, J. R.; Higgins, D. A.; Collinson, M. M. Separation of transition and heavy metals using stationary phase gradients and thin layer chromatography. *Journal of Chromatography A* **2016,** *1446,* 141-148.

31. Kannan, B.; Higgins, D. A.; Collinson, M. M. Aminoalkoxysilane reactivity in surface amine gradients prepared by controlled-rate infusion. *Langmuir* **2012,** *28,* 16091-16098.

32. Dewoolkar, V. C.; Jeong, L. N.; Cook, D. W.; Ashraf, K. M.; Rutan, S. C.; Collinson, M. M. Amine Gradient Stationary Phases on In-House Built Monolithic Columns for Liquid Chromatography. *Analytical chemistry* **2016**.

33. Dewoolkar, V. C.; Kannan, B.; Ashraf, K. M.; Higgins, D. A.; Collinson, M. M. Amine-phenyl multi-component gradient stationary phases. *Journal of Chromatography A* **2015,** *1410*, 190-199.

34. Kannan, B.; Marin, M. A.; Shrestha, K.; Higgins, D. A.; Collinson, M. M. Continuous stationary phase gradients for planar chromatographic media. *Journal of Chromatography A* **2011,** *1218*, 9406-9413.

35. Ashraf, K. M.; Giri, D.; Wynne, K. J.; Higgins, D. A.; Collinson, M. M. Cooperative Effects in Aligned and Opposed Multicomponent Charge Gradients Containing Strongly Acidic, Weakly Acidic, and Basic Functional Groups. *Langmuir* **2016,** *32* (16), 3836-3847.

36. Wang, C.; Nair, S. S.; Veeravalli, S.; Moseh, P.; Wynne, K. J. Sticky or Slippery Wetting: Network Formation Conditions Can Provide a One-Way Street for Water Flow on Platinum-cured Silicone. *ACS applied materials & interfaces* **2016,** *8* (22), 14252-14262.

37. Wilhelmy, L. About the dependence of capillary constants of alcohols on substance and shapes of moistened solid bodies. *Ann. Physik* **1863,** *119*, 177.

38. Elwing, H.; Welin, S.; Askendal, A.; Nilsson, U.; LundstrÖm, I. A wettability gradient method for studies of macromolecular interactions at the liquid/solid interface. *Journal of Colloid and Interface Science* **1987,** *119* (1), 203-210.

39. Gölander, C.; Lin, Y.; Hlady, V.; Andrade, J. Wetting and plasma-protein adsorption studies using surfaces with a hydrophobicity gradient. *Colloids and Surfaces* **1990,** *49,* 289-302.

40. Lin, Y.; Hlady, V.; Gölander, C.-G. The surface density gradient of grafted poly (ethylene glycol): Preparation, characterization and protein adsorption. *Colloids and Surfaces B: Biointerfaces* **1994,** *3* (1-2), 49-62.

41. Lin, Y.; Hlady, V. The desorption of ribonuclease A from charge density gradient surfaces studied by spatially-resolved total internal reflection fluorescence. *Colloids and Surfaces B: Biointerfaces* **1995,** *4* (2), 65-75.

42. Decker, E.; Garoff, S. Contact line structure and dynamics on surfaces with contact angle hysteresis. *Langmuir* **1997,** *13* (23), 6321-6332.

43. Rupp, F.; Scheideler, L.; Geis-Gerstorfer, J. Effect of heterogenic surfaces on contact angle hysteresis: dynamic contact angle analysis in material sciences. *Chemical engineering & technology* **2002,** *25* (9), 877-882.

44. Wang, C.; Nair, S.; Wynne, K. J. Wilhelmy balance characterization beyond contact angles: Differentiating leaching from nanosurface reorganization and optimizing surface modification. *Polymer* **2017**.

45. Wang, J.-H.; Claesson, P.; Parker, J.; Yasuda, H. Dynamic contact angles and contact angle hysteresis of plasma polymers. *Langmuir* **1994,** *10* (10), 3887-3897.

46. Uilk, J. M.; Mera, A. E.; Fox, R. B.; Wynne, K. J. Hydrosilation-cured poly (dimethylsiloxane) networks: Intrinsic contact angles via dynamic contact angle analysis. *Macromolecules* **2003,** *36* (10), 3689-3694.

47. Graf, N.; Yegen, E.; Gross, T.; Lippitz, A.; Weigel, W.; Krakert, S.; Terfort, A.; Unger, W. E. XPS and NEXAFS studies of aliphatic and aromatic amine species on functionalized surfaces. *Surface Science* **2009,** *603* (18), 2849-2860.

48. Moses, P.; Wier, L. M.; Lennox, J. C.; Finklea, H.; Lenhard, J.; Murray, R. W. X-ray photoelectron spectroscopy of alkylaminesilanes bound to metal oxide electrodes. *Analytical Chemistry* **1978,** *50* (4), 576-585.

49. Wang, Y.; Pitet, L. M.; Finlay, J. A.; Brewer, L. H.; Cone, G.; Betts, D. E.; Callow, M. E.; Callow, J. A.; Wendt, D. E.; Hillmyer, M. A. Investigation of the role of hydrophilic chain length in amphiphilic perfluoropolyether/poly (ethylene glycol) networks: towards high-performance antifouling coatings. *Biofouling* **2011,** *27* (10), 1139-1150.

50. Eral, H. B.; t Mannetje, D.; Oh, J. M. Contact angle hysteresis: a review of fundamentals and applications. *Colloid and Polymer Science* **2013,** *291* (2), 247-260.

51. Lander, L. M.; Siewierski, L. M.; Brittain, W. J.; Vogler, E. A. A Systematic Comparison Of Contact-Angle Methods. *Langmuir* **1993,** *9* (8), 2237-2239.

52. Dettre, R. H.; Johnson Jr, R. E. Contact Angle Hysteresis. IV. Contact Angle Measurements on Heterogeneous Surfaces1. *The journal of physical chemistry* **1965,** *69* (5), 1507-1515.

53. Johnson Jr, R. E.; Dettre, R. H. Contact angle hysteresis. III. Study of an idealized heterogeneous surface. *The journal of physical chemistry* **1964,** *68* (7), 1744-1750.

54. Eick, J.; Good, R.; Neumann, A. Thermodynamics of contact angles. II. Rough solid surfaces. *Journal of Colloid and Interface Science* **1975,** *53* (2), 235-248.

55. Neumann, A.; Good, R. Thermodynamics of contact angles. I. Heterogeneous solid surfaces. *Journal of Colloid and Interface Science* **1972,** *38* (2), 341-358.

Chapter 5: On the importance of gradient infusion order on the microscopic and macroscopic properties of bi-functional charge gradients

5.1. Abstract

Four multicomponent charge gradients were prepared by a combination of sol-gel process and the controlled rate infusion (***CRI***) method. The concentration and time of infusion of the individual of silane solutions were kept constant. Only the sequence of infusion of the individual silane solutions was changed. The first set of samples were prepared by infusing APTEOS first followed by MPTMOS solution either in an aligned or opposed fashion. The second set of samples were prepared by infusing the MPTMOS solution first and then the APTEOS solution in an aligned or opposed fashion. After infusion of MPTMOS, the gradients were immersed into H_2O_2 solution to produce charged gradients (NH_3^+, SO_3^-). The effect of one functional group over the other on the gradient properties was analyzed in this work. The extent of modification due to NH_3^+ + SO_3^- and SO_3^- + NH_2 gradients was studied by **XPS** spectroscopy. It was found that NH_3^+ + SO_3^- gradients have higher modification than SO_3^- + NH_2 gradients. Surface wettability of these gradients were probed by **DCA**. NH_3^+ + SO_3^- gradients were shown to have greater surface heterogeneities than SO_3^- + NH_2 gradients as observed from the contact angle hysteresis.

5.2. Introduction

A multicomponent gradient surface is one where more than one functional group is spatially distributed in an increasing or decreasing fashion. A gradient is one that exhibits a gradual variation in a chemical or physical property along its length or width, and/or height.[1] Many different approaches have been used to form gradient materials as explained in the recently published reviews. [1–8] Chemical gradient materials have been used to drive and control transport and as high-throughput tools to study biomolecule adsorption and crystallization, cell adhesion, charge interactions, and phase separation.[1,3,5,7] Recently, they have been used to investigate reaction kinetics,[9,10] surface basicity,[9] and synergistic interactions[10,11,12] and to separate mixtures of similar compounds.[13,14] Multicomponent charge gradients are especially important since charged species show preferential adsorption to some of the biomolecules.[1-5, 15] For example Riepl *et al*.[16] reported protein-adsorption experiments on a unidirectional surface-net-charge gradient. The positively charged lysozyme adsorbed preferentially on the negatively charged carboxylic acid side and the negatively charged pepsin on the positively charged amine side. Gessner *et al*.[17] observed higher protein adsorption on nanoparticles with different surface-charge densities for higher charge densities.

In **Chapter 3** we explored the cooperative interactions between acidic and basic functionalities (NH_3^+ + SO_3^-) on a multicomponent charge gradients in which the individual component gradients either align with or oppose each other. It was concluded that the spatial distribution of the individual components on the surface ultimately influenced the local microscopic charge and hence, localized interactions between surface-bound functional groups and reagents in solution. We showed how the distribution of charge on the surface is very different for opposed vs. aligned multicomponent gradients and how by simply aligning the individual

gradients differently, materials with very different surface chemistry could be obtained. All those gradients in that work were prepared by depositing the amine gradient first then the second gradient of thiol was placed on it. We assumed that there would a difference on the extent of immobilization of the different charge groups on the surface when we change the sequence of the silane infusion and thereby changing the surface wettability. It is known that surface amine having a lone pair of electron serves as a Lewis base which helps catalysis of the condensation reaction of thiol, thus, increasing the extent of thiol on the surface. We wanted to see the effect of thiol on the immobilization of amine and vice versa on the gradient properties. In a word, in this study, we explored the effect of the order of infusion (Amine + Thiol vs. Thiol + Amine) on the gradient characteristics. Such a comparative study will provide deeper understanding in optimizing their application in various fields as mentioned earlier.

In this work, four different gradients were prepared by the ***CRI*** method.[18] The first gradient was prepared on a tetramethoxysilane (TMOS) derived base layer by infusing a solution containing an aminosilane first and then a second solution consisting of thiolsilane in the same or opposed direction to make (NH_2 + SO_3^-) aligned or opposed multicomponent gradients. These gradients were then converted to (NH_3^++ SH) charged gradients by immersing them in 30% H_2O_2 solution. As explained in **Chapter 3** it converts thiol to sulfonate groups and sulfonate groups synergistically convert free amine to protonated amine. We, however, expected less protonation of free amine when thiol is infused first for several reasons. First, when thiol is infused first, a smaller amount of it will be anchored on the surface. Without the aminosilanes present on the surface and their self-catalyzing properties,[19] less thiol will be deposited. Additionally, the concentration of thiol is one-fourth of that of the aminosilane solution. Also, oxidation with H_2O_2 takes place first before amine deposition. With all of these being said, we expected a lower degree

of protonation of free amine on the gradient surface when thiol is infused first. Thus, after the preparation, we expect to have aligned and opposed (NH_3^+ + SO_3^-) and (SO_3^- + NH_2) multicomponent charge gradients. The chemistry involved in these two different gradients materials and subtle changes in the surface heterogeneity and their spatial density along the length of a gradients were studied by **XPS** spectroscopy, **WCA** and **DCA**.

5.3. Experimental

5.3.1 Sample preparation

The silica sol used for base layer preparation was composed of ethanol, TMOS, 0.1 M HCl, and water in a 0.4:0.2:0.06:0.06 volumetric ratio and was aged for 24−36 h prior to use. This sol was spin-coated on the wafers at 5000 rpm for 30 s and the modified substrates then dried in a desiccator overnight.

The aminosilane solution used for infusion was prepared by mixing ethanol, silane and water in a 5 : 0.25 : 0.06 volumetric ratio. Surface amine gradients were prepared by slowly infusing a freshly prepared aminosilane solution into a vial containing the vertically aligned substrate by ***CRI***.[9,18] During infusion, the base-layer-coated substrate was exposed to the aminosilane solution for 30 min along its length in a time dependent fashion, thus producing a gradual spatial variation in the extent of amine modification from top to bottom.

The mercaptosilane solution for subsequent use in ***CRI*** was prepared by mixing ethanol : silane : 0.1 M HCl in a 11.8 : 0.125 : 0.125 volumetric ratio. The solution was vigorously stirred for 5 min, after which 0.125 ml of 0.3 M NH_4OH solution was added to neutralize the acid and ultimately increase the rate condensation of the silanols.[20] The pH of the resultant solution was ~ 6.3 similar to one shown in **Chapter 3**. The solution was stirred for an additional 25 min and sat quiescent for 90 min before use in ***CRI*** with an infusion rate of ~0.3 mL/min.

5.3.2 Characterization

XPS spectroscopy[23, 24], **TM-AFM** and **WCA** measurement are described in **Chapter 3** and **DCA**[25-27] measurement is described in **Chapter 4**.

5.4. Results and Discussion

5.4.1 Gradient fabrication

A flow chart outlining the steps associated with gradient formation is shown in **Scheme 5.1**. At first, APTEOS and MPTMOS derived gradients were prepared separately on TMOS-derived base-layer coated substrates by ***CRI*** as outlined in the **Scheme 5.1**. These gradients denoted as "N gradient" and "S gradient" respectively. Multi-component gradients e.g., "NH_2+SH or $\boldsymbol{T}_{NH_2+SH}$" were prepared by infusing a freshly prepared MPTMOS sol along the same direction gradient, termed as "$\boldsymbol{T}_{NH_2+SH}$ aligned" gradient or in the opposite direction to produce "$\boldsymbol{T}_{NH_2+SH}$ opposed" gradient. Before further modification with APTEOS sol "S gradient" was immersed in H_2O_2. H_2O_2 was used to oxidize the thiol groups to sulfonic acid groups (SH→ SO_3H).[28, 29] Specifically, surface charge gradients were prepared as explained in **Chapter 3** by exposing the multi-component gradients to 30% H_2O_2 at 70 ^oC for 20 min. This treatment converts the "S gradients" to "SO_3^- gradients". Aligned and opposed "$\boldsymbol{T}_{SO_3^-+NH_2}$ gradients" were prepared by infusing the APTEOS sol along the same and opposite direction of the "SO_3^- gradients". H_2O_2 treatment was also performed on $\boldsymbol{T}_{NH_2+SH}$ gradients The oxidation of thiol to sulfonate group (SO_3^-) subsequently leads to the protonation of amine (NH_2 →NH_3^+). Therefore, $\boldsymbol{T}_{N+S}$ gradients convert into $\boldsymbol{T}_{NH_3^+ + SO_3^-}$ aligned and opposed gradients. The duration of the reaction time with H_2O_2 was optimized as described in **Chapter 3**. After ***CRI***, the samples were rinsed with ultrapure water, dried with a stream of N_2 and stored in a desiccator. We denote the "amine + thiol" aligned and

opposed charge gradients as ($\boldsymbol{T}_{NH_3^+ + SO_3^-}$ (A)) and ($\boldsymbol{T}_{NH_3^+ + SO_3^-}$(O)) respectively and "thiol + amine" aligned and opposed charge gradients as ($\boldsymbol{T}_{SO_3^- + NH_2}$ (A)) and ($\boldsymbol{T}_{SO_3^- + NH_2}$ (O)) respectively.

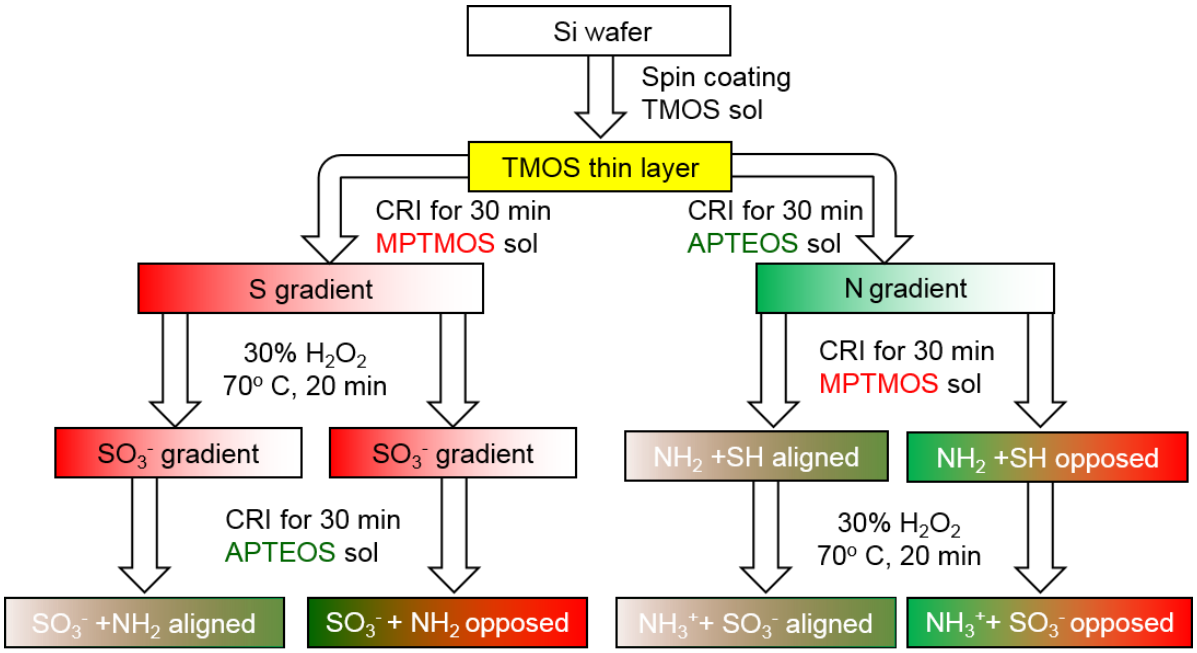

Scheme 5.1: Fabrication of aligned and opposed ($\boldsymbol{T}_{NH_3^+ + SO_3^-}$) (right side) and ($\boldsymbol{T}_{SO_3^- + NH_2}$) (left side) charge gradients by programmed rate infusion (CRI method)[18].

5.4.2 X-ray photoelectron spectroscopy

The presence and extent of modification of the surfaces with amine and thiol as well as the degree of protonation/oxidation were evaluated using **XPS** spectroscopy. **Figure 5.1** shows an overlay of five N1s and S2p **XPS** spectra for the aligned and opposed ($\boldsymbol{T}_{SO_3^- + NH_2}$) gradients acquired at ~3 mm intervals from the high amine end (position 5) to the low amine end (position 1). The N1s peak in the **XPS** spectra shown in **Figure 5.1** (**a**, **c**) appears as a doublet with binding energies (***BE***) ~399.5 and ~401.8 eV, corresponding to free amine and protonated/H-bonded amines, respectively, in accordance with the literature.[12, 16, 23 30-33] For S2p, the spectrum consists of one peak at a binding energy of 168.5 eV (see **Figure 5.1** (**b, d**)) in agreement with reported values.[35-37] For the aligned gradient, both the N1s and S2p signals increase from low amine end (sample #1)

to high amine end (sample #5), while for the opposed gradient the N1s signal increases while the S2p decreases from position sample # (1-5). These trends indicate the presence of multi-component gradients in the same or opposing directions.

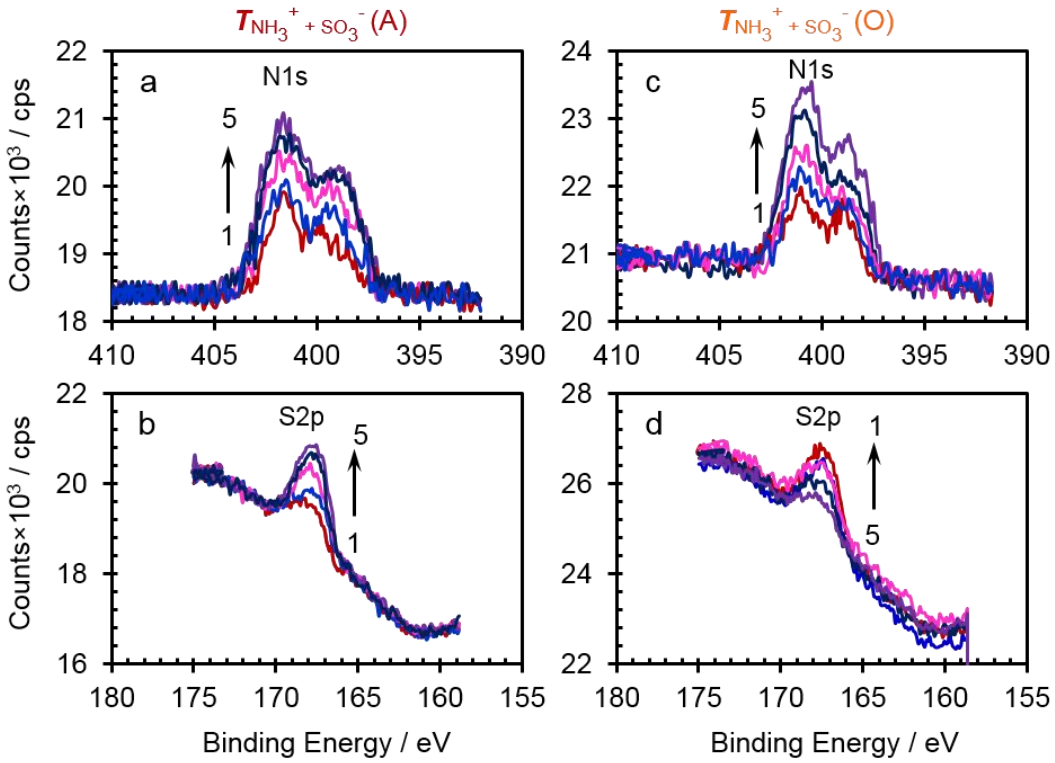

Figure 5.1: **XPS** spectra of N1s and S2p peaks. (a) and (b) correspond to ($\boldsymbol{T}_{NH_3^+ + SO_3^-}$(A)) gradients and (c) and (d) correspond to ($\boldsymbol{T}_{NH_3^+ + SO_3^-}$(O)) gradients.

As shown in **Figure 5.2**, the XPS spectra of N1s peaks for aligned and opposed ($\boldsymbol{T}_{SO_3^- + NH_2}$) gradients exhibit increasing intensity from low amine end (sample #1) to high amine bottom (sample #5). S2p peak intensity on the other hand, increases and decreases from (sample #1) to low amine top (sample #5) for the aligned and opposed gradients, respectively. However, the extent of protonation of the free amine on surface is different for the ($\boldsymbol{T}_{NH_3^+ + SO_3^-}$) and ($\boldsymbol{T}_{SO_3^- + NH_2}$) gradients. **XPS** results indicate that thiol (SH) group was totally converted to sulfonate group (SO_3^-). However, the percent conversion of amine into protonated amine group is lower for the ($\boldsymbol{T}_{SO_3^- +}$

$_{NH_2}$) gradients as judged by the larger peak at ~402 eV compared to ($\boldsymbol{T}_{NH_3^+ + SO_3^-}$) (compare **Figure 5.1** and **5.2**). For the opposed ($\boldsymbol{T}_{SO_3^- + NH_2}$) gradient, the extent of protonation is higher at the low amine (sample 1) than the high amine end whereas for aligned ($\boldsymbol{T}_{SO_3^- + NH_2}$), the extent of protonation at bottom and the top are similar. Deconvolution of the N1s spectra into two components (protonated and nonprotonated) for the ($\boldsymbol{T}_{NH_3^+ + SO_3^-}$ (O)) and ($\boldsymbol{T}_{NH_3^+ + SO_3^-}$ (A)) gradients yields a NH_3^+/N (***R***) in the dry state of ~0.66 - ~0.64 at the bottom or high amine end (sample #5) of the gradient and ~0.56 - ~0.61 and at the top or low amine end (sample #1) of the gradient as shown in **Table 5.1** indicative of a slightly greater protonation of the amine groups at the high amine end. The lower the value of ***R,*** the lower the protonated fraction on the surface and the higher the fraction of free amine. The value of ***R*** in the $\boldsymbol{T}_{SO_3^- + NH_2}$ (A) gradient is almost invariant (~0.5) along the length of the gradient indicating that 50% of the free amine was protonated due to the reaction. On the other hand, the value of ***R*** in the $\boldsymbol{T}_{SO_3^- + NH_2}$ (O) gradient increases from ~0.42 to ~0.66 from low amine end to the high amine end indicative of a significantly lesser protonation of the amine groups at the high amine end. At the other end of this gradient which is the low amine end containing the greater amount of sulfonate ions have mostly protonated amine groups little higher than the other. Note that from high amine end to the low amine end of $\boldsymbol{T}_{SO_3^- + NH_2}$ (O) gradient, the

Table 5.1: Deconvoluted N1s peak area into NH_3^+ and NH_2 and their ratio ***R*** ($NH_3^+ /NH_2 + NH_3^+$).

	$\boldsymbol{T}_{NH_3^+ + SO_3^-}$ (O)			$\boldsymbol{T}_{NH_3^+ + SO_3^-}$ (A)			$\boldsymbol{T}_{SO_3^- + NH_2}$ (O)			$\boldsymbol{T}_{SO_3^- + NH_2}$(A)		
Sample #	NH_3^+	NH_2	***R***	NH_3^+	NH_2	***R***	NH_3^+	NH_2	***R***	NH_3^+	NH_2	***R***
5	6350.0	3292.0	0.66	5692.0	3229.0	0.64	3355.0	4548.0	0.42	4052.0	4010.0	0.50
4	5530.0	2999.0	0.65	5110.0	2902.0	0.64	3022.0	4290.0	0.41	3793.0	3548.0	0.52
3	5147.0	3080.0	0.63	5061.0	2923.0	0.63	3246.0	3347.0	0.49	3592.0	2874.0	0.56
2	3342.0	2811.0	0.54	3967.0	2423.0	0.62	3764.0	2007.0	0.65	2677.0	2771.0	0.49
1	2846.0	2220.0	0.56	2960.0	1915.0	0.61	2981.0	1533.0	0.66	2542.0	2188.0	0.54

dominant fraction of nitrogen changes from free amine to protonated amine. The lower protonation at the high amine end of the gradients could result from changes in the pK_b of the immobilized base due to changes in hydrogen bonding and the local chemical environment.[34] Alternatively, it could be due to the fact that the percent ionization of a weak base (or acid) depends on its concentration.

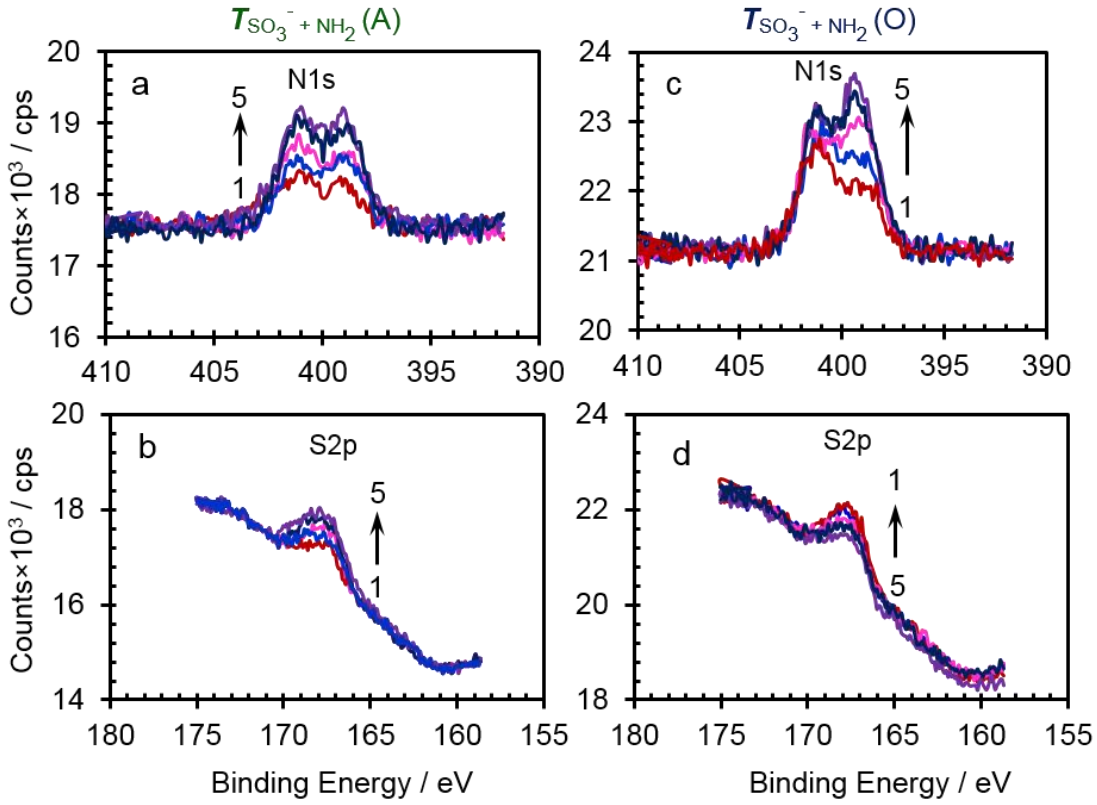

Figure 5.2: **XPS** spectra of N1s and S2p peaks. (a) and (b) correspond to ($\boldsymbol{T}_{SO_3^- + NH_2}$ (A)) gradients and (c) and (d) correspond to ($\boldsymbol{T}_{SO_3^- + NH_2}$ (O)) gradients.

To better evaluate the gradient profile, the integrated areas under the N1s and S2p peaks for both the ($\boldsymbol{T}_{NH_3^+ + SO_3^-}$) and ($\boldsymbol{T}_{SO_3^- + NH_2}$) charge gradients as function of distance along length of the substrate were plotted as shown in **Figure 5.3**. The area under the N1s peak increases from top to bottom for all the gradients. As evident in **Figure 5.3** (**A**), the area of the N1s in both the ($\boldsymbol{T}_{NH_3^+ + SO_3^-}$) gradients is higher than that of the SO_3^- to NH_2 analog. A similar analogy holds for

the aligned gradients. This result indicates that when surface is modified with thiol (SH) first, less modification by amine (NH_2) takes place. The reverse is true when the infusion of the modifying silanes flips. This is probably surface amine undergoes drastic condensation on the surface because of its self-catalyzing activity and at the same time catalyzes the condensation of the thiolsilane. Thus, there is more nitrogen as well sulfur on the surface when the aminosilane deposition takes place first.

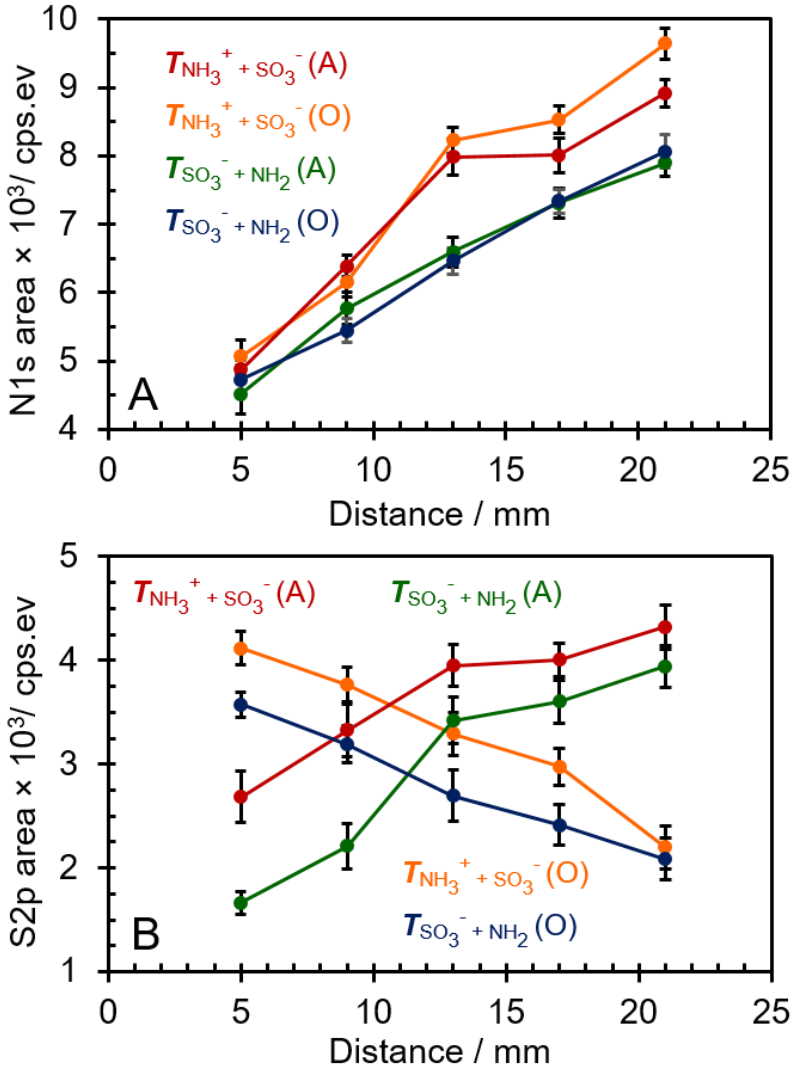

Figure 5.3: N1s and S2p area vs. distance profiles for ($\boldsymbol{T}NH_3^+ + SO_3^-$) and ($\boldsymbol{T}SO_3^- + NH_2$) samples for both aligned and opposed gradients.

For S2p, it can be observed that there is less sulfur on the surface at the top and bottom ends for the ($\boldsymbol{T}_{SO_3^- + NH_2}$) gradients as compared to ($\boldsymbol{T}_{NH_3^+ + SO_3^-}$(A)) gradients (green vs. red in **Figure 5.3**). The same holds true for the opposed gradients (yellow vs. blue in **Figure 5.3**) particularly at the low amine end.

It is clear from these results that sulfur (***S***) immobilizes more onto the "amine + thiol" or $\boldsymbol{T}_{NH_3^+ + SO_3^-}$ samples and it was always lower in the thiol + amine" or $\boldsymbol{T}_{SO_3^- + NH_2}$ samples. This is attributed to the fact that amine having a lone pair of electron works as a Lewis base and catalyzes the condensation of the thiolsilane to the surface thereby increasing the amount of immobilized sulfur on the surface in the amine + thiol samples.

5.4.3 WCA Analysis

WCA is a rapid acquisition of information about hydrophobicity and hydrophilicity originating from the polarity differences along the length of the samples. The surface polarity, and hence the WCA, is determined by the net effects of the various component functional groups present on the film surface. **Figure 5.4** shows images of water drops spaced ~ 5 mm apart along the length of the gradient surfaces. The degree to which the water wets the surface depends on its position along the length of the gradient film as well as the type of surface. It has been found that the size of the water drop depends on the type of gradients, for example, aligned vs. opposed, thiol vs. amine or amine vs. thiol. Water wets ($\boldsymbol{T}_{SO_3^- + NH_3^+}$) gradients more than ($\boldsymbol{T}_{SO_3^- + NH_2}$) as shown in the **Figure 5.4**. Interestingly, the **WCA** behavior of the aligned ($\boldsymbol{T}_{NH_3^+ + SO_3^-}$) and the aligned and opposed ($\boldsymbol{T}_{SO_3^- + NH_2}$) gradients is almost identical, i.e., the CA decreases from bottom (high amine end) to the top of the gradients. Water completely wets the opposed ($\boldsymbol{T}_{NH_3^+ + SO_3^-}$) gradient because of the presence of the charged species on both sides of the gradient.

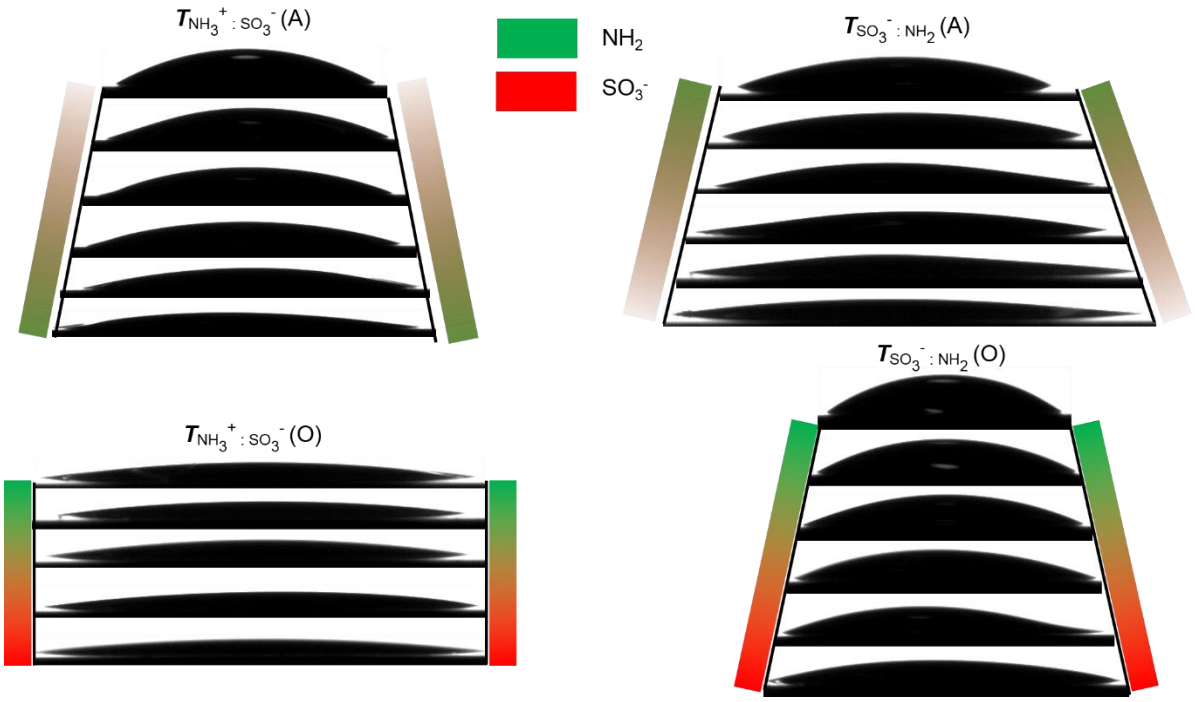

Figure 5.4: Shape of water droplets on the gradient surfaces. WCA was taken at every 5 mm along the length of gradients.

To better understand how the WCAs change with distance, profile plots were constructed. **Figure 5.5** shows WCAs obtained for the ($\boldsymbol{T}_{NH_3^+ + SO_3^-}$) and ($\boldsymbol{T}_{SO_3^- + NH_2}$) gradients. Other than the ($\boldsymbol{T}_{NH_3^+ + SO_3^-}$ (O)) gradient, all the gradients exhibit an increasing **WCA** from bottom (high amine end) to the top (low amine end). The rather low contact angle at the end of the gradient indicates the presence of charged species on the surface. The sample ($\boldsymbol{T}_{SO_3^- + NH_2}$ (O)) has a highest **CA** at the top, which is mostly dominated by the by the NH_2 species as evident from the **XPS** results. Normally amine modified TMOS surface has a **CA** around 65 ^{o} as explained in **Chapter 3**. In this case, the high amine end of ($\boldsymbol{T}_{SO_3^- + NH_2}$ (O)) gradient has obviously small amount of SO_3^- that inevitably lowers the **WCA**. The top of this gradient, however, is heavily modified with sulfonate group thereby turning the low amine end into a more hydrophilic surface and the **WCA** is reduced to 18 ^{o}. The **WCA** of ($\boldsymbol{T}_{SO_3^- + NH_2}$ (A)) gradient has a value of 14 ^{o} at the bottom (heavily modified

end) and 33 ^{o} at the top (least modified end). This gradient ($\boldsymbol{T}_{SO_3^- + NH_2}$ (A)) is prepared by infusing the thiolsilane first, followed by aminosilane in the same direction. Thus, the high amine end of the gradient is rich in SO_3^- and NH_2 functional groups which cause the surface to wet more by water. Sample ($\boldsymbol{T}_{NH_3^+ + SO_3^-}$ (A)) behaves similarly to ($\boldsymbol{T}_{SO_3^- + NH_2}$ (A)) only except it has NH_3^+ more than NH_2 causing the **WCA** is reduced to even more at the top (28 ^{o}). ($\boldsymbol{T}_{NH_3^+ + SO_3^-}$ (O)) has a **WCA** ~$(11\text{-}12)^0$ and is invariant along the length of the gradient. Since the gradient is dominated by the charged species across the surface, water wets the surface nearly completely.

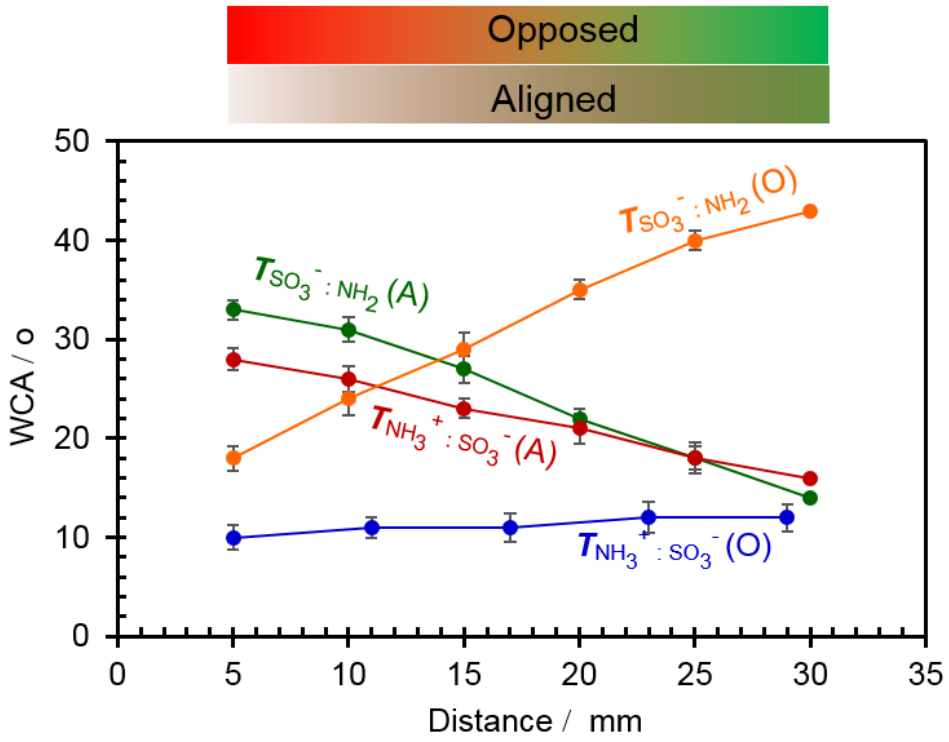

Figure 5.5: Contact angle profiles for ($\boldsymbol{T}_{NH_3^+ + SO_3^-}$) and ($\boldsymbol{T}_{SO_3^- + NH_2}$) samples for both aligned and opposed gradients.

5.4.4 DCA analysis

DCA measurements using the Wilhelmy plate method[25, 26] were performed to obtain information about the heterogeneity and/or phase separation effected by the reaction of the various charged species present on the gradient films. Since our samples were prepared by modifying the TMOS thin films by amine and the thiol groups and vice versa, **DCA** can provide valuable information regarding these effects on the gradients. Thus, the shape of the **DCA** graphs can tell us effect of the amine over thiol or thiol over amine gradients. The Wilhelmy plate method provides the average advancing and receding contact angle along the entire area at the solid-liquid-air interface. For heterogeneous samples, **DCA** is faster than the sessile drop method, which requires numerous water drops to be placed at various locations on the sample.[25] Furthermore, for a gradient sample that is macroscopically heterogeneous on the millimeter length scale, the Wilhelmy plate method is advantageous in providing a means to rapidly assess wettability along the perimeter of a substrate, typically 2-4 cm in length.[25] Contact angle hysteresis, θ_Δ ($\theta_\Delta = \theta_{adv} - \theta_{rec}$) can also be readily ascertained at various locations along the length of the substrate to obtain information regarding surface heterogeneity[38] originating from the different preparation methods. For gradient films, however, the Wilhelmy plate method requires a near-identical film on both sides of the substrate. For this we spin coated both sides of a polished Si wafer with the TMOS-derived sol and prepared aligned and opposed ($\boldsymbol{T}_{NH_3^+ + SO_3^-}$) and ($\boldsymbol{T}_{SO_3^- + NH_2}$) gradients using the ***CRI*** method as described in the experimental section. To verify that the water was not contaminated by components leaching out of the films during **DCA** analysis, pre- and post-water checks were performed and showed no significant contamination.

The hydrophilic end of the gradient samples was immersed first and the hydrophobic end was immersed last. For example, for aligned gradient irrespective of the sequence of preparation, the heavily modified bottom end was immersed first. For opposed ($\boldsymbol{T}_{SO_3^- + NH_2}$) gradient the end heavily modified with SO_3^- group was immersed first. ($\boldsymbol{T}_{NH_3^+ + SO_3^-}$ (O)) gradient the end heavily modified with NH_3^+ group was immersed first.

The change in θ_{adv} and θ_{rec} for the aligned and opposed ($\boldsymbol{T}_{NH_3^+ + SO_3^-}$) and ($\boldsymbol{T}_{SO_3^- + NH_2}$) gradient samples are shown in **Figure 5.6.** As can be seen from the graphs, the shape of DCA profile for these gradients prepared in different fashions are different. For example, ($\boldsymbol{T}_{NH_3^+ + SO_3^-}$ (O)) has **DCA** profile quite different from the other three. The **WCA** along this gradient is almost constant (~11-

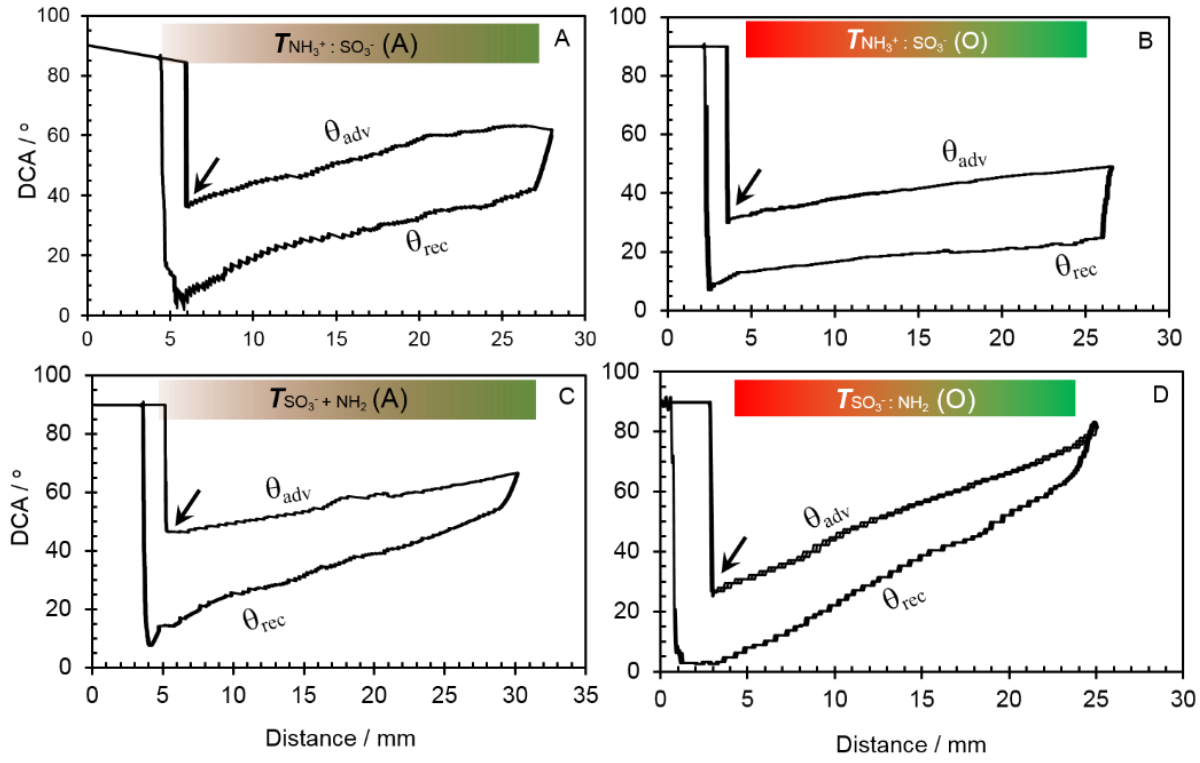

Figure 5. 6: DCA force distance curves for multicomponent charge gradient surfaces. As indicated by the arrow, the hydrophilic end was immersed first.

13^{o}). The **DCA** profile of the same gradient changes a little bit (33-48 ^{o} between the ends) when the NH_3^+ end was immersed first. Since both ends are rich in charged groups (either NH_3^+ or SO_3^- according to **XPS** results), the **DCA** does not change (17 ^{o}) much along the length of the gradient. On the other hand, the **WCA** along the length of the other three gradients was found to increase from one end to the other end. Similar to that, the **DCA** also increases when the hydrophilic end was immersed in the water first as shown in **Figure 5.6** (**A**, **C** and **D**). Since there exists a polarity difference along the length of these gradients, the **DCA** increases from a low value to high value. The DCA curve for the TMOS base layer was obtained and shown in the previous chapter (**Chapter 4**). The curve for the base layer was horizontal and the hysteresis was quite constant along the sample. The DCA curves for the charge gradients were found steeper. The steepness of the DCA curve indicates gradual variation of surface heterogeneity caused by chemical reaction. The initial DCA for all these gradients is higher than the corresponding WCA values. This is probably associated with the change in the surface hydrophilicity due to moisture adsorbed on the surface in-between preparation and the DCA measurements. Furthermore, we notice that both aligned and opposed ($\boldsymbol{T}_{SO_3^- + NH_2}$) gradients exhibit steeper DCA curves indicating that these regions of the gradients are rich in less polar NH_2 group but not highly polar NH_3^+ group in accordance with the **XPS** results.

The contact angle hysteresis at five different positions (4, 8, 12, 16 and 20 mm) is plotted for different gradient samples as shown in **Figure 5.7**. The average value of each position ±1 mm was acquired for plotting this graph. Position **4** mm for all ***aligned*** gradients is the heavily modified end with both thiol (SH → SO_3^-) and NH_2 or NH_3^+. Whereas it is the thiol (SH → SO_3^-) modified end for the ***opposed*** ($\boldsymbol{T}_{SO_3^- + NH_2}$) gradient and amine or NH_3^+ modified end for the ($\boldsymbol{T}_{NH_3^+ + SO_3^-}$) gradient. The smallest hysteresis is noted for TMOS-derived base layer and it is almost constant every point along the length of the substrate. Likewise, the hysteresis across the length of the substrate is approximately constant for the aligned ($\boldsymbol{T}_{NH_3^+ + SO_3^-}$) gradient. For $\boldsymbol{T}_{SO_3^- + NH_2}$ samples, the hysteresis noticeably decreased from position 4 mm to position 20 mm. Note that the hysteresis

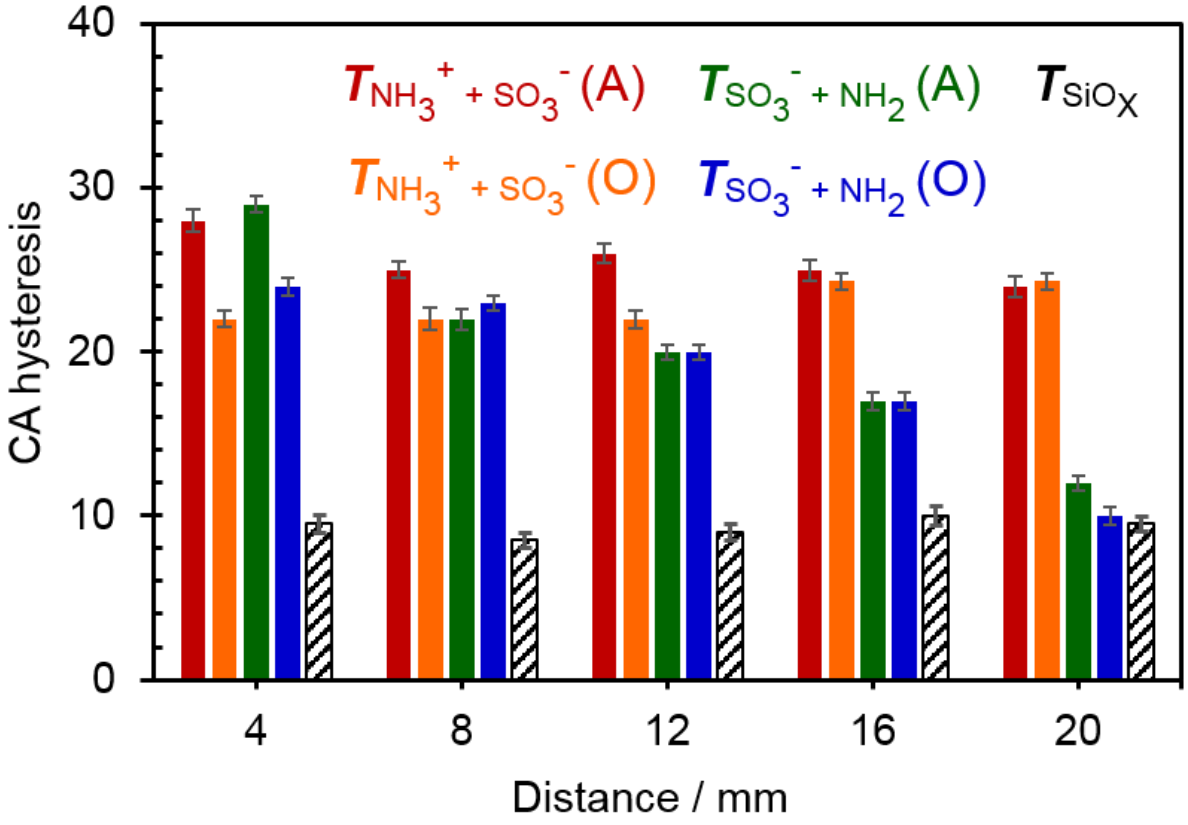

Figure 5.7: Dynamic contact angle hysteresis at five different points (4, 8, 12, 16 and 20 mm) along the length of the aligned and opposed ($\boldsymbol{T}_{NH_3^+ + SO_3^-}$) and ($\boldsymbol{T}_{SO_3^- + NH_2}$) gradients.

decreases from one end (4 mm) to the other end (20 mm) for the aligned ($\boldsymbol{T}_{NH_3^+ + SO_3^-}$) gradient and both aligned and opposed ($\boldsymbol{T}_{SO_3^- + NH_2}$) gradients. It can be observed that all the samples show higher hysteresis than that measured on the TMOS derived base layer, meaning that subsequent treatment brought about the heterogeneity in the gradient samples. We see that the hysteresis difference for the ($\boldsymbol{T}_{NH_3^+ + SO_3^-}$(O)) sample increases a little from 22 ° at NH_3^+ (high amine) end to 24° at SO_3^- end (high thiol). On the other hand, the surface heterogeneity decreases along the length of all other gradients. The highest decrease 17° (**Figure 5.7**) was observed for ($\boldsymbol{T}_{SO_3^- + NH_2}$) aligned gradient (from heavily modified end to least modified end then it is ($\boldsymbol{T}_{SO_3^- + NH_2}$) opposed gradient (14) and the lowest decreases is found in ($\boldsymbol{T}_{NH_3^+ + SO_3^-}$) aligned gradient (4°) as calculated from **Figure 5.7**.

The DCA is very good indicator to show that the various surface functional groups such as NH_2, NH_3^+, SO_3^-, SiO^- have a dominant effect in governing the surface wetting behavior. **XPS** results have already proved that when the surface is infused with aminosilane first, it results in more thiol on the surface whereas it is rather less when thiolsilane is infused first. The is ascribed to the ability of the amine group to act as a Lewis base that catalyzes the thiol condensation reaction. When amine is deposited first, a large fraction of the amine on the surface is converted from free amine to protonated amine whereas when the amine is deposited after the thiol, only about one third of the total free amine is converted to protonated amine. This means that for the $\boldsymbol{T}_{SO_3^- + NH_2}$(A) gradient, the heavily modified end is less rich in both SO_3^- and NH_2 group as compared to $\boldsymbol{T}_{NH_3^+ + SO_3^-}$(A) gradient. The other end of $\boldsymbol{T}_{SO_3^- + NH_2}$(A) gradient however has plenty of silanol and some NH_2 groups in contrast to NH_3^+ group in $\boldsymbol{T}_{SO_3^- + NH_2}$(A) gradient. For $\boldsymbol{T}_{NH_3^+ + SO_3^-}$ opposed gradient, one end is rich with NH_3^+ group and the other end is rich with SO_3^-group both

of which decrease from one end to the other. The amount of these species NH_2, NH_3^+ and SO_3^- are less in extent in the $\boldsymbol{T}_{NH_3^+ + SO_3^-}$ opposed gradient as compared to $\boldsymbol{T}_{SO_3^- + NH_2}$ opposed gradient.

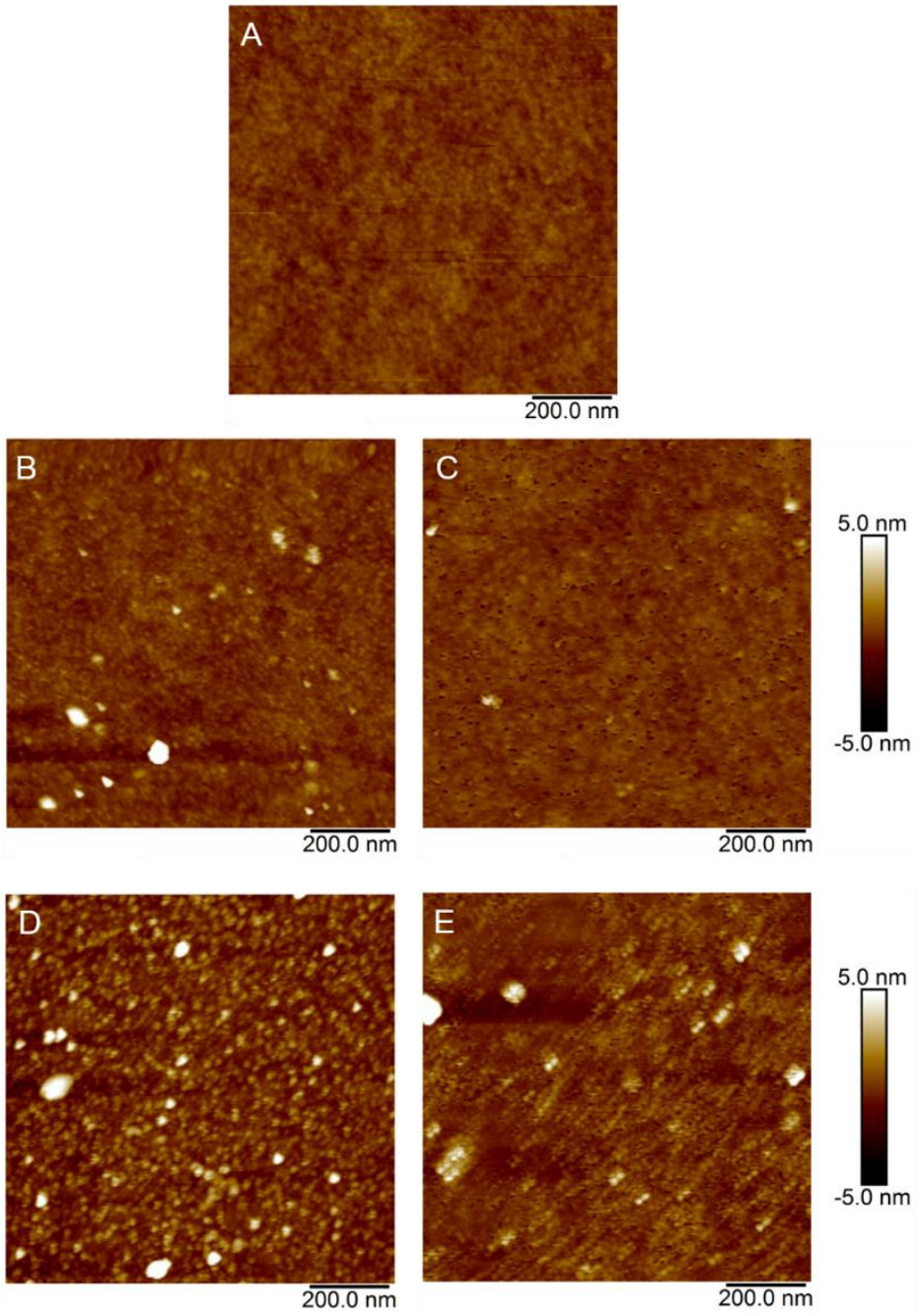

Figure 5.8: AFM images of (A) TMOS derived base layer, (B) ($\boldsymbol{T}_{SO_3^- + NH_2}$ (O)), (C) ($\boldsymbol{T}_{SO_3^- + NH_2}$ (A)), (D) ($\boldsymbol{T}_{NH_3^+ + SO_3^-}$) (O)) and ($\boldsymbol{T}_{NH_3^+ + SO_3^-}$ (A)) surfaces. All the images were taken near the middle point of the samples.

The data analysis of DCA graphs provides two interesting results. First, the contact angle hysteresis varies across the length of the gradient substrate. Dettre and Johnson reported that θ_Δ is very sensitive to hydrophobicity and coverage and the receding angle, in particular, can vary considerably over a relatively narrow change of coverage.[39] Gradient materials are particularly useful in this regard because coverage can be easily changed over a narrow range spanning short distances. Second, it can be observed that θ_Δ varies depending on the type of gradients e.g., amine over thiol or thiol over amine or aligned vs. opposed.

Because contact angle hysteresis can vary with roughness, the RMS surface roughness (***R*q**) of the base-layer supported films used herein was investigated by **TM-AFM** (1 μm x 1 μm area scans). The results are shown in **Figure 5.8**. ***R***q was typically on the order of ~0.3-1.1 nm (**Table 5.2**). Surface roughness alone does not usually contribute to contact angle hysteresis unless > 100 nm.[40-42] The next most likely contributor is chemical heterogeneity, which has been observed on amine and thiol functionalized gradient films.[12] For the gradient materials particularly (***T***$_{SO_3^- + NH_2}$) samples, we observe that the contact angle hysteresis at the hydrophilic end (bottom) is larger than that observed on the more hydrophobic side on the gradient for three of the four samples. A

Table 5.2: Roughness factor (***R*q**) of the base layer and the charged surfaces.

Samples	Roughness (nm) in 1 cm × 1 cm area
TMOS base layer	0.48±0.10
T$_{NH_3^+ : SO_3^-}$ (A)	1.00±0.16
T$_{NH_3^+ : SO_3^-}$ (O)	0.93±0.20
T$_{NH_3^+ : SO_3^-}$ (O)	1.11±0.29
T$_{NH_3^+ : SO_3^-}$ (O)	1.13±0.23

possible reason for this observation is that the hydrophilic end of the gradient has both hydrophilic SO_3^- and NH_3^+ and NH_2 groups; the coexistence of these groups generates a nanoscale heterogeneous surface. The more hydrophobic side, however, has fewer SO_3^-, and NH_3^+ groups but more SiOH and some NH_2 groups, resulting in lower observed hysteresis. For the ($\boldsymbol{T}_{NH_3^+ + SO_3^-}$ (O)) gradient film, both ends have hydrophilic groups that keeps the hysteresis almost unchanged and similar on both the hydrophilic end and hydrophobic end. ($\boldsymbol{T}_{NH_3^+ + SO_3^-}$ (A)) gradient has both hydrophilic SO_3^-, and NH_3^+ groups at which decreases in number from bottom to the top. These groups generate a nanoscale heterogeneity which spans the whole film causing the hysteresis to decrease only slightly (28 → 24).

5.5 Summary

The NH_3^+ to SO_3^- and SO_3^- to NH_2 gradients were prepared by the controlled rate infusion method on TMOS-derived siloxane base layer. The effect of the order of deposition (thiol + amine or amine + thiol was thoroughly investigated by the **XPS** spectroscopy, **WCA** and **DCA** in conjunction with the **AFM** microscopy. The examination of the **XPS** results, **SCA**, and **DCA** indicate that the extent of nitrogen and sulfur on the surface and the wettability of the surface depends on the order of infusion. The extent of nitrogen and sulfur was found to be less when thiol was deposited first. **DCA** data coupled with **AFM** explains that the varying degree of nanoscale heterogeneity produced along the gradient due to the interaction of the surface charge groups causes the varying contact angle hysteresis.

5.6. References

1. Genzer, J. Surface-bound gradients for studies of soft materials behavior. *Annu. Rev. Mater. Res.* **2012**, *42* (42), 435−468.
2. Genzer, J.; Bhat, R. R. Surface-bound soft matter gradients. *Langmuir* **2008**, *24* (6), 2294−2317.
3. Kim, M. S.; Khang, G.; Lee, H. B. Gradient polymer surfaces for biomedical applications. *Prog. Polym. Sci*. **2008**, *33* (1), 138−164.
4. Lin, X. K.; He, Q.; Li, J. B. Complex polymer brush gradients based on nanolithography and surface-initiated polymerization. *Chem. Soc. Rev*. **2012**, *41* (9), 3584−3593.
5. Morgenthaler, S.; Zink, C.; Spencer, N. D. Surface-chemical and -morphological gradients. *Soft Matter* **2008**, *4* (3), 419−434.
6. Pulsipher, A.; Yousaf, M. N. Surface chemistry and cell biological tools for the analysis of cell adhesion and migration. *ChemBioChem* **2010**, *11* (6), 745−753.
7. Wu, J. D.; Mao, Z. W.; Tan, H. P.; Han, L. L.; Ren, T. C.; Gao, C. Y. Gradient biomaterials and their influences on cell migration. *Interface Focus* **2012**, *2* (3), 337−355.
8. Zhang, J. L.; Han, Y. C. Active and responsive polymer surfaces. *Chem. Soc. Rev*. **2010**, *39* (2), 676−693.
9. Kannan, B.; Higgins, D. A.; Collinson, M. M. Aminoalkoxysilane reactivity in surface amine gradients prepared by controlled-rate infusion. *Langmuir* **2012**, *28* (46), 16091−16098.
10. Lee, J.; Choi, I.; Yeo, W. S. Preparation of gradient surfaces by using a simple chemical reaction and investigation of cell adhesion on a two-component gradient. *Chem. Eur. J.* **2013**, *19* (18), 5609−5616.

11. Ma, Y. R.; Zheng, J. K.; Amond, E. F.; Stafford, C. M.; Becker, M. L. Facile fabrication of ″dual click″ one- and two-dimensional orthogonal peptide concentration gradients. *Biomacromolecules* **2013**, *14* (3), 665−671.

12. Ashraf, K. M.; Giri, D.; Wynne, K. J.; Higgins, D. A.; Collinson M. M. Cooperative effects in aligned and opposed multicomponent charge gradients containing strongly acidic, weakly acidic, and basic functional groups *Langmuir*, **2016**, *32*, 3836−3847.

13. Kannan, B.; Marin, M. A.; Shrestha, K.; Higgins, D. A.; Collinson, M. M. Continuous stationary phase gradients for planar chromatographic media. *J. Chromatogr. A* **2011**, *1218* (52), 9406−9413.

14. Pucci, V.; Raggi, M. A.; Svec, F.; Frechet, J. M. J. Monolithic columns with a gradient of functionalities prepared via photoinitiated grafting for separations using capillary electrochromatography. *J. Sep. Sci.* **2004**, *27* (10−11), 779−788.

15. Beurer, E.; Venkataraman, N. V.; Sommer, M.; Spencer, N. D., Protein and Nanoparticle Adsorption on Orthogonal, Charge-Density-Versus-Net-Charge Surface-Chemical Gradients. *Langmuir* **2012**, *28*, 3159−3166.

16. Riepl, M.; Ostblom, M.; Lundstrom, I.; Svensson, S. C. T.; van der Gon, A. W. D.; Schaferling, M.; Liedberg, B. Molecular gradients: An efficient approach for optimizing the surface properties of biomaterials and biochips. *Langmuir* **2005**, *21* (3), 1042−1050.

17. Gessner, A.; Lieske, A.; Paulke, B. R.; Muller, R. H. Influence of surface charge density on protein adsorption on polymeric nanoparticles: analysis by two-dimensional electrophoresis. Eur. J. Pharm. *Biopharm*. **2002**, *54* (2), 165−170.

18. Kannan, B.; Dong, D.; Higgins, D. A.; Collinson, M. M., Profile Control in Surface Amine Gradients Prepared by Controlled-Rate Infusion. *Langmuir* **2011**, *27* (5), 1867-1873.

19. Schubert, U.; Husing, N.; Lorenz, A., Hybrid inorganic-organic materials by sol-gel processing of organofunctional metal alkoxides. *Chemistry of Materials* **1995,** *7* (11), 2010-2027.

20. Brinker. C. J. Hydrolysis And Condensation Of Silicates - Effects On Structure, *Journal of Non-Crystalline Solids* **1988,** *100* (1-3), 31-50

21. Brinker, C. J.; Keefer, K. D.; Schaefer, D. W.; Ashley, S. Sol-gel transition in simple silicates, *Journal of Non-Crystalline Solids* **1982,** *48* (1), 47-64.

22. Fidalgo, A.; Ilharco, L. M. Chemical tailoring of porous silica xerogels: Local structure by vibrational spectroscopy, *Chemistry-a European Journal* **2004,** *10* (2), 392-398.

23. Graf, N.; Yegen, E.; Gross, T.; Lippitz, A.; Weigel, W.; Krakert, S.; Terfort, A.; Unger, W. E. S. XPS and NEXAFS studies of aliphatic and aromatic amine species on functionalized surfaces, *Surface Science,* **2009,** *603* (18), 2849-2860.

24. Kristensen, E. M. E.; Nederberg, F.; Rensmo, H.; Bowden, T.; Hilborn, J.; Siegbahn, H. Photoelectron spectroscopy studies of the functionalization of a silicon surface with a phosphorylcholine-terminated polymer grafted onto (3-aminopropyl)trimethoxysilane, *Langmuir,* **2006,** *22* (23), 9651-9657.

25. Yuan, Y.; Lee, T. R. Contact angle and wetting properties. In *Surface science techniques*; Springer, 2013, pp 3-34.

26. Eral, H. B.; Mannetje, D.; Oh, J. M. Contact angle hysteresis: a review of fundamentals and applications. *Colloid Polym. Sci.,* **2013,** *291* (2), 247-260.

27. Uilk, J. M.; Mera, A. E.; Fox, R. B.; Wynne, K. J. Hydrosilation-cured poly (dimethylsiloxane) networks: Intrinsic contact angles via dynamic contact angle analysis. *Macromolecules,* **2003,** *36* (10), 3689-3694.

28. Cano-Serrano, E.; Blanco-Brieva, G.; Campos-Martin, J. M.; Fierro, J. L. G. Acid-functionalized amorphous silica by chemical grafting-quantitative oxidation of thiol groups, *Langmuir*, **2003,** *19*, 7621-7627.

29. Cano-Serrano, E.; Campos-Martin, J. M.; Fierro, J. L. G. Sulfonic acid-functionalized silica through quantitative oxidation of thiol groups., *Chem. Com. (Cambridge, England)*, **2003**, DOI: 10.1039/b210766j, 246-247.

30. Zhang, F. X.; Srinivasan, M. P. Self-assembled molecular films of aminosilanes and their immobilization capacities, *Langmuir*, **2004,** *20* (6), 2309-2314.

31. Vandenberg, E. T.; Bertilsson, L.; Liedberg, B.; Uvdal, K.; Erlandsson, R.; Elwing, H.; Lundstrom, I. Structure Of 3-Aminopropyl Triethoxy Silane On Silicon-Oxide, *J. Colloid Interface Sci.*, **1991,** *147* (1), 103-118.

32. Metwalli, E.; Haines, D.; Becker, O.; Conzone, S.; Pantano, C. G. Surface characterizations of mono-, di-, and tri-aminosilane treated glass substrates *J. Colloid Interface Sci.*, **2006,** *298*, 825-831.

33. Castner, D. G.; K. Hinds, K.; Grainger, D. W. X-ray photoelectron spectroscopy sulfur 2p study of organic thiol and bisulfide binding interactions with gold surfaces, *Langmuir*, **1996,** *12*, 5083-5086.

34. Kim, K.; Kwak, J. Faradaic impedance titration of pure 3-mercaptopropionic acid and ethanethiol mixed monolayers on gold, *J. Electroanalytical Chem.*, **2001,** *512* (1-2), 83-91.

35. Corum, L. E.: Hlady, V. Screening platelet-surface interactions using negative surface charge gradients, *Biomaterials* **2010,** *31*, 3148-3155.

36. Ding, Y. X. Streitmatter, S. Wright, B. E. Hlady, V. Spatial variation of the charge and sulfur oxidation state in a surface gradient affects plasma protein adsorption. *Langmuir,* **2010,** *26*, 12140-12146.

37. Shen, C. H.; Lin, J. C. Surface characterization and platelet compatibility evaluation of binary mixed self-assembled monolayers containing novel sulfonic acid terminated alkanethiol. *Colloids Surf. B: Biointerfaces,* **2010,** *79*, 156-163.

38. Wartz, L.W.; Garoff, S. Contact angle hysteresis on heterogeneous surfaces. *Langmuir,* **1985**, 1, 219.

39. Wang, J.-H.; Claesson, P.; Parker, J.; Yasuda, H. Dynamic contact angles and contact angle hysteresis of plasma polymers. *Langmuir,* **1994,** *10* (10), 3887-3897.

40. Dettre, R. H.; Johnson Jr, R. E. Contact Angle Hysteresis. IV. Contact Angle Measurements on Heterogeneous Surfaces1. *J. Phys. Chem.,* **1965,** *69* (5), 1507-1515.

41. Eick, J.; Good, R.; Neumann, A. Thermodynamics of contact angles. II. Rough solid surfaces. *J. Colloid Interface Sci.,* **1975,** *53* (2), 235-248.

42. Neumann, A.; Good, R. Thermodynamics of contact angles. I. Heterogeneous solid surfaces. *J. Colloid Interface Sci.,* **1972,** *38* (2), 341-358.

Chapter 6: Charge Distribution in Aligned Bi-functional Gradients as a function of surface concentration and base layer

6.1 Abstract

Charge gradients containing NH_3^+, SO_3^-, SiO^- and OH species on TMOS and OTMOS (C8) base layers were prepared by infusing APTEOS and MPTMOS of varying concentration by the ***CRI*** method in a way so that the total infusion time of individual silane solution is kept constant. The extent of modification of each charge groups were examined by **XPS** spectroscopy. It has been found that extent of modification largely depends on the initial concentration of silane used for infusion and the type of base layers. The higher the initial amine concentration, the higher the extent of modification of charged groups. On the other hand, modification is significantly low when a hydrophobic base layer (OTMOS) is used. Surface wettability also widely varied from depending on the different concentration and type of base layers. The zeta potential of these gradients exhibited a point of intersection (***POI***) where the ζ at every point of a gradient remains constant at a particular pH of the solution. The ***POI*** significantly varied from TMOS gradients to OTMOS gradients largely dependent on the extent of different charge species. The results are discussed in detail in the result and discussion section.

6.2 Introduction

Multicomponent charge gradients provide a continuous varying surface charge on a single substrate. By strategically modifying the surface with various acid-base functional groups, a spatial distribution of the charged groups along the length of the gradient can be obtained. Such a surface charge gradient can be used as smart tool for studying the local effect on adsorption of proteins over a variety of chemistry.[1-6] In addition, the surface charge gradient can provide a high throughput method to evaluate a variety of surface properties and a deeper insight in the potential cooperative effect between multiple functional groups.[5,7-10] For example charge gradients have been used to study the adhesion of platelets[7], proteins[5,8,9] and nanoparticles on surfaces.[10,11] For example, the adsorption of proteins on a unidirectional surface charge gradient where the positively charged lysozyme adsorbed preferentially on the negatively charged carboxylic acid side and the negatively charged pepsin on the positively charged amine side has been reported.[6] Chuang and Lin[7] reported the local acid base effect on platelet adhesion on mixed amine and carboxylic acid terminated self-assembled monolayers (SAMs). It was reported that protein adhesion on OH terminated SAMs was reduced in comparison with that on carboxylic-acid-terminated SAMs.[12] One common ground of studies involving charge gradients in the above mentioned biological systems is to investigate the effect of the local surface charge orientation on those biological processes in one single experiment.

In one of our previous works,[13] we have reported in detail the effect of the spatial distribution of surface charge groups (cationic and anionic) on the variations of various macroscopic properties along the multicomponent charged gradients. Depending on the distribution of the charge groups (cationic and anionic), oriented either unidirectionally or in opposed fashion, the gradients exhibited entirely different surface wettability, Au nanoparticle

adsorption, and charge variation along the surfaces. The variations of the net localized charge were found to be dependent on whether the charged species were oriented aligned or opposed to each other. The aligned multicomponent charged gradient showed a distinct point of intersection (***POI***) where the ζ along the gradient at pH ~6.6 was constant and also the direction of charge reverses at pH 8 compared to pH 3.

In the present work, we attempted to study in detail the effect of the ratio of the cationic and anionic surface charged species on the ***POI*** and the net localized charge variation along length of six different aligned gradients prepared by varying the concentration of the silanes in the original solution. Two different base layers, e.g., hydrophilic tetramethoxysilane (TMOS) and hydrophobic octyltrimethoxysilane (OTMOS) were chosen to study the effect of the base layer on the charge variation along the length. At first the gradients were characterized by **XPS** spectroscopy to see how the components vary across the surface and then their spatial variation was studied by the **WCA**. The variation of local charge density along the length of samples was studied by an electrokinetic analyzer which measured the ζ at different pHs. The distribution of local charge density/groups for the different samples was found to be different and their distribution depended on the composition of the surface charge groups as well as on the base layer.

6.3 Experimental

6.3.1 Materials

The substrate was then spin-coated with either a TMOS based sol or a hybrid sol prepared from OTMOS and TMOS in a 1 to 3 volume ratio. The TMOS sol was prepared by mixing ethanol, TMOS, HCl and water in the following composition, EtOH : TMOS : 0.1 M HCl : H_2O = 400 : 200 : 70 : 70 μL. The hybrid sol has the following composition, EtOH : TMOS : OTMOS : 0.1 M

HCl : H_2O = 400 : 200 : 70 : 70 : 70 μL. The sol was then spin coated on a clean Si wafer at 5000 rpm for 30 sec. The base-layer coated substrates were desiccated again overnight. This siloxane base layer helps to ensure a uniform surface containing reactive silanol groups for the subsequent chemical modification regardless of the substrate.[14]

Sols used to prepare the gradient materials were freshly prepared. The aminosilane sol was prepared by mixing ***x*** mL (***x*** = 0.5, 1 or 2) of APTEOS (3-aminopropyltriethoxysilane) with 20 mL of ethanol and ***y*** mL (***y*** = 0.125, 0.25 or 0.5 mL, respectively) of water. Since APTEOS has aNH_2 functional group which catalyzes the condensation reaction upon mixing with water and ethanol, it was used immediately after preparation. The mercaptosilane sol was prepared by stirring the ***x*** mL (**x** = 0.125, 0.25 or 0.5) of MPTMOS (3-mercaptopropyltrimethoxysilane) with 20 mL of EtOH and ***y*** mL (***y*** = 0.125, 0.25 or 0.5 mL, respectively) of 0.1 M HCl for 5 min on a magnetic stirrer. Then, ***z*** mL of (***z*** = 0.125, 0.25 or 0.5 mL, respectively) of 0.3 M NH_4OH was then added to the mixture and stirred for additional 25 min. The NH_4OH increases the pH of the sol and helps catalyze the condensation reaction of the mercaptosilane to surface silanol groups. The mixture was then put to rest for 90 min to facilitate the condensation to form the reactive silanols.

Six different samples were prepared for the experiment as shown in **Table 6.1**. For simplicity, we give an id of each sample as ***T*** or ***C8***, where ***T*** stands for the TMOS-derived base layer coated substrate and ***C***8 stands for the ***C***8-derived base layer. The subscripts indicate the volumes (mL) of silanes used to make the gradients and uniformly modified substrates. The first number at the subscript indicates the volume of aminosilane and the second number indicates the mercaptosilane volume in the respective modifying sol solutions. So, $\boldsymbol{T}_{1:0.25}$ indicates that 1 mL of amine was mixed with 20 mL ethanol to prepare the amine sol and separately 0.25 mL

Table 6.1: Composition of different the gradient samples

Sample Id	APTES (mL) in 20 mL EtOH	MPTMS (mL) in 20 mL EtOH	R (NH_2/SH)
$T_{1:0.5}$	1	0.5	2
$T_{2\text{-}0.25}$	2	0.25	8
$T_{1:0.125}$	1	0.125	8
$T_{0.5:0.25}$	0.5	0.25	2
$C8_{1:0.5}$	1	0.5	2
$C8_{2:0.25}$	2	0.25	8

MPTMOS was mixed with 20 mL ethanol to the prepare the SH sol. Two different base layers were used for making these gradients; one chosen to be hydrophilic e.g., the TMOS-derived base layer and the other is hydrophobic, e.g., ***C***8-derived base layer. Thus, the samples were prepared on these base layers by changing the volume ratio of the amine and thiol silanes in the deposition solution.

6.3.2 Gradient preparation

The gradient of NH_2 and SH functional groups on the base- layer coated substrates were prepared by infusing the appropriate deposition sol into a vial containing the vertically aligned substrate. In the infusion process, the sol containing amine groups always infused first followed by the sol containing thiol groups, as the amine helps catalyze the condensation of the hydrolyzed mercaptosilane to the substrate. The gradient was prepared as depicted in **Scheme 6.1** by a method recently developed by our lab called controlled-rate infusion or ***CRI.***[15] The ***CRI*** method consists of a syringe pump (Harvard apparatus, PHD 2000 infusion), which can control the rate of infusion

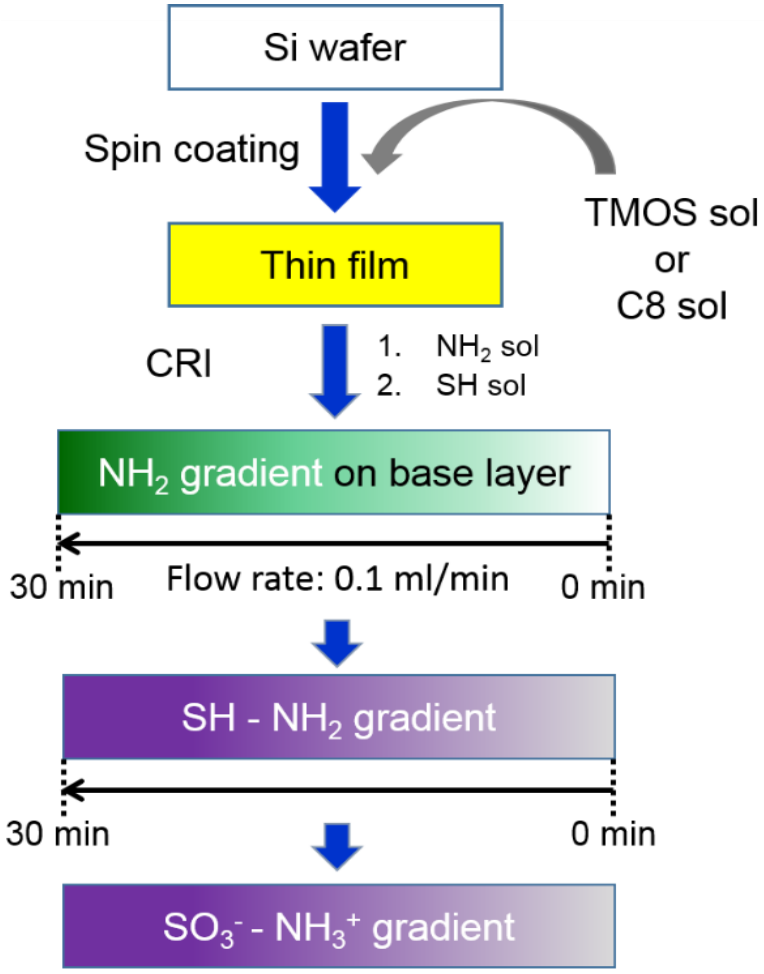

Scheme 6.1: Fabrication of NH_3^+ charge gradients on base-layer coated substrates of different polarity by varying the amount of NH_2 and SH by programmed ***CRI***.

of the modifying sol contained in a syringe. During infusion, the base-layer-coated substrate is exposed to the aminosilane solution for 30 min along its length, thus producing a gradual spatial variation in amine modification from top to bottom. The time gap between the two infusions was 12 hours. The amine gradient was desiccated for 12 hours prior to thiol gradient formation.

Multi-component gradients were prepared by infusing a freshly prepared mercaptosilane sol into the glass vial containing the vertically aligned amine gradient in such a fashion so that the two components (amine and thiol) align in the same direction. These gradients are called aligned multicomponent gradients. The time gap between the two infusions was 12 hours. After the infusion, the substrates were rinsed with ethanol and desiccated for 12 hours. The prepared multi-component gradients were then immersed in 30% H_2O_2 for 20 min to convert SH to SO_3^- and simultaneously NH_2 to NH_3^+ as described in **Chapter 3**.[13] The duration of the reaction time with H_2O_2 was optimized as described in our earlier work.[13] The charge gradients were then characterized using **XPS** spectroscopy, **WCA** and ζ measurements.

6.3.3 Characterization

XPS spectroscopy, **WCA,** and Zeta potential (ζ) measurements are described in **Chapter 3**. The preparation of samples for the ζ measurements is also described in Chapter **3**.

6.4 Results and Discussion

6.4.1 Gradient fabrication

Gradient fabrication begins by spin coating a silica sol prepared from either TMOS or OTMOS/TMOS onto a silicon or glass substrate to form a homogeneous base layer for covalently bonding the organoalkoxysilanes to the surface and in the case of the ***C***8, to impart hydrophobicity to the surface.[14,15] Using ***CRI***, the base-layer coated substrate was exposed first to a solution

containing APTEOS and then after 12 hours to a solution of MPTMOS in a time-dependent fashion.[15] As a result of the condensation reaction between surface silanol groups and the hydrolyzed APTEOS or MPTMOS precursors, the organic groups were covalently bonded to the planar substrate in a gradient fashion. The surface immobilized amine groups catalyze the condensation of mercapto group bearing alkoxysilane as explained in **Chapter 5**. It is thus likely that the mercapto and amine functionalities are located near to each other. The ***CRI*** method provides an advantage by affording a means to prepare multicomponent gradients where the changes in surface density of the individual components can be controlled easily. The rate of infusion, the rate of reaction and the silane concentration regulate the overall gradient formation.[15,16] By changing the concentration of the APTEOS and MPTMOS in the original silane solution, we prepared four multifunctional chemical gradients on TMOS and two on OTMOS/TMOS siloxane base layers. The simultaneous oxidation of the sulfhydryl to sulfonate groups and protonation of the amine groups NH_3^+ groups was achieved via immersion in 30% H_2O_2 for 20 min. In these materials, sol-derived surface silanol groups will also be present with surface concentrations that will vary from bottom to top depending on the level of modification.

6.4.2 Gradient characterization

6.4.2.1 XPS spectroscopy

The presence and extent of modification of the surfaces with NH_3^+ and SO_3^- as well as the degree of protonation/oxidation were evaluated using **XPS** spectroscopy. **Figure 6.1** shows an overlay of six N1s and S2p **XPS** spectra for the $\boldsymbol{T}_{1:0.5}$ and $\boldsymbol{T}_{2:0.25}$ gradients acquired at ~3 mm intervals along the length. The N1s peak in the **XPS** spectra shown in **Figure 6.1** (**A, B**) appears as a doublet when fitted with binding energies of ~400 and ~402 eV, corresponding to free amine and protonated/H-bonded amines, respectively.[13,15] As expected and similar to previous work (**Chapter 3**), the peak intensity is higher for the protonated form of the amine group. It is expected that thiols upon treatment with hydrogen peroxide, convert to SO_3^- groups.[17] However, H_2O_2

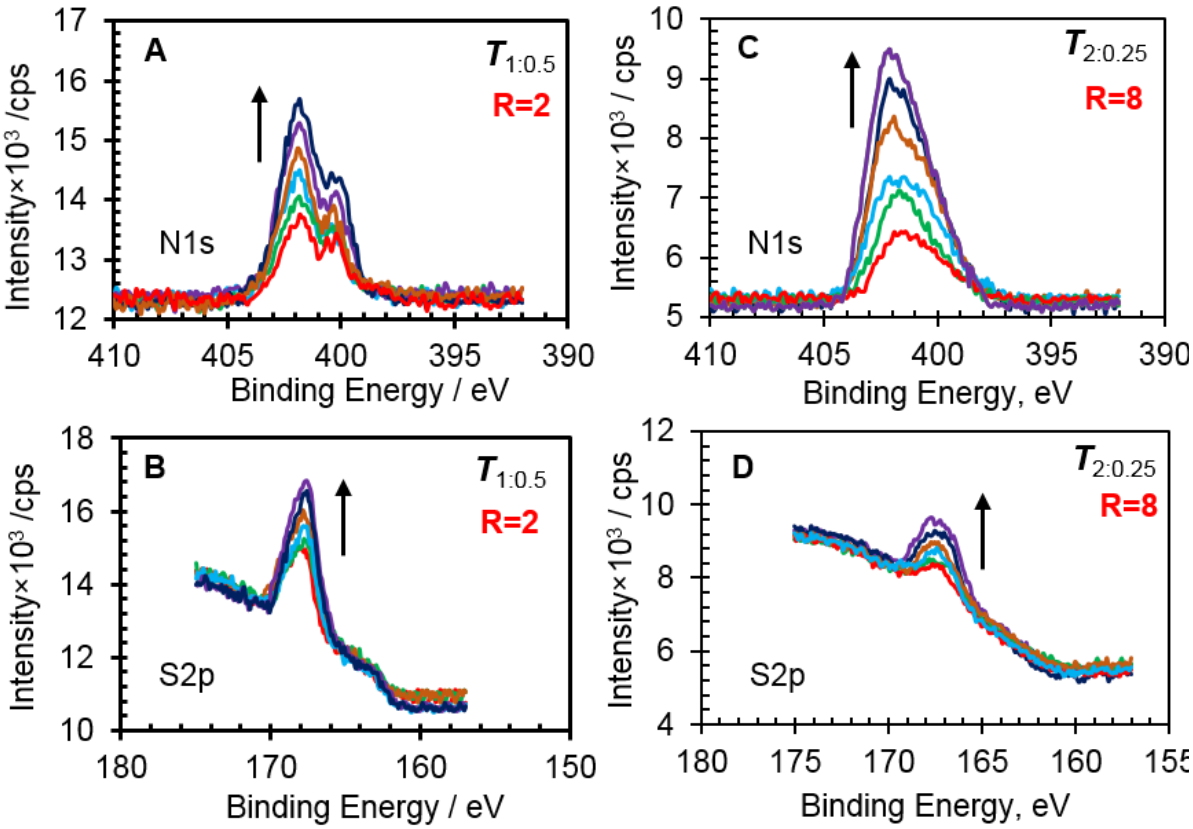

Figure 6.1: XPS N1s and S2p spectra in the $\boldsymbol{T}_{1:0.5}$ (A and B) and $\boldsymbol{T}_{1:0.5}$ (C and D) gradients. Both the samples exhibit a gradual decrease in the concentration of S and N along the length of the substrate as depicted by the arrows.

cannot protonate the amine groups to NH_3^+ groups because the pKa of H_2O_2 is 11.6[18] and it is unlikely that hydrogen peroxide is responsible for amine group protonation. As already explained in **Chapter 3**, that amine protonation parallels thiol oxidation, indicating that thiol oxidation leads to simultaneous amine protonation. Neighboring SO_3^- groups can then act as counter ions for nearby NH_3^+ groups. The complete disappearance of the SH peak indicates that sulfhydryl groups have been oxidized, but some free amine group remains (**Figure 6.1 & 6.2 A**, **C**). This result suggests that the surface concentration of thiol is lower than that of the amine. This observation is consistent with the (2×, 4×, 8×) lower concentration of thiol relative to amine in the respective deposition solutions.

For S2p, the spectra consist of one peak at ~168.5 eV (see **Figure 6.1** (**B, D**)) in agreement with reported values.[19-21] For both the gradients, both the N1s and S2p signals increase from the top to the bottom of the substrate. These trends indicate the presence of multi-component gradients aligned in the same direction. Note that for sample $\boldsymbol{T}_{1:0.5}$ some SH remains unoxidized as shown by a small shoulder near 163 eV. It is likely that the 20 min immersion time in the H_2O_2 was not sufficient to oxidize all the SH groups, given the relatively high concentration of SH present in the $\boldsymbol{T}_{1:0.5}$ sample.

Figure 6.2 shows the **XPS** spectra of N1s and S2p along the length of the substrate for ***C8***$_{1:0.5}$ and ***C8***$_{2:0.25}$. Similar to ***T*** samples, ***C***8 samples also exhibit an N1s doublet. The free amine is at ~ 400 eV and the protonated amine is at ~ 402 eV. As observed in the ***T*** samples, the majority of the amine is in protonated form. The presence of the unprotonated N 1s peak in the **XPS** of the ***C***8 samples are attributed to the same fact as explained for the ***T*** samples. S2p peak is found to be around 168.5 eV representing the S in the SO_3^- group. These peaks were found to decrease from the bottom of the gradients to the top indicating the formation of aligned gradients of N and S. A higher peak intensity for N1s is found on the ***T*** samples compared to the ***C8*** samples. These results are similar to previous ones as shown in **Chapter 3 and 4**. As explained in **Chapter 4**, the lower

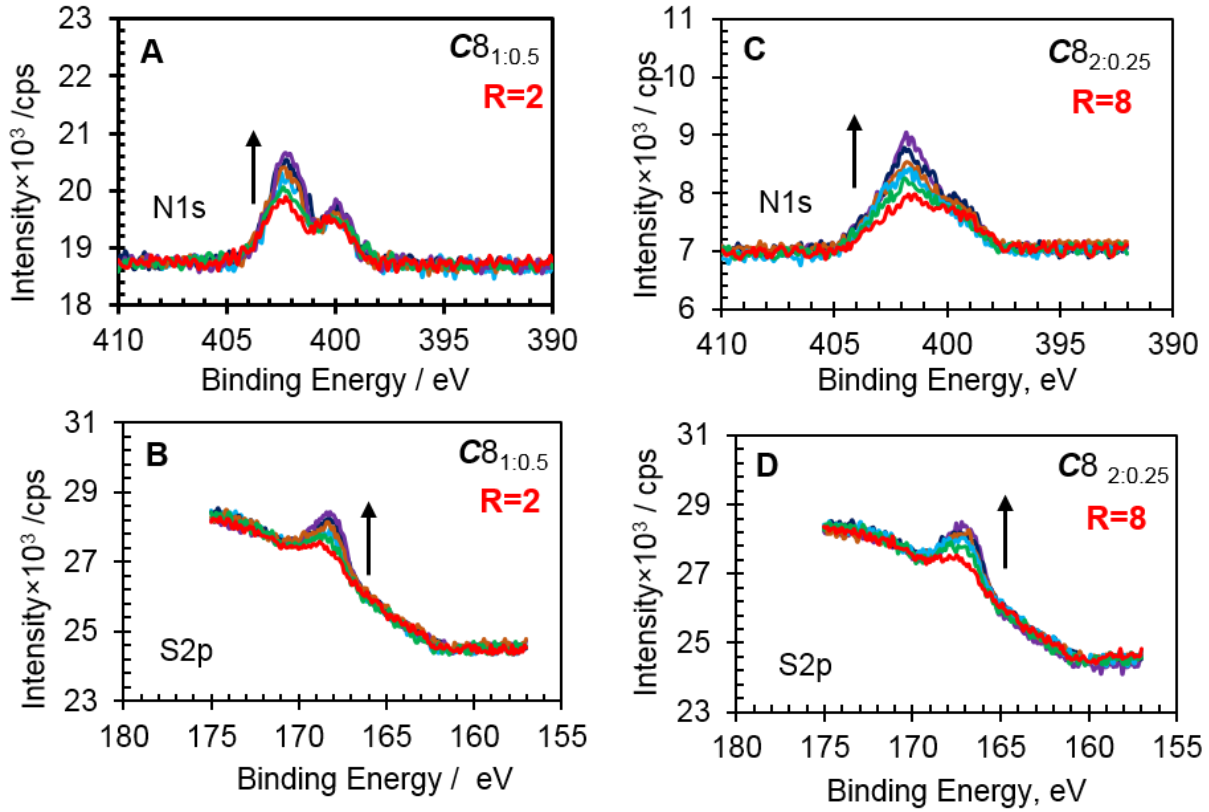

Figure 6.2: XPS N1s and S2p spectra in the ***C8***$_{1:0.5}$ (A and B) and ***C***8$_{1:0.5}$ (C and D) gradients. The intensity of the S and N peaks decrease from bottom to top of the substrate as depicted by the arrows.

degree of amine modification in the ***C8*** samples is attributed to the steric effect of the bulky ***C8*** organic group covalently bonded to the central Si atom as well as a reduced amount of surface silanol groups on the ***C8*** derived base-layer. Similarly, the peak intensity of the S2p peak was found to be greater in ***T*** samples as compared to the ***C8*** samples. On the other hand, more sulfur was found to be attached to $\boldsymbol{T_{1\text{-}0.5}}$ sample as the ratio of (***R***) NH_3^+ / SO_3^- increased. The additional amine immobilized on $\boldsymbol{T_{1\text{-}0.5}}$ sample enhances the condensation of the mercaptosilane to the surface. The ***C***8 samples, however, did not show a significant change in S2p peak intensity when the (***R***) NH_3^+ / SO_3^- increased.

Because it is possible that amine groups can be oxidized by the H_2O_2 when the samples are immersed in it, we carried out another experiment. In this experiment, two control samples were prepared by soaking the TMOS-derived base-layer coated substrate in amine (APTEOS : EtOH:: 1:20 mL) for 30 minutes. One of the control samples was then soaked in the H_2O_2 for 20 minutes. Two N1s **XPS** spectra acquired for the H_2O_2 treated and untreated samples were overlaid as shown in **Figure 6.3**. As can be seen, no change in the position of the N1s peak (~400 eV) in the H_2O_2 treated and an untreated sample was observed. Furthermore, no additional peaks can be seen for oxidized amine groups. For example, N1s in nitrate occurs at 406 eV,[22] nitrite at 405 eV[22] and nitroso occurs at 400 eV.[23] Oxidation of amine to a nitroso compound is also not possible because

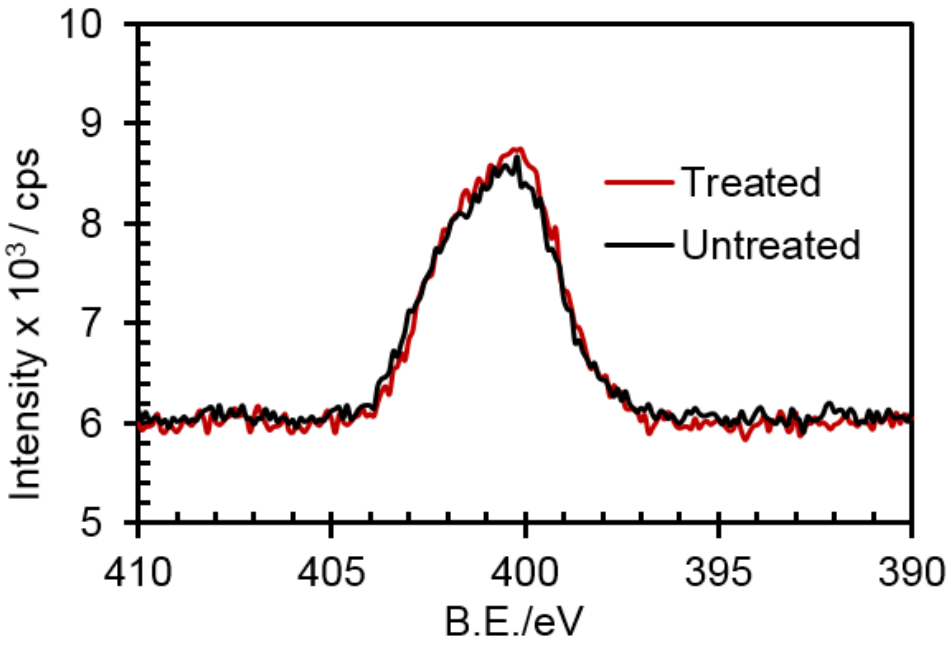

Figure 6.3: **XPS** N1s spectra obtained for the uniformly modified NH_2 samples prepared on TMOS-derived base layers following exposure to H_2O_2 for 20 min (treated) and without exposure to H_2O_2 (untreated). The base-layer coated substrates were soaked in the APTEOS sol for 30 min.

if it occurs at 400 eV, the peak intensity would drop instead of increase. These results confirm that the H_2O_2 does not oxidize the amine functional group but only the sulfur.

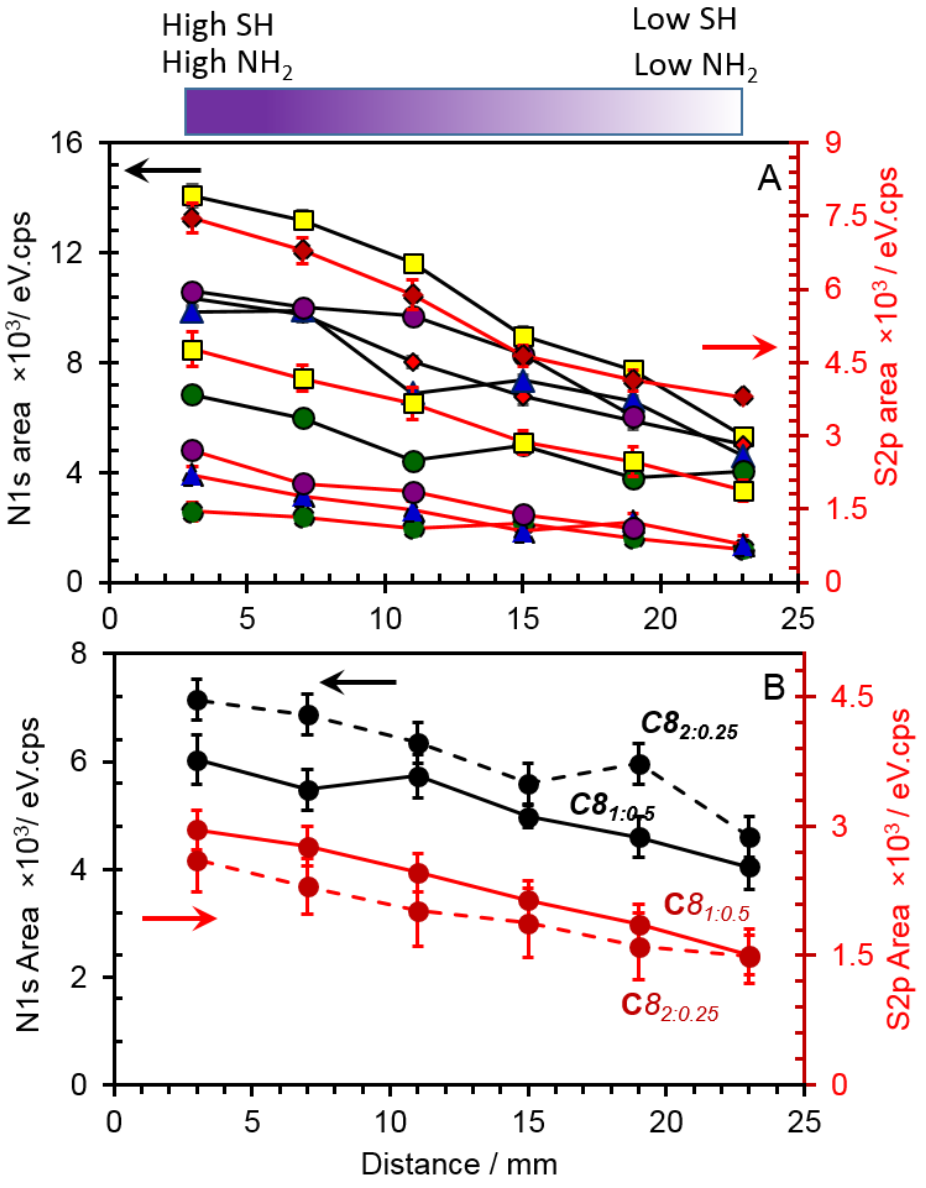

Figure 6.4: The profiles of the XPS peak area for nitrogen (**N**) and sulfur (**S**) as a function of distance along the gradient samples. (**A**) ***T*** samples; (**B**) ***C***8 samples. (**A**): yellow square ($T_{2:0.25}$), purple circle ($T_{1:0.25}$), red diamond ($T_{1:0.5}$), blue triangle ($T_{1:0.125}$) and dark green circle ($T_{0.5:0.125}$) and (**B**): as mentioned in the plot.

To better understand the gradient profile, we plotted the integrated areas under the N1s and S2p peaks for all ***T*** (A) and ***C8*** (B) gradients samples and these results are shown in **Figure 6.4 (A, B)**. This figure also includes the result from sample id $\boldsymbol{T}_{1:0.25}$ (from **Chapter 3)** for comparison. The subscripts in the reference sample $\boldsymbol{T}_{1:0.25}$ indicates 1 mL of APTEOS and 0.25 mL of MPTMOS were added in the sample preparation. For all the gradient profiles, the amount of both N and S in both ***T*** and ***C8*** samples increase from top (25 mm) to the bottom (0 mm). This is expected since the bottom was exposed to the sols for longer period of time than that of the top. As can be seen, samples prepared with the same amount of APTEOS in the sol $\boldsymbol{T}_{1:0.5}$ (red diamond line) and $\boldsymbol{T}_{1:0.25}$ (purple circle line) show similar integrated peak areas that are lower than that found for the sample prepared with double the amount of APTEOS ($\boldsymbol{T}_{2:0.25}$ (yellow square), as expected. It can also be noted in **Figure 6.4,** that the N and S surface concentration is higher in the ***T*** samples compared to the ***C8*** samples as mentioned earlier. The amount of immobilized thiol on $\boldsymbol{T}_{2\text{-}0.25}$ is greater than that observed on $\boldsymbol{T}_{1\text{-}0.25}$ because there is more amine on the $\boldsymbol{T}_{2\text{-}0.25}$ surface and amine catalyzes the deposition of thiol to the surface. So, the big picture of these **Figures** is that higher the concentration of the amine and thiol silanes in the deposition sol, the higher the N and S immobilized onto the siloxane base layer. On the other hand, when a bulky organic group as in **Figure 6.4 (B)** is attached to the siloxane layer, surface modification by these groups is greatly reduced because of the steric effect of the bulky group and reduction in available reactive SiOH groups.

6.4.2.2 WCA analysis (Wettability)

To see the spatial variation across the gradient, the **WCA** at 3 mm intervals lengthwise was acquired on the four representative samples ***T***$_{2\text{-}0.25}$ (A), ***C8***$_{2\text{-}0.25}$ (B), ***T***$_{1\text{-}0.5}$ (C) and ***C8***$_{1\text{-}0.5}$ (D) as shown in **Figure 6.5.** Gradients on the TMOS-derived base layer were more hydrophilic at the bottom end due to the presence of the charged species whereas the top end show character more like the siloxane surface.[13] The contact angles gradually increase from 13^{o} and 12^{o} at the bottom to 43^{o} and 41^{o} at the top of the gradient for ***T***$_{2\text{-}0.25}$ and ***T***$_{1\text{-}0.5}$, respectively. On the other hand, the

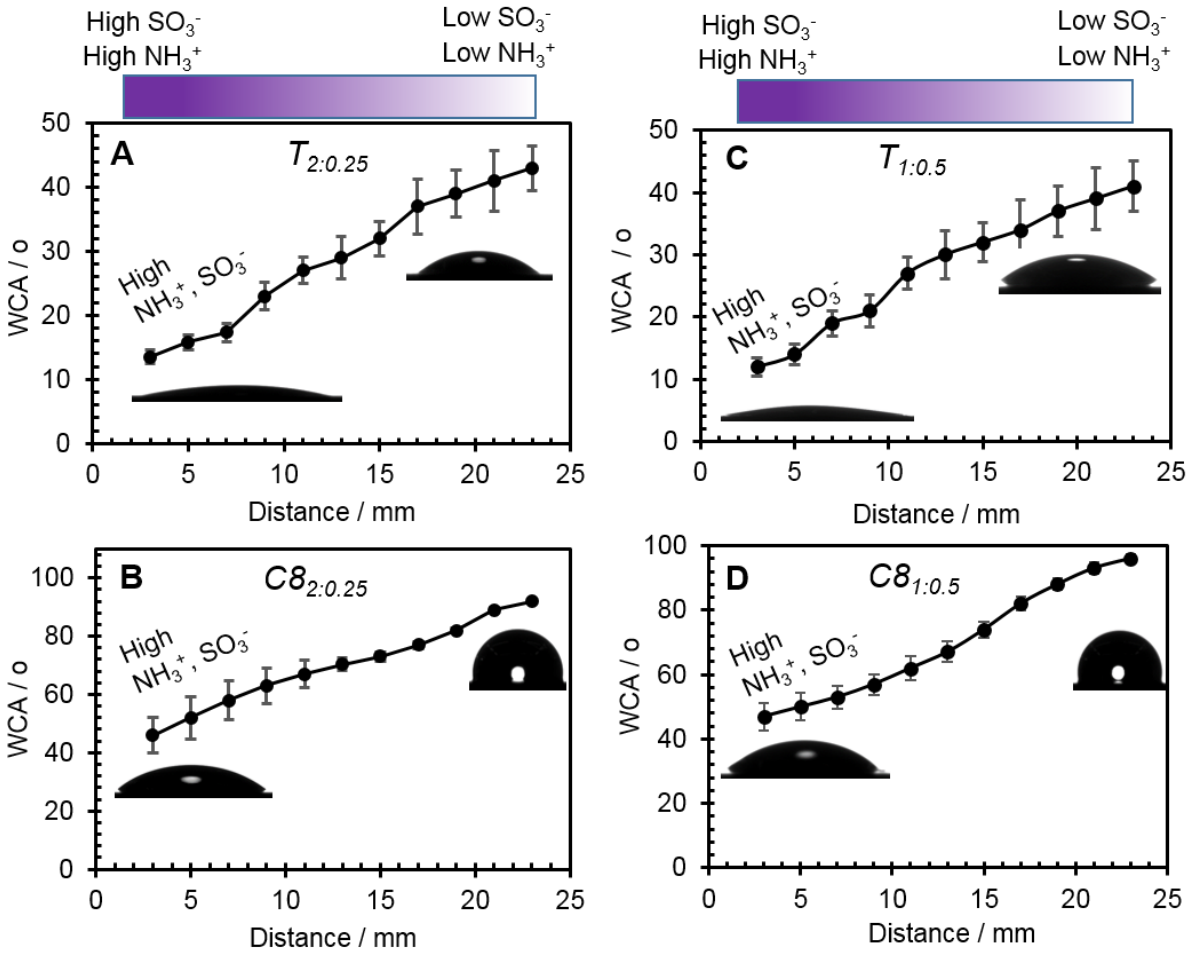

Figure 6.5: Photographs of water droplets on the top (low NH_3^+ : low SO_3^-) and bottom (high NH_3^+ : high SO_3^-) of the gradient films and their contact angle profiles prepared on TMOS derived base layer (A, C) and ***C***8 derived base layer (B, D) coated substrates.

top of the gradients prepared on the ***C8***-derived base layer was significantly more hydrophobic with a WCA of 92º - 96 º compared to 46º - 47 º at the top end of the ***T*** gradients. Although small changes in the composition did not bring about a large change in the WCA at the top of the gradients where the extent of modification is smaller (as in $\boldsymbol{T}_{1\text{-}0.5}$ or $\boldsymbol{T}_{1\text{-}0.5}$), more base layer characteristics show up. The ***C8*** samples appear to be more uniform than the ***T*** samples as evident from the smaller standard deviation of the three replicate measurements. The small error bar on the OTMOS surface is ascribed to the spherical shape of the water drops on its surface. A higher amount of protonated amine is found at the bottom of TMOS-derived base layers, thus the WCA decreases drastically near the bottom of the gradients.

6.4.2.3 Electrokinetic measurements

Chapter 3 discusses the principle of the electrokinetic measurements and provides detailed information correlating surface composition and charge density[13, 24 - 26], and ultimately interactions between functional groups. References 27-29 discuss the characterization of charged glass surfaces modified with aminosilanes, silica nanoparticles, and a glass capillary. Before measurement of a

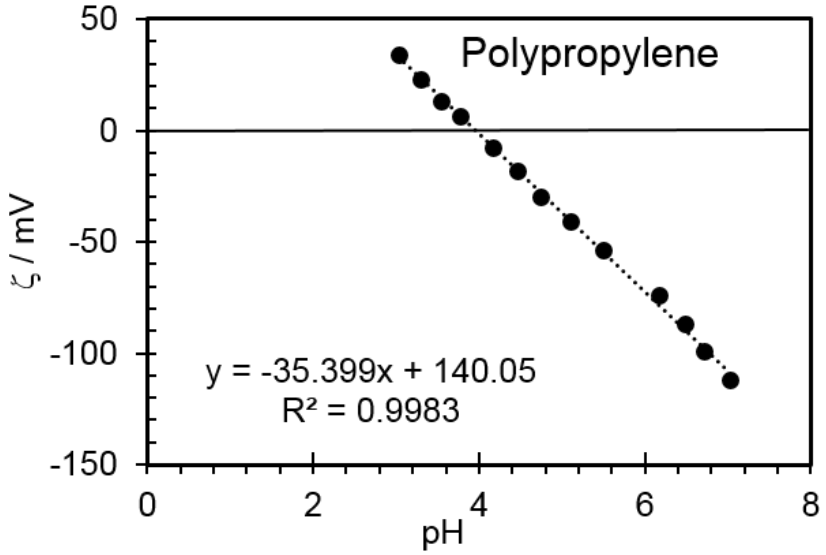

Figure 6.6: ζ of the reference (polypropylene) sample from pH 3-7.

new set of samples, it is mandatory to measure the ζ of the ***PP*** reference to check the instrument. In this case, the ζ and isoelectric point (***IEP***) of the ***PP*** reference sheet was found consistent with the Anton Paar electrokinetic analyzer specifications (***IEP*** = 4±0.2) as shown in **Figure 6.6**.

With a gradient substrate, only the average ζ can be measured. To obtain information about surface charge at discrete positions along the gradient, six samples (size: 2 × 5 cm^2) were prepared. The sample preparation procedure is explained in detail in **Chapter 3**. Each sample mimics a certain surface chemical composition along the length of the multi-component gradient as shown in the **Scheme 6.2**. Thus, sample 6 was soaked in the aminosilane for 30 min followed by mercaptosilane for 30 min to represent a position at the high amine/high sulfur end (bottom) of a gradient, while sample 1 was immersed in the respective solutions for 5 min each to represent a position at the low amine/low sulfur end (top) of the multi-component charge gradient. To oxidize/protonate the surface, the samples were immersed in H_2O_2 for 20 min.

The ζ as a function of pH for the mimics of ***T*** and ***C***8 samples (**Scheme 6.2)** measured by the Anton Paar electro-kinetic analyzer is presented in **Figures 6.7 - 6.9,** respectively. Each line corresponds to the ζ for each mimic shown in **Scheme 6.2**. As described in previous work (**Chapter 3**)[13], ζ largely depends on the quantity of charged species such as NH_3^+, SO_3^-, SiO^- etc. present on the surface, their pKas, their relative position, and the solution pH. In solution, the pKa's of SO_3H and NH_3^+ are ~ -2.0 and ~10.0, respectively,[31,32] while the majority of SiOH groups

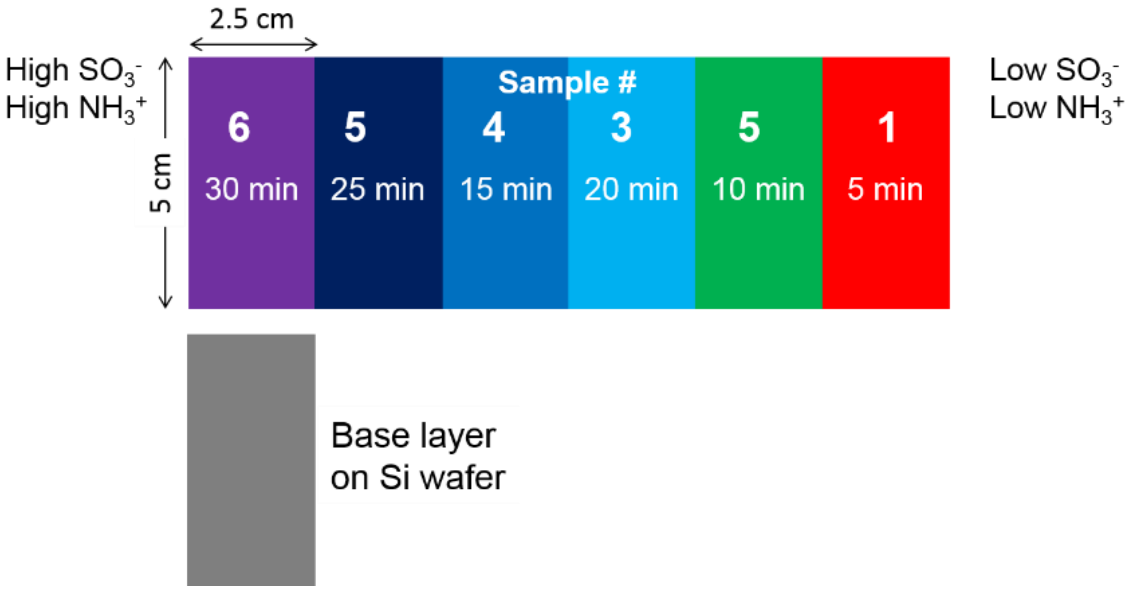

Scheme 6.2: Each sample for the ζ measurement has a dimension of 5×2.5 cm^2. There were a total of six samples, each representing a specific point across the gradient. Each sample was prepared by modifying the TMOS derived base layer with the APTEOS and MPTMOS silane sols by immersing the base layer in the respective silane sol. Samples #6-#1 indicate six points as we move from the high NH_3^+ / SO_3^- end to low end. The time in each figure represent the time of immersion in the respective silane sols containing either the amine or thiol functional groups.

exhibit a pKa ~ 8.[33] On a surface, however, the pKa's of acidic and basic functionalities can be significantly different from their solution values and can also depend of the local chemical environment.[34–36]

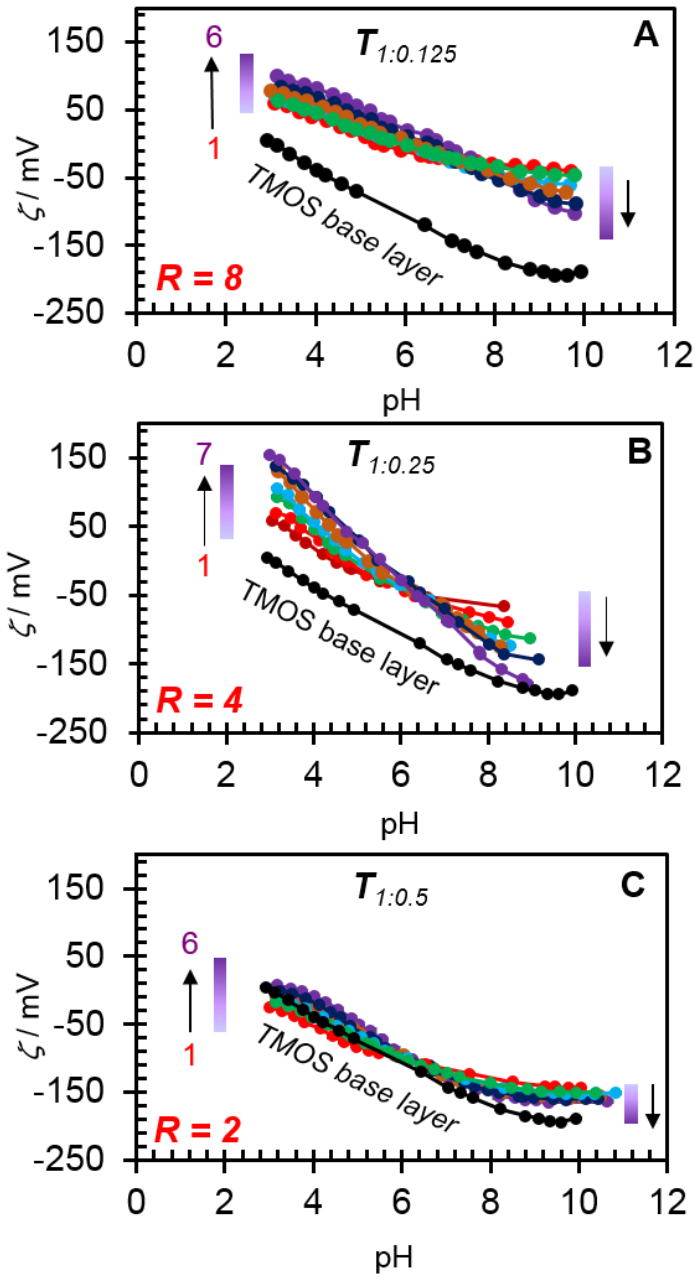

Figure 6.7: Change of ζ with pH for the gradient mimics (samples 1→6) prepared on the ***TMOS***-derived base layers. (A), (B) and (C) correspond to $\boldsymbol{T}_{1:0.125}$, $\boldsymbol{T}_{1:0.25}$, $\boldsymbol{T}_{1:0.5}$ respectively. The gradient bar to the left and right of the profiles represent the direction of modification.

As can be seen in **Figures 6.7-6.9**, the ζ shifts negative as the pH of the solution increases and the surface bound species become depronated leading to the formation of SO_3^-, SiO^-, NH_2. The larger the amount of SO_3^- on the surface as in the case of ***T*** $_{1:0.5}$ or ***C8*** $_{1:0.5}$, the more negative the surface is at acidic pHs and the closer the ζ vs. pH profile approaches that obtained for the base layer. Also, noteworthy in each of the profiles is the appearance of a cross over at a point which

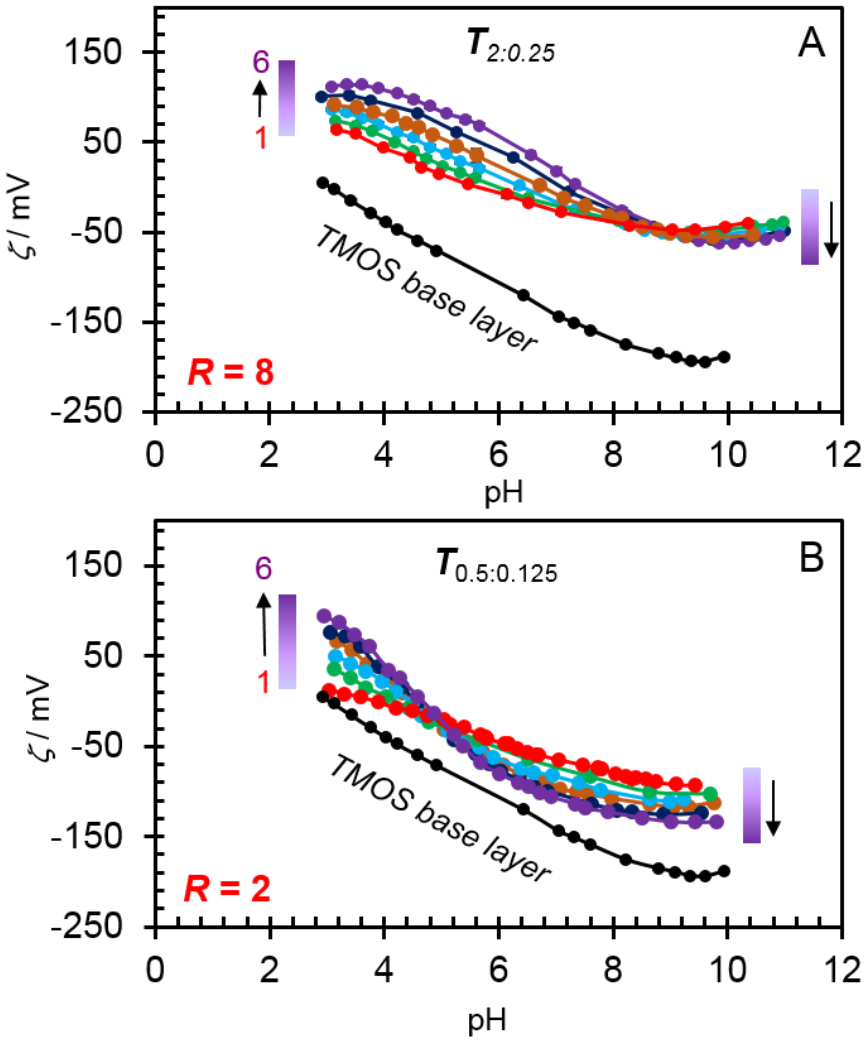

Figure 6.8: Change of ζ with pH for the gradient mimics (samples 1→6) prepared on the ***TMOS***-derived base layers (A) and (B) correspond to $T_{2:0.25}$, and $T_{0.5:0.125}$ respectively. The gradient bar to the left and right of the profiles represent the direction of modification.

we term the point of intersection (***POI***) where the ζ of all six samples is the same. This ***POI*** shifts its position depending on the composition of the surface, its charge and on the siloxane base layers and is discussed further below. At pHs acidic of the ***POI***, the surface charge becomes more positive the greater the extent of modification while after the ***POI***, the surface charge becomes more negative with increasing modification.

Figure 6.7 shows the ζ-pH profile from 3.4 to 9 when the volume of ATPEOS is kept constant while that of MPTMOS in the deposition sol decreases (**R** = 2 → 8). As the pH of the solution increases, the ζ becomes more negative due to the deprotonation of the surface bound functional groups leading to the formation of SO_3^-, SiO^-, and NH_2. When the surface concentration of protonated amine groups is high as in **Figure 6.7A and B**, the ζ is fairly positive at acidic pHs. A large fraction of positively charged species (NH_3^+) makes the surface less rich in negatively charged species, thereby shifting ζ to more positive values. As **R** decreases to 2, the ζ becomes significantly more negative particularly at low pH values and the ζ-pH profile approaches that of the base layer (black curve). This indicates that the surface is rich in isolated negatively charged SO_3^- groups as the volume of MPTMOS is increased in the deposition sol relative to APTEOS, which contributes to the negative ζ.

Figure 6.8 shows the ζ-pH profiles for samples $\boldsymbol{T}_{2:0.25}$, and $\boldsymbol{T}_{0.5:0.125,}$ where the volume of aminosilane is decreased by a factor of 4 and the volume of the mercaptosilane is decreased by a factor of 2. As the ratio ***R*** decreases from ***R*** = 8 to ***R*** = 2 and the amount of surface bound amine drops, the curves shift toward that acquired for base layer coated substrate particularly at pH <8.

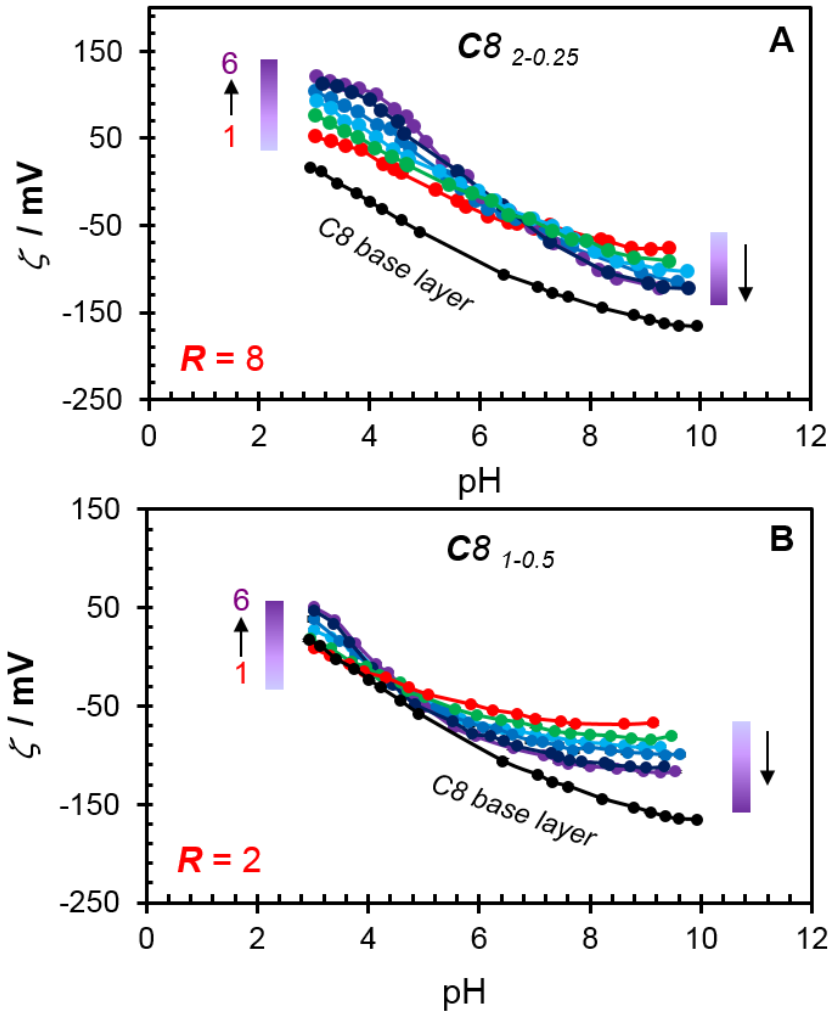

Figure 6.9: Change of ζ with pH for the gradient mimics (samples 1→6) prepared on the ***C*8** derived base layers. (A) and (B) correspond to $\boldsymbol{C8}_{1:0.5}$, and $\boldsymbol{C8}_{2:0.25}$, respectively. The gradient bar to the left and right of the profiles depict the direction of modification.

Also, noteworthy, the pH at the ***POI*** noticeably shifts to more acidic values as the amount of amine on the surface decreases (**Figure 6.8A** vs. **6.8B**).

The ***ζ-pH*** profiles for the two samples prepared on the more hydrophobic base layers, e.g., $\boldsymbol{C8}_{1:0.5}$ and $\boldsymbol{C8}_{2:0.25}$, are presented in **Figure 6.9** (**A**) and (**B**) respectively. As observed for the ***T*** samples, the shape of the ζ vs. pH curves depends on ratio ***R***. The sample with the greater amount of amine on the surface has a more positive charge relative to the one with a lower fraction. Likewise, the sample $\boldsymbol{C8}_{1:0.5}$ having a smaller ***R*** exhibits ζ behavior similar to the base layer coated substrate. Again, the pH at the ***POI*** also noticeably shifts to more acidic values with a decrease in ***R***.

To better evaluate how the ζ and pH at the ***POI*** change with the composition of charged groups on the surface, the ζ and pH at the ***POI*** are plotted in **Figure 6.10.** The results are very interesting. For the gradient samples prepared from sols with the same volume of aminosilane (e.g., 1 mL) but decreasing volumes of the mercaptosilane (0.5 mL → 0.25 mL; as marked by arrow in **Figure 6.10**), the pH at the ***POI*** shifts slightly to higher values (6.4 → 7.3) as ***R*** increases. At the same time, the ζ at the ***POI*** also becomes increasingly positive. This is expected as the amount of SO_3^- decreases (see **XPS**). While comparing samples where the ratio ***R*** = 4 (e.g., $\boldsymbol{T}_{0.5:0.125}$ and $\boldsymbol{T}_{1:0.25}$), the ζ at the ***POI*** is more positive for the $\boldsymbol{T}_{0.5:0.125}$ sample consistent with the lower amount of SO_3^- on the surface as evaluated by **XPS**. Also, the pH at the ***POI*** is slightly more acidic for $\boldsymbol{T}_{0.5:0.125}$ consistent with the lower amount of NH_3^+. Likewise, samples with ***R*** = 8 (e.g., $\boldsymbol{T}_{1:0.125}$ and $\boldsymbol{T}_{2:0.25}$) can be compared. The ζ at the ***POI*** is more positive for the $\boldsymbol{T}_{1:0.125}$ sample and the pH at the ***POI*** is considerably more acidic again consistent with smaller amount of SO_3^- and NH_3^+ on the surface relative to $\boldsymbol{T_{2:0.25}}$. The higher value of the ***POI*** for the $\boldsymbol{T_{2:0.25}}$ is attributed to the increased basicity caused by the increased number NH_2 anchored on the surface.

In the case of ***C8*** samples, e.g., $\boldsymbol{C8}_{1:0.5}$ and $\boldsymbol{C8}_{2:0.25}$, the pH at that ***POI*** becomes more basic from 4.5 to 6.9 as ***R*** increases from 2 to 8. The ζ at the ***POI*** increases to more negative values with an increase in the ratio ***R***. In case of ***C***8 samples the APTEOS modification largely depends on the bulky octyl group, higher the silane concentration higher the modification. Thus, $\boldsymbol{C8}_{2:0.25}$ is more basic than $\boldsymbol{C8}_{1:0.5}$. On the other hand, higher amine modification leads to higher thiol condensation on the surface thereby increasing the extent of SH groups on the surface. Thus, at high pH $\boldsymbol{C8}_{2:0.25}$ sample is dominated by the negative species more than $\boldsymbol{C8}_{1:0.5}$ sample leading to more negative ζ at the ***POI***.

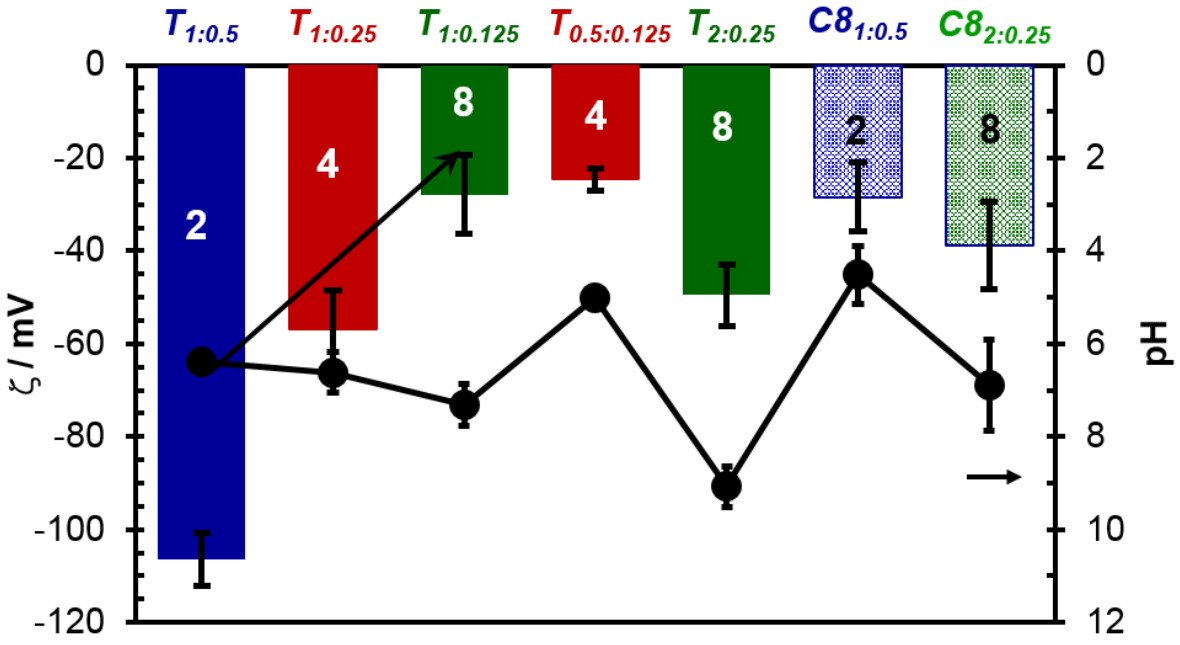

Figure 6.10: ζ and pH at the ***POI*** as a function of the ratio of NH_3^+/SO_3^-.

Figure 6.11 shows how the pH at the iso-electric point (***IEP***) for each of the six samples at the different ratios (**R**) change. The pH at the ***IEP*** for samples prepared on the TMOS derived base layer (**Figure 6.11A**) and the ***C***8/TMOS derived base layer (**Figure 6.11B**) shifts to basic values as the extent of modification increases (sample 1 → sample 6). Furthermore, for each sample, the ***IEP*** moves significantly to more basic values with the increase in the NH_3^+/SO_3^- (***R***)

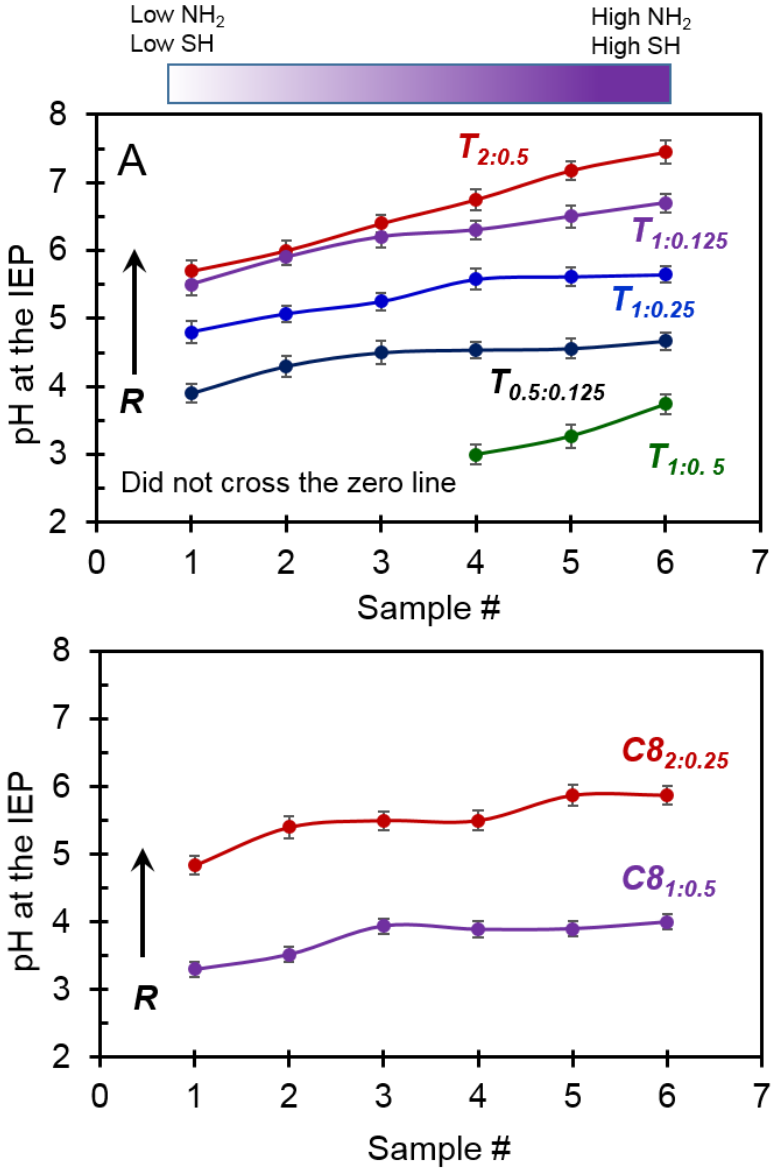

Figure 6.11: pH at the iso-electric for the gradient mimics (samples 1→6) prepared on the **(A)** TMOS-derived base layers) and (**B**) the TMOS/***C8*** derived base layer.

ratio. At very low ***R*** (***R*** = 2) sample ($\boldsymbol{T}_{1:0.5}$) the pH at the ***IEP*** fell behind the experimental range. Because of the relatively high amount of SO_3^- on the surface and the relatively high amount of SiO^- groups present on the surface particularly for samples 1-4, the pH at the ***IEP*** is lower than 3 and could not be obtained. The effect of the composition of the base layer on the ***IEP*** is evident in the **Figure 6.11 (B).** $\boldsymbol{C8}_{1:0.5}$ has fewer negatively charged silanol groups on its surface and thus a pH at the ***IEP*** can be obtained for all six samples that represent the gradient. Again, the pH is fairly low ranging from ~3.2 to 4 while moving from top to the bottom of the gradient (sample 1→6). For the sample with fewer SO_3^- and more NH_3^+, e.g., $\boldsymbol{C8}_{2:0.25}$, the pH at the ***IEP*** is more basic and shifts from 4.8 to 5.8. In comparison, pH shifts from 5.7 to 7.4 for its TMOS analog consistent with a greater amount of amine on the TMOS derived substrates.

The variation of ζ with surface modification (***R***) at three different pH values (e.g., 3, 5 and 8) was analyzed and shown in **Figure 6.12**. For simplicity, we focused on the ***T*** samples having the same volume of amine but gradually decreasing volume of mercaptosilane where ***R*** = 2, 4 and 8 ($\boldsymbol{T}_{1:0.25}$, $\boldsymbol{T}_{1:0.25}$ and $\boldsymbol{T}_{1:0.125}$). At acidic pHs, the surfaces are mostly positive due to the relatively high concentration of amine in the deposition sols and thus the strong presence of NH_3^+. For all the samples at pH 3 and 5.5, it can be observed that ζ increases to more positive values from top (least modified, sample 1) to bottom (heavily modified, sample 6) at lower pH (3). However, at higher pH ~ 9, the surfaces are mostly negative because the amine groups have been deprotonated. ζ is found to be increase to more negative values when we move from top (sample 1) to the bottom (sample 6). It is shown in the **Figure 12B** and **C** that ζ becomes more positive with increasing silane ratio (***R*** = 2, 4, 8). At low pH however, an exception is seen for sample $\boldsymbol{T}_{1:0.25}$ and $\boldsymbol{T}_{1:0.125}$ where we observe ζ for sample $\boldsymbol{T}_{1:0.125}$ changes to a little more positive value than that of $\boldsymbol{T}_{1:0.25}$ sample. At pH 3 the modified end shows a difference of around 85 mV whereas it about 146 mV

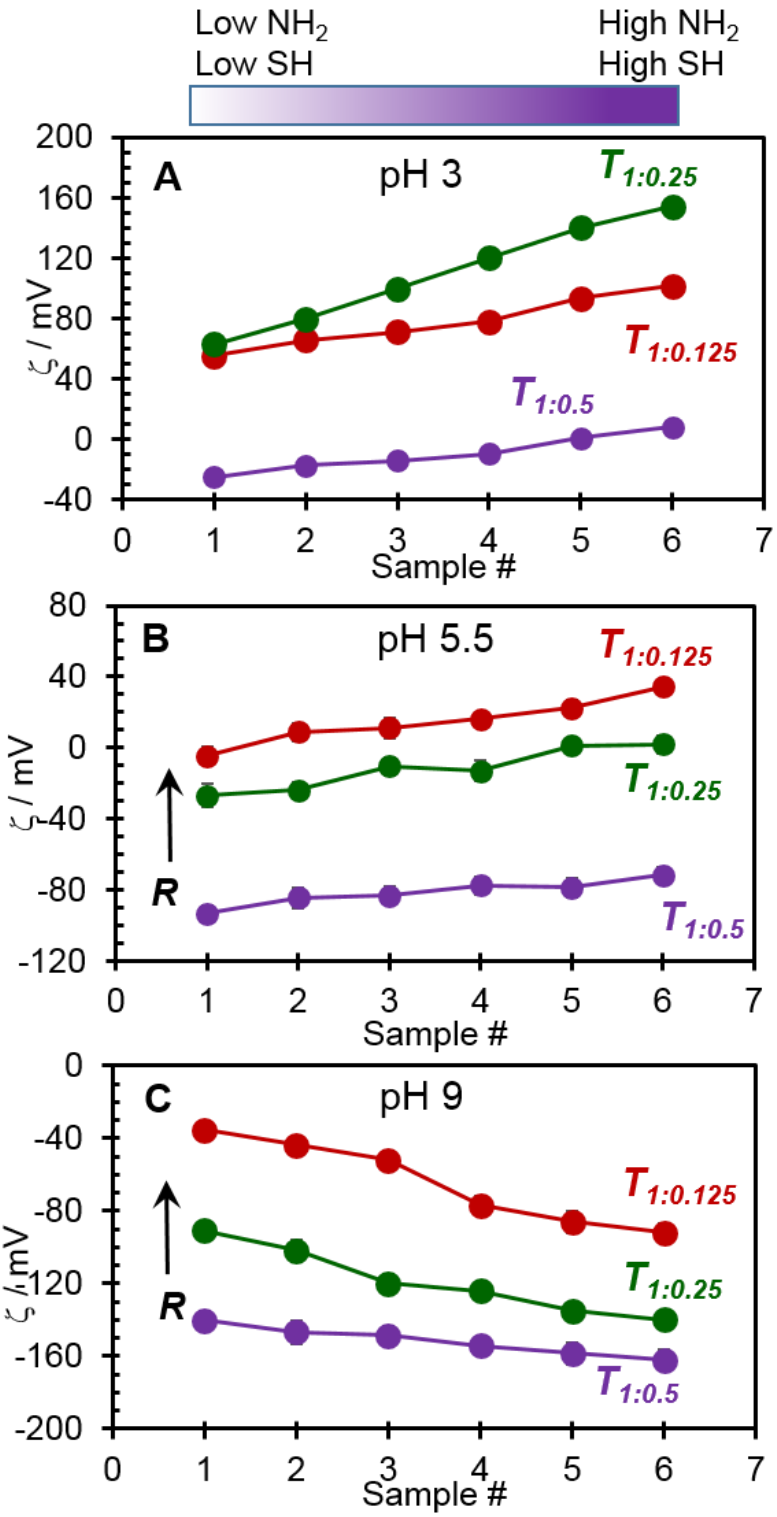

Figure 6.12: Changes in ζ with the extent of surface modification at three different pHs. For simplicity only $\boldsymbol{T}_{1:0.25}$, $\boldsymbol{T}_{1:0.125}$ and $\boldsymbol{T}_{1:0.5}$ are shown.

a balance between the acidic and basic species at that pH.

Table 6.2 and **6.3** shows surface charge density and charged groups of the various samples calculated at pH 5.5. The samples having greater (***R*** = 8) have mostly positive charge density on the surface and vice versa. Similarly, the number of the charge groups vary significantly from top to bottom of the gradients for higher ***R*** and vice versa.

Table 6.2: Charge density of the samples measured at pH 5.5

			Charge density × 10^3 (C/m^2) at			pH 5.5	
$T_{immersion}$	Sample #	$T_{2:0.25}$	$T_{1:0.5}$	$T_{0.5:0.125}$	$T_{1:0.125}$	$C8_{2:0.25}$	$C8_{1:0.5}$
30	6	7.90	-7.30	-4.10	2.70	1.33	-7.10
25	5	4.95	-8.40	-3.93	1.70	1.29	-6.15
20	4	3.30	-8.20	-4.11	1.20	0.04	-5.62
15	3	1.93	-9.30	-3.87	0.67	-0.17	-5.25
10	2	0.91	-9.50	-3.12	0.65	-0.44	-4.44
5	1	0.53	-12.0	-2.44	-0.04	-1.5	-3.59

Table 6.3: # of charge group of the samples measured at pH 5.5

$T_{immersion}$	Sample #	Net # of Charge groups at pH 5.5					
		$T_{2:0.25}$	$T_{1:0.5}$	$T_{0.5:0.125}$	$T_{1:0.125}$	$C8_{2:0.25}$	$C8_{1-0.5}$
30	6	4.90×10^{16}	-4.54×10^{16}	-2.56×10^{16}	1.70×10^{16}	8.32×10^{15}	-4.4×10^{16}
25	5	3.10×10^{16}	-5.27×10^{16}	-2.44×10^{16}	1.06×10^{16}	8.07×10^{15}	-3.8×10^{16}
20	4	2.10×10^{16}	-5.13×10^{16}	-2.56×10^{16}	7.52×10^{15}	2.68×10^{14}	-3.5×10^{16}
15	3	1.21×10^{16}	-5.80×10^{16}	-2.41×10^{16}	4.17×10^{15}	-1.05×10^{15}	-3.3×10^{16}
10	2	5.68×10^{15}	-5.96×10^{16}	-1.95×10^{16}	4.09×10^{15}	-2.75×10^{15}	-2.8×10^{16}
5	1	3.32×10^{15}	-7.16×10^{16}	-1.53×10^{16}	-2.48×10^{14}	-9.32×10^{15}	-2.2×10^{16}

6.5 Summary

The sample surfaces both TMOS and OTMOS in this paper have complex chemical nature and a complex distribution of NH_3^+, SO_3^-, SiO^- and OH species from one end to the other end of the gradients surfaces. So, the ζ is the net resultant effect of all these species at certain pH depending on the pKa values of various species present. Here we examined the ζ dependence on the extent of modification by the various charged species and the different base layers. One

interesting observation is that all six samples in the different samples prepared on both TMOS and OTMOS cross at the same pH. We call this point of intersection (***POI***) where the ζ basically remains constant i.e., at that particular pH the samples do not show any charge gradient. The same ***POI*** was also observed in our previous work at pH around ~6.6, sample id $\boldsymbol{T}_{1\text{-}0.25}$. In this work, we analyzed that point by varying the amount of the different charged species and base layers. Increasing the SO_3^- fraction on the surface leads to the more negative ζ whereas increasing the NH_3^+ fraction on the surface leads to the more positive ζ.increasing the NH_3^+ fraction gives more basic character to the surface as a result the pH at the ***POI*** shifts to more basic values irrespective of the nature of the siloxane base layers.

6.6. References

1. Becker, A. L.; Henzler, K.; Welsch, N.; Ballauff, M.; Borisov, O. Proteins and polyelectrolytes: A charged relationship. Curr. Opin. *Colloid Interface Sci.*, **2012**, *17*, 90−96.

2. Ekblad, T.; Andersson, O.; Tai, F. I.; Ederth, T.; Liedberg, B. Lateral Control of Protein Adsorption on Charged Polymer Gradients. *Langmuir*, **2009**, *25* (6), 3755−3762.

3. Chung, Y. C.; Chiu, Y. H.; Wu, Y. W.; Tao, Y. T. Self-assembled biomimetic monolayers using phospholipid-containing disulfides. *Biomaterials*, **2005**, *26* (15), 2313−2324.

4. Beurer, E.; Venkataraman, N. V.; Sommer, M.; Spencer, N. D. Protein and nanoparticle adsorption on orthogonal, charge-densityversus-net-charge surface-chemical gradients. *Langmuir*, **2012**, *28*, 3159−3166.

5. Yang, R.; Xu, J. J.; Ozaydin-Ince, G.; Wong, S. Y.; Gleasont, K. K. Surface-Tethered Zwitterionic Ultrathin Antifouling Coatings on Reverse Osmosis Membranes by Initiated Chemical Vapor Deposition. *Chem. Mater.*, **2011**, *23* (5), 1263−1272.

6. Ding, Y. X.; Streitmatter, S.; Wright, B. E.; Hlady, V. Spatial variation of the charge and sulfur oxidation state in a surface gradient affects plasma protein adsorption. *Langmuir*, **2010**, *26*, 12140 − 12146.

7. Chuang, W. H.; Lin, J. C. Surface characterization and platelet adhesion studies for the mixed self-assembled monolayers with amine and carboxylic acid terminated functionalities. *J. Biomed. Mater. Res., Part A*, **2007**, *82A* (4), 820 − 830.

8. Riepl, M.; Ostblom, M.; Lundstrom, I.; Svensson, S. C. T.; van der Gon, A. W. D.; Schaferling, M.; Liedberg, B. Molecular gradients: An efficient approach for optimizing the surface properties of biomaterials and biochips. *Langmuir*, **2005**, *21* (3), 1042 − 1050.

9. Gessner, A.; Lieske, A.; Paulke, B. R.; Muller, R. H. Influence of surface charge density on protein adsorption on polymeric nanoparticles: analysis by two-dimensional electrophoresis. Eur. *J. Pharm. Biopharm*. **2002**, *54* (2), 165 − 170.

10. Beurer, E.; Venkataraman, N. V.; Rossi, A.; Bachmann, F.; Engeli, R.; Spencer, N. D. Orthogonal, Three-Component, Alkanethiol-Based Surface-Chemical Gradients on Gold. *Langmuir*, **2010**, *26* (11), 8392 − 8399.

11. Ooi, Y.; Hobara, D.; Yamamoto, M.; Kakiuchi, T. Ideal nonideality in adsorption of 2-aminoethanethiol and 2-mercaptoethane sulfonic acid to form electrostatically stabilized binary selfassembled monolayers on Au(111). *Langmuir*, **2005**, *21* (24), 11185 − 11189.

12. Lestelius, M.; Liedberg, B.; Tengvall, P. In vitro plasma protein adsorption on omega-functionalized alkanethiolate self-assembled monolayers. *Langmuir*, **1997**, *13* (22), 5900 − 5908.

13. Ashraf, K. M.; Giri, D.; Wynne, K. J.; Higgins, D. A.; Collinson M. M. Cooperative effects in aligned and opposed multicomponent charge gradients containing strongly acidic, weakly acidic, and basic functional groups *Langmuir*, **2016**, *32*, 3836−3847.

14. Kannan, B.; Dong, D.; Higgins, D. A.; Collinson, M. M. Profile Control in Surface Amine Gradients Prepared by Controlled-Rate Infusion. *Langmuir*, **2011**, *27*, 1867 − 1873.

15. Kannan, B.; Higgins, D. A.; Collinson, M. M. Aminoalkoxysilane reactivity in surface amine gradients prepared by controlled-rateinfusion. *Langmuir*, **2012**, *28*, 16091 − 16098.

16. Kannan, B.; Higgins, D. A.; Collinson, M. M., Aminoalkoxysilane Reactivity in Surface Amine Gradients Prepared by Controlled-Rate Infusion", *Langmuir*, **2012**, *28*, 16091-16098.

17. Margolese, D.; Melero, J. A.; Christiansen, S. C.; Chmelka, B. F.; Stucky, G. D. Direct Syntheses of Ordered SBA-15 Mesoporous Silica Containing Sulfonic Acid Groups. *Chem. Mater.*, **2000**, *12*, 2448−2459.

18. Sundara, R. Hot peroxide bleaching. *Can. Chem. News*, **1998**, *17*, 15−17.

19. Corum, L. E.; Hlady, V. Screening platelet-surface interactions using negative surface charge gradients. *Biomaterials*, **2010**, *31*, 3148 − 3155.

20. Ding, Y. X.; Streitmatter, S.; Wright, B. E.; Hlady, V. Spatial variation of the charge and sulfur oxidation state in a surface gradient affects plasma protein adsorption. *Langmuir*, **2010**, *26*, 12140 − 12146.

21. Shen, C. H.; Lin, J. C. Surface characterization and platelet compatibility evaluation of binary mixed self-assembled monolayers containing novel sulfonic acid terminated alkanethiol. *Colloids Surf. B*, **2010**, *79*, 156 − 163.

22. Ivashenko, O.; van Herpt, J. T.; Feringa, B. L.; Browne, W. R.; Rudolf, P. Rapid reduction of self-assembled monolayers of a disulfide terminated para-nitrophenyl alkyl ester on roughened Au surfaces during XPS measurements. *Chem. Phys. Lett.*, **2013**, *559*, 76−81.

23. Batich, C. D.; Donald, D. S. X-Ray Photoelectron-Spectroscopy of Nitroso-Compounds - Relative Ionicity Of The Closed And Open Forms. *J. Am. Chem. Soc*. **1984**, *106* (10), 2758−2761.

24. Gupta, M. L.; Brunson, K.; Chakravorty, A.; Kurt, P.; Alvarez, J. C.; Luna-Vera, F.; Wynne, K. J. Quantifying surface-accessible quaternary charge for surface modified coatings via streaming potential measurements. *Langmuir*, **2010**, *26*, 9032 − 9039.

25. Pu, Q.; Elazazy, M. S.; Alvarez, J. C. Label-free detection of heparin, streptavidin, and other probes by pulsed streaming potentials in plastic microfluidic channels. *Anal. Chem.* **2008**, *80*, 6532 − 6536.

26. Berezkin, V. V.; Volkov, V. I.; Kiseleva, O. A.; Mitrofanova, N. V.; Sobolev, V. D. The Charge of the Pores of Poly (ethylene terephthalate) Nucleopore Membranes. *Colloid J.* **2003**, *65* (1), 119 − 121.

27. Kim, K.; Kwak, J. Faradaic impedance titration of pure 3-mercaptopropionic acid and ethanethiol mixed monolayers on gold. *J. Electroanal. Chem.* **2001**, *512* (1 − 2), 83 − 91.

28. Ivashenko, O.; van Herpt, J. T.; Feringa, B. L.; Browne, W. R.; Rudolf, P. Rapid reduction of self-assembled monolayers of a disulfide terminated para-nitrophenyl alkyl ester on roughened Au surfaces during XPS measurements. *Chem. Phys. Lett.* **2013**, *559*, 76 − 81.

29. Kannan, B.; Nokura, K.; Alvarez, J. C.; Higgins, D. A.; Collinson, M. M. Fabrication of Surface Charge Gradients in Open-Tubular Capillaries and Their Characterization by Spatially Resolved Pulsed Streaming Potential Measurements. *Langmuir*, **2013**, *29*, 15260 − 15265.

30. Bard, A. J.; Faulkner, L. R. Electrochemical Methods: Fundamentals and Applications; John Wiley & Sons, Inc.: New York, **2001**.

31. Zeidan, R. K.; Davis, M. E. The effect of acid-base pairing on catalysis: An efficient acid-base functionalized catalyst for aldol condensation. *J. Catal.* **2007**, *247*, 379 − 382.

32. Hall, H. K. Steric Effects on the Base Strengths of Cyclic Amines. *J. Am. Chem. Soc*. **1957**, *79*, 5444 − 5447.

33. Ong, S.; Zhao, X.; Eisenthal, K. B. Polarization of water molecules at a charged interface: second harmonic studies of the silica/water interface. *Chem. Phys. Lett.* **1992**, *191*, 327 − 336.

34. Creager, S. E.; Clarke, J. Contact-Angle Titrations of Mixed Omega-Mercaptoalkanoic Acid Alkanethiol Monolayers on Gold -Reactive vs. Nonreactive Spreading, and Chain-Length Effects on Surface Pk(a) Values. *Langmuir*, **1994**, *10*, 3675 − 3683.

35. Van der Vegte, E. W.; Hadziioannou, G. Acid-base properties and the chemical imaging of surface-bound functional groups studied with scanning force microscopy. *J. Phys. Chem. B,* **1997**, *101*, 9563 − 9569.

36. Vezenov, D. V.; Noy, A.; Rozsnyai, L. F.; Lieber, C. M. Force titrations and ionization state sensitive imaging of functional groups in aqueous solutions by chemical force microscopy. *J. Am. Chem. Soc*. **1997**, *119*, 2006 − 2015.

Chapter 7. Conclusion

7. Conclusion

A number of surface charge gradients were prepared from 3-aminopropyltrieethoxysilane 3-mercaptopyltriemethoxysilane using controlled-rate infusion (***CRI***). This approach described in this work takes advantage of the reactivity of these silanes, which can be controlled by the concentration, amount and type of catalyst and the amount of water in the silane solution. Among the various organoalkoxysilanes commercially available, aminoalkoxysilanes have an advantage of self-catalyzing the reaction with surface silanol groups through the basic amine moiety. This research mainly concentrates on the preparation of charge gradients containing NH_3^+, SO_3^- and SiO^- or NH_3^+, and SiO^- on siloxane base layer coated substrates. Siloxane base layers were chosen to have varying degree of hydrophilicity and hydrophobicity. Both 3-aminopropyltriethoxysilane and 3-mercaptopropyltriemethoxysilane have widespread application in various fields in analytical and inorganic chemistry. In the very first project, aligned and opposed gradients containing NH_3^+, SO_3^- and SiO^- charge groups on TMOS derived siloxane base layers were prepared by the ***CRI*** method. Very different surface chemistry was observed when the 3-mercaptopropyltrimethoxysilane precursors and the 3-aminopropyltriethoxysilane precursors were deposited in the same direction (aligned) vs. opposite directions (opposed). Surface charge and charge distribution from the bottom to the top of the substrate strongly influenced **WCA**, binding of metal nanoparticles, and ζ. The surface wettability and nanoparticles absorption patterns of these gradients were also found to dramatically different from each other.

In the second project, NH_3^+ gradients on different base layer modified substrates were prepared via the ***CRI*** method to elucidate the effect of different base films on surface wettability.

In this case, the rate of infusion of the silane solution was programmed so that the substrate has three distinct regions: one-third having slow infusion and a high degree of modification, the middle one-third with medium infusion rate and last one-third having the fast infusion rate having a low degree of modification. This way the chemistry at different points along the substrate was changed. Static and dynamic contact angle experiments were used to probe the surface wettability of these charged gradients and **XPS** was used to evaluate the gradient profile. It has found that surface wettability and gradient profiles are entirely different from each other and are largely dependent on the base layer chemistry. The higher the hydrophobicity of the base layer, the lower the extent of the modification. The contact angle hysteresis of the gradients also widely varied; the gradient deposited on the most hydrophobic base layer showed the greatest hysteresis and one having the highest hydrophilicity showed the smallest hysteresis.

In the third project, the effect of the order of infusion NH_3^+ to SO_3^- or $SO_3^-$to NH_3^+ on aligned and opposed gradients was studied by **XPS** spectroscopy and **DCA** analysis. The samples were prepared by sequentially infusing amine and thiol silanes into a glass vial housing a silicon wafer containing a TMOS derived base layer and subsequently converting these functionalities into charge groups by reacting them with 30% H_2O_2. The effect of amine catalysis on the condensation of thiol was evident as **XPS** spectroscopy result clearly showed the extent of modification with thiol was the greatest when the order of infusion was amine + thiol in contrast to thiol + amine.

In the final project, a total of six charge gradients on TMOS (four) and octyltrimethoxysilane- (OTMOS) (two) derived base layers containing SO_3^-, NH_3^+ and SiO^- oriented in an aligned fashion were prepared by the ***CRI*** method. We evaluated the ζ dependence on the extent of modification by the various charged species on the different base layers. One

interesting observation was that all six samples in the different samples prepared on both TMOS and OTMOS derived base layers cross at the same pH. We called it the "point of intersection (***POI***)" where the ζ basically remains constant i.e., at that particular pH the samples do not show a charge gradient. The same ***POI*** was also observed in the very first work at pH ~6.6 for the aligned gradient. In this work, we attempted to analyze that point by varying the amount of the different charged species on the surface and also by changing the base layers. Increasing the SO_3^- fraction on the surface leads to the more negative ζ whereas increasing the NH_3^+ fraction on the surface leads to the more positive ζ values. Increasing the NH_3^+ fraction also gives more basic character to the surface and, as a result, the pH at the ***POI*** shifts to more basic values irrespective of the nature of the siloxane base layers.

Kayesh M Ashraf Vitae

Professional Overview

A dedicated, flexible, and result oriented individual possesses problem solving and organizational skills and able to communicate effectively to all levels of an organization, and confident to adapt rapidly to any new environment and also to the demands of a fast-paced work place.

Education

Doctor of Philosophy, Analytical Chemistry and Nanoscience 05/2017

Virginia Commonwealth University, USA.

Research Interest: Thin films (Raman, FTIR, UV-VIS), Coating technology, Sol-gel chemistry, and multifunctional charged surface (AFM, SEM, XPS, Zeta potential, dynamic CA).

Doctor of Engineering, Environment Science, 09/2012

Yokohama National University, Japan.

MS, Applied Chemistry & Chemical Engineering 06/2005

University of Dhaka, Bangladesh.

BS, Applied Chemistry & Chemical Engineering, 06/2003

University of Dhaka, Bangladesh.

Experience

Research Assistant, Virginia Commonwealth University, Virginia, USA 01/2012 – 05/2017

Achievements

1. Developed approaches to strategically modify siloxane thin layers with cationic and anionic species in a gradient fashion.
2. Designed and developed new methods to characterize the gradients' micro-properties and quantify surface charge along the gradients.
3. SOP writing (LabRAM HR Evolution - HORIBA, ramé-hart, Contact Angle Goniometer)
4. Coordinating various research activities.

Research Assistant, Yokohama National University, Japan 2008 –2012

Achievements

1. Designed and developed new techniques/methods for determining conditions (thermal and catalytic) for the termination of sol-gel reaction.
2. Participated in the university science grant completion and obtained grant as the best speaker.
3. Conducted literature reviews for research particularly on sol-gel process

thermal analyses and spectroscopy.
4. Led group research meetings based on literature reviews and laboratory work on environmental science.

QC officer, Aristopharma Ltd

Generic products Manufacturer, Dhaka, Bangladesh 2006 - 2008

Achievements

1. Strengthened knowledge in handling advanced instruments like HPLC, UV-Vis and FT-IR.
2. Maintained all documentation in laboratory, supervised and investigated the team members.

Research Assistant

Bangladesh Atomic Energy Commission, Savar, Bangladesh 2004 – 2006

Achievements

1. Improvement of the physico-mechanical and biodegradable properties of the natural fiber and polymer composites by UV and Gamma radiation.
2. Characterization of the composite products by Materials testing machine (INSTRON), Hydraulic pressure testing machine, UV-Vis, FT-IR etc.
3. Small scale production of commercial chairs and tables from the produced composites.

Other Experiences

1. **Industrial training** on chemical process and engineering at Jamuna Fertilizer Co. Ltd. Bangladesh. 10/2003 -12/2003

2. **Hands-on Experience** on "Industrial process unit operation & process control techniques" at Training Institute for Chemical Industries (TICI), Polash, Bangladesh. 04/2003 - 05/2003

Skills

1. Instrumental and chemical

- X-ray photoelectron spectroscopy (XPS), Scanning electron microscopy (SEM), Peak force QNM and Tapping mode atomic force microscopy (AFM), Dynamic and static water contact angle, Surpass electrokinetic analyzer, Wide angle X-ray spectroscopy, Transmission electron microscopy (TEM), Spin coating, TLC, GC, UV-Vis, FTIR, Raman spectroscopy, Stober process, Dissolution test and sol-gel process.

2. Computer

- MS office, Sigma plot, Origin, Mathlab, FORTRAN, Chemdraw, Chemometrics, Adobe Photoshop and Illustrator.

Excellent communication skills, ability to work as part of a team and on own. Versatile team player with excellent interpersonal and technical documentation skills and handling multiple projects simultaneously.

Language skills

English: Advanced,
Japanese: Intermediate,
Hindi: Speaking only,
Bengali: Native,
French: Beginner

Please visit

linkedin.com/in/kayesh-ashraf-phd for more info

Publications

1. **Kayesh M. Ashraf**, Chenyu Wang, Sithara S. Nair, Kenneth J. Wynne, Daniel A. Higgins, Maryanne M. Collinson*,[1] Base Layer Influence on Protonated Aminosilane Gradient Wettability, *Langmuir*, **2017**.
2. Zi Li, **Kayesh M. Ashraf**, Maryanne M. Collinson and Daniel A. Higgins "Single Molecule Catch and Release: Potential-Dependent Plasmid DNA Adsorption along Chemically Graded Electrode Surfaces", *Langmuir*, **2017**, *doi: 10.1021/acs.langmuir.7b00044.*
3. Dipak Giri, Zi Li, **Kayesh M. Ashraf**, Maryanne M. Collinson and Daniel A. Higgins, Molecular Combing of λ-DNA using Self-Propelled Water Droplets on Wettability Gradient Surfaces, *ACS Applied Materials & Interfaces*, **2016.**
4. Veeren C. Dewoolkar, Lena N. Jeong, Daniel W. Cook, **Kayesh M. Ashraf**, Sarah C. Rutan, Maryanne M. Collinson Amine Gradient Stationary Phases on In-House Built Monolithic Columns for Liquid Chromatography, *Analytical Chemistry*, **2016**.
5. **Kayesh M Ashraf**, Dipak Giri, Kenneth J Wynne, Daniel A Higgins, Maryanne M Collinson, Cooperative Effects in Aligned and Opposed Multicomponent Charge Gradients Containing Strongly Acidic, Weakly Acidic, and Basic Functional Groups, *Langmuir*, **2016**.
6. Stacy L. Stegall, **Kayesh M. Ashraf**, Julie R. Moye, Daniel A. Higgins, Maryanne M. Collinson, Separation of Transition and Heavy Metals Using Stationary Phase Gradients and Thin Layer Chromatography, *J. Chromatog. A*, **2016**.
7. Veeran C. Dewoolkar, Balamurali Kannan, **Kayesh M. Ashraf**, Daniel A. Higgins and Maryanne M. Collinson, Amine-Phenyl Multi-Component Gradient Stationary Phases, *J. Chromatog. A*, **2015.**
8. Dipak Giri, **Kayesh M. Ashraf**, Maryanne M. Collinson and Daniel A. Higgins, A Single Molecule Perspective on Mass Transport in Condensed Water Layers over Gradient Self-Assembled Monolayers, *J. Phys. Chem. C*, **2015**.
9. Ken-ichi Kurumada, **Kayesh M. Ashraf**, Shinya Matsumoto, Effects of Heat Treatment on Various Properties of Organic–Inorganic Hybrid Silica Derived from Phenyltriethoxysilane, *Mat. Chem. Phys.*, **2014**.
10. **Kayesh M. Ashraf**, Ken-ichi Kurumada, Shinya Matsumoto, Determination of Heat Treatment Temperature for Completing Polycondensation of Vinyl Substituted Silica Particles Prepared by Sol-Gel Method, *Chem. Eng. Tech*., **2012**.
11. Juganta K. Roy, Nousin Akter, Haydar U. Zaman, **Kayesh. M. Ashraf**, Sabrina Sultana, Shahruzzaman, Nuruzzaman Khan, M. Arifur Rahman, Tuhidul Islam, Mubarak. A. Khan · Ruhul A. Khan Preparation and properties of coir fiber-reinforced ethylene glycol dimethacrylate-based composite, *J. Thermoplast. Comp. Mater*. **2012**.
12. **Kayesh M. Ashraf**, T. J. Ferdous, Ahmed. I. Mustafa, Mubarak A. Khan, Photocuring of Empty Fruit Bunches of Oil Palm (Elaeis guineensis) Fibers with Allyl Methacrylate (AMA): Effect of Additives on Mechanical and Degradable Properties, *Polym. Plast. Tech. Eng.*, **2008**.

Manuscripts ready for submission

1. On the importance of gradient infusion order on the microscopic and macroscopic properties of bi-functional charge gradients. Kayesh M Ashraf, Sithara S. Nair, Kenneth J. Wynne, Daniel A. Higgins and Maryanne M. Collinson.
2. Charge Distribution in Aligned Bi-functional Gradients as a function of surface concentration and base layer. Kayesh M Ashraf, Md Rezaul K Khan, Daniel A. Higgins and Maryanne M. Collinson.

Presentation

1. Single-Molecule Tracking Study of Mass Transport in Nanoscale Water Condensed over Gradient Self-Assembled Monolayers. Kansas Physical Chemistry Symposium, Dec, **2015**, USA. Dipak Giri, Kayesh M. Ashraf, Maryanne M. Collinson, and Daniel A. Higgins.
2. Multicomponent charge gradients using silane chemistry Sol-Gel 2015 Conference Sep, **2015**, Kyoto, Japan. Kayesh M. Ashraf, Daniel A. Higgins and Maryanne M. Collinson.
3. Method of determining heat treatment condition for completing polycondensation of organic silica containing bulky phenyl groups. SCEJ (The Society of Chemical Engineers, Japan) 79th Annual Meeting, Feb 2014, Gifu, Japan. Kurumada Kenichi, Matsumoto Shinya and Kayesh M Ashraf.
4. Effects of catalyst and heat treatment on polycondensation of sol-gel derived organic-inorganic hybrid silica from phenyltriethoxysilane (PTES). Core-to-Core 2010 World Network Seminar on Advanced Particle Science and Technology Nov, 2010, Kyoto, Japan. Kayesh M Ashraf, Matsumoto Shinya, and Kurumada Kenichi.